ICARUS

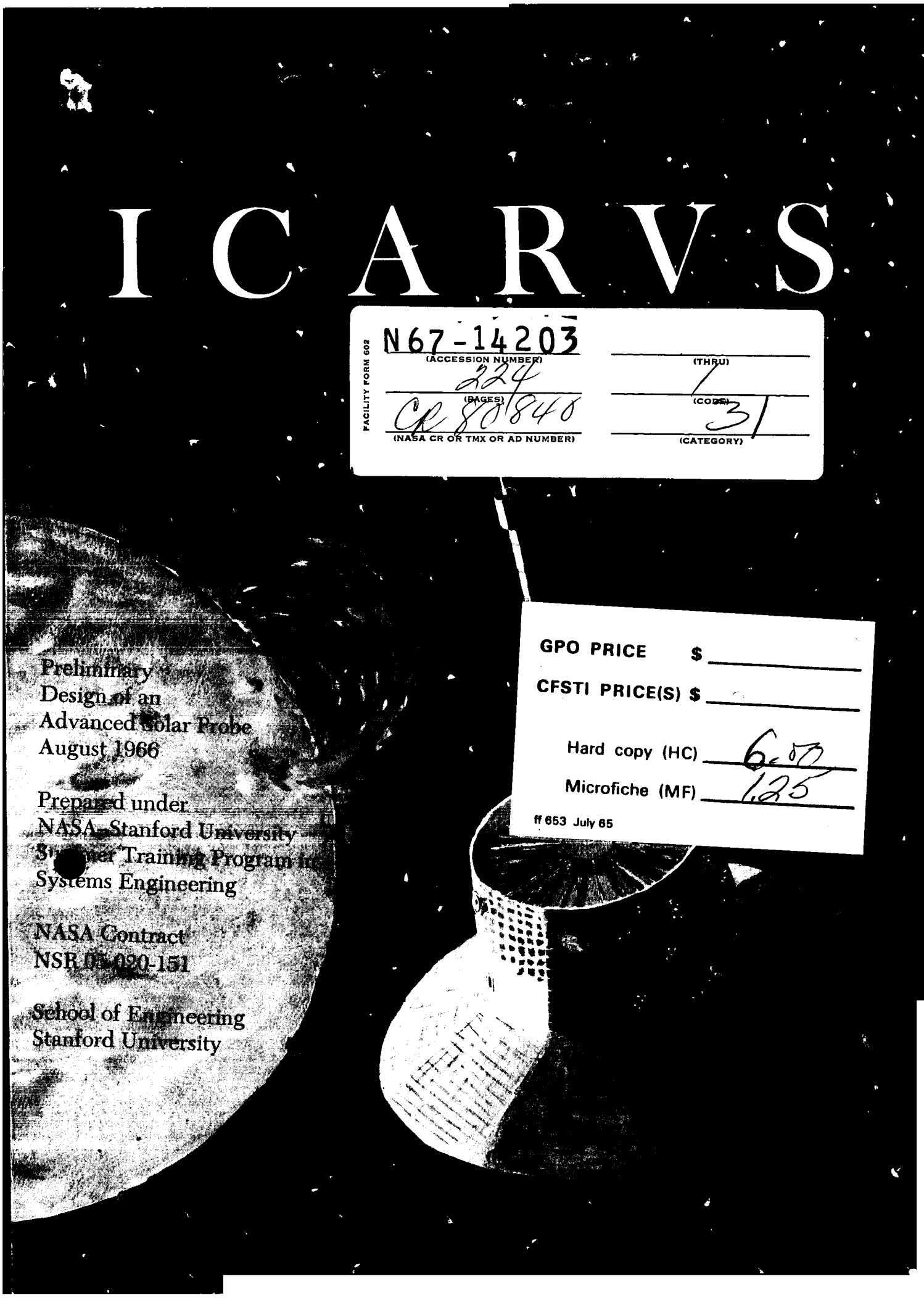

Preliminary Design of an Advanced Solar Probe
August 1966

Prepared under NASA-Stanford University Summer Training Program in Systems Engineering

NASA Contract NSR 05-020-151

School of Engineering
Stanford University

I C A R V S

INTER-PLANETARY CRAFT FOR ADVANCED RESEARCH IN THE VICINITY OF THE SUN

STANFORD-NASA SPACE SYSTEMS PROJECT

Edited by:
Varada P. Charyulu

August 1966

LIST OF PARTICIPANTS

GROUP A:	Experiments and Data Handling (Advisor: Dr. B. Lusignan)
Varada P. Charyulu†	University of Tulsa B.E. - Osmania Univ., India; 1956 M.E. - Univ. of Roorkee, India; 1958 M.S. - Purdue Univ.; 1960 Ph.D. - Iowa State Univ.; 1964
M. Don Merrill	New Mexico State University B.S.E.E. - Univ. of Utah; 1958 Ph.D. - Univ. of Utah; 1964
Robert P. Merrit	University of Alaska B.S.E.E. - Oregon State; 1949 M.S. - Oregon State; 1957
Thomas M. White, Jr.*	Georgia Institute of Technology B.S.E.E. - G.I.T.; 1947 M.S.E.E. - G.I.T.; 1948 Ph.D. - G.I.T.; 1963
John R. Osborn*	Purdue University Ph.D. - Purdue Univ.; 1957
Paul A. Wintz*	Purdue University Ph.D. - Purdue Univ.; 1964
GROUP B:	Boosters, Trajectories and Stabilization (Advisors: Dr. W. Bollay, Dr. D. De Bra)
Madeline Goulard	Purdue University M.S.A.E. - ENSAE (Paris); 1950 Ph.D. - Purdue; 1958
J. J. Jonsson*	Brigham Young University B.S.G.E. - Univ. of Utah; 1944 B.S.E.E. - Univ. of Utah; 1947 M.S.E.E. - Purdue; 1948 Ph.D. - Purdue; 1951
Ross M. McDonald*,**	University of Tulsa B.S. - Univ. of Tulsa; 1950 M.S. - Univ. of Tulsa; 1959 Ph.D. - Iowa State Univ.; 1965

Corrado Poli*	Air Force Institute of Technology B.A.E. - Rensselaer Polytechnic. Inst.; 1957 M.S. - Rensselaer Polytechnic. Inst.; 1958 Ph.D. - Ohio State Univ.; 1965
GROUP C:	Spacecraft (Advisor: Prof. J. Mayers)
A.E. Andreoli**	Calif. State Polytechnic College B.S.A.E. - Univ. of Colorado; 1954 M.S. - Calif. Inst. of Tech.; 1956
Stephen L. Dickerson*	Georgia Inst. of Technology B.S. - Ill. Inst. of Tech.; 1962 M.S. - Univ. of Calif., Berkeley; 1963 Sc.D. - M.I.T.; 1965
Virgil Smith*	Georgia Institute of Technology B.C.E. - Georgia Tech.; 1958 M.S.C.E. - Stanford Univ.; 1959 Sc.D. - M.I.T.; 1963
Emil J. Steinhardt*,**	West Virginia University B.S.M.E. - U. of Pittsburgh; 1959 M.S.M.E. - U. of Pittsburgh; 1961 Ph.D. - U. of Pittsburgh; 1965
Otto E. Widera	University of Illinois (Chicago) B.S. - Univ. of Wisconsin; 1960 M.S. - Univ. of Wisconsin; 1962 Ph.D. - Univ. of Wisconsin; 1965

* Group Leaders
** Project Leaders
† Editor of Final Report

ABSTRACT

This report presents a preliminary design study of ICARUS, an advanced solar probe. It was prepared during a NASA - Stanford training program on space systems engineering by a group of 15 professors from various US universities during the summer of 1966.

The objective of ICARUS is to explore the region of space between 1 AU and 0.1 AU* from the Sun, both in and out of the ecliptic plane. This program thus supplements the current NASA Pioneer project which investigates solar particles and fields in the region to 0.8 AU with the current Pioneer and to 0.5 AU with later versions of Pioneer. The experiments planned for ICARUS are similar to Pioneer, namely, the measurement of cosmic rays, solar particles, and magnetic fields.

The major new problem encountered in this study was the design of a spacecraft which could survive and function under the 100-fold increase in solar radiation which is encountered at 0.1 AU. Many configurations were studied and a simple arrangement finally evolved which can withstand this severe thermal environment and still weigh only 160 pounds. The spacecraft consists of a relatively flat spin stabilized body of revolution with its axis normal to the orbit plane. This arrangement minimized the heat inflow from the Sun and maximized the heat rejected by radiation. The basic load carrying structure is of Beryllium. The outer shell is made up of fiberglass reinforced plastic in the form of a frustum of a cone.

The solar cell power supply is on a flared conical skirt, attached to the bottom of the main body. It provides a minimum of 40 watts near Earth and 242 watts near the Sun. Active thermal control is effected by louvers (actuated by bimettalic springs) located at the top and bottom ends of the spacecraft. Minimum heat inflow into the spacecraft is achieved by means of optical solar reflectors and superinsulation. A suitable combination of travelling-wave tubes provide communication data rates of greater than 500 bits/sec using a ground antenna of 210 ft. diameter and an error rate not to exceed 10^{-3} bits/sec. Data rates as high as 1800 bits/sec at 0.3 AU and 800 bits/sec at 0.1 AU are available with this communication system. Data reduction and processing and analog to digital conversion for both the scientific and engineering data is performed by a central data system in the spacecraft.

The spacecraft system is design to be launched by the Atlas-Centaur, plus two solid propellant upper stages for flights in the vicinity of 0.2AU. For flights in the vicinity of 0.1AU the Saturn IB-Centaur plus two solid propellant upper stages are required. The launch schedule is as follows:

* 1 AU is the mean distance from the Sun to the Earth.

ACKNOWLEDGMENTS

The participants of Stanford-NASA Space Systems Project wish to thank Professors William Bollay, Bruce Lusignan, Jean Mayers and Dan DeBra for their interest and excellent direction throughout the ICARUS project. Special thanks are due to Mr. John Foster and Mr. Howard Mathews of Systems Engineering Division at NASA-Ames who not only delivered lectures and gave their words of wisdom and experience to us, but also for their genuine interest in the educational aspect of the Systems Engineering.

We wish we could express our thanks to all the individuals, who helped us with valuable advice, and the organizations which we had the pleasure of visiting, but the list would be too long.

Since the entire project, ICARUS, including the final report was completed in a short period of ten weeks, the final report could not get all the required editorial attention and any slight discripancies are to be blamed only on the ever-running time.

Most of us, with the exception of the bachelor and the lady, wish to thank our respective and respectable wives who foresook their vacations and cooperated in the successful completion of ICARUS up to this stage.

The painting of ICARUS on the cover is by Dr. Bruce Lusignan.

Finally, all of us wish to express our sincere thanks to Miss Barbara Durham, our good friend and secretary, but for whose valuable legal and other advice and help - this project would not have taken this shape.

Launch No.	Date	Perihelion	Ecliptic Inclination
	ICARUS Skirt Angle 30°		
1	Spring 1971	0.18AU	1½°
2	Fall 1971	0.23AU	15°
3	Summer 1972	0.18AU	1½°
4	Spring 1973	0.23AU	15°
	ICARUS Skirt Angle 20°		
5	Fall 1973	0.09AU	3°
6	Spring 1974	0.11AU	15°

An estimate of the ICARUS program costs is as follows.

Four missions to 0.2 AU

Spacecraft - R & D	$24 million
4 vehicles	8
Five experiments	12
Boosters	56
Total	$100 million

Two missions to 0.1 AU

Spacecraft - additional R & D	$ 8 million
2 vehicles	4
Experiments	6
Boosters	84
Total	$102 million

Missions for solar exploration between 3 solar radii and 0.1 AU would require a radically different thermal design of the spacecraft and would probably utilize Jupiter swing-by to achieve the very high velocities ($\Delta V \approx$ 100,000 ft/sec) required for such flights.

TABLE OF CONTENTS

LIST OF FIGURES

LIST OF TABLES

I. INTRODUCTION

IA. Stanford-NASA Program in Space Systems Engineering

IA1. Objective

This report presents the conclusions of a preliminary design study carried out during the summer of 1966 as a space systems engineering project at Stanford University under the sponsorship of the National Aeronautics and Space Administration.

The participants were a group of fifteen professors of engineering representing seven specialties from ten universities in the United States. The objective of the project was a dual one, viz., technical and educational. The technical objective was to develop a preliminary design of a solar probe to a perihelion of about 0.1 AU, using the present state-of-the-art. The educational objective was to acquaint the participants with the techniques of systems engineering so that upon return to their respective universities they could initiate similar programs.

IA2. Program

Systems engineering seeks to optimize the design of a project from an overall mission point of view rather than on an individual component design basis by resolving the often conflicting requirements imposed by the subsystems. In the systems approach, the function which must be performed, i.e. the mission, is the prime factor to which each subsystem must be sub-servient. Subsystems are designed with respect to each other, rather than as separate aspects, so that the end result is an optimum over-all design.

To become qualified in the field of systems engineering the designers must be able to understand the concepts in other fields and how these fields interact with their own in a systems design; they must be able to talk and work with other engineers in a design team, and they must be able to handle system design problems, where often the questions can not even be properly asked until they are at least partially answered.

A course of this kind was conceived and conducted at MIT by Dr. William Bollay, who was a visiting professor at MIT, in the year 1962. The design problem selected was an equatorial weather satellite system. This experiment in creative engineering proved to be a tremendous success. The following year Dr. Bollay initiated a similar program, the preliminary design of a satellite based data collection

system at Stanford University. Since then both Stanford and MIT have continued this course. The encouraging results from this type of course prompted the sponsoring of the present study whose educational objective is to spread the technique to various other universities.

Course structure: The class was divided into three working groups, each with an elected group leader, a faculty advisor and a defined area of responsibility:

Group A: Experiments, communications and data handling
Group B: Boosters, trajectories and stabilization
Group C: Spacecraft

An elected project manager directed the entire effort of the three groups. The time span of ten weeks was split into three phases of approximately equal duration. At the end of each phase new group leaders and project managers were elected.

During the first phase of the program the necessary background lectures were presented by the Stanford faculty and specialists from the NASA-Ames research center. By the end of phase I the participants were able to organize a preliminary joint report comprising of a brief description of the overall system and its objective, and the major alternatives of overall system and for each subsystem.

During phase II the team was engaged in detailed evaluation of alternatives and preliminary design and analysis. At the same time, additional lectures, as needed, were delivered by NASA and industry representatives. Also, the group visited a few industries engaged in related endeavor. Daily, during the phase II, the group took part in active discussions and fruitful trade-off sessions. By the end of phase II of the program the group was able to reach an agreement on the major system decisions after having justified them quantitatively and considering the advantages and disadvantages of the alternatives.

Technical system integration and organization of the final report formed the major task during the third phase. At the end a verbal presentation of the final report was made to invited guests from the universities, NASA and other governmental organizations and industry. The comments from the invited guests were reviewed and minor modifications to the final report were made wherever necessary.

IB. Advanced Pioneer History

The value of scientific observations of interplanetory

phenomena has long been recognized by the NASA. NASA's program for unmanned space exploration includes the objectives of detailed observations of the solar disk and comprehensive mapping of the solar atmosphere. The result of these efforts is to gain a better understanding of solar phenomena and the relation of these phenomena to the dynamics of the solar corona.

The launching of Pioneer V in March 1960 marked the first specific step taken by the United States toward mapping the solar atmosphere. This provided magnetic field measurements up to 36 million km (22.5 million miles) from the Earth. About a year later Explorer X provided the first significant measurements of interplanetary plasma and of the boundary between the magnetosphere and the interplanetary regions.

The successful flights of OSO-I and Mariner II in 1962 made further contributions to the knowledge about the Sun. The OSO I accomplished detailed optical observations of the solar disk; Mariner II made the first measurements of solar wind away from the Earth's magnetic sphere. Later launches such as Explorer XII and Pioneer VI have provided valuable data on space radiation and magnetic fields. More extensive measurements of particles and fields in the solar atmosphere, between 0.8 and 1.2 AU, are the objectives of the current NASA Pioneer program.

The experimental results obtained thus far, through these programs, are reinforced by the various theoretical models of the Sun and its dynamic corona, in showing the desirability of conducting scientific experiments as close and as far away from the Sun and as far out of the ecliptic plane as is possible. This report presents a preliminary design proposal of a solar probe designed for nominal 0.1 and 0.2 AU orbits both in and out of ecliptic plane.

II. Program Summary

2A. Introduction and Experiments

The mission of the probe described herein is to transport five instruments through interplanetary space to the vicinity of the Sun, and transmit the data collected to Earth. The instruments selected are a triaxial fluxgate magnetometer, an electrostatic plasma probe, a cosmic ray detector, a neutron detector, and a device for measuring the electron density in space.

The fluxgate magnetometer will investigate dynamic magnetic phenomena in interstellar space, especially in the solar wind, and is designed to measure three orthogonal components of the magnetic field. The plasma probe will investigate the energy spectrum and angular distribution of solar plasma; it will measure the energy and direction of low energy charged particles (from about 10^2 ev to about 10^5 ev). The cosmic ray detector investigates the heliocentric radial gradients of proton and alpha particle intensities. It will measure the number of high energy protons and alpha particles. The neutron counter will investigate the solar flare phenomena by measuring neutron spectra. A bistatic radar experiment measures the electron density between Earth and the probe, and time variations of that quantity. This is accomplished by determining the phase differences of a fixed frequency UHF signal and a fixed frequency VHF signal.

The total mass of all instruments, including electronics, is 13.78 kg, and the power requirement is 11 watts. In addition, the fluxgate magnetometer requires 3.5 watts intermittantly for calibration.

A special booster and spacecraft system, ICARUS, has been designed to accomodate these instruments. The remainder of this Chapter is a summary of the booster and spacecraft system, and associated design philosophy.

2B. Design Philosophy

The program philosophy which guided the development of the ICARUS space research vehicle encompasses the following points:

a. Minimize program costs
b. Maintain multi-mission capability
c. Utilize space qualified components
d. Minimize mechanically actuated members
e. Maximize scientific data returned.

National acceptance of scientific unmanned space probes will probably depend critically on keeping the system cost to a minimum.

Decisions concerning booster selection, spacecraft design and utilization, and specific electronic and scientific equipment packages were therefore greatly influenced by cost considerations.

The ICARUS concept is built around multi-mission capability. Such capability offers, in addition to obvious economic advantages, the ability to fly identical scientific instruments in identical spacecraft environments to different sectors of inward solar system space. The "core" spacecraft is designed to perform satisfactorily in many heliocentric orbits.

Another point of philosophy was to take full advantage of the many systems and components already developed for the Pioneer program. A spin stabilized platform with the spin axis perpendicular to the orbit plane still appears to be the most effective way of providing two dimensional space scanning for the instruments. It was concluded that a fixed pole, high gain fan antenna is still the best compromise solution to achieve high data rates, and that a number of highly refined and space qualified electronics packages and scientific instruments could be adopted in toto.

Major emphasis in the design was placed upon improving reliability through simplicity. Articulated members were eliminated wherever possible. The only remaining adjustable members are the bimetallic actuated thermal louvers.

Every effort was made to maximize data gathering and transmission capacity in the region of greatest scientific interest, i.e. near the Sun. Highest transmission rates are needed near perihelion for two reasons, viz., the extremely large spacecraft velocity and a corresponding clustering of events in this region.

2C. Trajectories and Booster

Logical extension of the present Pioneer program and economic considerations resulted in the selection of an Atlas/Centaur/TE-364-3/FW-4S combination as the booster system. An outline drawing of the spacecraft and the two upper solid propellant kick stages mounted on the Centaur is shown in Fig. 2C1.1.

The booster system will effect hyperbolic escape from the Earth and transfer into a heliocentric orbit about the Sun

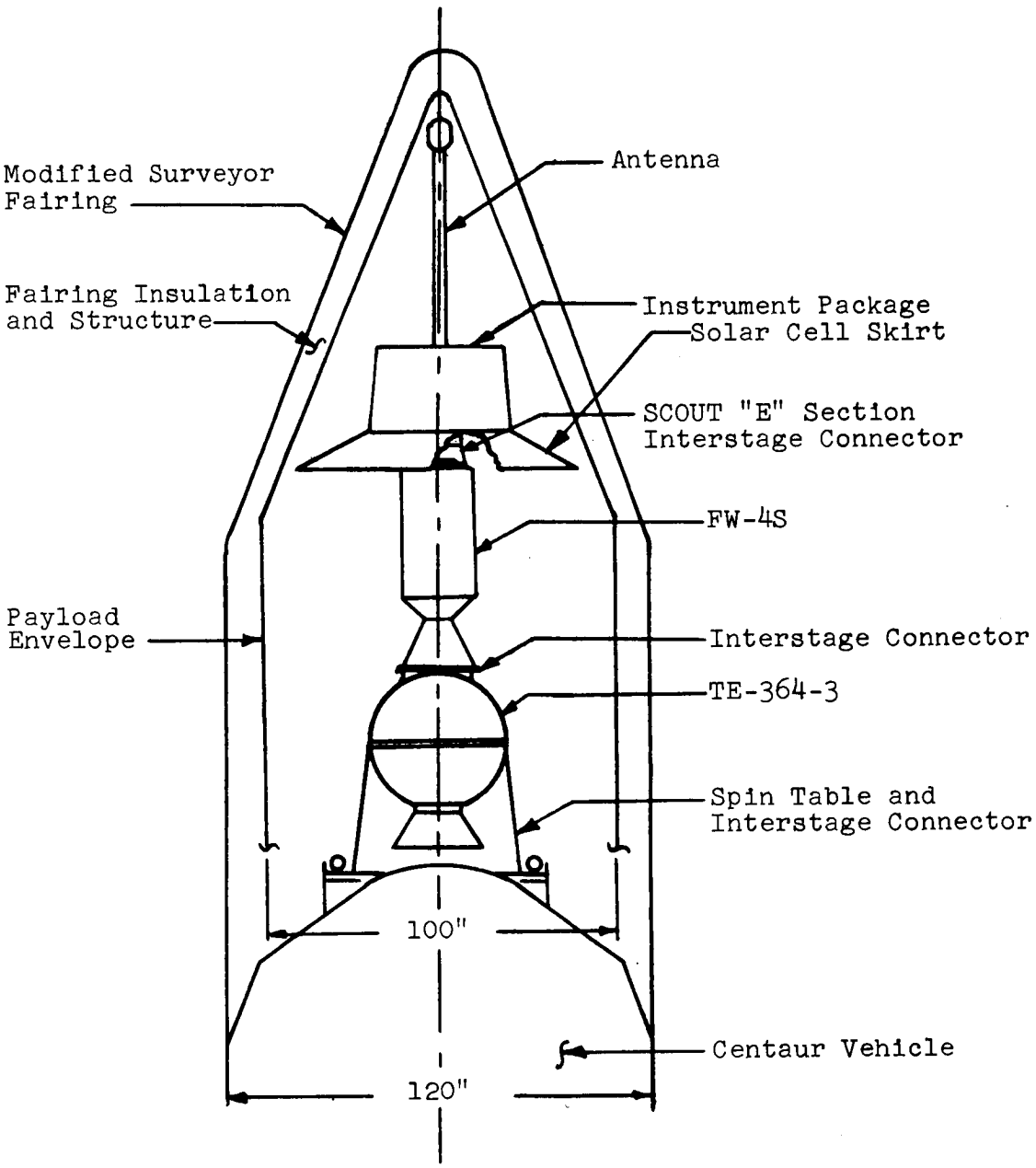

Figure 2C1.1 Upper Stage Congiguration of ICARUS

with an injection velocity of 57,500 ft/sec and a resultant perihelion of 0.17 AU in the ecliptic plane. The same booster produces a perihelion of 0.23 AU for a launch 15 degrees out of the ecliptic. Launches such as these are generally referred to as 0.2 AU missions. More powerful boosters, such as the Saturn IB, are needed for 0.1 AU launches since the corresponding injection velocity requirement is 67,1000 ft/sec.

Attitude stabilization is achieved by spinning the spacecraft at 100 rpm by means of a spin table attached to the Centaur; attitude control is obtained using a Pioneer-like gas expulsion system with the nozzle mounted on the solar cell skirt.

2D. Spacecraft

Figures 2D1.1 and 2D1.2 are sketches of ICARUS. The vehicle consists of a frustum of a cone for the body; a conical solar cell skirt attached to the larger end of the body; and an antenna on the spin axis attached to the smaller end of the body. Some characteristic dimensions are:

	MKS	FPS
Diameter, solar cell skirt	2 m	6.5 ft
Diameter, body cone, large end	1.1m	3.6 ft
Diameter, body cone, small end	1.0m	3.3 ft
Height, body cone	0.6m	2.0 ft
Height, antenna	1.3m	4.3 ft

Other parameters of interest are:

Range of operation, design	1 AU - 0.1 AU
Range of operation, ultimate (est.)	1 AU - 0.07 AU
Weight	157 lbs
Volume, instrument compartment	0.37m^3, (13 ft^3)
Electric Power, regulated	40w - 242w

The solar cell skirt cone angle depends on the perihelion of the vehicle's orbit. Perihelions of 0.2 AU and 0.1 AU have been studied in detail. The power supply will provide at least 40 watts of regulated power at injection for both missions. This increases to a minimum of 242 watts in the region of perihelion. The 242 watts first becomes available at 0.33 AU from the Sun on the 0.2 AU mission, and at 0.3 AU on the 0.1 AU mission. For the 0.2 AU mission the conical skirt will be flared at 60° from the spin axis and will have 2.8m^2 (30 ft^2) of area. For the 0.1 AU mission two conical skirts are required. The inner one will have 2.6m^2 (28 ft^2) at 70° angle from the spin axis. The outer skirt will have 0.85m^2 (9 ft^2) at 40°. The outer skirt will overheat and

permanently degrade on the first pass near the Sun. The total power available after the first pass is only that provided by the inner skirt.

Active thermal control is effected by louvers actuated by bimetal springs. These louvers are located on the outboard side of the top and bottom equipment plates. Thermal input into the louvers and the solar cell array is minimized by using correctly shaped highly specular surfaces, with low solar absorptance, on those surfaces which re-radiate to the louvers and solar cells. Heat flux through the walls is minimized by using the recently developed optical solar reflector (OSR) as the main body coating with new high-temperature aluminized plastic super-insulations. The OSR has an extremely low ratio of solar absorption to infrared emittance (α_s/ε_T = 0.06) which limits maximum outside wall temperatures to 500°K for missions to 0.1 AU. These new material applications maintain the instrument compartment at 0°C to 50°C.

The structural design of the spacecraft is dictated by thermal and power requirements as well as structural considerations. Beryllium is used where possible because of its high ratio of thermal conductivity to density (resulting in minimum temperature gradients) and high ratio of stiffness and strength to density (resulting in excellent static and dynamic structural behavior). Fiberglass reinforced plastic is used where a low thermal conductivity structure is required, such as in the outer body shell and attachment structures for the solar cell cone, the super-insulation, and the antenna. Wherever feasible, sandwich or waffle (integrally stiffened) construction is used for structural efficiency. An outstanding feature of the structural design is the solar cell construction which results in low weight and excellent heat radiation properties. The proposed structure including the solar array structure is 17.3% of the total weight of the vehicle.

2E. Communications

Data transmission from the solar probe to Earth is limited by noise as well as the large distances involved. The large loss of energy must be compensated by various combinations of RF power output, transmitting antenna gain, and receiving antenna gain. The following paragraphs summarize these aspects of the program.

The Deep Space Instrumentation Facility with no improvement in capability is considered to be available with receiving antenna gains of 53 db for 85 ft. antennas, and 61 db for the 210 ft. antenna.

The spacecraft uses a high gain (11 db) fan-beam antenna,

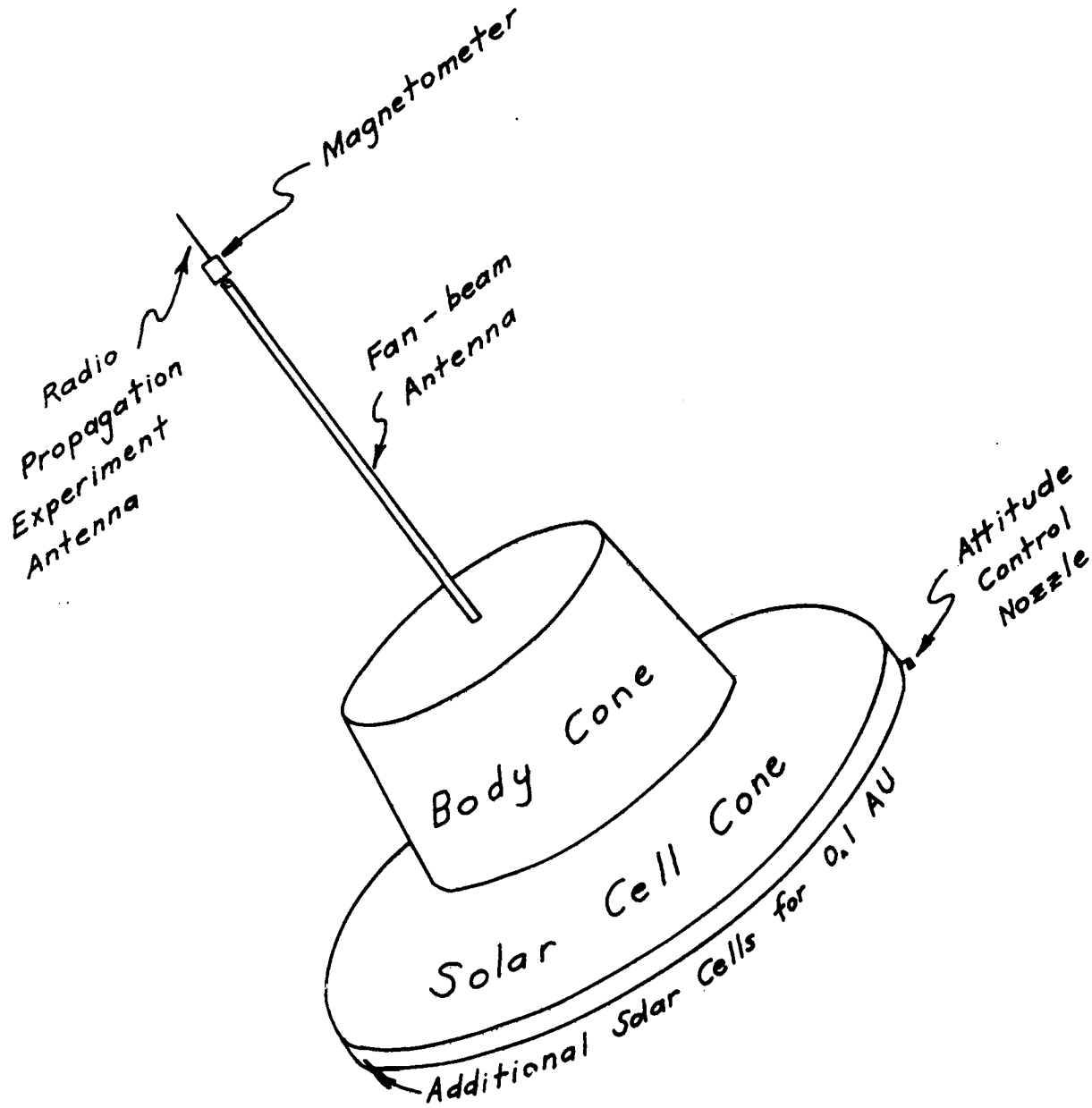

Figure 2D1.1 ICARUS -- An Artist's Conception

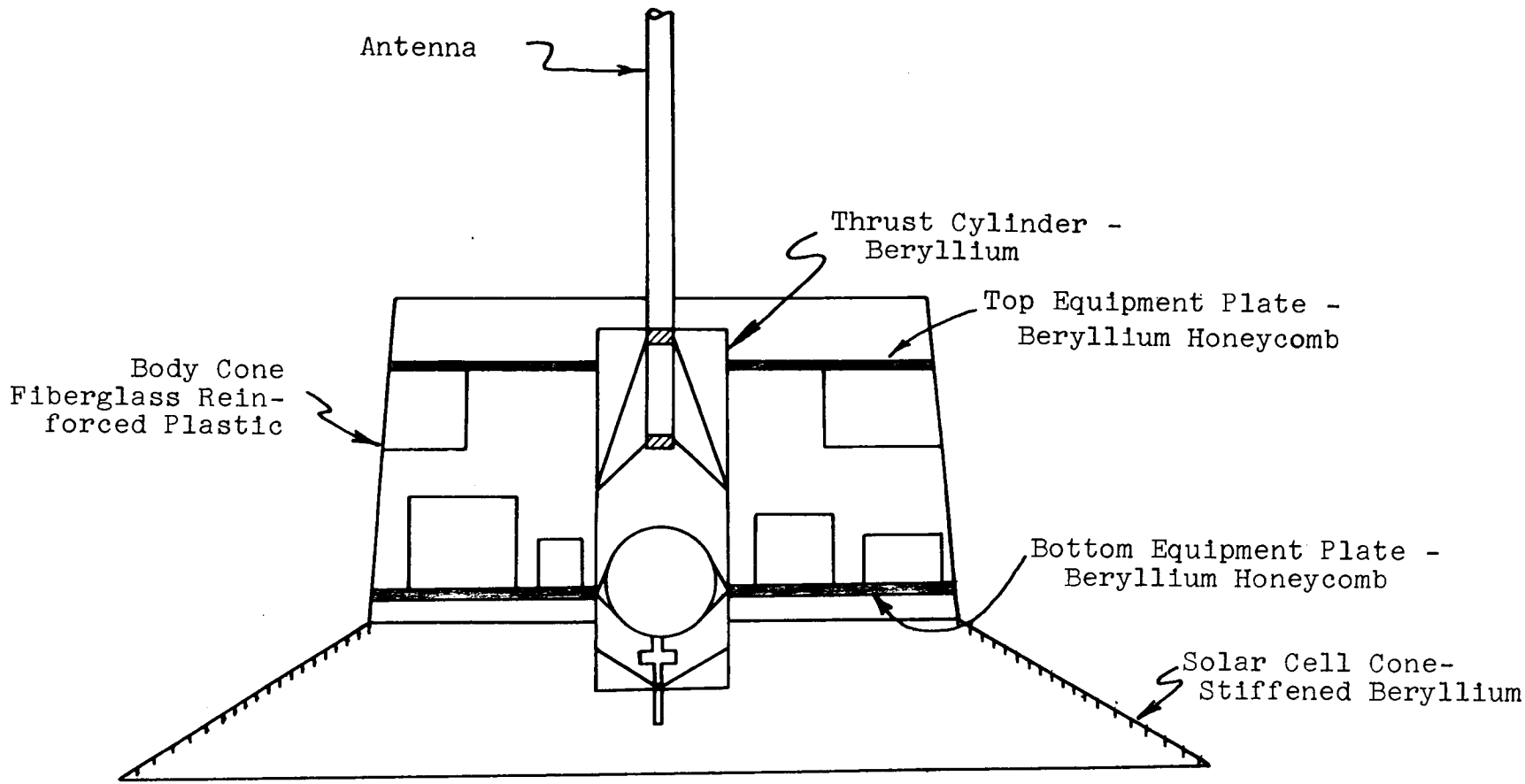

Figure 2D1.2 Basic ICARUS Structure

similar to that of Pioneer, for near-ecliptic orbits, and it uses the same antenna with a modified cone-shaped beam, obtained by phase shifting between antenna elements, for out-of-the-ecliptic orbits. The directional aspect of the beam is adjusted for optimum Earth reception when the spacecraft is in the region of greatest scientific interest.

There are three TWT power amplifiers on board capable of 3 watts, 20 watts, and 100 watts output power respectively.

The 20 watt tube can be operated at a 50 watt level. Logical switching, as a function of available solar cell energy, enables the proper amplifier. At the available power levels, and an error rate not to exceed 10^{-3}, transmission rates are obtained no lower than 64 bits per second with the 85 ft. antenna, and no lower than 500 bits per second with the 210 ft. antenna. These bit rates are available as the spacecraft goes in from 0.65 AU to 0.2 AU perihelion and out to 0.3 AU. Approximately 10% lower data rates are obtained for the 0.1 AU mission.

2F. Central Data System

The Central Data System (CDS) combines in a lightweight, efficient low-power-drain unit, the functions now being performed in many separate portions of the usual spacecraft data system. The CDS generates the time code, 16 bits, for inclusion in each data format. The master oscillator frequency of 262,144 Hz is counted down with a series of binary counter stages to provide 2048, 1024, or 512 Hz subcarriers for modulation of the radio frequency carrier. The binary counter chain provides data rates of 1024, 512, 256. 128, 64, 32, 16, 8, and 4 bits/sec. In conjunction with the Sun pulse sensor and an overflow and reset counter, the CDS formulates Sun sector identification and data sampling control pulses. The Sun sector counter provides 128, 64, 32, 16, 8 or 4 sector identification codes for each revolution of the spacecraft. Gating pulses for data sampling and readout are provided by the Sun sector counter.

Data reduction and processing, and analog to digital conversion for both the scientific and engineering data is performed by the CDS. Buffer storage has been provided to ensure the smooth flow of data or simultaneous recording of data from the experiments requiring this feature; e.g. magnetometer sensors. Data encoding in a simple convolutional code, using a 24 bit shift register and combinational logic for 1/2 rate code, and the phase shift keying of the coherent subcarrier is combined with the selected format and information bit rate. Commands sent from the ground control station are decoded and stored in the CDS. Permanenet storage of spacecraft

command and eight data formats is provided as well as subroutines for special data processing. The central data system constitutes a mass of 10 kilograms with 12 watts of electrical power required. The unit will be built using presently available integrated circuits. Bulk data storage is accomplished by transferring the information, assembled into a format ready for transmission, into a digital tape recorder (1.36 kg. and 2.7 watt). The CDS has a program memory section that can be loaded by ground command which controls the data sequencing format and bit rate for transmission.

2G. Launch Schedule

The ICARUS program is a series of orbiting solar laboratories launched into different orbits during various portions of the solar cycle. Initial launches should be phased in shortly after the Pioneer program terminates, thus the first flight will be in 1971, just past the next period of maximum sunspot activity.

The first ICARUS launched will be boosted by the Atlas/Centaur/2 Kick launch vehicle into a near ecliptic orbit, and the second one into an orbit inclined at 15°. The spacecraft solar cell skirt is set at 30° for these launces. A summary of the initial launch schedule follows:

ICARUS (Skirt Angle 30°)

Launch No.	Date	Perihelion	Ecliptic Inclination
1	Spring 1971	0.18AU	1½°
2	Fall 1971	0.23AU	15°
3	Summer 1972	0.18AU	1½°
4	Spring 1973	0.23AU	15°
	* ICARUS (Skirt Angle 20°)		
5	Fall 1973	0.09AU	3°
6	Spring 1974	0.11AU	15°

* Launches to a perihelion of 0.09 AU can be accomplished by replacing the Atlas with a Saturn IB. The decision of whether or not to use a Saturn IB booster should be made only after the 0.20 AU data is examined. The large booster cost increment, approximately $28 million more per launch, can be justified only on the basis of the scientific merit of the deeper penetration. If the decision is that perihelions of 0.09 are economically worthwhile, launches Nos. 5 and 6 should be carried out according to the schedule shown above.

III. EXPERIMENTS

3A. Scientific Objectives

3A1. Introduction

During the past several years, the United States has been conducting investigations in the various space sciences utilizing Earth satellites and deep space probes (1). The success of this program thus far is indicated by the number and significance of the discoveries (2). An objective of this program as stated by NASA is: "To produce scientific data on the space environment, the Sun, the Earth and planets, and the galaxy, using unmanned spacecraft equipped with instrumentation and telemetry to relay data to the ground. This information is essential to all utilization of space and to an understanding of the physical universe and its relation to man." A deep space probe approaching the Sun (within from 0.1 to 0.3 AU) is, therefore, a logical extension of the program outlined above. The primary goal of such a mission is to obtain a more valid understanding of the Sun and the solar system.

3A2. Description of the Sun

The Sun is a typical star which dominates the interplanetary environment throughout its solar system. Since the Sun comprises most of the material of the solar system and since it supplies the energy for the solar system, it has a material effect on the solar system. The Sun itself provides a continuous and quite variable source of plasma which flows throughout the solar system. It also affects the spatial and time distribution of the interplanetary medium. The distribution of the interplanetary dust is essentially determined by the solar gravitational and electromagnetic radiation fields. The ionization of neutral interplanetary gas occurs due to solar ultraviolet radiation and possibly from charge exchange with the solar plasma wind. A brief examination of the features of the solar surface consists of three principle layers, (a) the photosphere, (b) the chromosphere, and (c) the corona. A brief description of each follows.

The photosphere is the name given to the visible disk of the Sun. It has a black body temperature of about 6000°K (4). However, the uppermost portion of the photosphere appears to have a temperature as low as 4500°K. Scattered around the surface of the photosphere are brightened "granules." These "granules" have lifetimes of several minutes and are approximately 1000 km in diameter (4). At any one time there are about a million of these granules visible on the photosphere

and they cover about a third of the total surface of the visible area. On this surface one sees the development of centers of activity. These appear in general to be bipolar magnetic regions which are thought to be due to twisted irregular magnetic field strands, which were initially submerged below the solar surface and became twisted as a result of the differential velocities of solar rotation. The solar equator rotates with a period of 25 days, and the period lengthens at successively higher latitudes, reaching about 30 days at the poles. Having come to the surface, these centers of activity, called photospheric faculae, contain a number of sunspots. The sunspot is a darker region which has a magnetic field with a strength estimated at several thousand gauss. The darkness indicates a lower temperature, evidently due to restricted motion in the large magnetic field. The magnetic fields in the facular region surrounding the sunspots appear to be less than 100 gauss. The sunspot groups evolve in about a week from the appearance of the first spots to the maximum development and then decay again over a period of several weeks. The gas density at the photospheric surface is deduced from the light intensity to be about 10^{-8} gm/cm^3(5).

The next layer to be discussed is the chromosphere. Its boundaries are defined in terms of the optical diameter of the photosphere at one extreme, and in terms of temperature and density of neutral hydrogen atoms at the other extreme. Just above the photosphere, the chromospheric temperature begins a rapid rise from an estimated 50,000°K at 1000 km to about 1 million °K at a height of about 3500 km (5). While the height of the chromosphere-corona interface varies in both time and space, the 3500 km represents an average height of this interface above the photosphere. Photospheric faculae, which contain the sunspots, have chromospheric faculae (plages) above them which are particularly bright in the K line of singly ionized calcium and extend to dimensions of 10^5 km around the sunspots (5). The material in the chromosphere shows definite upward and downward motions although the relative amounts of each are a matter of considerable uncertainty. The vertical velocities seem to be of the order of 15 km/sec, although on the plages they appear to be about half this value due to the stronger magnetic fields in the plages which is estimated to be between 20 and 100 gauss (4). On looking more closely at the chromosphere, one sees many fine spicules or columns rising in the chromosphere, with many of them rising well up into the corona. The plage areas are seen to be simply a denser packing of spicules. It is also quite suggestive that energy transfer through the spicules accounts for the great heating of the upper chromosphere and the corona. The supergranulation on the photosphere appears to be the base of the spicules whereas no

spicules appear to arise from the normal granulation. This chromospheric network of spicules is topographically identical with a magnetic network with a field strength comparable to plage field strengths. Thus the spicules, observed as a fine mottling of the chromosphere, are the seats of the chromospheric magnetic network:

The last layer is called the corona. It is the region beyond the chromosphere starting at about 3500 km above the photosphere. The outer boundary of the corona has often been described as the outer part of the "visible" corona seen in eclipse photographs although it is probably more realistic to describe the entire interplanetary space as part of the corona. The activity in the corona is evidently very dependent on the activity in the chromosphere below it. The coronal regions above plages seem to have an increased density. A density ratio of an order of magnitude higher than the surrounding corona has been seen above plages at a height of 10^5 km. The temperature in this condensation is somewhat higher than the surrounding corona (roughly twice) and the magnetic field is about 2 to 6 gauss at 10^5 cm (6). The high temperature of the corona results most probably from a flux of acoustic energy rising through the chromosphere in the spicules. Calculations have shown that the flux of acoustic energy from a region with a magnetic field of about 50 gauss is about five to ten times greater than the flux from the quiet parts of the Sun. The acoustic energy transforms into a shock wave, dissipating its energy in the upper parts of the chromosphere and causing the increased density and heating in the corona above it.

In addition to the above layers, another item of interest is the "solar wind". The idea of the solar wind was first proposed to explain the antisolar direction of comet tails and was confirmed on Mariner II. Data from Mariner II showed large peaks in plasma current lasting for one or two days with a recurrence in the solar rotational period. These peaks are strongly correlated with terrestrial magnetic disturbances (7) and thus also, apparently, with central solar meridian passage of active solar regions (8). A theory exists (9) for the expansion of the solar plasma along a tube of flow, but the theory cannot account for the change in cross-section of the tube or its overall shape with distance from the Sun. Nevertheless, using reasonable assumptions, the theory provides conclusions for the variation with heliocentric distance of the plasma velocity and density. To obtain a complete understanding of the solar wind, more data must be obtained as to its temperature, velocity, and density and as to the distance from the Sun. Parker's model (10) of the solar wind consists of an isotropic flow of gas radially outward from the Sun. The general solar magnetic fields are dragged

out by the outblowing solar wind. Due to the rotation of the Sun, however, these magnetic fields would describe something approximating an Archimedes spiral. In addition, Parker would expect, on the basis of cosmic ray modulation data, that the magnetic spiral becomes highly disordered somewhere beyond the region of the earth's orbit. Mustel describes a rather different concept of the coronal expansion. He envisions the expansion in terms of the continuous ejection of isolated clouds of plasma with their frozen-in magnetic fields oriented at random. Mustel argues that such a random character of the magnetic fields of the solar wind is consistent with the observed radial and continuous motions from the Sun of ionized gases in comet tails. The enhanced coronal density and elevated temperature above the magnetic structure in the spicules of the chromosphere are seen as the sources of gas outflow from the Sun. Very slight increases in coronal temperature cause a great increase in mass flow. The greatest mass flow would come from the coronal condensations above the plages, since the temperatures and densities are a little higher here than above the spicules in the general chromospheric magnetic network. The gas which thus escapes from the magnetic regions of the chromosphere carries with it the magnetic field of the region. Thus the outflow of gas is seen as a conglomeration of individual gas clouds, each carrying a magnetic field. The large variations seen in the coronal occultation of radio stars are cited as evidence of this emission of elongated plasma clouds. These plasma clouds end up forming a rather amorphous group of "classical streamers", which would extend out to only 0.15 to 0.25 AU. Mustel also describes plasma emissions from faculae or young activity centers as being of a more filamentary nature. These R-rays, as he calls them, which move radially out, and tend to be wound up spiral-like at greater distances to the Sun, consist of many thinner threads which do not expand outward, presumably kept together by the magnetic fields they carry with them. These magnetic fields are probably much stronger than those carried by the "classical streamers," since they originate in the facular regions where the chromospheric magnetic fields are stronger. These R-rays can extend up to great distances from the Sun and have been postulated as identified largely with the streams of particles responsible for the 27-day recurrent geomagnetic storms. There is apparently quite a variance between Parker's and Mustel's concepts of the structure of the solar wind. According to Mustel's model, one should see intense R-rays sweeping past a spacecraft as the Sun rotates. Then as the craft reaches about 0.3 AU, one should begin to see the amorphous plasma which he describes as arising from the general magnetic structure of the chromosphere. The probability of intercepting the narrow R-rays should increase with approach to the Sun. Parker's picture shows a much more uniform wind, which decreases in velocity

with approach to the Sun. The Mariner plasma data tends to favor Parker's picture, but actually appears to be somewhat of a compromise between the two. However, the Mariner data could be equally well fitted with a model solar atmosphere that is heated isothermally to the Earth or by one which is heated only at the base of the corona. In order to disentangle these ambiguities, the mean velocity, average density and temperature of the solar wind must be known as a function of distance from the Sun. The intensity and direction of the magnetic field as a function of distance from the Sun are measurements which are also vital in the interpretation of the above theories since this acts as a memory for the distortions and variations in the solar wind. Since these quantities need to be measured as a function of distance from the Sun, a deep space probe which approaches the sun (from 0.1 to 0.3 AU) could provide much useful data.

Another item of interest is the solar "flare" which is an occasional brightening in the vicinity of a center of activity in the upper chromosphere or lower corona. The essential feature of the flare is that it has a great and suddenly acquired density (10^3 to 10^5 times greater than the surrounding region). It appears as many thin knots and threads having thicknesses of about 10 km (6). The flare seems to arise when two bipolar spot groups approach each other. The magnetic energy density due to these groups in the high chromospheric region far exceeds the kinetic energy of the plasma, so that the approaching magnetic fields greatly condense the plasma. This eventually reaches a point where instabilities occur, causing some sort of sudden collapse of the plasma and the subsequent optical flare. The mechanism of energy emission is not well understood. It is very important to the understanding of solar flares to know something about the particle composition and energy spectrum of the particles emitted. These factors are very largely unknown from measurements made at 1 AU by the poorly understood propagation history of the particles. Since one cannot predict when a solar flare will occur, it is not correct to discuss planning of vehicle position for the most significant observation of flare phenomena. A deep space probe which approaches the Sun (from 0.1 to 0.3 AU) could provide useful data on the solar flare phenomena if these flares were to occur when the space probe was in close proximity to the Sun.

3A3. Scientific Objectives of the Solar Probe Mission

It would be of considerable advantage, from the scientific standpoint, to observe the Sun and its space environment from vantage points nearer to the Sun than the orbit of the Earth. For such locations nearer the Sun, one would obtain

a better physical understanding of the Sun and its environment. That is, the nature of solar phenomena is such that an observer at Earth is not capable of detecting all that transpires on or near the Sun. In particular, magnetic field configurations near the Sun may change markedly with little or no detectable change at the orbit of Earth. Moreover, clouds of solar plasma may be ejected from the Sun in connection with many flares, or other solar phenomena. Such effects may not produce a measurable effect at the orbit of Earth. In addition, an observer at Earth can make only very restricted observations of such phenomena as occur in the solar wind. Finally, the influence of the magnetic field and atmosphere of the Earth are negligibly small for a solar probe near the Sun. Experimental investigations of the solar magnetic field, in addition to yielding information regarding the interplanetary medium and charged particle propagation, offer a distinct possibility for adding to knowledge of the Sun itself. An understanding of the structure of the solar magnetic field nearer the Sun would aid in an understanding of the corona and its change in structure with the solar cycle. Neutrons, which are suspected as part of the solar flare emissions, can be detected by an experiment on the probe. A great advantage is gained by going closer to the Sun, since the neutron half-life is short compared to the time required for it to travel to the Earth from the Sun.

In view of the fact that no space probe has as yet approached the vicinity of the Sun, it is expected that the first mission(s) will be launched essentially in the plane of the ecliptic. That is, the trajectory of the solar probe will lie in the plane formed by the orbit of the Earth. It is also to be expected that later launches of the solar probe will have trajectory planes which are inclined to the plane of Earth's orbit. Such trajectories are of considerable scientific interest. In particular, mapping the magnetic field may yield much information about the structure of the magnetic field of the Sun. Such information will aid in the understanding of the corona and its change in structure with the solar cycle. The particle detection experiments will also yield much information about solar flares and solar flare emissions. Thus, it can be concluded that the probe travelling in the ecliptic trajectory will yield new information. Moreover, the out-of-the-ecliptic trajectory may yield useful information regarding the symmetry or asymmetry of the Sun.

As space research progresses, a comprehensive understanding of the Earth-Sun relation and of the solar system is emerging. Considering the past surprise discoveries, such as the Van Allen radiation belt, it would be somewhat

presumptuous to try to predict the more important future findings. At this time, however, it can be stated with some confidence which of the several scientific experiments will probably yield the more important information in the near future using the solar probe described herein. These more important experiments are outlined in the next section.

To summarize the preceding sections, it may be concluded that by employing suitable experiments on board a deep space probe, scientific contributions of some scientific merit could be expected in the following areas:

a) the structure of the magnetic field in space and near the Sun
b) particles and galactic cosmic rays
c) the solar wind near the Sun
d) the plasma clouds
e) the electron density over long paths
f) the possibility of solar magnetic field line detachments
g) the solar cycle
h) the size distribution of micrometeoroids
i) the asymmetry of the above properties

This knowledge, in turn, will lead to a new insight into the structure of the universe and permit the evolution of more realistic cosmological models.

3A4. Experiments Considered for the Advanced Solar Probe

The summary of the experiments considered for the advanced solar probe is listed in the table below. The table names the several experiments, states their objective, and describes very briefly their function. In addition, the scientific merit of each experiment is listed, based upon the majority opinion of the six members of the Experiments Group of the Stanford University NASA Program in Space Systems Engineering. Finally, the relative observation advantage for a mission near the Sun is stated. The experiments selected for installation on the solar probe are those of scientific merit of 1 and z. This selection was based upon a weight estimate for the total space craft. The experiments selected are described in more detail in the next section.

Table 3AI Summary of Experiments Considered

Name	Objective	Function	Merit	Orbit Advantage
Fluxgate Magnetometer	Investigate Magnetic phenomena in space	Measure three components of the ambient magnetic field	1	Place as near the sun as possible - continuou measurement all the way
Plasma Probe	Investigate energy spectrum and angular distribution of solar plasma	Measure energy and direction of low energy charged particles	1	" "
Cosmic Ray	Investigate the heliocentric radial gradients of proton and alpha particle intensities	Measure high energy protons and alpha particles	1	" "
Neutron Counter	Investigate solar flare phenomena	Measure neutron and charged particle spectra	2	" "
Dual Frequency VHF Radio Propagation	Investigate electron density between earth and probe and time variations	Measure phase difference of UHF and VHF signals	2	" "
VHF Propagation	Investigate coronal electron density	Measure coronal electron density	3	Must be near and behind Sun
Rubidium Vapor Magnetometer	Investigate magnetic phenomena in space	Measure total magnetic field	4	Same as fluxgate
Micrometeoroid Detection	Investigate origin and the distribution of micrometeoroids	Measure Impact of particles	4	
Solar Flare Monitor	Investigate Solar flare activity	Measure X-rays (1 to 0.1 Å)	4	
Mass Specrometer	Investigate species of the interplanetary gas	Measure the mass number of the interplanetary gas	4	
White Light Corona Meter	Investigate coronal light	Measure intensity and polarization of light scattered by coronal electrons	4	

3B. Description of Experiments

3B1. Introduction

The primary purpose of a space probe is the transportation of scientific instruments into regions of space that are otherwise inaccessible. A deep space probe is one such that it permits instruments to be placed near the Sun. There are several important considerations for selection of instruments in addition to their scientific merit. They are as follows: size, weight, power requirements, and a qualitative factor, reliability. Space instruments in general resemble those made for Earth applications except that they are reduced in size, weight, and power requirements. In addition, they are in general better constructed, for they must withstand a more hazardous environment. In the final competition for payload space, the desirability of an experiment is measured by its scientific merit, the availability of proven instruments, and the ease of spacecraft integration. It was on these criteria that the final selection was made. The instruments selected for installation are described in the next section.

In addition to the requirements listed for each of the instruments, a general requirement may be listed regarding the attitude of the probe. This attitude requirement is necessary for reducing the complexity of data reduction. The attitude of the probe should be controlled within $\pm 5^{\circ}$, and the attitude should be known within $\pm 1^{\circ}$. Another general requirement for the instruments is a method of scanning. Two of the instruments selected have been developed using a spinning vehicle or a spinning coordinate system as a method for scanning. Therefore, the method of scanning for the ICARUS instruments involves spinning the spacecraft. The angular speed was selected to be between 90 and 100 rpm.

3B2. Fluxgate Magnetometer

In comparing the fields measured by spacecraft magnetometers with those customarily recorded by Earth-based and satellite instruments, one distinction stands out: probe magnetometers must measure fields of from 1 to possibly 100 gamma compared to the 50,000 gamma at the Earth's surface (11). It should be pointed out that the field in space can easily be overwhelmed by the magnetic field of the spacecraft if great care is not taken. Moreover, the magnetometer calibration (12) may drift a few gammas and grossly incorrect data will be telemetered. From the viewpoint of the magnetometer designer, the most sensitive spacecraft interface is undeniably magnetic in character. To avoid submerging the ambient field in that of the spacecraft, non-magnetic materials must be used in space craft construction and current-generated

fields should be canceled by opposing currents. Careful design can push the spacecraft fields down below one gamma as it did on the Pioneer 6 and IMP (13, 14).

The adjective "fluxgate" is derived from a key physical feature of this magnetometer: the "gating" of the ambient field being measured. Consider the two long ferromagnetic cylinders shown in Fig. 3B1. Two external fields are applied to each: H_1, the field being measured; and $H_o \sin\omega t$, an alternating gating field impressed by the primary winding around the cylinders. Inside the cylinders, the total impressed field is $H = H_o \sin\omega t + H_1$. The magnetic induction, found from $B = \mu\mu_o H$, is modified by the saturability of the ferromagnetic core. During the peaks of the gating field, the cylinder cores are saturated at $\pm B_o$, and the ambient field is gated. In between the peaks, the induction is $B = \mu\mu_o(H \pm H_1)$ as shown in Fig. 3B1. The presence of the ambient field, H_1 thus introduces an asymmetry into the induction cycle. It is this asymmetry that provides the measure of the ambient field, and the asymmetry appears only in the presence of the gating field. If the total induction is expanded in a Fourier series,

$$B = a_o + \Sigma a_n \cos n\omega t + \Sigma b_n \sin n\omega t$$

it can be shown that the source of the asymmetry, the ambient field, is also the source of the even harmonics in the expansion. The logic of the coil arrangement shown in Fig. 3B1 is now apparent. The oppositely wound primaries impress a gating signal at a frequency X. The output secondary coil is wound around both cores and feeds a filter, which passes only the second harmonic, frequency 2X. The fundamental and all its odd harmonics are canceled out by the stratagem of winding the primaries in opposite directions. The magnetometer circuit shown in Fig. 3B1 is of the open-loop type; that is, there is no feedback of the output signal. Its output is an analog signal whose amplitude is proportional to the ambient field. A fluxgate can be sensitive to a tenth of a gamma and can span the range up to thousands of gammas. In order to reduce the space craft field to about one gamma, the magnetometer must be mounted on a boom about a meter long.

Specifications

	Inboard electronics	Outboard sensor
Size	6.6 cm long by 28 cm wide by 16 cm high	cylinder 10 cm OD x 16 cm long

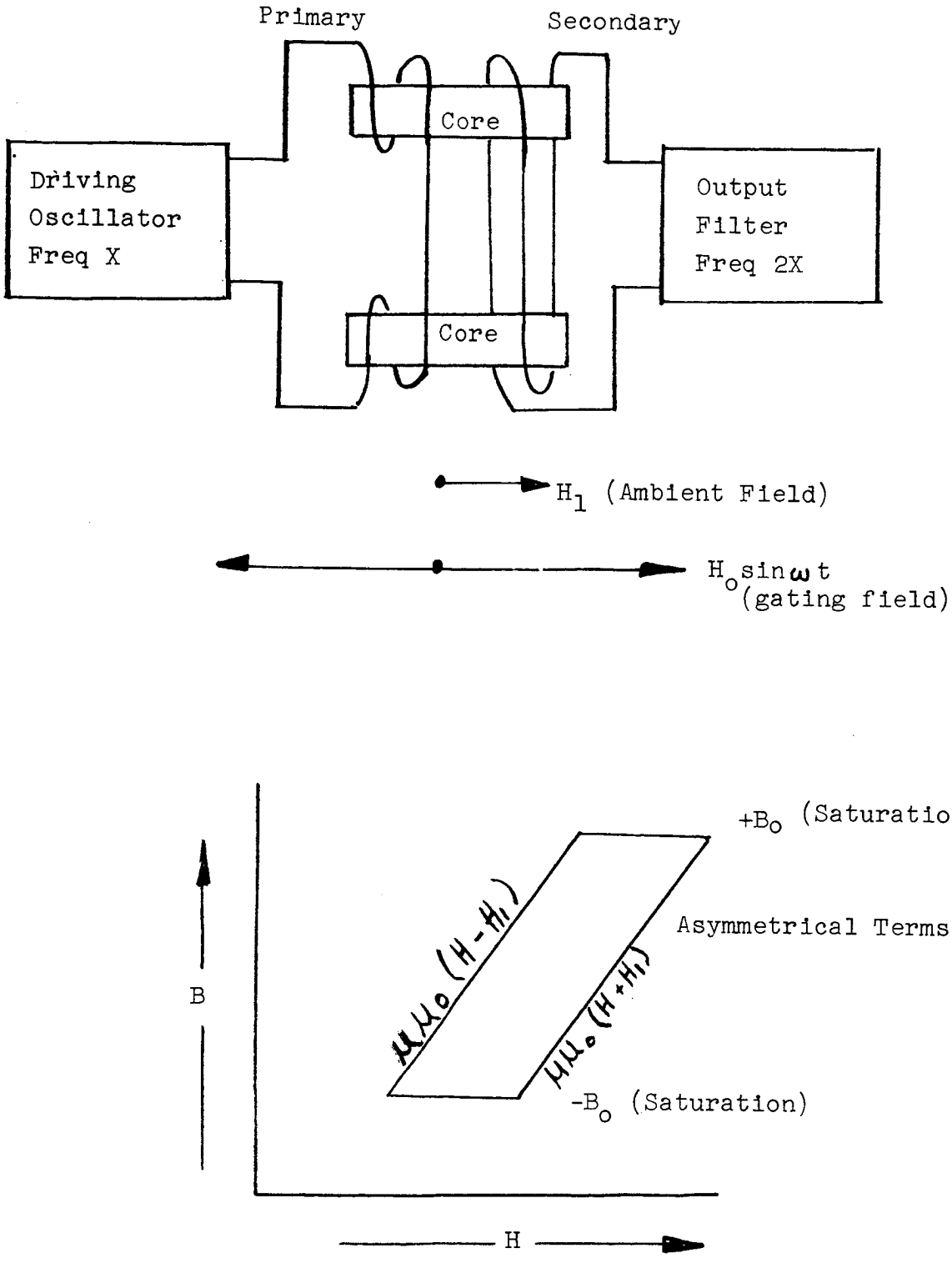

Figure 3B1 Fluxgate Magnetometer

Specifications (continued)

	Inboard electronics	Outboard sensor
Power	3.5 watts	3.5 watts for ten minutes during calibration
Window	none	none
Temperature		
high	390 K	370 K absolute upper limit
low	270 K	270 K
Weight	2.27 kg	0.34 kg
	(cable between electronics and sensor 0.17 kg/m)	
View	none	none

3B3. Plasma Probe

The energies, direction, and scalar fluxes making up the interplanetary plasma can be partly sorted out by electrostatic analyzers (15). There is a superficial resemblance between this instrument and the better-known mass spectrometer. While the mass spectrometer separates a monoenergetic beam of charged particles into groups with different mass-to-charge ratios by means of a magnetic field, the electrostatic analyzer splits a flux of charged particles into equal energy-to-charge ratio groups with an electric field. The functions of the two instruments are actually complementary. The use of both together would provide both mass and energy discrimination, leading to unequivocal analysis of plasma fluxes. Figure 3B2 is a block diagram of the Electrostatic Analyzer. A positively charged particle entering the space between the plates will be pulled downward by a negative voltage on the lower plate. If the plates were flat, the particle would quickly impact and be neutralized. Their curvature, however, permits particles with a certain energy-to-charge ratio to travel circular trajectories and reach a detector located at the other ends of the plates. Particles entering the space between the plates with energy-charge ratios substantially different from that dictated by the dimensions and applied voltage of the analyzer will collide with the walls and not be detected. There is, of course, a small energy range of particles which will just clear the rims of the plates and be detected. The same is true for particles not aligned with the particle beam shown in Fig. 3B2, so that there is a fan of flux that will be accepted and

detected. The acceptance angle in the aximuthal plane may be nearly 180 degrees for instruments like that shown in the above figure. At a fixed voltage, the analyzer acts as a narrow energy-to-charge ratio filter. Voltage stepping allows it to sample different portions of the energy spectrum with time. By synchronizing the detector readings with the voltage steps, energy groups like those shown in Fig. 3B3 can be distinguished by electrostatic analyzers. Charges of both signs can be analyzed by reversing the polarity of the plates during the stepping process. If the incident plasma flux consists of predominantly protons and electrons, the analysis is quite simple. If alpha particles are present, for example, they will be indistinguishable from protons with the same energy-to-charge ratio. This ambiguity can be resolved only with further separation by a magnetic field.

Specifications

Size	25 cm long by 25 cm wide by 25 cm high
Power	1 watt
Window	4 cm^2
Temperature	390 K to 270 K
Weight	2 kg
View	$\pm$ 50 degrees meridional plane $\pm$ 30 degrees equatorial plane

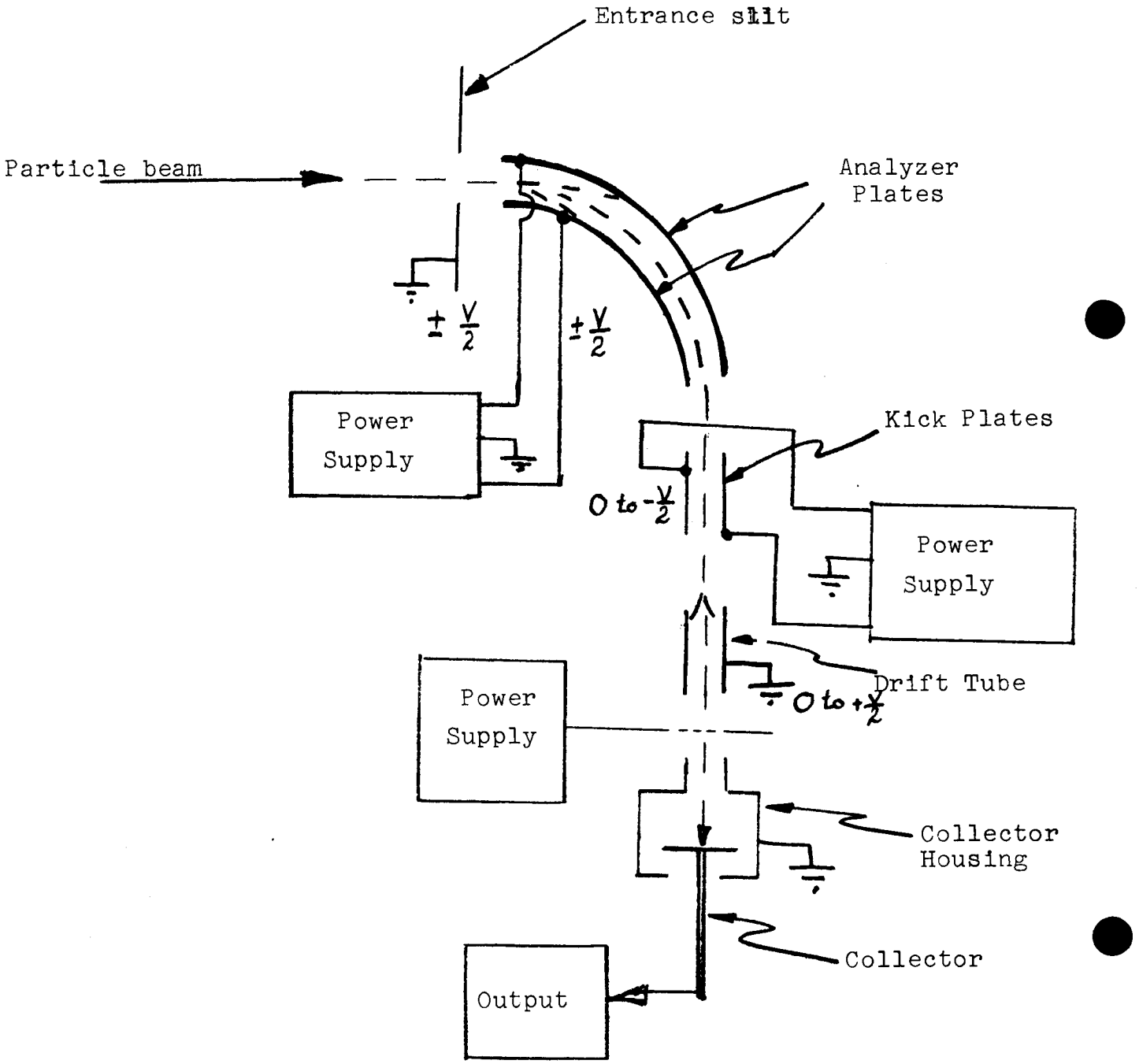

Figure 3B2 Electrostatic Analyzer

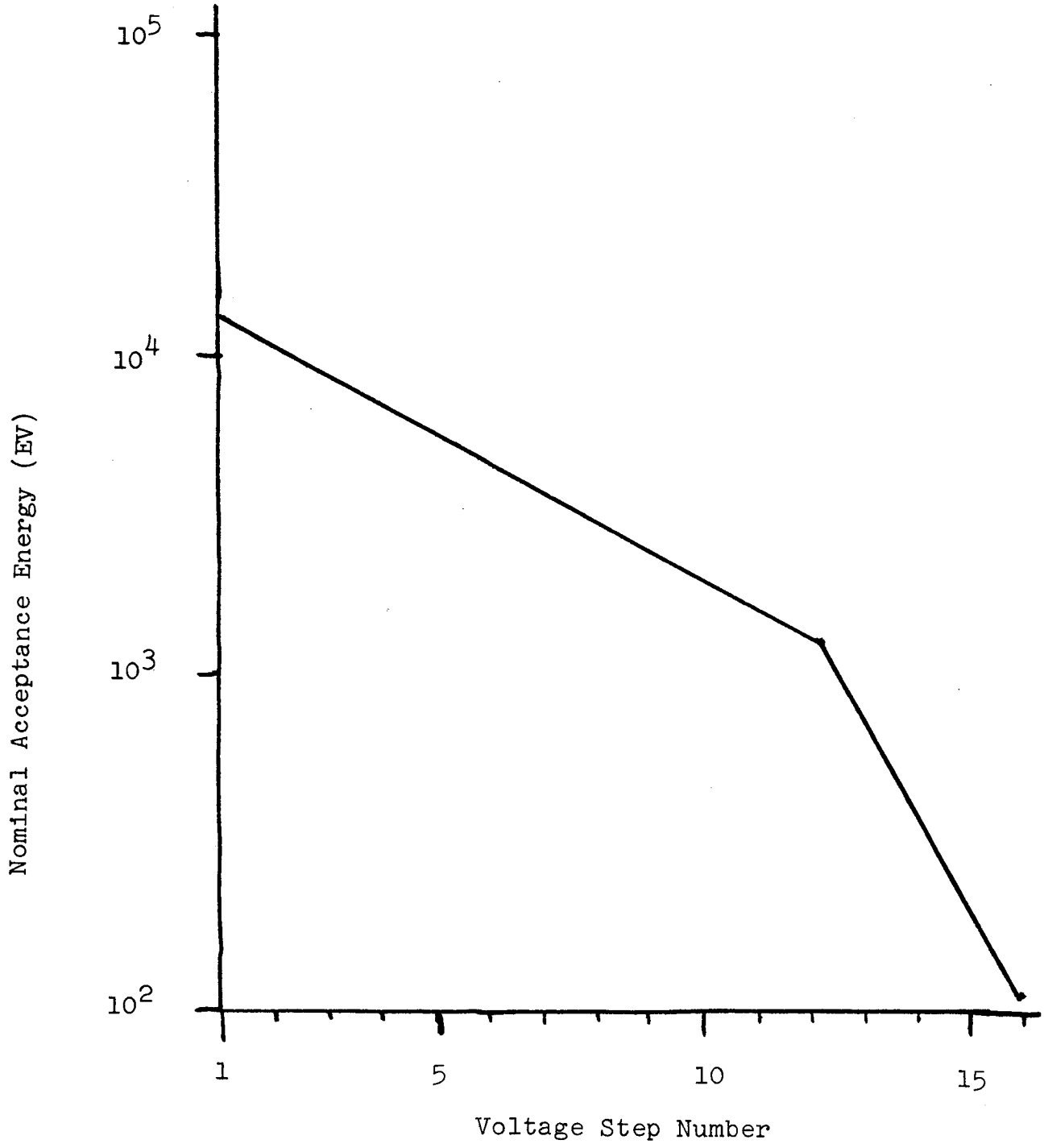

Figure 3B3 Energy Scanning

3B4. Cosmic Ray

The cosmic ray detector is a form of a radiation telescope. Different types of radiation telescopes can be distinguished by their special geometrical and/or electrical arrangement of two or more detectors. A radiation telescope will resolve particle energies and directions, but it will not magnify anything. The energies of charged particles can be measured either by a detector whose output is proportional to the energy lost in passage by the ionizing particles or by linear stacks of detectors which signal the depth of penetration of a particle into the stack. Depth of penetration is related to energy. To measure total particle energy by the pulse-height analysis method, the particle has to be completely stopped in one of the detectors. Assurance that this occurs must be provided by a guard detector in anti-coincidence, which discards particles that completely penetrate the internal detectors. Detector anisotropy can obviously be used to measure direction by scanning space with its open or sensitive area if attitude data are available. It is important to realize that a telescope's anisotropy, in both energy and direction, may be due to either the geometrical stacking of detectors or the electrical selectivity of coincidence and anticonicidence circuitry of an otherwise isotropic group of detectors. A block diagram of a cosmic ray telescope is shown in Fig. 3B4, and it has three surface barrier detectors shown as D_1, D_2, and D_3. Each detector produces an electrical pulse with an amplitude proportional to the energy lost in the barrier region by the impinging charged particle. The detectors are connected through separate amplifiers to five pulse-height discriminators. The discriminator D_3' passes pulses representing energy losses of 400 kev or more. The four other discriminators are set with their lower limits at 180 kev. In addition, the discriminator D_1 is connected to a height-to-time converter, which sorts pulses into 128 channels between 180 kev and 5.2 mev. The coincidence-anticoincidence logic provides output signals when the following events occur: $D_1'\bar{D}_2$; $D_1'D_2\bar{D}_3$; and $D_1'D_2D_3$ where the null bar indicates anticoincidence. When the absorbers placed between the detectors are taken into account, the energy ranges represented by these three events are:

Energy Range of Primary Particles (mev)

Event	Protons	Alphas	Electrons
$D_1'\bar{D}_2$	0.80 to 15	2 to 60	0.18 to 0.35
$D_1'D_2\bar{D}_3$	15 to 80	60 to 320	no sensitivity
$D_1'D_2D_3$	90 to 190	320 to infinity	no sensitivity

The small alpha source shown adjacent to each of the detectors in the above figure provides coincidence-noncoincidence calibrating pulses at a constant rate.

Specifications

Size	25 cm long by 25 cm wide by 25 cm high
Power	1.5 watts
Window	2.5 cm^2
Temperature	390 K to 270 K
Weight	2.0 kg
View	$\pm$ 30° unobstructed view

3B5. Neutron Experiment

The aim of this experiment is to measure the flux and energy spectrum of solar neutrons in the energy range between 1 and 20 Mev. The presence of other radiation, primarily the high energy protons, causes some difficulty in distinguishing the neutrons from the other ionizing radiation. This can be overcome by the use of a "phoswich". The basic theory of the phoswich is described below.

The phoswich counter (16) selected uses four lithium-iodide scintillators, surrounded by a plastic guard scintillator. The lithium-iodide crystals are made neutron-sensitive by using lithium enriched with Li^6 isotope, which has a high cross section for the neutron-alpha reaction. The pulses triggered by these alphas give a measure of the number and energy of the primary neutrons. The proton interference is eliminated in the following manner. A shield over the sensor of 3 gm/cm^2 of aluminum is used to limit the incoming protons to those having energy greater than 50 Mev. This will decrease the number of neutrons by about 10%, but this can be corrected for by ground processing. The plastic guard scintillator, connected in anti-coincidence, produces a pulse every time a charged particle penetrates its active volume. By discarding all the coincident pulses from both the detectors, only neutron counts remain.

An additional factor to be considered is gamma rays over the energy range of 0.5 Mev to 2 Mev. These are identified primarily through the Compton scattered electrons absorbed in the plastic. These are distinguished from neutrons by

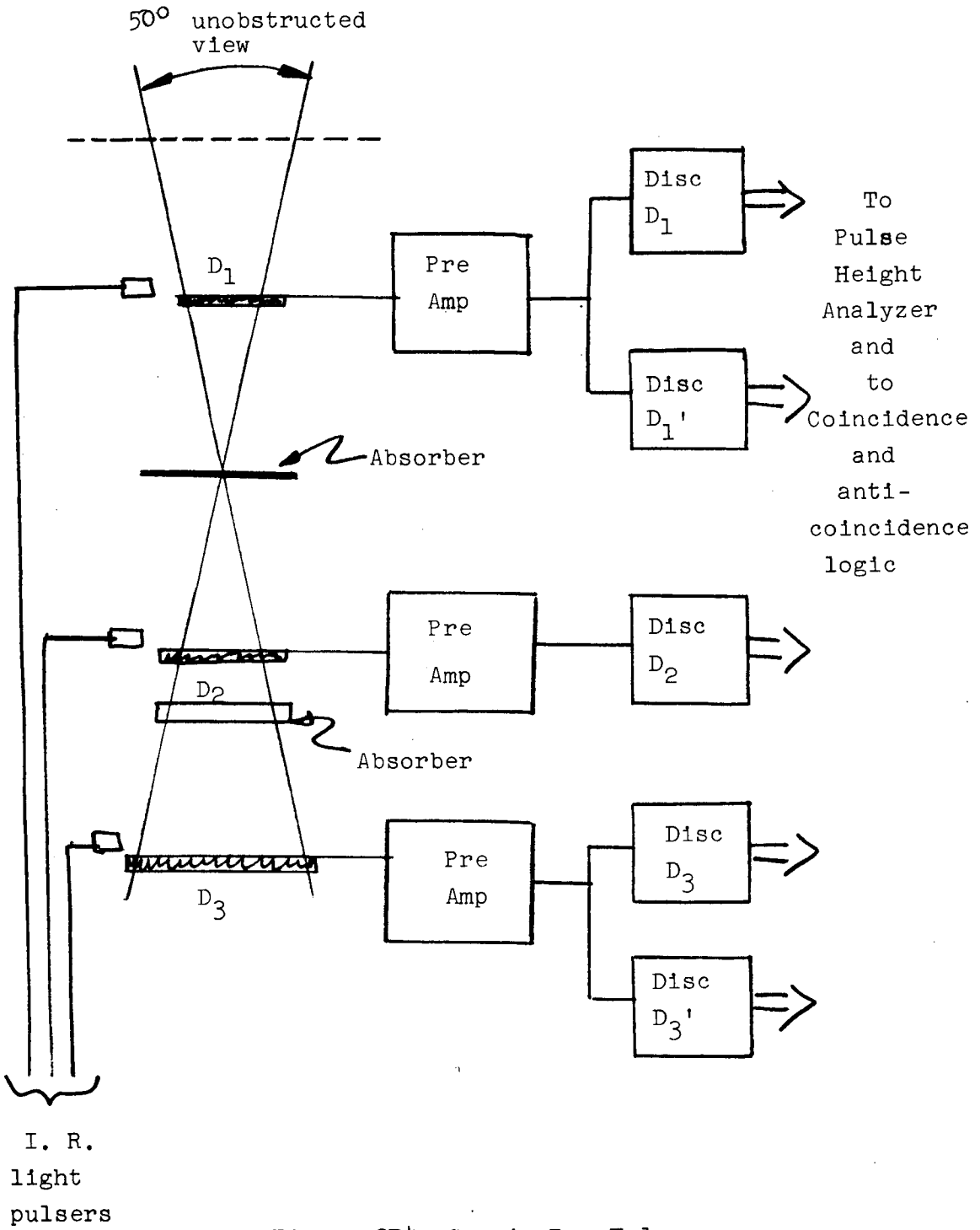

Figure 3B4 Cosmic Ray Telescope

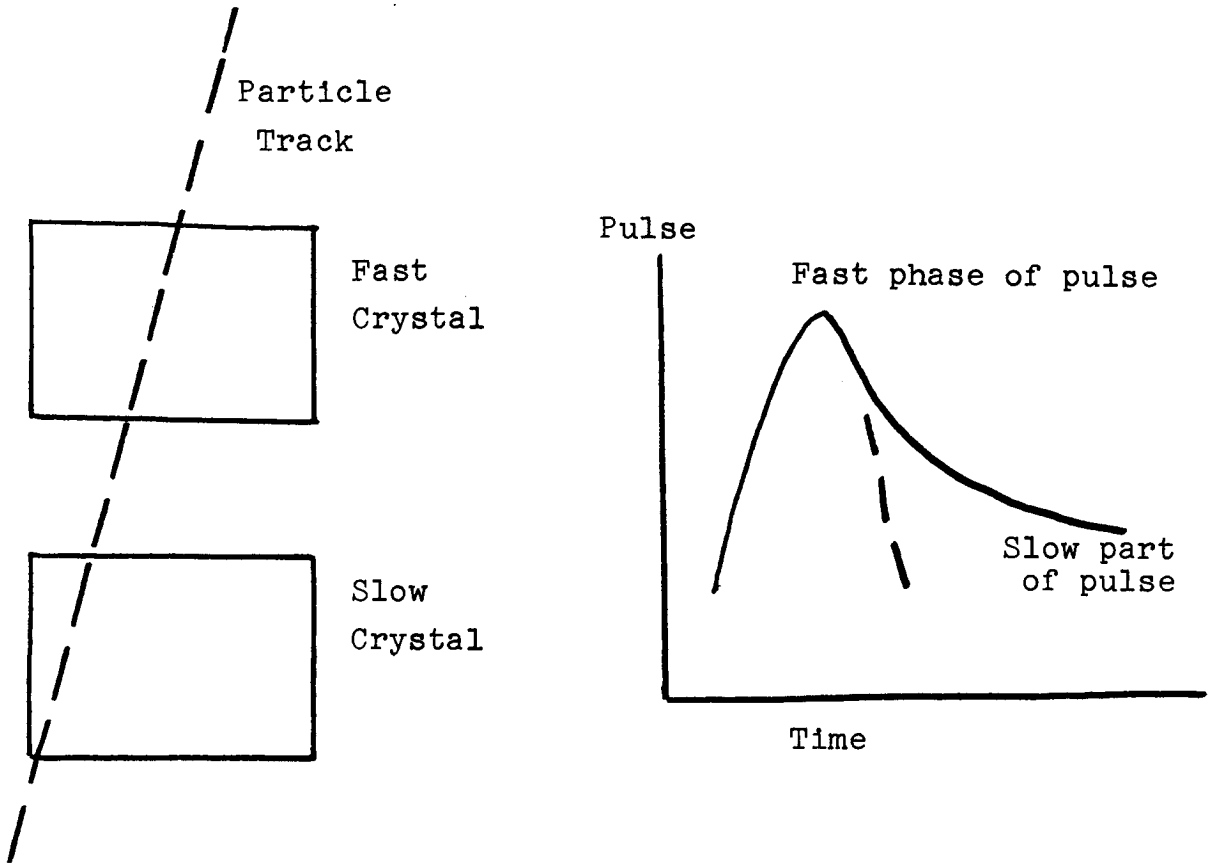

Figure 3B5 Neutron Counter

the fact that the ionizing proton produced in the neutron decay has a greater number of slow component than the Compton scattered electrons, see Fig. 3B5.

The instrument should be capable of detecting fluxes as high as 5×10^3 particle/cm^2/sec of neutrons of energy between 1 - 20 Mev. An omnidirectional sensor is desired for this measurement. This sensor should view the Sun at all times. Solar aspect referenced multiple sensors are required on the spin-stabilized spacecraft.

Specifications

	Out board (window)	In board
Size cylinders	35 cm long x 18 cm OD	35 cm long x 18 cm OD
Power	3.5 watts both	---
Window	4 cm^2	
Temperature	390°K to 270°K	
Weight	3.3 kg	1.1 kg
View	60° unobstructed	

3B6. Dual frequency VHF Radio Propagation Experiment

The radio propagation experiment provides a means of measuring the integrated electron density from a spacecraft to a ground based termainal station. This measurement is implemented by transmitting from the ground station two modulated, coherent radio frequency carriers, receiving the signals on the spacecraft and determining the relative phase and group velocity of the two radio waves. The measurements of the relative phase and group velocity are transmitted back to Earth by the spacecraft telemetry system.

Signal strength and conditions of phase-lock loop are also transmitted to Earth. The two radio frequency signals are chosen such that the higher frequency will be relatively unaffected by the ionization along the raypath and the lower frequency, although shifted in phase, must follow substantially the same ray path to the receiver. In a space probe mission 0.6 to 0.8 AU from the Sun the frequencies chosen have been approximately 50 and 400 mc/s. For a mission close in to the Sun (0.2 AU) the higher ionization density would cause a

50 mc/s radio wave to follow a substantially different ray path than the 400 mc/s radio wave. 200 mc/s and 400 mc/s will be provided as the operating frequencies for this space probe mission. The antenna on board the spacecraft for receiving the signals could be a simple whip antenna extending from the end of the communication antenna.

The radio propagation experiment, although providing data on the total integrated electron density along the ray path from the spacecraft to ground and indicating any change in this value of ionization, does not provide any information of the location of an increase in the ionization along the ray path. If a radio wave coherent with the radio signal received on the spacecraft were retransmitted back to Earth a time correlation study could be performed by a computer relating the recorded effect of an ionization "blob" on the down-path radio wave intensity and the delayed effect by this same "blob" on the up-path radio wave intensity as retransmitted back to earth from the spacecraft. Such a system would require an additional transmitter and a medium gain antenna on the spacecraft or the combining of this experiment with the existing telemetry system. The latter method would complicate the operation of the "Deep Space Instrumentation Facility". The additional weight and power required for implementing this valuable extension of the radio propagation experiment by separate transmitter and antenna on board the spacecraft suggests that the system should be considered for inclusion at a later time with the telemetry transmitter system and integrated with the Deep Space Instrument Facility.

Specifications

Main Instrument Package

Weight	4 lbs (2kg)
Power	2 watts
Volume	144 in^3 (225 cm^3)

REFERENCES

1. Ludwig, G. H.: The NASA Program for Particles and Fields Research in Space, NASA TND-1173, April, 1962.
2. Hess, W., Mead, G., and Nakada, M. P.: Significant Achievements in Particles and Fields, 1958 - 1964, NASA SP-97, 1966.
3. NASA - Industry Program Plans Conference, Goddard Space Flight Center, July 28-29, 1960.
4. deMoraes, C. A., and Gage, D.D.: Mission Objectives and Design Considerations for a Scientific Solar Probe, AIAA Publication CP-12, Unmanned Space Craft Meeting, pp 413-442, March 1965.
5. Solar Probe Study, Final Report, ER 13110, The Martin Company, August, 1963.
6. Solar Probe Study, Technical Report WDL-TR 2133, The Philco Corporation, August, 1963.
7. Nazarova, T. N.: Meteroric Matter Along the Trajectory of the Mars I Probe Flight, 1963 COSPAR Symposium, Warsaw, Poland.
8. Snyder, C.: Direct Measurements of Solar Plasma, Symposium on Plasma Space Science, Catholic University.
9. Kuiper, G.: The Sun, University of Chicago Press.
10. Parker, E.N.: Astrophysical Journal, vol. 128, p. 664, 1958.
11. Corliss, W.: Space Probes and Planetary Exploration, D. Van Nostrand, New York, p. 296, 1965.
12. Sonett, C.P.: Modulation and Sampling of Hydromagnetic Radiation, NASA TN D-2950, Oct., 1965.
13. Stambler, I.: Interplanetary Probes, Space/Aeronautics, vol. 42, p. 36, 1964.
14. Ludwig, G.H.: The NASA Program for Particles and Fields Research in Space, NASA TN D-1173, April, 1962.
15. Bader, M., Fryer, T.B., and Witteborn, F.C.: Two Instruments for Measuring Distributions of Low-Energy Charged Particles in Space, NASA TN D-1035, July, 1961.
16. Smith, R.V., Reagan, J.B., and Alber, R.A.: Use of Scintillation Detectors for Space Radiation Measurements, IRE Transactions, vol. NS-9, p. 386, June, 1962.

IV. DATA HANDLING AND COMMUNICATIONS

4A. Data Handling

4A1. Introduction

The purpose of the solar probe is to collect data in the vicinity of the Sun and transmit this information to Earth. The outputs of the experiment sensors are either analog waveforms or counter readings. Hence, the down link (spacecraft to earth) communication system must be capable of reproducing at the ground station waveforms that resemble the waveforms appearing at the sensor outputs. Along with this "experiement" data, certain "engineering" data such as spacecraft temperature, power supply voltage, etc. must also be transmitted to the ground terminal. The purpose of the on board data processing and communication system is to transmit these data in some orderly fashion to the ground terminal.

Both "analog" systems and "digital" communication systems were considered. Of the analog modulation methods available, some form of frequency or phase modulation is most suitable because of the relatively straight forward exchange of bandwidth for signal-to-noise ratio permitted by these techniques. Of the digital modulation methods available, some form of pulse code modulation is most suitable, again because of the ease of trading bandwidth for signal-to-noise ratio, and for a number of other reasons discussed in the following paragraphs.

A digital system was chosen for this mission because of the significantly greater degree of flexibility it allows. For example, the five experiments provide more than 25 analog (waveforms) and digital (counter reading) outputs, all of which, along with some 50 engineering measurements, must be transmitted to the ground terminal. The problem of multiplexing these data is significantly easier to solve using digital techniques. Furthermore, digital techniques permit the use of a single on board "central data processor" (described in section 4A2) capable of performing a variety of operations on these data.

A digital system does, however, involve a few inherent problems that must be considered. First, consider the problem of transmitting a single sensor output to the ground terminal. Let $x(t)$ represent the amplitude of the sensor output over the time interval $(0,T)$ and, $z(t)$ represent the reconstructed waveform at the ground terminal. Ideally, we would like for $z(t)$ to be identical to $x(t)$, but this is not possible because of three inherent sources of system errors.

The first error is due to the analog-to-digital conversion process. Most systems time sample the analog waveform. Unfortunately, most waveforms cannot be precisely represented by a finite number of time samples. Besides this theoretical error, various equipment errors enter in. For example, to accurately reconstruct a waveform from a set of time samples requires an ideal low pass filter which can only be approximated with practical equipment. Although these errors could undoubtedly be reduced by resorting to a sampling technique other than time samples very little is known about this area, and present day technology requires that we too resort to time samples.

A second source of error in digital systems is due to quantization error and is sometimes referred to as quantization noise. Quantization error is simply the round-off error due to replacing the actual sample value with one of a number of preset discrete levels. This error can, of course, be decreased by increasing the number of quantization levels, but this, unfortunately, increases the magnitude of the third type of error.

The third source of error in digital communication systems is the communication channel between the spacecraft transmitter and the ground-based detector. System noise results in some detection errors, and these bit errors result in errors in the reproduced waveform. The bit error rate can be decreased by increasing the energy per bit transmitted. However, this can only be accomplished (under an average transmitter power constraint and a given receiver noise temperature) by increasing the bit duration. Unfortunately, increasing the transmission time of each bit implies that fewer bits can be transmitted in any time interval. Hence, for each sample value to be transmitted, a trade-off between the number of bits used to represent the sample value (quantization error) and the transmission time per bit (error due to bit errors) is possible. It follows that an optimum trade off resulting in the least overall error exists. However, following standard practice, we neglect the optimum solution and independently choose quantization levels for each sensor that result in allowable errors and a transmission time that results in a reasonable error rate. The "telemetry problem" is discussed in more detail in Appendix A

4A2. Central Data System

A central data system (CDS) has been selected for the spacecraft. This system, with the use of integrated circuits, combines in an efficient package the following functions:

1. Clock and timing generators

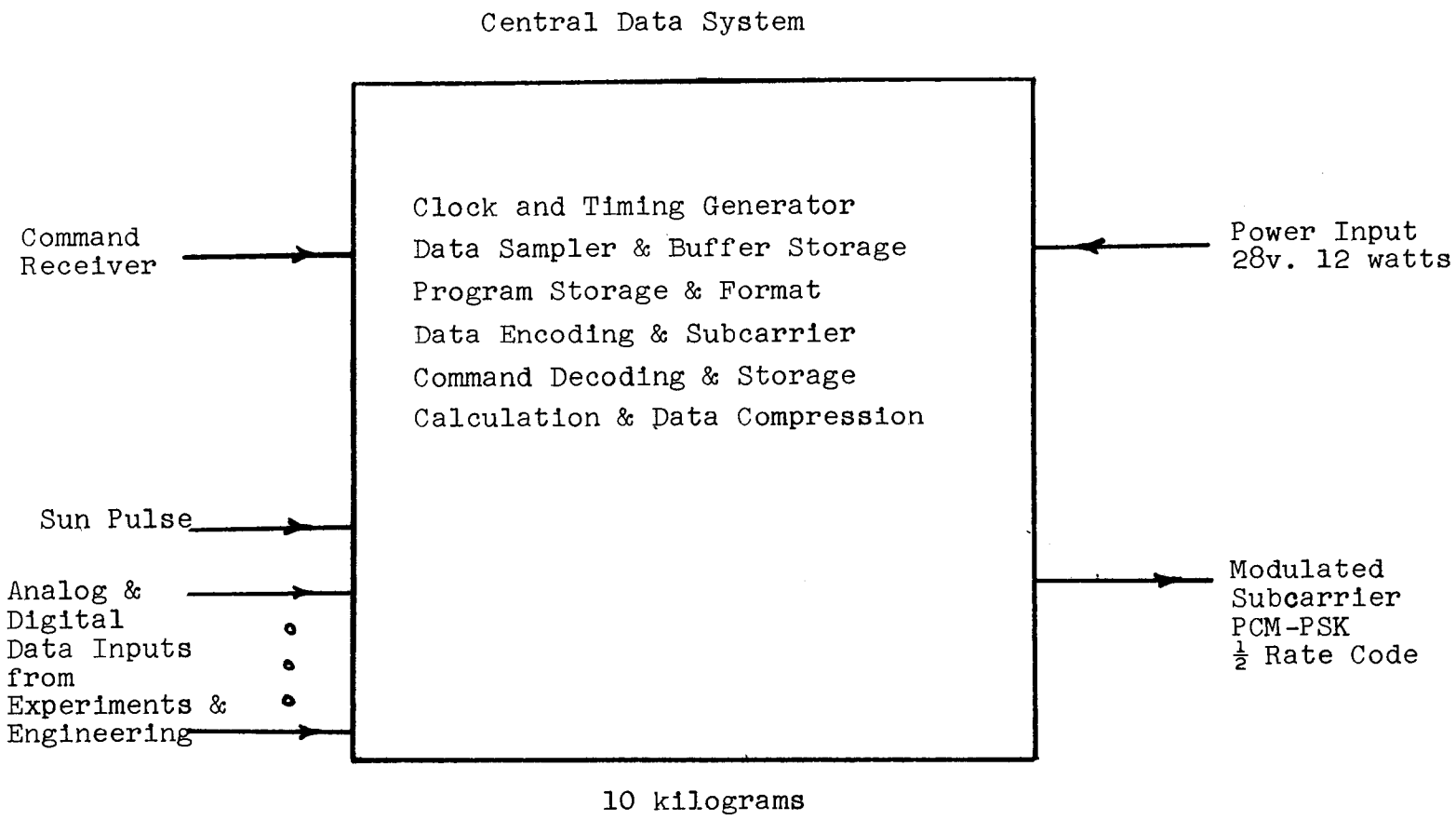

Figure 4A2.1 Schematic Diagram of Central Data System

2. Data sampler and buffer storage
3. Program storage and format
4. Data encoding and subcarrier modulation
5. Command decoding

The clock and timing generator on board the spacecraft provide all the basic time pulses required for data sampling, processing and storage. An elapsed time counter provides a time word in each data frame to assist the experimentors in establishing a time base for these data. See Fig. 4A2.1.

The master oscillator of the clock system is a stable crystal controlled oscillator operating at a frequency corresponding to a power of 2. For example, 2^{18} = 262,144 Hz, a frequency which may be easily obtained with crystal oscillators. The output of the master oscillator is connected to a series of binary counter stages and gate circuits to provide timing pulses to the elapsed time counter, the bit rate generator, the data sampler logic control, and, the sun sector code generator. The data subcarrier required by the modulation system is also extracted from the binary counter chain.

Consideration has been given to providing for all analog to digital conversions in the central data unit. However, experience with other spacecraft has indicated that it is difficult to carry the analog data from the experiment package to the central data unit without introducing errors due to ground loops, noise, and contact differences of potential. Therefore, although a central analog-to-digital converter is provided, it may be necessary for some of the experiments with analog outputs to provide their own analog to digital conversions using timing and sequencing pulses from the central data system. Temporary buffer storage of experimental and engineering data is also provided in the central data system.

Space qualified experiment hardware will be available in the next few years providing measurements at better than 0.25% accuracy. Therefore, an 8 bit binary data word resulting in a maximum quantization error of approximately .20%, has been selected.

Data rates of 1024, 512, 256, 128, 64, 32, 16, 8 and 4, bits per second are available on ground command.

The central data system has a program memory section that can be loaded by ground command. This section controls the data sequencing format and bit rate for data transmission.

The CDS represents a step toward a general purpose

computer on-board a spacecraft.

4A3. Experiment Data

The three analog outputs from the triaxial fluxgate magnetometer are simultaneously sampled four times per spacecraft revolution, held, and applied sequentially to the A/D converter in the CDS. These three 8 bit data words are then transferred to a buffer storage unit. The Sun sector position, dynamic range, D.C. offset value, and Z axis flux gate physical orientation codes require 8 additional bits. Therefore, a total of 32 bits per reading or 128 bits per spacecraft revolution are acquired. At approximately 2 rev/sec of the spacecraft with sampling every other revolution the data is accumulated at the rate of 128 bits per second. Other data processing, such as digital bandwidth reduction, scale changing, etc., can also be performed by the CDS.

The cosmic ray experiment is sampled in twelve sectors of the spin axis and requires 82 bits per revolution. 12 revolutions are required for a total scan of all energy levels up to 190 Mev. A logarithmic scale is used to reduce the counting rate which may exceed 10^6 counts/sec near the Sun.

The plasma probe experiment can determine the energy spectrum of protons over a range of 100 ev to 15,000 ev and of electrons over a range 3 ev to 500 ev in twenty-four steps. The experiment is sampled in 16 sectors of the spin axis and 8 collectors out of the spin plane. The plasma probe scanning divides the active volume into 128 regions which, combined with the step voltage energy analysis, generates 3072 data points. A data rate of 120 bits per spececraft revolution is obtained by using 384 spacecraft revolutions to complete a data cycle. A maximum flux mode of operation measures the channel and sector number (related to Sun-pulse timing) that contains a maximum number of particles for a given energy range. This mode generates approximately 8.5 bits per spacecraft revolution.

The dual frequency VHF radio propagation experiment measures the integrated electron density over the ray path from the spacecraft to the earth transmitting station. By counting phase changes in a given time (up to 1024 Hz) between the two radio waves of different frequency as they pass through the ionized medium, the relative phase delay is obtained, this allows the electron density in the total path to be computed. An analog voltage is generated proportional to the group path phase delay obtained from the coherent 10 kHz FM modulation present on both of the radio frequency carriers.

The amplitudes of the two frequency carriers provide additional information on the radio path to the spacecraft. These analog signals are sampled and converted to digital form, during the normal scientific data format, at a rate of one sample per five seconds. A special format for the radio proagation experiment provides thirty-two samples per second of each radio frequency amplitude to measure the scintillation of the radio signal passing through the ionized regions of space. An indication of continuing satisfactory operation of the radio propagation experiment is provided by the measurement of the control voltage in the phase-lock loop circuit. This loop stress signal is digitized and read out at a rate of one sample per five seconds in the normal mode of operation. The phase path counter output requires ten bits and should be sampled at least once per second. Other measurements need not be transmitted more often than one data point every ten seconds.

The fast neutron experiment provides omnidirectional detection and energy range measurement of the neutron flux. One type of neutron counter now under consideration for use in a solar probe detects high energy charged particles and gamma rays as well as high energy neutrons. The individual events are separated by pulse shape detectors that provide separate outputs for charged particles, gamma photons and fast neutrons. Sampling and digitizing of the pulse height from the detector gives a measure of the energy of the incoming particles. The CDS is used to accumulate the number of counts in a given time for the charged particles, digitize the pulse peak detector outputs, and provide a buffer storage. Data is accumulated for one spacecraft revolution and these 225 data bits are read approximately once per minute.

The experiment data rates are summarized in Table 4A3.1.

Table 4A3.1

Experiment	Bit rate		
Magnetometer	32	or	64
Cosmic ray	8		16
Plasma probe	64		64
VHF radiopropagation	16		32
Neutron	24		32
Engineering	16		16
	160		208

4A4. Format

The selection of a data format requires co-ordination among the scientists with experiments selected for the ICARUS mission. Since the spacecraft passes in close proximity to the Sun an extensive engineering surveillance requirement exists. Several format configurations are available on command from the Earth. The CDS initiates a different data sampling rate for the different data transmission rates. As an example when data transmitted at the 1024 bits/sec rate the magnetometer is sampled at 128 bits/sec, the plasma probe at 512 bits/sec the cosmic ray detector at 256 bits/sec, the radio propagation experiment at 32 bits/sec and so on. At slower data transmission rates several of the experiments are sampled at a greatly reduced rate. The magnetometer data are sampled at as low a bit rate as 8 bits/sec; cosmic ray data, plasma probe, as well as the VHF experiment are also sampled at 8 bits/sec each. The neutron experiment could be read out once an hour or slower if required.

A standard scientific data format is used for most of the mission. However, special scientific formats are provided that place emphasis on one or two of the experiments. During the transmission of the scientific format, engineering data is subcommutated during each frame. A frame of data consists of 32 words, 8 bits/word or a total of 256 bits. The first word in each frame is for frame synchronization. The second and third words in the formats represent the time code. Following this, fram identification and scientific subcommutation identification are included. Figure 4A4.1 represents a format layout for 256 bits/sec transmission. This format provides the magnetometer 64 bits/sec, cosmic ray 16 bits/sec, plasma probe 64 bits/sec, and the neutron experiment 32 bits/sec. The engineering service is also provided with 16 bits/sec. At different data transmission rates some compromise in the rate for individual experiments is required. On command from the ground the special engineering format is transmitted in two frames, of 26 engineering words each, a total of 52 engineering data points. Table 4A4.1 lists the 52 engineering measurements for this spacecraft.

4A5. Modulation and Coding

The data and communication system is compatible with the Deep Space Instrumentation Facility operated by the Jet Propulsion Laboratory(JPL) for NASA. The down link frequency 2295 $\pm$ 5 MHz is generated by an on.board crystal controlled oscillator. Assuming that the crystal frequency does not change during launch and operation, a precise measurement of the frequency received at the ground station may be used to

Table 4A4.1 Engineering Measurements

1. Temperatures	
magnetometer	1
electronic packages	8
antenna	(3)
battery	4
solar cells	6
cold gas storage	1
side wall	(3)
	26
2. Power System	
solar cell voltage	1
solar cell current	1
battery voltage	1
battery current	1
bus voltage	1
bus current	1
	6
3. Attitude Control	
sun sensor	(3)
cold gas storage pressure	1
mode switch positions	(5)
	9
4. Data and Communications	
TWT voltage	(5)
transmitter mode	(3)
receiver mode	(3)
	11
TOTAL	52

MAG - Magnetometer
CR - Cosmic Ray
ND - Neutron Detector
PP - Plasma Probe
VHF - Dual Freq. VHF Radio Prop.

Frame Sync.	16 Bit Clock		Format and Science Sub. ID
MAG	MAG	MAG	MAG
MAG	MAG	MAG	MAG
CR	CR	VHF	VHF
Frame Sync.	Engr. Sub. ID	Engr.	Engr.
PP	PP	PP	PP
PP	PP	PP	PP
ND	ND	ND	ND

Figure 4A4.1 Normal Scientific Format 32 Words 256 Bits

calculate the component of the velocity of the spacecraft along the line between the spacecraft and the ground station. This "one-way" doppler measurement results in a velocity calculated within an accuracy of $\pm$ 30 meters/sec.

A more accurate doppler measurement is possible by transmitting a radio frequency signal to the spacecraft at the up-link frequency of 2115 $\pm$ 5 MHz. At the spacecraft this frequency is converted by the exact ratio of 221/240 in a coherent translator and then retransmitted back to the origninating ground station. The received frequency is converted by the ratio of 240/221 in a coherent translator and compared with the original transmitted frequency. The frequency difference measures the two-way doppler shift from which the component of velocity along a line between the spacecraft and the ground station may be calculated to an accuracy on the order of $\pm$ 0.003 meter/sec (1). As soon as the uplink frequency is received and converted to the down-link frequency, and stability is established, the converted signal is used in place of the onboard crystal oscillator as the exciter for the on board transmitter.

The doppler measurement yields the velocity component of the spacecraft but not the range to the spacecraft. The range to the spacecraft is determined by combining the velocity data from many measurements with the antenna pointing data and other factors into a computer program that generates a solution to the range, velocity and orbit parameters for the flight of the spacecraft.

Another range-determining technique, called the pseudo-noise (PN) code system (1) requires a long pseudo-noise pulse code to be transmitted from the ground station and then retransmitted from the spacecraft. The returned signal is correlated with a delayed replica of the transmitted signal to determine the transit time, from which the range is computed. Of these two systems, the PN code, though slower to acquire, requires less power and bandwidth and is available in the Deep Space Instrumentation Facility.

Digital data may be impressed on a radio frequency carrier in a number of ways. In each of these systems factors that must be considered are simplicity of implementation, weight, efficient use of the available power on the spacecraft, ease of decoding at the ground station, availability of real time data display, and complexity of ground equipment required both at the receiving station and the spaceflight operation facility.

All data transmission in the presence of noise is subject to error. The average error rate per information

bit (P_e) or signal error probability is related to the received energy per bit per noise spectral density. Figure 4A5.2 shows the relationship between the average error rate and the pertinent system parameters defined in the figure.

Two modulation schemes were considered. In the first a binary serial bit stream modulates a subcarrier by reversing or not reversing the phase of the subcarrier by π radians. This form of modulation is called differential phase shift keying (PSK), a form of pulse code modulation, and it is presently employed on several vehicles in space, e.g. Pioneer 6. The second form of modulation which was considered for this spacecraft consists of several tones generated with a specific frequency relationship between tones and transmitted in one phase position or π radians reversed in phase (3). This system with M/2 tones and the two phase positions provides M signals. The modulation process associated with a biorthogonal system amounts to a data encoding device. The information bits are taken as a group, k-bits at a time, and encoded as a 2^{k-1} bit waveform. This process requires k-shift register stages and a k-bit buffer storage. This implies the transmission of $2^{k-1}/k$ additional bits to represent the information content, i.e. 16 bits transmitted for 5 information bits (16,5). This system is easy to implement on board the spacecraft but presents a formidable decoding requirement at the ground station (3). The system using pulse code modulation with a phase shift keyed subcarrier that phase modulates the radio frequency carrier has been selected after careful study. An elementary convolutional code with a form of maximum likelihood decoding (4) is employed to reduce the required transmitter power for a given data rate and error probability.

The proposed encoding system requires two transmitted bits for each information bit. This relation is referred to as a half rate code or a clock ratio of 2. The information bit stream is read into a 24 bit shift registration and at each count of the shift register a signal is drawn from selected register stages to a combinational logic circuit that produces a parity bit for each information bit. The parity bit is inserted after each information bit in a buffer storage unit and then fed into the subcarrier modulator. The modulation of the subcarrier is accomplished using a non-return-to-zero-mark-on-one system with several cycles of coherent subcarrier per bit period. See Fig. 4A5.2.

The lowest error probability for a given power and data rate requires phase coherent reception of the radio frequency carrier and the telemetry subcarrier. The phase-lock loop circuit used to obtain phase coherent reception contains a

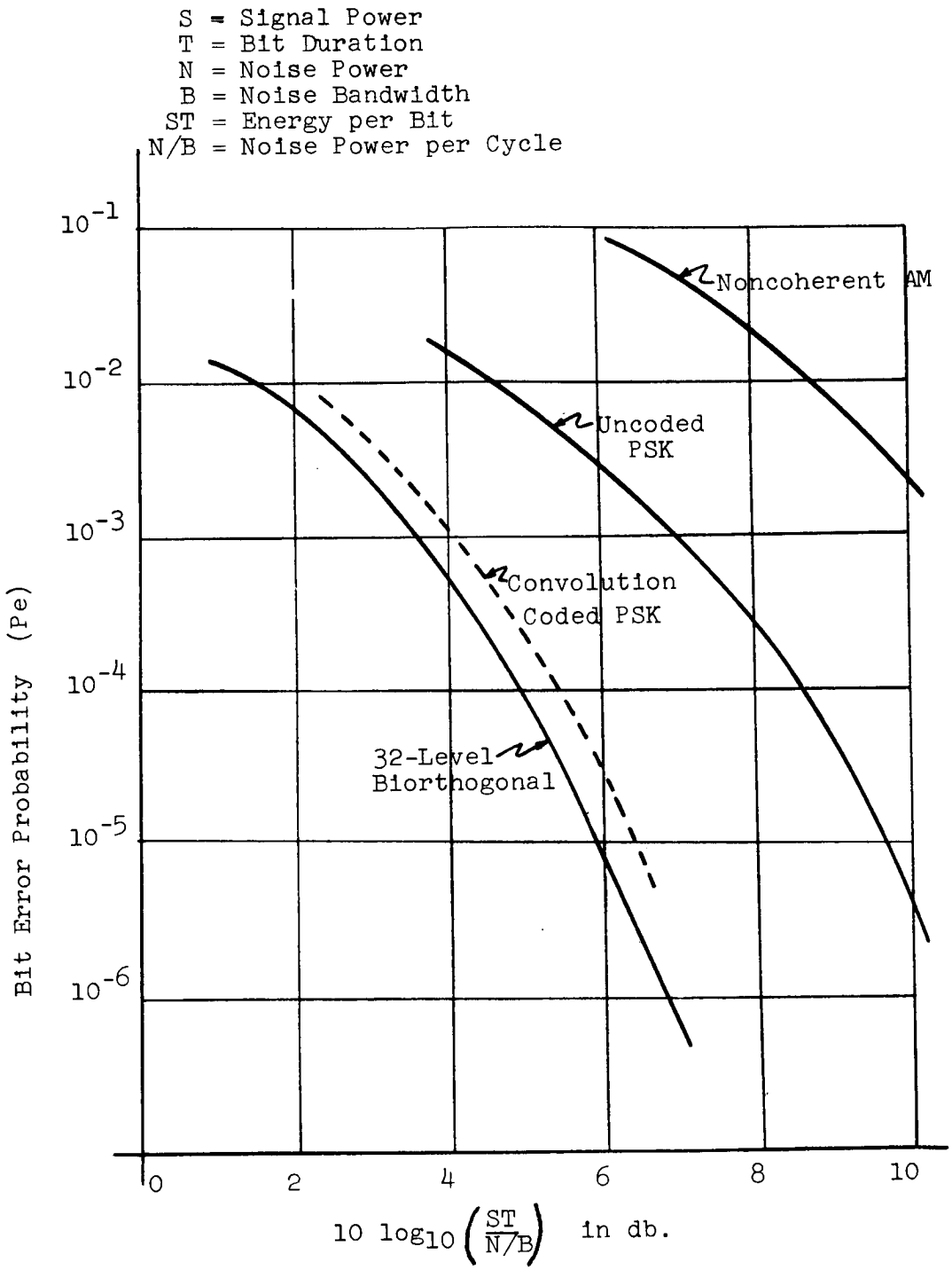

Figure 4A5.1 Bit Error Probability as a Function of Energy per Bit per Noise Density

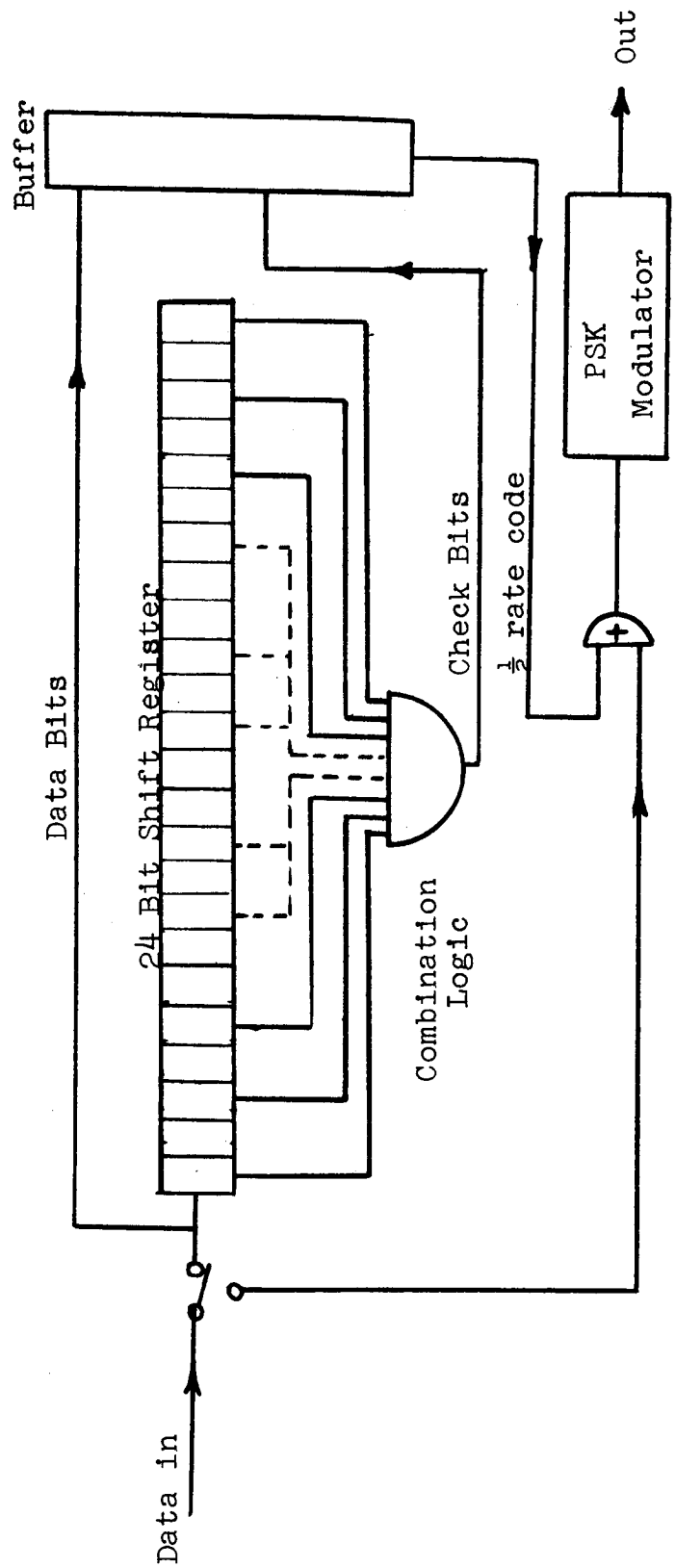

Figure 4A5.2 Convolutional Code Generator Schematic

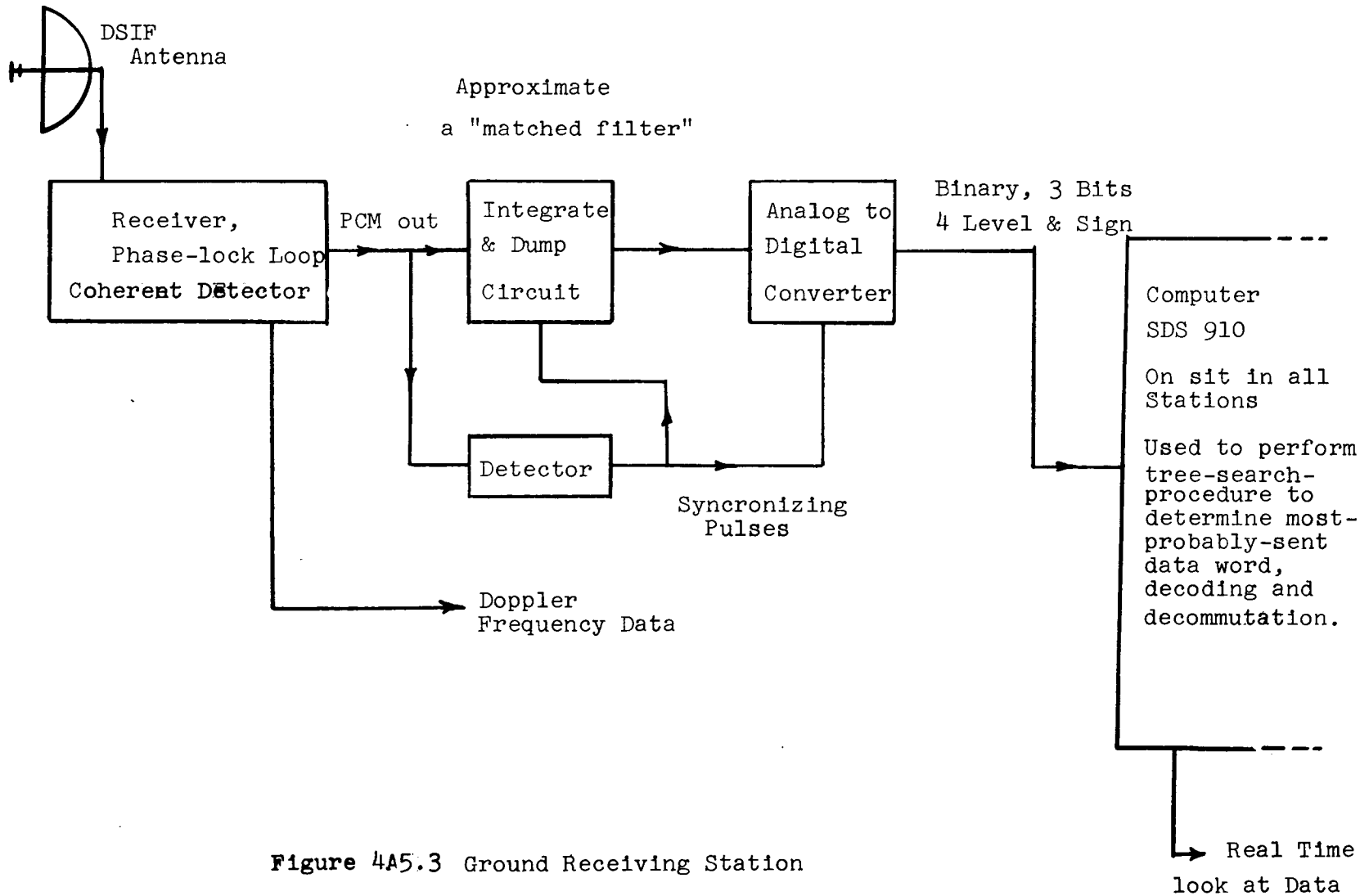

Figure 4A5.3 Ground Receiving Station

multiplier (mixer) with inputs which are the undetected signal and the output of a voltage controlled oscillator. The output frequency and phase of the voltage controlled oscillator are controlled by a voltage obtained from the multiplier output through a low pass filter. The band width of the phase-lock loop circuit (the low pass filter) is normally on the order of 10-12 Hz.

The subcarrier is demodulated by first squaring the signal, to remove the modulation. It is divided by two, and compared to the original subcarrier in a phase sensitive detector. The output of this detector is connected to an integrate and dump circuit. This system approaches an ideal matched filter detector. The voltage level obtained is then digitized and the voltage is returned to zero. This procedure requires bit syncronization in order to control the integrate and dump and digitising circuits. The bit synchronization signal to noise ratio may be the limiting factor in the telemetry system. See Fig. 4A5.3.

The output voltage from the integrate and dump circuit is digitized into a 3 bit code (4 levels and sign). No firm dicisions have been made at this point as to whether the signal represents a 1 or 0 data bit. The digital information will be fed into a SDS 910 computer available at the DSIF receiving station for decoding and decommutation of the information. The computer performs a search procedure (6) to determine the most probable data word. The computer program is now being written and the demodulation equipment has been built and operated to demonstrate an expected improvement of 3db to 4db over the present Pioneer 6 telemetry system.

4B. On-Board and Ground Antenna, Transmitting, and Receiving Systems

4B1. Introduction

Communication with a solar probe at bit rates high enough for sufficient data transmission is difficult because of the large distances involved. The following sections outline the general details of what can be called a satisfactory compromise. Topics covered are: the Deep Space Instrumentation Facility, a discussion of the on-board sub-system, reasons for the choice of TWTs as power output devices, a description of the on-board antennas, listing of the losses encountered in the system, a discussion of bit rates associated with various missions, and the need for on-board data storage.

4B2. Deep Space Instrumentation Facility

The antenna-tracking facilities of the DSIF consist of 85 ft. diameter cassegrain antennas located at Goldstone, California, Woomera, Australia and Johannesburg, South Africa. In addition to the 85 ft. antennas there is one 210 ft cassegrain antenna located at Goldstone, California. The antennas are designed to receive signals at a frequency of 2295 $\pm$ 5 mHz. This frequency was chosen so that the sum of the galactic and atmospheric noise is a minimum. The 85 ft. antennas have a receiving gain of 53 db and a beamwidth of 0.35 degrees. The 210 ft. antenna has a receiving gain of 61 db and a beamwidth of 0.1 degrees. The effective noise temperature of the receiving system using the 85 ft. antennas is $55^{\circ} \pm 10^{\circ}$K. The effective noise temperature of the receiving system using the 210 ft. antenna is 25°K.

During the summer, the spacecraft near the Sun can be tracked continuously for 12 hrs by the 210 ft receiving antenna. During the winter, because of the Earth axis tilt, the tracking time is reduced to 8 hours. In either season full 24 hour coverage can be obtained with the 85 ft. receiving systems.

At present the 85 ft. antennas are capable of simultaneously tracking and transmitting (gain of 51 db) powers up to 10KW for communication from Earth to the spacecraft. Also available is an 85 ft. antenna capable of transmitting powers of 100KW. This 100KW system can only be used if emergency conditions arise. Although the 210 ft. antenna does not have transmitting capabilities, it is needed to provide increased data rates near perihelion, 0.5 to 0.1 AU. See Figs. 4B7.1 and 4B7.2. The increased data rates will greatly improve the significance of the scientific information gathered. Even though the 210 ft.

antenna is likely to be available for 14 to 21 days (7), 24 hour coverage can be guaranteed only if two additional 210 ft. antennas are constructed. Table 4B2.1 summarizes the major parameters of the DSIF.

Table 4B2.1

Antenna	Gain Listen	Gain & Power Transmit.	System Noise Temperature	Beamwidth
85 ft	53db	51db 10kw	$55^{\circ} \pm 10^{\circ}K$	0.35 degrees
85 ft	--	51db 100 kw	--	0.35 degrees
210 ft	61db	--	$25^{\circ}K$	0.10 degrees
		listen frequency 2295mHz	transmit frequency 2115mHz	

Although the ICARUS program is planned around the use of the existing DSIF it is obvious from the information in the preceding paragraph that more 210 ft. antennas are needed with their higher (greater than 6 times the rate possible with the 85 ft. antennas) data rate capability. These antennas are permanenet installations and they would give all the future space missions of any kind the added data capacity. The saving in cost of on-board communication equipment, requiring an on-board power output increase of 6 to 1 (with associated thermal problems) to accomplish the same data rate increase, would soon pay for adding new 210 ft. antennas. Additional antennas would also ease the DSIF scheduling problem which becomes more severe with the increased number of missions each year.

4B3. Communication Subsystem

The communication subsystem shown in block diagram form in Fig. 4B3.1 is similar to, but more versatile than, the subsystem on the present Pioneer spacecraft. The antenna system consists of one high gain (11 db) antenna on top of the spacecraft, one omni antenna on top of the high gain antenna, and one omni antenna below the spacecraft. The RF power amplifiers can be switched to take full advantage of the available solar cell ouput energy.

Immediately after launch, but before the spacecraft is oriented with respect to the Sun, only a small amount of

energy is used on the spacecraft. This energy is battery supplied and the same battery is part of the power conditioning system. Commands are sent to either of the two omnis and their associated receivers. Choice of system is made automatically by signal level. Engineering information is the only telemetry requirement at this stage and it is sent back to Earth by using one of the driver stages (about 200 mw) with the upper omni antenna.

After the Sun has been acquired and the spacecraft is properly oriented, there is enough energy from the solar cells to operate the 3 watt TWT. The driver then provides the input to the 3 watt TWT through the power divider for telemetry purposes. Command signals, after orientation, are received by the upper omni and receiver number one or by the high gain antenna and receiver number two. Signal levels are compared and the higher level signal is fed to one of the decoders. If one receiver and/or one decoder fails, spacecraft control is maintained through the remaining receiver and/or decoder.

As the spacecraft nears the Sun more energy is available from the solar cells. As power becomes available the 20 watt TWT, the 50 watt TWT, and finally the 100 watt TWT are used for telemetry purposes. The high output power near the Sun provides a high bit rate where data of maximum interest is available. Note that, by changing the primary voltages, the 20 watt TWT is used as a 50 watt ouput device. This provides a guarantee of no more than a three db loss in output if the 100 watt TWT fails.

The RF switches used are mechanical switches similar to those on the Pioneer. Although there is some question of their reliability, they are flight tested and they do not have to operate many times. They are lightweight compared with RF circulators and they produce no disturbing magnetic fields. For the sake of reliability an additional switch could be placed in the line of the diplexer of the high gain antenna. If one of the other switches failed this switch could be operated to connect the ouput of the 20/50 watt TWT directly to the diplexer.

4B4. RF Power Amplifiers (8,9)

Communication from a spacecraft at any appreciable distance from the earth depends to a great extent on the device generating the output signal. At the frequency of 2.3 gHz solid state devices can not generate sufficient power to be considered and vacuum tube devices alone are suitable for use. The primary types of vacuum tube amplifiers considered are triodes, klystrons, amplitrons and TWTs.

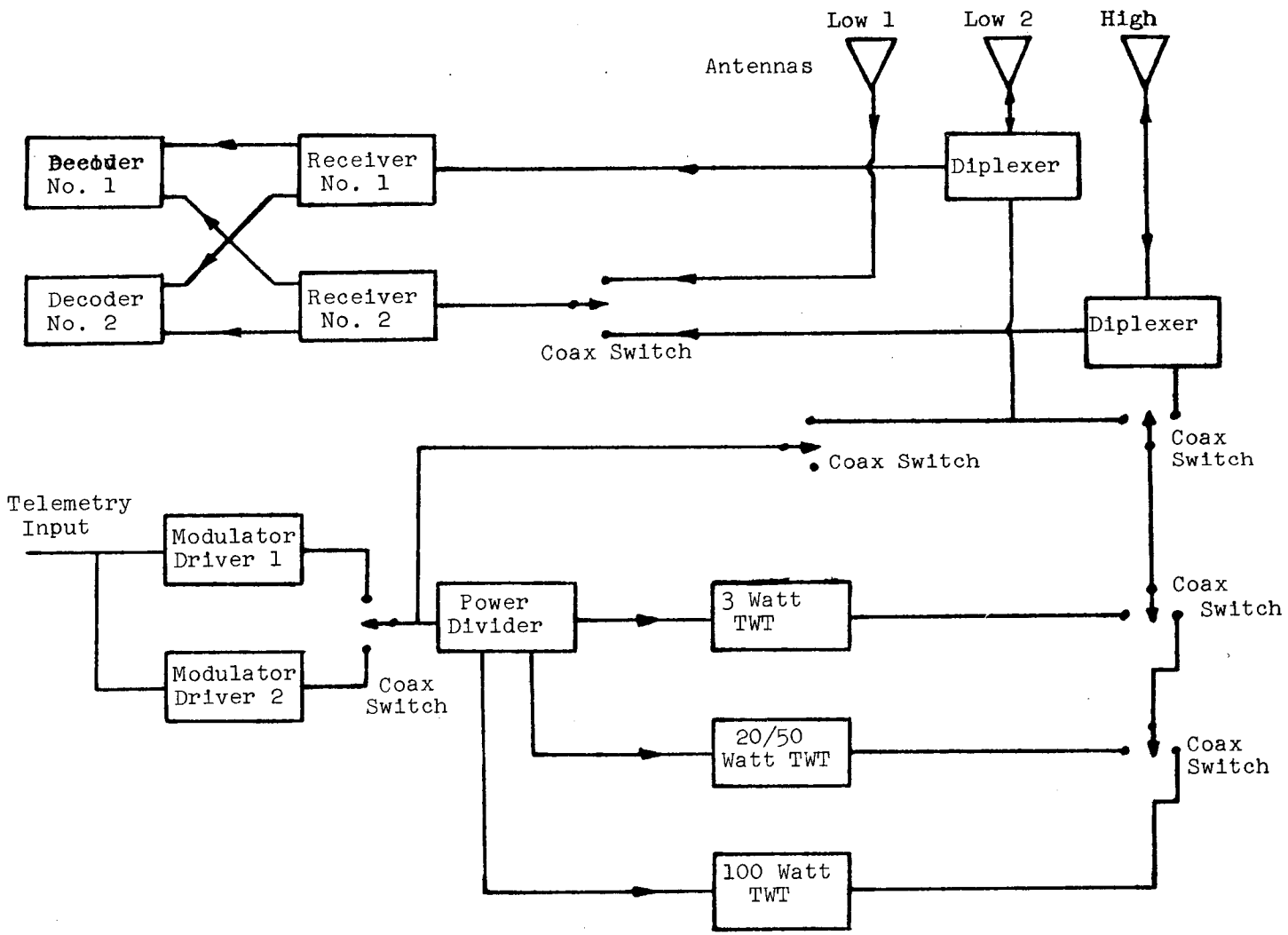

Figure 4B3.1 Simplified Block Diagram of Communications Subsystem

Typical complete triode telemetry transmitter packages at 2.3 gHz may offer 4-5 watts output with 10 percent overall efficiency and a minimum life of 5000 hours. The poor efficiency and the short lifetime rule out the use of triodes.

Klystrons are efficient and reliable at 2.3 kw but low and intermediate power klystrons have anticipated efficiencies no better than 20% maximum. Electrostatically focused klystrons are light and they, as well as hybrid klystron-traveling wave tubes, may be available in the distant future.

Lightweight amplitrons have been developed in the 20-25 watt range with efficiencies of 40 to 55 per cent and a gain of approximately 17 db. They are attractive because of their high efficiencies but there is not enough data available to know what lifetime is to be expected from them. They may be in the 5000 hour class. They require a complex power supply but in the event of tube failure they have the possible advantage that energy can be fed directly through them without appreciable loss.

Traveling wave tubes have demonstrated typical lifetimes of around 30,000 hrs. They are presently available in many power ratings such as 3 watts at 20 per cent efficiency and 20 watts at 28 per cent efficiency (these figures include power converter efficiencies.) Tests on a WJ-274-2 indicate that an overall efficiency of 35% can be expected by careful selection and matching of the tube and pwer supply. Tests also indicate that the 20 watt tube can be operated at a 50 watt level with 40% efficiency by changing the power supply voltages. It seems likely that switching of the primary voltages can accomplish the change although the tests were made by changing secondary voltages. Watkins-Johnson is presently developing for JPL the TWT, WJ-395, which will have an efficiency of 55% (47% with converter) and an output power of 100 watts. The preliminary tubes should be completed by the end of September 1966 and the production models should be ready for delivery before the scheduled solar mission.

A combination of TWTs, 3 watt, 20 watt (which is used at 50 watts), and the 100 watt under development have been chosen to furnish the spacecraft RF output. The decision to use TWTs was based on their long life and reliability. (The new tube will meet NASA specifications and should have the same life and reliability built in.) Amplitrons were considered but their efficiencies are no better at 100 watts than the new TWT and their dependability is unknown.

4B5. Spacecraft Antenna Systems

The spacecraft will have three separate antennas. Two of the antennas will have an isotropic (omni) pattern; the remaining antenna will be high gain.

The high gain antenna will be essentially the same as the one used on the present Pioneer, with the exception that a surface material will be added to meet the thermal conditions involved. The present Pioneer antenna has a beam width of 5.5° and a gain of 11 db. The only modification in pattern would be for out-of-the-ecliptic orbit planes as indicated in section 4B8.

One of the omni antennas will be located on the high gain antenna as was done on the Pioneer. The second omni of the Pioneer will be removed so that the cabling of the magnetometer and the VHF antenna can use the coxial cable space thus made vacant.

The remaining omni of the spacecraft will be placed on the end opposite to the high gain antenna. Since this antenna will be located inside the skirt on the spacecraft it will provide antenna coverage during the pre-orientation trajectory. This antenna will be used only for receiving.

The upper omni and high gain antennas will both be capable of receiving and transmitting, therefore, they must be able to transmit 100 watts of power.

4B6. Communication System Losses

Tables 4B6.1 and 4B6.2 are design tables showing power distributions in the system. The tables are self explanatory. They are conservative estimates because they use a figure of 8.8 db for ST/N/B, which is the value associated with the present Pioneer coding system. The proposed new coding scheme (discussed in section 4A will save three to four db over the present system. Also, it may be noted that for the 210 ft. antenna the 3 db polarization loss could be avoided with a linear feed. It is assumed that the 85 ft. dishes will use linear feeds for receiving.

4B7. Communication Data Rates

The communication data rates will change because of two factors. The first of these factors is the changing Earth-spacecraft distance which produces a changing space loss of transmission power. The second factor is the discontinuous change in the power transmitted as the Sun-spacecraft

Down Link with 100 watt s/c transmitter, high gain s/c antenna, and 85 ft. parabola on ground. Distance to Earth = 0.8 AU.

Telecommunication Design Control Table

No.	Parameter	Value	Tolerance		Source
1.	Total Transmitter Power 100 watts	50 dbm	+1	-1	Estimated
2.	Transmitting Circuit Loss	-1.5 db	+0.5	-0.5	Estimated, Present Pioneer
3.	Transmitting Antenna Gain	11 db	+1.0	-0.5	Estimated, Present Pioneer
4.	Transmitting Antenna Pointing Loss	Included in 3			
5.	Space Loss @ 2295mc R = 1.2×10^8km(0.8AU)	-261.3 db			Calculated
6.	Polarization Loss	0 db			With use of linear feed
7.	Receiving Antenna Gain	+53.0 db	+1	-0.5	NASA
8.	Receiving Antenna Pointing Loss	0 db			NASA
9.	Receiving Circuit Loss	-0.2 db	+0.1	-0.1	Estimated, Present Pioneer
10.	Net Circuit Loss	-199 db	+2.6	-1.6	Computed
11.	Total Received Power	-149 dbm	3.6	-2.6	Computed
12.	Receiver Noise Spectral Density(N/B)@50°K	-181.6 dbm/cps	+0.4	-0.2	NASA
13.	Carrier Modulation Loss, θ = 1 rad.	-5.4 db	+016	-0.8	NASA
14.	Received Carrier Power	-154.4 dbm	+4.2	-3.4	Computed
15.	Carrier APC Noice BW($2B_{lo}$=12H)	10.8 db	+0.0	-0.5	Estimated, Present Pioneer
	CARRIER PERFORMANCE FOR TELEMETRY				
16.	Threshold SNR in 2 B_{lo}	+6 db			
17.	Threshold Carrier Power	-164.8 dbm	0.7	-1.4	Pres. Pioneer
18.	Performance Margin	10.4 db	5.3	-5.0	Computed

Table 4B6.1, continued.

	DATA CHANNEL			
19.	Modulation Loss	-1.5 db	+0.26 -0.3	Present Pioneer
20.	Received Data Subcarrier Power	-150.5 dbm	+3.86 -2.9	Computed
21.	Bit Rate (1/T) 32 bps	15.1 db		
22.	Required ST/N/B Pe = 10^{-3}	8.8 db		NASA
23.	Threshold Subcarrier Power	-157.7 dbm	+0.7 -0.9	
24.	Performance Margin	70.2 db	+4.76 -3.6	

Table 4B6.2

Down Link with 20 watt s/c transmitter, high gain s/c antenna, and 210 ft. parabola on ground. Distance to Earth = 1.2 AU.

Telecommunication Design Control Table

No.	Parameter	Value	Tolerance		Source
1.	Total Transmitter Power 20 watts	43 dbm	+0.5	-0.5	Estimated
2.	Transmitting Circuit Loss	-1.5 db	+0.5	-0.5	Estimated, Present Pioneer
3.	Transmitting Antenna Gain	11 db	+1.0	-0.5	Estimated, Present Pioneer
4.	Transmitting Antenna Pointing Loss	Included in 3			
5.	Space Loss @ 2295 mkg. $R=1.8\times10^{8}$ km (1.2AU)	-264.8 db			Calculated
6.	Polarization Loss	-3 db	+0.3	-0.3	Present Pioneer data
7.	Receiving Antenna Gain	61 db	+1.0	-015	
8.	Receiving Antenna Pointing Loss	0 db			
9.	Receiving Circuit Loss	-0.2 db	+0.1	-0.1	Estimated, Present Pioneer
10.	Net Circuit Loss	-197.5 db	+2.9	-1.9	Computed
11.	Total Received Power	-154.5 dbm	+3.4	-2.4	Computed
12.	Receiver Noise Spectral Density(N/B)@40°K	-182.6 dbm/cps	+0.4	-0.2	NASA
13.	Carrier Modulation Loss, θ = 1 rad.	-5.4 db	+0.6	-0.8	NASA
14.	Received Carrier Power	-159.9 dbm	+4.0	-3.2	Computed
15.	Carrier APC Noise BW($2B_{lo}$=12 cps)	10.8 db	+0.0	-0.5	Present Pioneer
	CARRIER PERFORMANCE FOR TELEMETRY				
16.	Threshold SNR in 2 B_{lo}	+6 db			

Table 4B6.2 continued.

17.	Threshold Carrier Power	-165.8 dbm	+0.7	-1.4	Present Pioneer
18.	Performance Margin	5.9 db	+5.1	-4.8	Computed
	DATA CHANNEL				
19.	Modulation Loss	-1.5	+0.26	-0.3	Present Pioneer
20.	Received Data Subcarrier Power	-156 dbm	+3.66	-2.7	Computed
21.	Bit Rate (1/T) 32 bps	15.1 db			
22.	Required ST/N/B Pe = 10^{-3}	8.8 db			NASA
23.	Threshold Subcarrier Power	-158.7 dbm	+0.7	-0.9	
24.	Performance Margin	21.7 db	+4.56	-3.4	

distance changes.

The data rate T, in db, as a function of the various parameters of the system is given by Eq. 4B7.1,

$$T = P_T + G_T + G_R - \phi_K - L_S - L_T - E/(N/B) \qquad 4B7.1$$

where P_T is power in dbw transmitted

G_T is gain in db of the transmitter antenna

G_R is gain in db of the receiver antenna

ϕ_K is receiving system noise spectral density (db/cps)

L_S is space loss in db

L_T is total losses in the system in db

$E/(N/B)$ is energy/bit per noise spectral density

For the data rate calculations used in this section the following parameters are used:

P_T is variable - 3 watts, 20 watts, 50 watts, and 100 watts

G_T is 12 db

G_R is 53 db for the 85 ft antenna and 61 db for the 210 ft antenna

ϕ_K is -211.6 dbw (noise temperature of 50°K)

L_S is variable as the Earth-spacecraft distance changes

L_T is 6 db

$E/(N/B)$ is 6.7 db (psk with matched filter detection and $Pe = 10^{-3}$)

On the basis of these parameters the data rates are calculated for a 0.1 AU and 0.2 AU in-the-ecliptic mission. Figure 4B7.1 is for the 0.2 AU mission and Fig. 4B7.2 is for the 0.1 AU mission. The discontinuous jumps in the data rates are due to the changing of the power transmitted. As the spacecraft gets closer to the Sun, the solar flux increases thus producing more power from the solar cells. When the power gets sufficiently

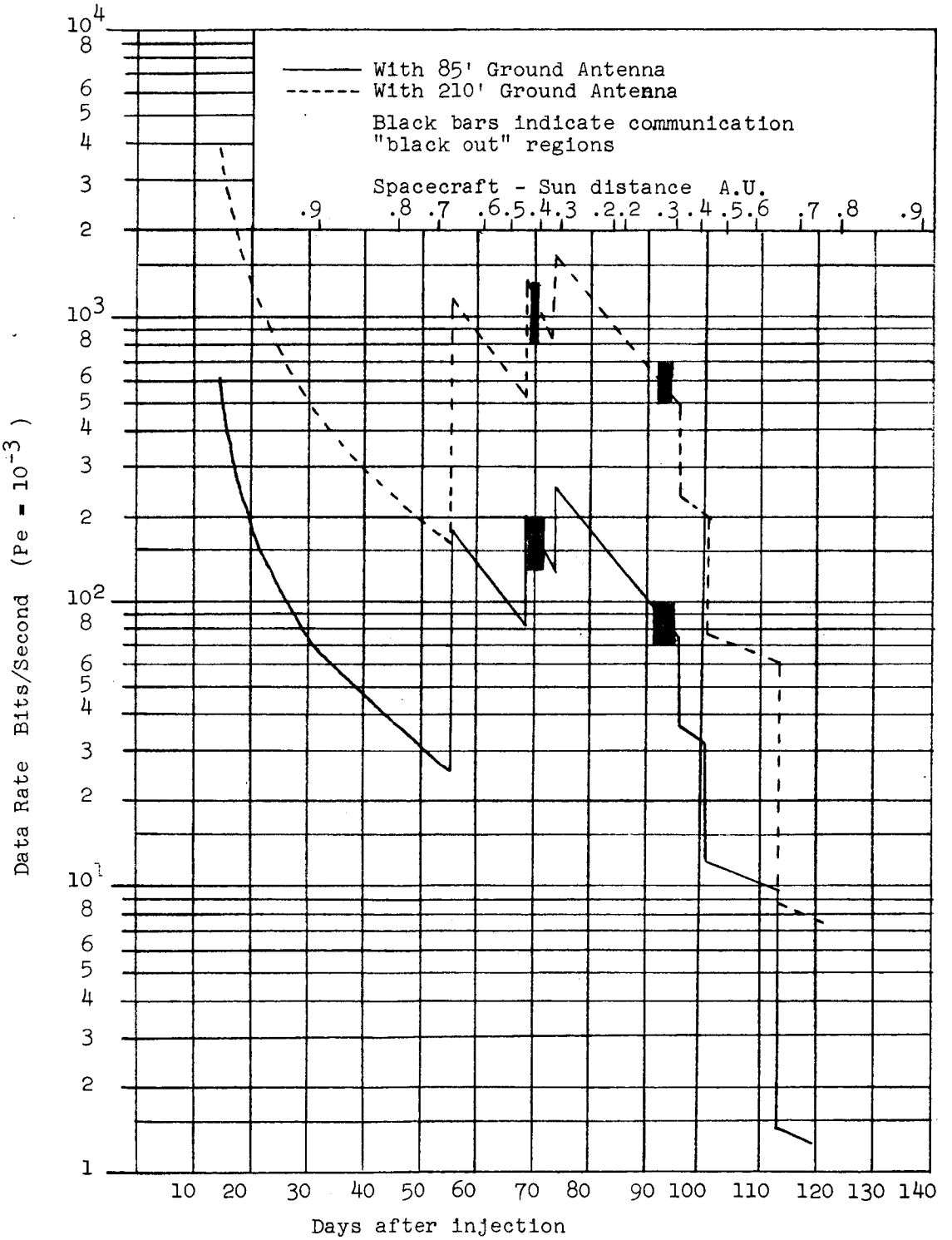

Figure 4B7.1 Data Rate vs Time after Injection - 0.2 AU Perihelion

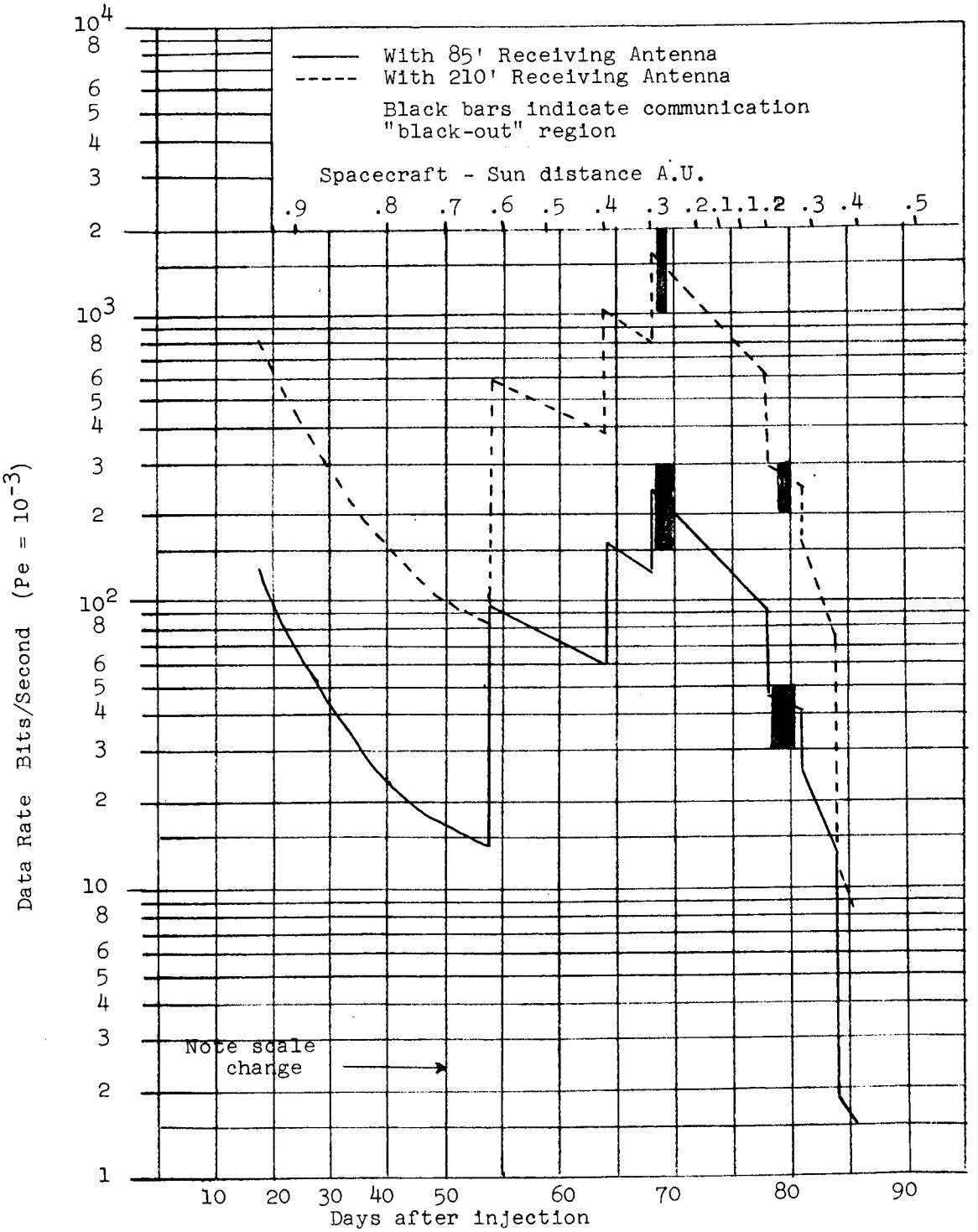

Figure 4B7.2 Data Rate vs Time After Injection - 0.1 AU Perihelion

high the next power level is switched on. Similarly as the spacecraft gets farther from the Sun and the power drops the next lower power is switched on. Table 4B7.1 shows the various times at which the power level is changed. The Earth-spacecraft distance and the Sun-spacecraft distance are also shown in the same table.

Table 4B7.1

Power Switching Time Table

Mission	Days	Power Switched From	To	Sun-spacecraft distance	Earth-spacecraft distance
0.1 AU	54	3 watt	20 watt	0.65 AU	0.52 AU
0.1 AU	64	20 watt	50 watt	0.41 AU	0.62 AU
0.1 AU	68	50 watt	100 watt	0.31 AU	0.70 AU
0.1 AU	78	100 watt	50 watt	0.22 AU	1.18 AU
0.1 AU	81	50 watt	20 watt	0.28 AU	1.24 AU
0.1 AU	84	20 watt	3 watt	0.42 AU	1.50 AU
0.2 AU	56	3 watt	20 watt	0.66 AU	0.38 AU
0.2 AU	69	20 watt	50 watt	0.44 AU	0.56 AU
0.2 AU	74	50 watt	100 watt	0.33 AU	0.70 AU
0.2 AU	96	100 watt	50 watt	0.33 AU	1.33 AU
0.2 AU	101	50 watt	20 watt	0.44 AU	1.43 AU
0.2 AU	114	20 watt	3 watt	0.66 AU	1.62 AU

In-the-ecliptic trajectories will result in a communication "black out" during portions of the flight. This "black out" occurs when the spacecraft is between the Sun and Earth or when the Sun is located between the spacecraft and Earth. Either of these two occurrences produces very high noise temperatures for the tracking antenna, and thus no data can be received. The "black-out" angle is dependent on the size of the tracking antenna beamwidth. For the 85 ft antenna the angle is within $\pm 2^{\circ}$ of the Sun center. For the 210 ft antenna the angle is within $\pm 1^{\circ}$ of the Sun center with an increase of noise temperature to about 300°K at $\pm 0.5^{\circ}$. This data shows the desirability of tracking the spacecraft with the 210 ft antenna near the region of the communication "black out". Table 4B7.2 summarizes the "black out" times for the 0.2 and 0.1 AU perihelion missions. The communication "black out" will be eliminated by injecting the spacecraft into a 1 or 2 degree out-of-the-ecliptic orbit as indicated in section 4B8.

Table 4B7.2

Communication "black out" times and duration for 0.1 and 0.2 AU in the ecliptic orbits. (85 ft. receiving antenna $\pm 2^{\circ}$; 210 ft. receiving antenna $\pm 1^{\circ}$)

Perihelion AU	Black out Angle Degrees	Days beyond approx.	Days ends approx.	Duration (hrs)
0.2	± 2	68	71	54
0.2	± 2	91	95	72
0.2	± 1	69	70	24
0.2	± 1	96	97	36
0.1	± 2	70	72	42
0.1	± 2	80	82	54
0.1	± 1	71	72	21
0.1	± 1	80	81	27

4B8. Out-of-the-Ecliptic Communication

For a mission in the ecliptic orbit no data can be received during the communication "black out", therefore, the information in this region must be lost, unless the data can be stored during this time for later transmission. The elimination of the communication "black out" is possible, however, by injecting the spacecraft into a non-ecliptic orbit for which the Earth-spacecraft and Earth-Sun angle can be made larger than the 1 or 2 degree "black out" angle given in Table 4B7.2. Table 4B8.2 shows the various orbit plane inclination angles necessary for the achievement of the no "black out" communication angles for the first "black out" region. For the 0.2 AU perihelion mission, the spacecraft will be injected into an orbit which is 1.5° out of the ecliptic. The spacecraft will be tracked by the 210 ft. antenna which will eliminate the communication "black out" and thus provide continuous "in-the-ecliptic" scientific information.

Other out-of-the-ecliptic missions are desirable so that more complete scientific information about the Sun can be obtained. For inclination angles greater than 3 degrees, problems of communication result if the present fan-beam antenna is used because the antenna beam does not always intercept the Earth. The variation of the angle between the Earth-spacecraft line and the orbit plane is shown in Figure 4B8.1 for inclination angles of 10° and 20° for a 0.1 AU perihelion. The spacecraft is injected in orbit

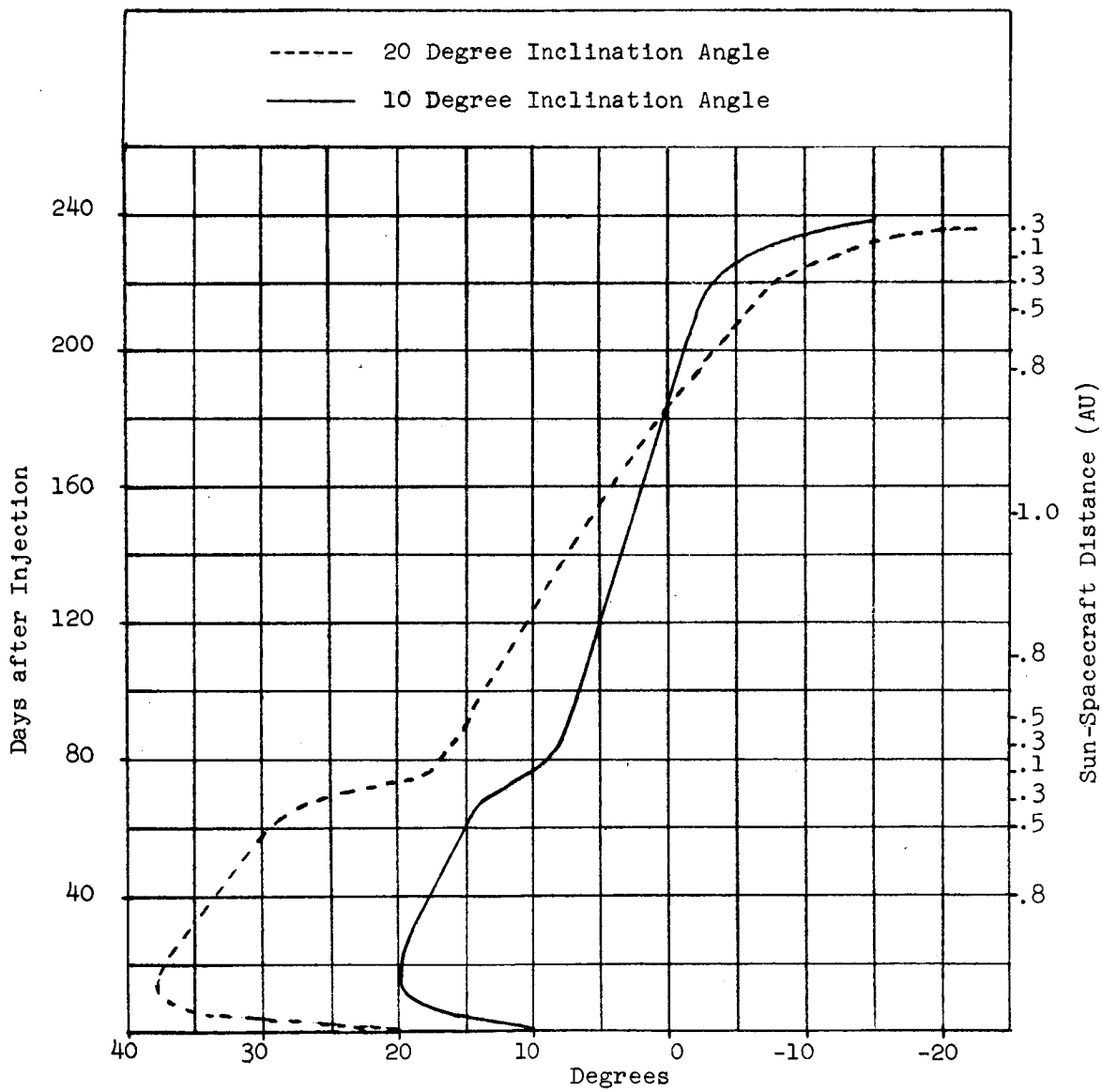

Figure 4B8.1 Angle between Earth - Spacecraft line and Orbit Plane for 0.1 AU Perihelion (out of the ecliptic)

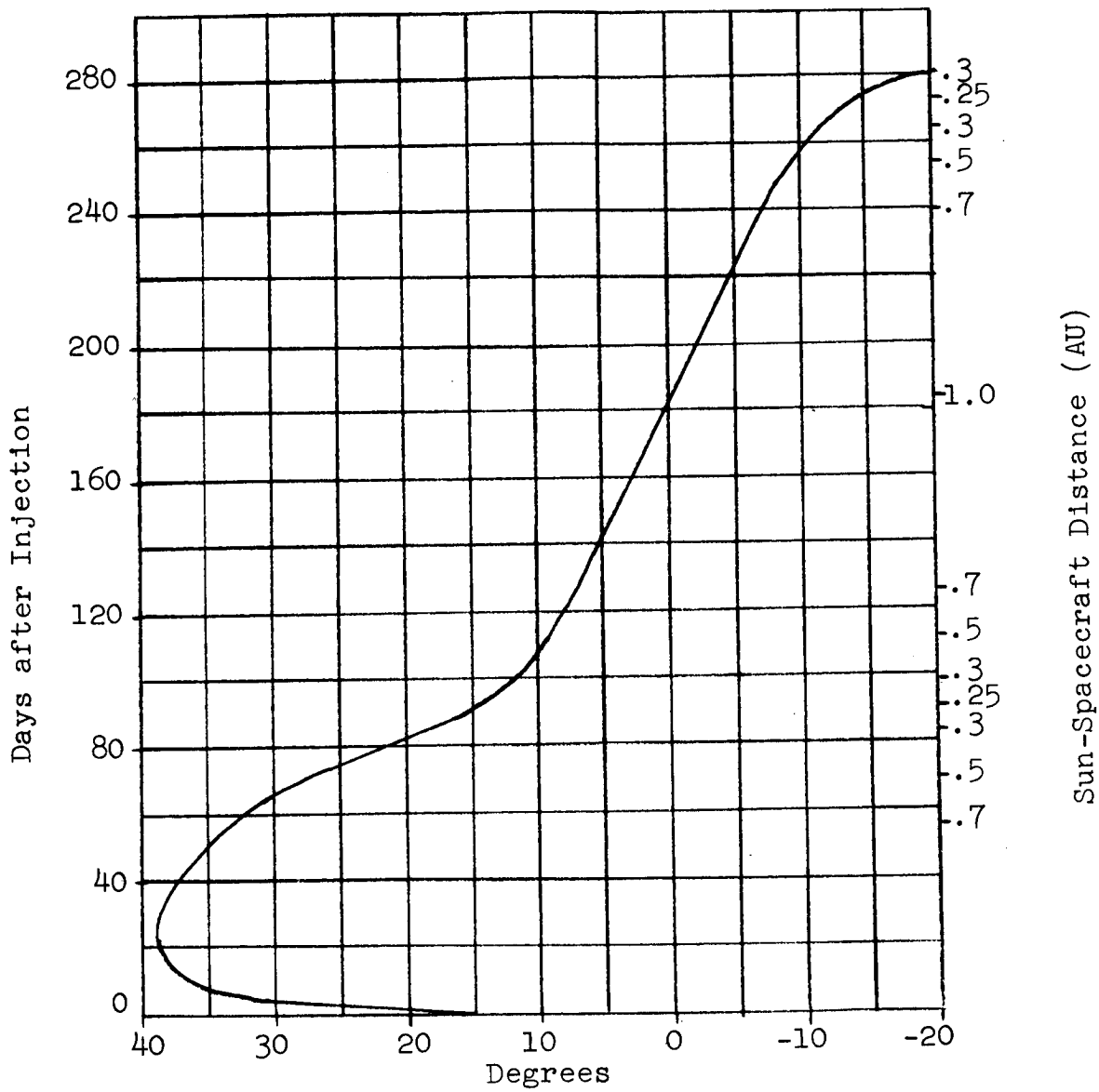

Figure 4B8.1a. Angle between Earth - Spacecraft line and Orbit Plane (15° inclination) vs Time after Injection

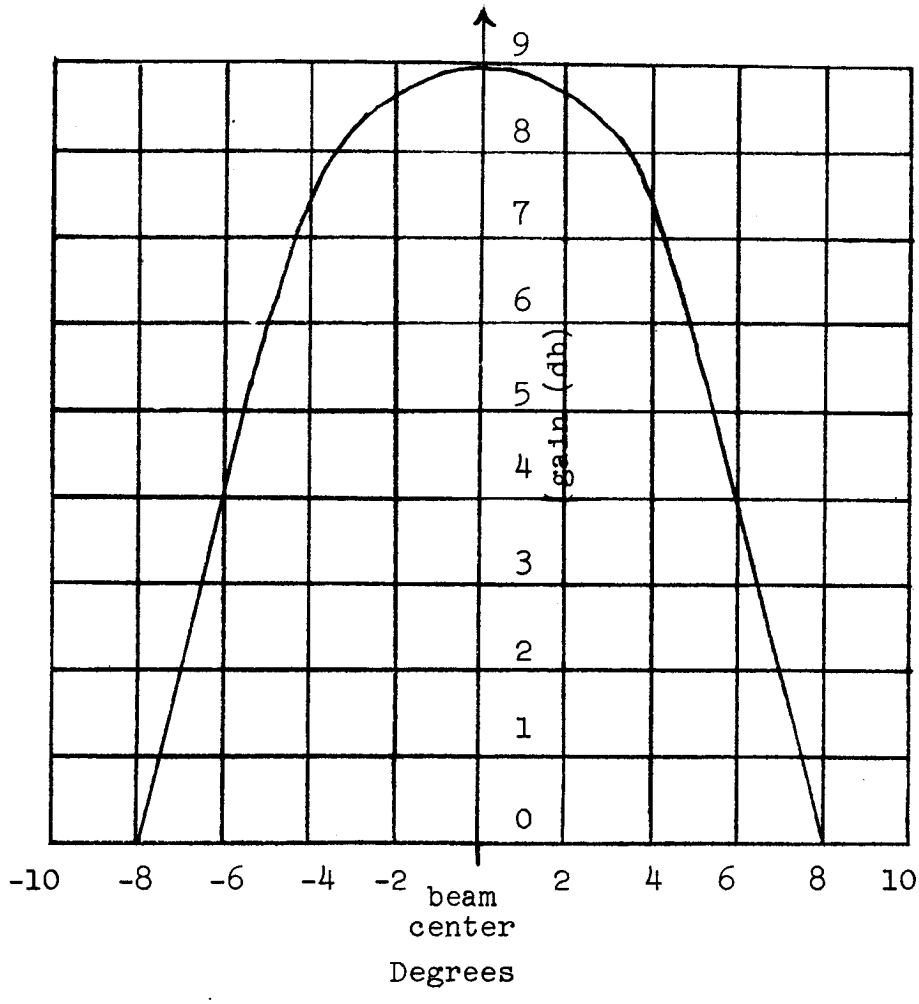

Figure 4B8.2 Pattern of the High Gain Antenna

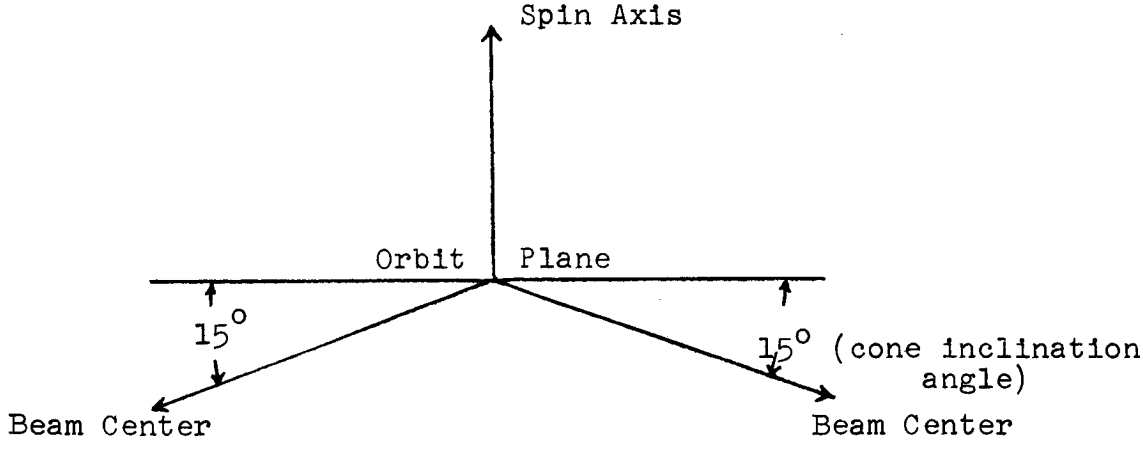

Figure 4B8.3 Location of the High Gain Antenna Beam (cross section view)

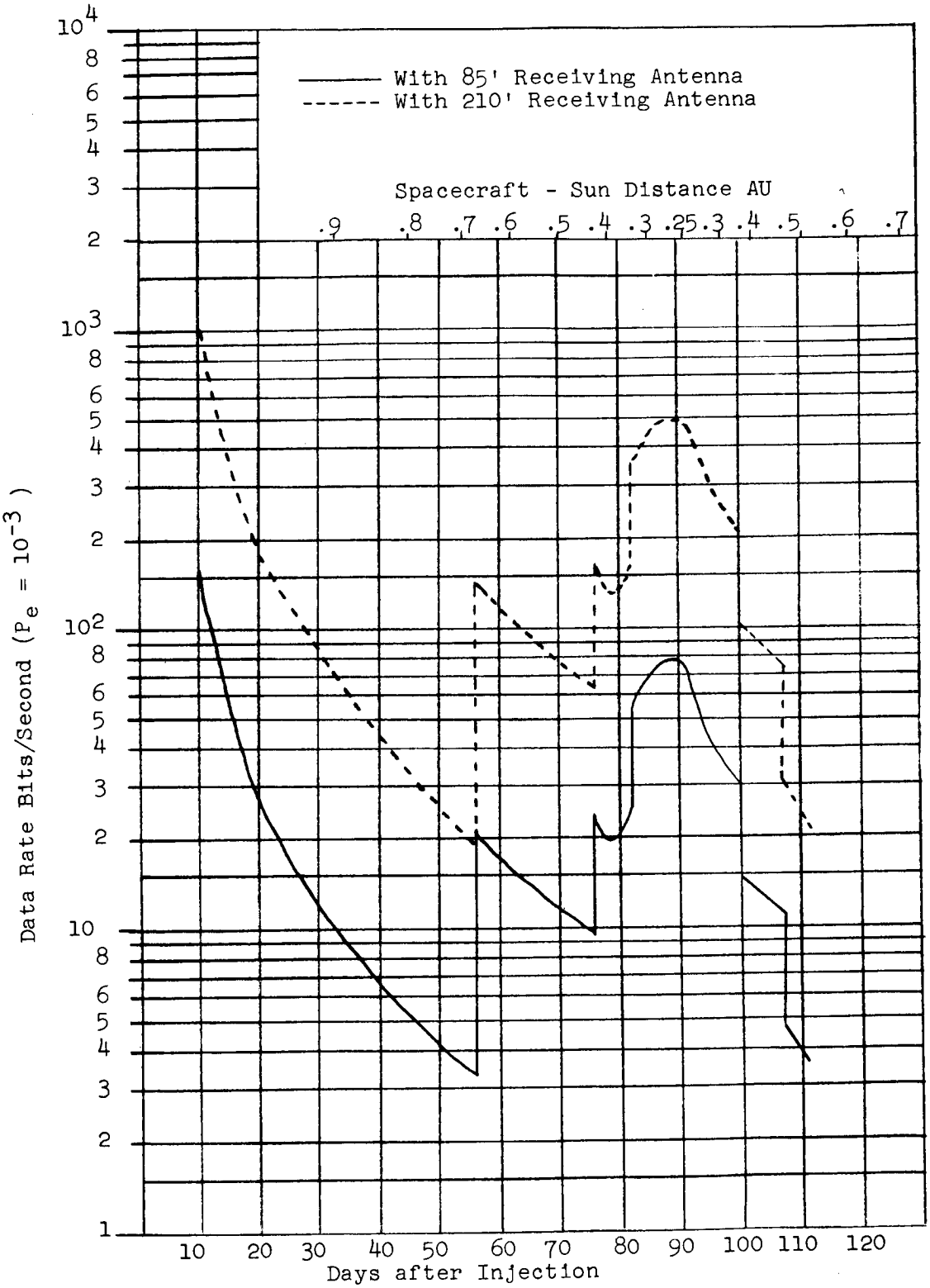

Figure 4B8.4 Data Rate vs Time after Injection for a 0.25 AU Perihelion 15° out of the Ecliptic

so that the spin axis is normal to the orbit plane.

The proposed solution to the communication problem for the out-of-the-ecliptic orbit requires transmission from the omni during the early part of the flight. When the spacecraft reaches a distance of 0.3 AU from the Sun, the transmission is switched to the fan-type antenna which has been modified. The modification produces a cone shaped antenna pattern which is adjusted for the specific out-of-the-ecliptic mission. The inclination angle of the cone (the angle between the unmodified antenna beam and the modified antenna beam) is adjusted to 10° and 20° out-of-the-ecliptic angles.* Figure 4B8.1 shows that these beamwidths will provide high gain and thus high data rates during the important portions of these missions. The modification of the antenna beam into a cone requires adjustment of the phasing arrangement of the antenna elements. If a second pass of the spacecraft is achieved, a 180° rotation is necessary so that high data rate transmission can occur from 0.1 AU to 0.3 AU.

The ICARUS program provides for at least one out-of-the-ecliptic trajectory of 15°. Although the perihelion distance for an in-the-ecliptic trajectory would be 0.2 AU, the result of injecting the spacecraft into a 15° out-of-the-ecliptic orbit produces a perihelion of 0.25 AU. For this orbit, the angle between the Earth-spacecraft line and the orbit plane as a function of time is shown in Fig. 4B8.1. The main beam of the high gain antenna has been altered to produce the pattern shown in Fig. 4B8.2 and the inclination cone angle of 15° as shown in Fig. 4B8.3. By using an upper "omni", which has been designed so that a gain of 3 db results, and the modified high gain antenna of Figs. 4B8.2 and 4B8.3, the data rate as a function of time was calculated and is shown in Figure 4B8.4

Table 4B8.2

Inclination angle to the ecliptic for elimination of communication "black out"

Perihelion (AU)	Inclination angle, θ to ecliptic (degrees)	Resultant Earth-Sun Earth s/c angle 1st "black out" (degrees)	Resultant Earth-Sun Earth s/c angle 2nd "black out" (degrees)
0.2	$\theta = 1.5$	1	0.55
0.2	$\theta = 3$	2	1.1
0.1	$\theta = 3.5$	1	0.42
0.1	$\theta = 7.1$	2	0.84

*10°, with 5° beam width, and 20°, with 7.5° beam width, respectively.

4B9. Data Storage

For any of the orbits considered for the solar probe there will be periods of time when communication with the Earth is restricted because of the Sun and lack of availability of tracking facilities. The on-board experiments require a minimum data rate of 32 bits per second. At this data rate the on-board tape recorder with 3×10^6 bits capacity can store all experimental data taken over a 24 hour period. Although the primary communication system does not depend on this storage (a slightly out-of-the-ecliptic orbit eliminates "black out") there are several other reasons for including the storage. Storage provides backup if partial limiting does occur. It allows easier and more flexible scheduling of the DSIF and it is needed if one of the ground stations fails for a short period of time.

4B10. Test Program

The communication subsystem is made up of components very similar to or identical to those used on the Pioneer. The TWTs are advanced models and are designed to meet NASA specifications. A minimum test program should be sufficient for the subsystem. The only area that might require significant investigation and testing is magnetic cleanliness. (This may be troublesome because of increased magnetic fields from the higher power TWTs.)

The antenna is a thermally redesigned Pioneer antenna with one omni removed and the magnetometer and VHF antenna added. There may be a need for thermal testing. The coating to reduce thermal effects may cause changes in the antenna pattern. These changes will have to be checked out and compensated for if they are present. The antenna for out-of-the-ecliptic orbits will require additional development and testing because of the different pattern requirements.

The tape recorder is flight tested and reliable. It should require no testing except for magnetic cleanliness.

REFERENCES

1. JPL,Technical Memorandum No. 33-83, April, 1964.
2. Space Communication, McGraw-Hill Book Co., New York, 1963.
3. Solar Probe Study, Book B, Appendix 5, NAS 2-1397 (Philco).
4. Lumb, Dr. Dale.: Personal Communication, NASA-AMES Research Center, System Engineering, Div.
5. Golomb, S.W., ed.: Digital Communications, Prentice-Hall, Inc., Englewood Cliffs, 1964.
6. Nozencraft, J.M., and Jocobs, I.M.: Principles of Communication Engineering, John Wiley & Sons, New York, 1965.
7. JPL, Technical Memorandum No. 33-83, System Capabilities and Development Schedule of the Deep Space Instrumentation Facility, 1964-68.
8. Rectin, Eberhard.: Personal Communication, Director DSIF of JPL.
9. Feldman, N.E.: Communication System Output Devices, The Rand Corporation, p. 2997-1, June, 1965.
10. Telephone Conversation and Correspondence with Watkins-Johnson Representative.

V. TRAJECTORIES AND LAUNCH VEHICLES

5A. Orbit Analysis

5A1. Introduction

The Sun, due to its mass being over one thousand times that of the largest planet, is the dominant gravitational field in the solar system. This means that in space a few million miles away from any planet, a spacecraft moves in a gravitational field closely resembling that of a simple central force field with the Sun as the main attracting body. Hence, the formulas and conclusions reached in two-body problem theory and the theory of transfer orbits in a single force field may be used with confidence in interplanetary operations. The correction necessary for the exact trajectory is small enough that it will not effect the choice of boosters or missions.

In those regions where the force field of both the Earth and the Sun are approximately of the same order of intensity, and for precision studies, special perturbation techniques must be used to determine the orbit of a spacecraft. However, for preliminary design and/or feasibility studies the approximate methods, such as those mentioned above, can be used. By using sphere of influence arguments (1), it can be reasoned that when the spacecraft is within 0.00619 astronomical units (AU) of the Earth, the Earth is the dominant influencing body, while for distances greater than 0.00619 AU, the Sun is the dominant body.

Hence, a mission from the surface of the Earth to a region between 0.10 and 0.20 AU of the Sun can be broken into two phases:

1) Ascent from the surface of the Earth to the boundary of the sphere of influence. This phase is known as the hyperbolic escape from the geocentric orbit.

2) Transfer into heliocentric space to the region of the Sun.

It is the purpose of this section to determine the velocity requirements necessary to inject a spacecraft into a heliocentric orbit about the Sun with a perihelion distance ranging between 0.10 and 0.20 AU. Motion both in and out of the ecliptic plane will be considered. The use of direct ascent and parking orbits will also be investigated. In addition, the effect of errors in the injection velocity on the interplanetary orbit will be determined.

5A2. Motion in the Ecliptic Plane

In this section, the spacecraft will be assumed moving in the ecliptic plane. In the first portion the heliocentric orbit will be considered, while in the second portion the hyperbolic escape phase will be considered.

Heliocentric Orbit

Figure 5A2.1 shows the heliocentric orbit in question, namely, one which has an aphelion distance, r_A, equal to the distance of the Earth from the Sun, a perihelion distance, r_p, equal to the closest approach of the spacecraft to the Sun, and f, the true anomaly or angle between perihelion and the Sun-vehicle line. If the orbit of the Earth about the Sun is taken to be circular, then, the velocity of the Earth is given by

$$V_E = \left[\frac{GM_s}{r_A}\right]^{1/2} \qquad 5A2.1$$

where

G is the universal gravitation constant
M_s is the mass of the Sun

Now

$$GM_s = \mu = 4.68679 \times 10^{21} ft^3/sec^2 = 1.327 \times 10^{11} km^3/sec^2$$

and

$$r_A = 93 \times 10^6 \text{ miles} = 150 \times 10^6 km$$

hence,

$$V_E = 97,702 \text{ ft/sec} = 29.77 \text{ km/sec} \qquad 5A2.2$$

The distance of the spacecraft from the Sun is given by

$$r = \frac{a(1-e^2)}{1+e\cos f} \qquad 5A2.3$$

where

a is the semi-major axis
e is the eccentricity
f is the true anomaly, measured from perihelion

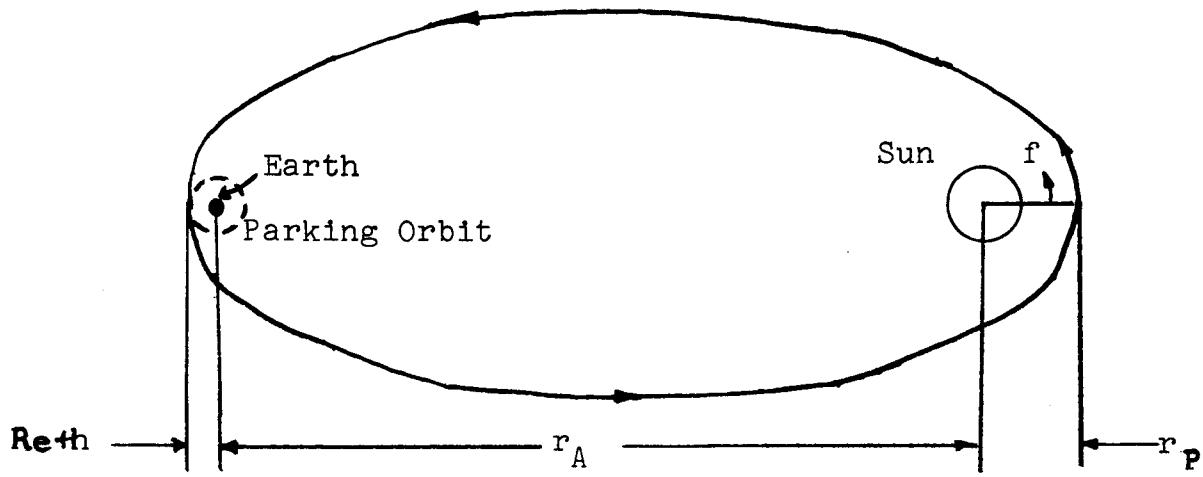

r_P = perihelion distance

r_A = aphelion distance

f = true anomaly (Angle between perihelion and the spacecraft)

R_e = radius of Earth

h = altitude of the parking orbit

Figure 5A2.1 Heliocentric Orbit of the Spacecraft

At perihelion f = 0, hence, the distance from the Sun becomes

$$r_p = a(1-e) \qquad 5A2.4$$

while at aphelion f = 180° and the distance from the Sun becomes

$$r_A = a(1+e) \qquad 5A2.5$$

These two equations combine to give

$$\frac{r_A}{r_p} = \frac{1+e}{1-e} \qquad 5A2.6$$

or, upon solving this equation for e we obtain

$$e = \frac{r_A - r_p}{r_A + r_p} \qquad 5A2.7$$

The velocity at any point in the heliocentric elliptic orbit is given by

$$V^2 = \mu\left(\frac{2}{r} - \frac{1}{a}\right) \qquad 5A2.8$$

If Eq. 5A2.4 is substituted into Eq. 5A2.8 then the velocity at perihelion is found to be given by

$$V_p^2 = \frac{\mu}{a}\left(\frac{1+e}{1-e}\right) \qquad 5A2.9$$

Similarly, by substituting Eq. 5A2.5 into Eq. 5A2.8 the velocity at aphelion is obtained as

$$V_A^2 = \frac{\mu}{a}\left(\frac{1-e}{1+e}\right) \qquad 5A2.10$$

The time for the spacecraft to go from its "launch" point at aphelion to a point nearest the Sun is given by

$$\tau = \frac{T}{2} = \pi\left[\frac{a^3}{\mu}\right]^{1/2} \qquad 5A2.11$$

Figure 5A2.2 shows a plot of the eccentricity, the velocities at aphelion and perihelion, and the time to go from aphelion to perihelion as a function of the perihelion distance, r_p. This information will be useful in making booster selections in the consideration of trade-off costs.

Geocentric Orbit

The orbit dynamics of a solar probe involves essentially escape from the Earth and then motion about the central body, the Sun. In the previous section the motion of a spacecraft about the Sun was investigated. Now the escape phase of the mission will be investigated.

It is well known that motion about a central body may be either elliptical, parabolic, or hyperbolic. In general, however, motion will be elliptical in order to minimize energy. It is also well known, from two-body theory, that escape from a body involves in the limiting case, parabolic velocity. However, a parabolic orbit would require a longer time in order to escape, hence, in general, hyperbolic orbits are used to provide escape from the Earth's attraction.

The velocity for a spacecraft moving along a hyperbolic orbit is given by

$$V^2 = \mu\left(\frac{2}{r} + \frac{1}{a}\right) \qquad 5A2.12$$

at $r = \infty$, the escape distance from the Earth, the velocity becomes

$$V_\infty^2 = \frac{\mu}{a} \qquad 5A2.13$$

This velocity is often called the hyperbolic excess velocity. Hence, the velocity at any point along the hyperbolic orbit is given by

$$V^2 = \frac{2\mu}{r} + V_\infty^2 \qquad 5A2.14$$

Of importance in this problem is the velocity required at burnout in order to inject the spacecraft into a hyperbolic orbit. This velocity will be denoted by V_b and can be obtained from Eq. 5A2.14.

By inspection of Eq. 5A2.14 it is seen that as the radius vector increases, the actual velocity approaches the hyperbolic excess velocity. Similarly, the distance between the hyperbola and the asymptote becomes small as r increases.

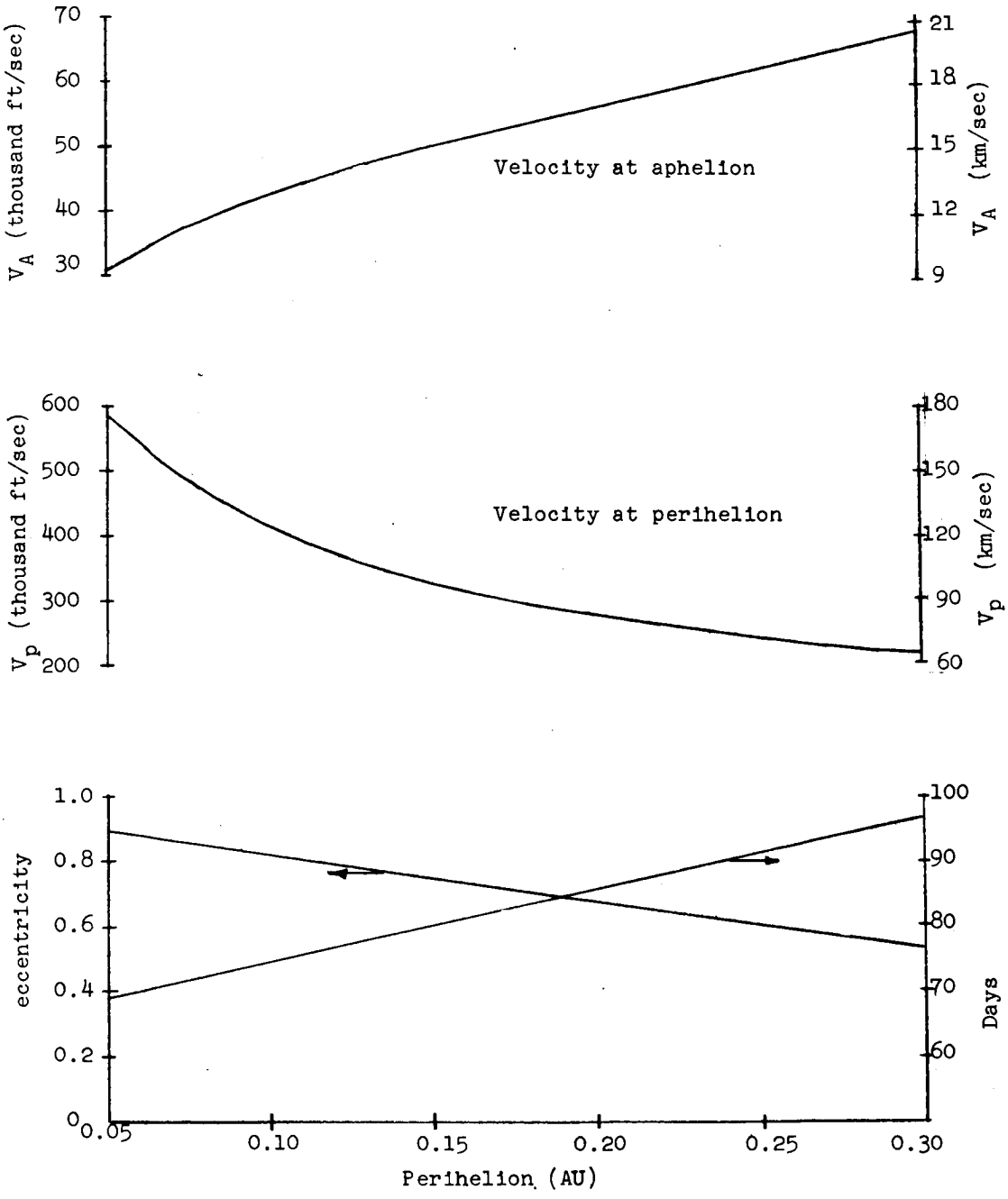
70
60
50
40
30
V_A (thousand ft/sec)
Velocity at aphelion
21
18
15
12
9
V_A (km/sec)
600
500
400
300
200
V_p (thousand ft/sec)
Velocity at perihelion
180
150
120
90
60
V_p (km/sec)
1.0
0.8
0.6
0.4
0.2
0
eccentricity
100
90
80
70
60
Days
0.05
0.10
0.15
0.20
0.25
0.30
Perihelion (AU)

Figure 5A2.2

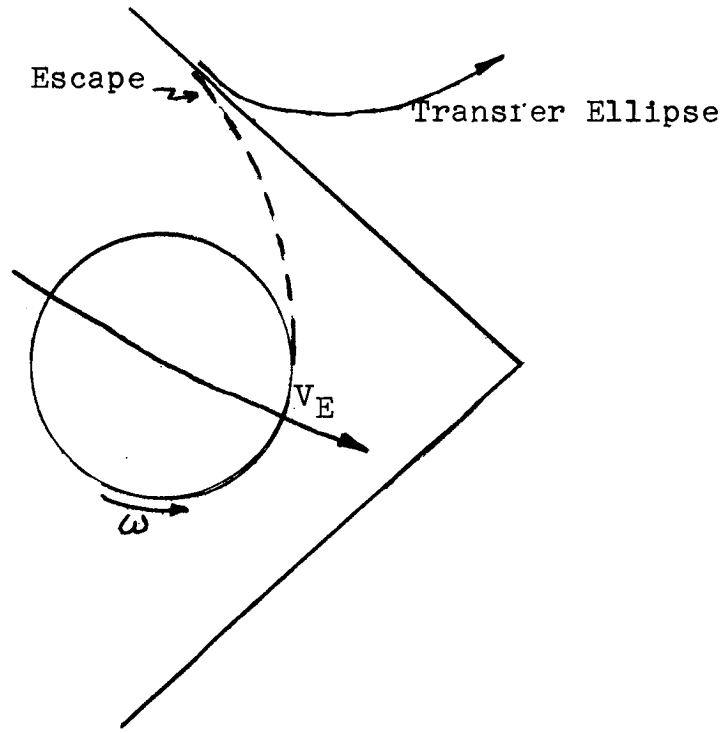

Figure 5A2.3 Axis orientation for escape from earth

Hence, at large values of r we can safely assume that the body is moving along the asymptote at the hyperbolic excess velocity.

In the present case, the Earth is assumed to be moving about the Sun in a circular orbit. In addition, the Earth is also rotating. In order to take advantage of the Earth's motion the vehicle is launched as shown in Fig. 5A2.3. From this figure and from the considerations of minimum energy transfer it is evident that the escape portion of the hyperbola must be oriented nearly parallel to the Earth's velocity vector about the Sun. Hence, for this inferior transfer V_∞ subtracts from the orbital velocity of the Earth. That is

$$V_t = V_E - V_\infty \qquad 5A2.15$$

where V_t denotes the transfer velocity. Since transfer takes place at aphelion of the heliocentric ellipse, then $V_t = V_A$ and from Eq. 5A2.15

$$V_\infty = V_E - V_A \qquad 5A2.16$$

For initial estimates it is also safe to assume that

$$r_t = r_A$$

and

$$f_t = f_A$$

Figure 5A2.4 shows values of V_∞ as a function of r_p.

Direct Ascent

In order to obtain the booster requirements for launch, the "ideal velocity" of the rocket, that is, the velocity of a rocket without gravity or drag losses, required to launch the vehicle into the escape hyperbola is necessary.

The energy equation within the sphere of influence of the earth is given by Eq. 5A2.14. If the burnout velocity, V_b, is assumed to take place on the surface of the Earth, then

$$V_b^2 = V_\infty^2 + \frac{2\mu}{R_E} \qquad 5A2.17$$

where in this case $\mu = GM_E = 1.408 \times 10^{16}$ ft^3/sec^2 = 3.986×10^5 km^3/sec^2.

Figure 5A2.4 shows how the injection velocity, V_b, varies as a function of r_p. From this plot it is seen that for a 0.10 AU mission an injection velocity of around 67,000 ft/sec (20.4 km/sec) is required. At 0.20 AU the injection velocity is seen to fall off to about 55,000 ft/sec (16.6 km/sec). The meaning of these injection velocities, in terms of booster requirements and payload capabilities, will be discussed later.

Parking Orbits

In most interplanetary, lunar, and orbital flights, performance optimization and systems considerations have shown that it is usually most efficient to park in a low altitude orbit and at the proper location to inject into the transfer orbit. For round trip missions, these parking orbits can be used as storage dumps about the Earth and destination planet. In addition these orbits could be used in order to check out any equipment and to make any necessary corrections to the orbit before launch into its transfer orbit. From many previous studies (1) a parking orbit of around 100 nautical miles has been found to be ideal. For this reason the velocity requirements for transfer from a 100 n.mi. circular orbit into a hyperbolic orbit will be determined.

Consider the situation as shown in Fig. 5A2.5. From the conservation of energy

$$\frac{V^2}{2} - \frac{GM_E}{\rho_0} = \frac{V_\infty^2}{2} - \frac{GM}{\rho_\infty} \approx \frac{V_\infty^2}{2} \qquad 5A2.18$$

Now,

$$V = V_c + \Delta V \qquad 5A2.19$$

where ΔV is the velocity increment required to transfer from the circular orbit into the hyperbolic escape orbit. If Eq. 5A2.19 is substituted into Eq. 5A2.18

$$\Delta V = \left[\frac{2GM_E}{\rho_0} + V_\infty^2\right]^{1/2} - V_c \qquad 5A2.20$$

Figure 5A2.6 contains a plot of ΔV as a function of the perihelion distance for transfer out of a 100 n.m. circular parking orbit. Here it is seen that a ΔV of around 41,500 ft/sec (12.65 km/sec) is required for a 0.10 AU mission while only 30,000 ft/sec (9.15 km/sec) is required for a 0.20 AU mission.

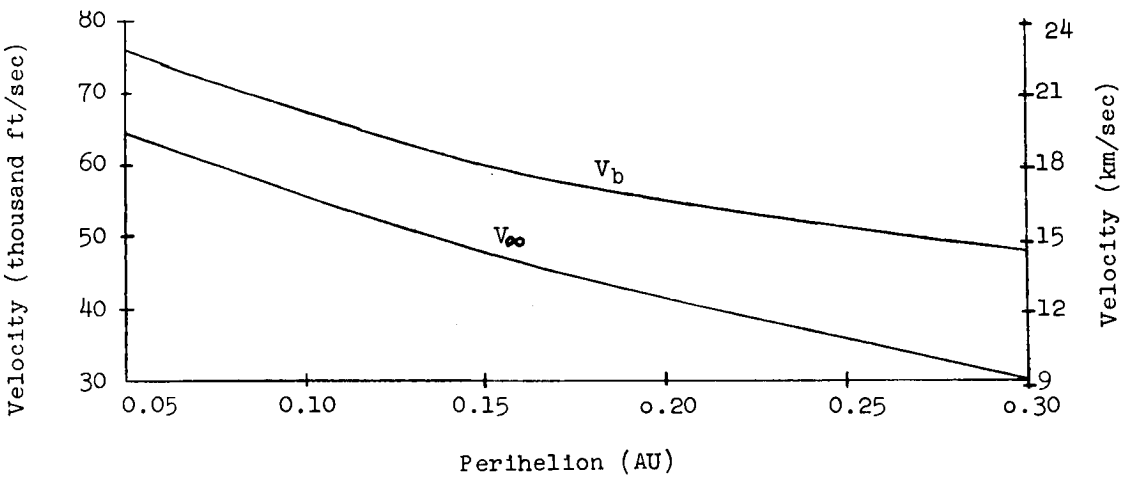

Figure 5A2.4 Velocity requirements for direct ascent

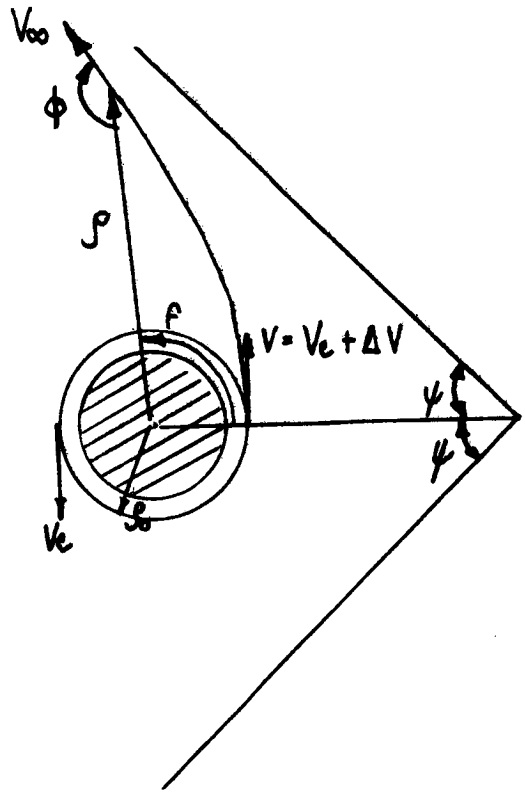

Figure 5A2.5 Transfer from a parking orbit

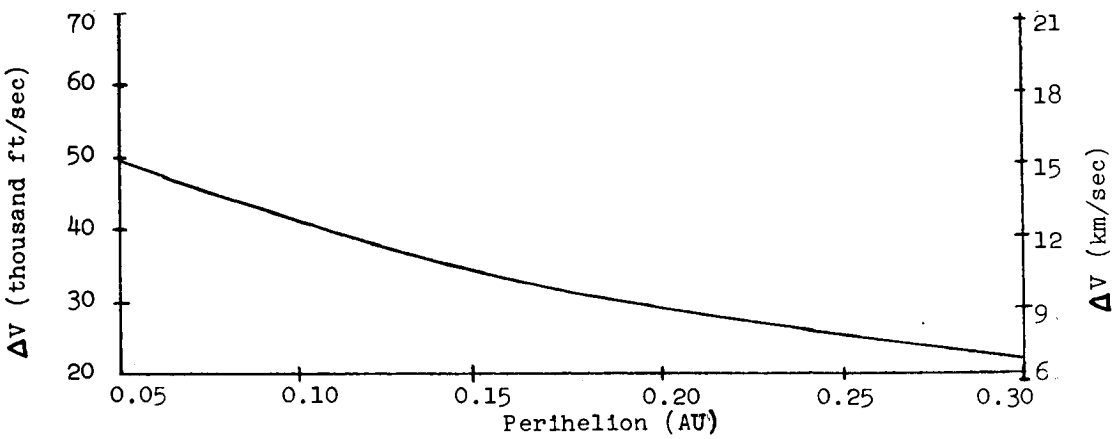

Figure 5A2.6 Impulse velocity to transfer from a 100 n.m. parking orbit

Position versus Time for the Heliocentric Orbit.

The equation describing the radial distance, r, of the spacecraft from the Sun is given by

$$r = \frac{a(1-e^2)}{1+e\cos f} \qquad 5A2.21$$

The time required for the spacecraft to go from perihelion, f = 0, to any other point on the orbit can be shown (4) to be given by

$$t = \frac{a^{3/2}}{\sqrt{\mu}}\left[2\tan^{-1}\left(\sqrt{\frac{1-e}{1+e}}\tan\frac{f}{2}\right) - \frac{e\sqrt{1-e^2}\sin f}{1+e\cos f}\right] \qquad 5A2.22$$

This equation in non-dimensional form, $\tau = \frac{t_e\sqrt{\mu}}{2\pi a^{3/2}}$, is shown plotted in reference (4). Hence by utilizing that plot along with Eq. 5A2.21 a time plot of the position of the spacecraft is obtained. These time plots are shown in Fig. 5A2.7 for both the 0.10 and 0.20 AU missions. The respective times are 74.5 and 85 days to reach perihelion and gives some indication of equipment reliability requirements.

For communication purposes it is necessary to know the trajectory of the spacecraft with respect to the Earth-Sun line. Fig. 5A2.8 shows this trajectory for two complete orbits of the spacecraft about the Sun. Again, only 0.10 and 0.20 AU missions are shown.

5A3. Motion out of the Ecliptic Plane

In the previous sections the velocity requirements for orbital missions in the plane of the ecliptic were considered. In this section the requirements for motion out of the ecliptic plane will be determined.

Figure 5A3.1 shows the relationship between the ecliptic plane and the spacecraft's orbit plane. The angle of inclination between the two planes is denoted by i.

The heliocentric orbit in this case is the same as for motion in the plane of the ecliptic. Hence, the velocities at aphelion and perihelion, the eccentricity, and the time of flight from aphelion to perihelion can all be obtained from Fig. 5A2.2.

As for the geocentric orbit, much of what was said earlier can also be said here. However, Eq. 5A2.16 in this case must be written as a vector equation, namely,

$$\bar{V}_\infty = \bar{V}_E - \bar{V}_A \qquad 5A3.1$$

In this case the excess hyperbolic velocity is given by

$$V_\infty = \left[(V_E - V_A \cos i)^2 + V_A^2 \sin^2 i \right]^{1/2} \qquad 5A3.2$$

and the burnout velocity for direct ascent is given by

$$V_b^2 = V_\infty^2 + \frac{2\mu}{R_E} \qquad 5A3.3$$

where

$$\mu = G M_E$$

Figures 5A3.2 and 5A3.3 show plots of V_∞ and V_b as functions r_p and i. By use of these plots it is possible to translate the results into booster requirements and payload capabilities. This will be done in a later section.

5A4. Effect of Injection Velocity Errors on Perihelion

It can be shown without much difficulty, see for instance reference 1, that an error in the injection velocity and hence, an error in the velocity at aphelion can be translated into errors in perihelion distance by the following expression, namely.

$$\frac{\Delta r_p}{r_p} = \frac{4}{1+e} \frac{\Delta V_A}{V_A} = - \frac{4}{1+e} \frac{V_b}{V_\infty} \frac{\Delta V_b}{V_A}$$

Hence, an error of -100 ft/sec in injection velocity results in a Δr_p of 6×10^{-4} AU, a negligible quantity.

5A5. Discussion on the Use of Gravity Assists

Niehoff (5) presents some analytical and numerical results of gravity assisted trajectories to the Sun. Niehoff shows that a large reduction in ideal velocity can be achieved by a Jupiter swing-by. A comparison of the velocity requirements and time of flight for a direct flight and for Jupiter fly-by missions is shown in the table below.

θ (deg)	10	20	40	60	80	100	120	140	160	180
$t_{\odot}$ (days)	19	42	60	68	70	72	73	73½	74	74½
$t_{\triangle}$ (days)	15	32	54	66	73	77	80	82	84	85

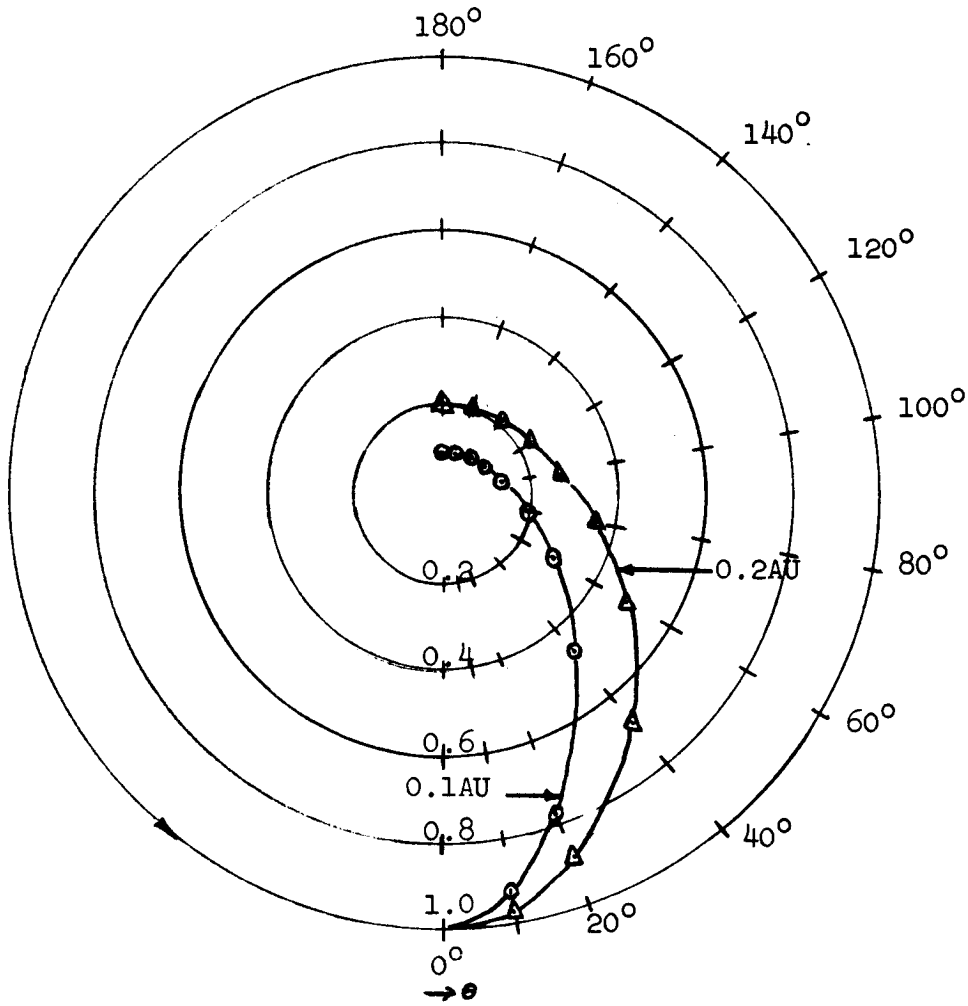

Figure 5A2.7 Heliocentric orbits

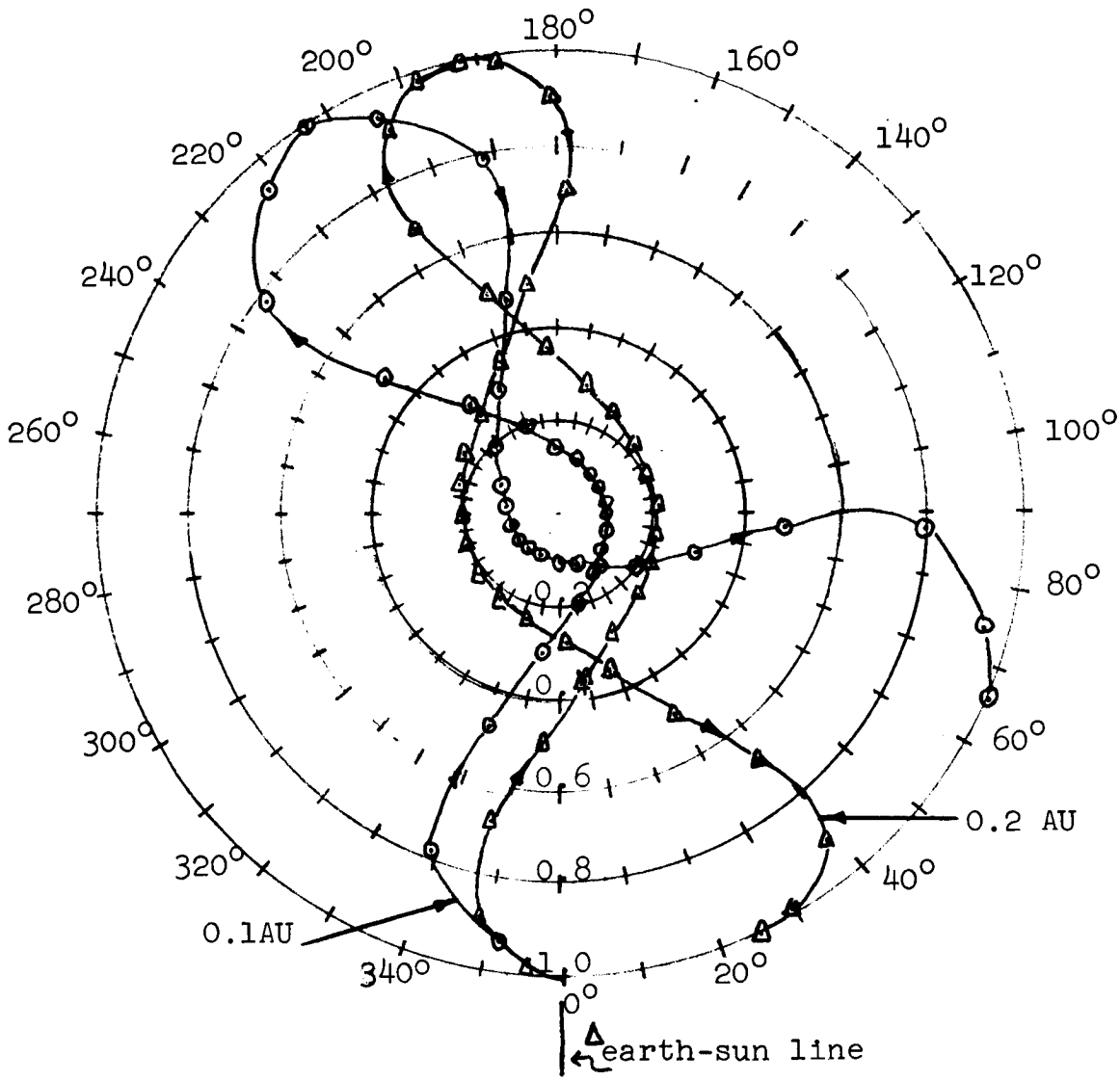

Figure 5A2.8 Trajectory relative to earth-sun line

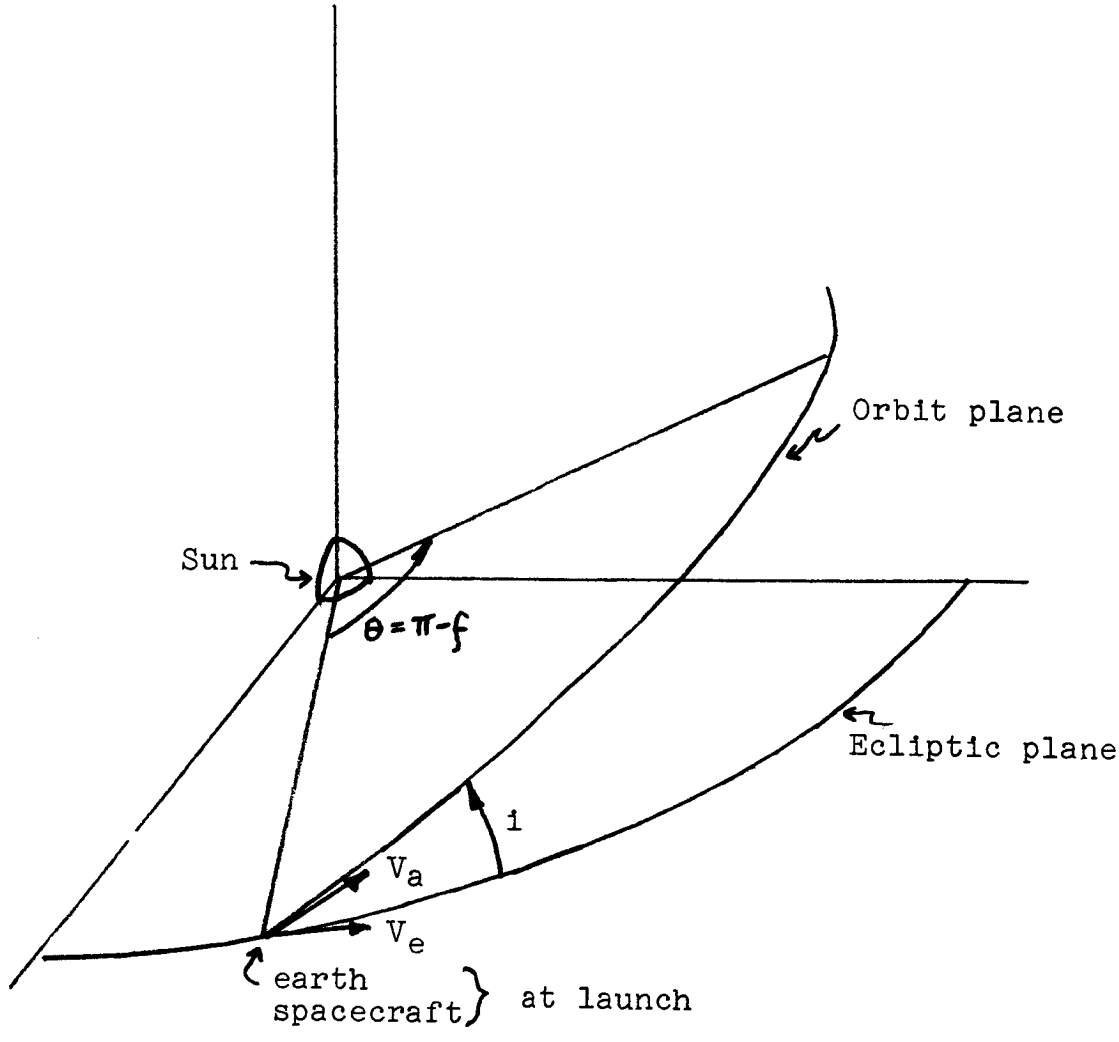

Figure 5A3.1
Motion out of the Ecliptic Plane

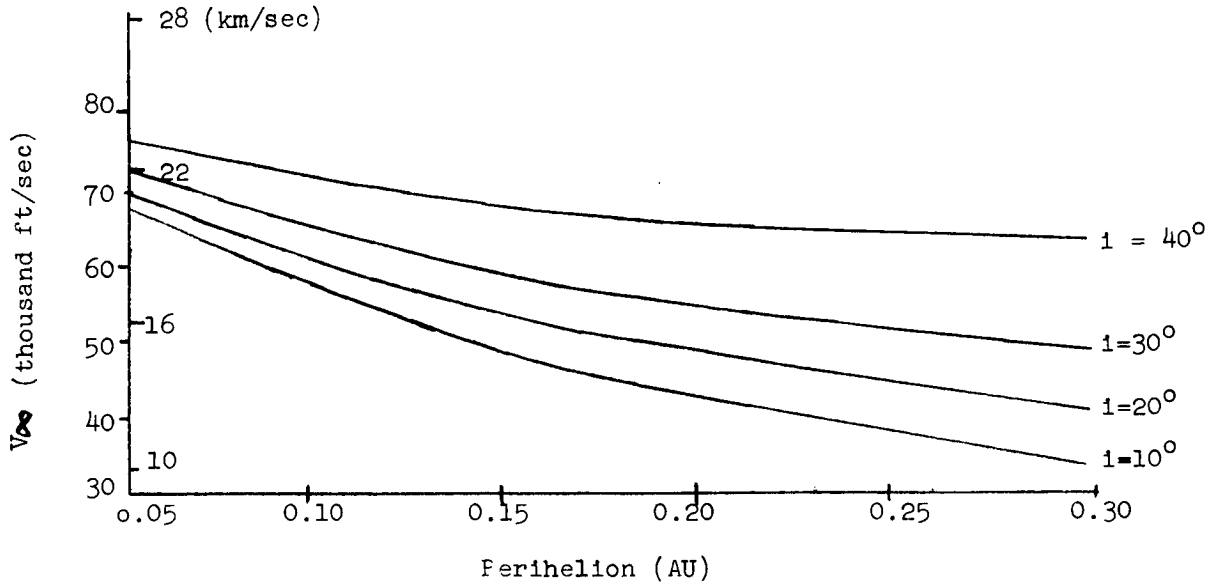

Figure 5A3.2 V_∞ as a function of r_p and i

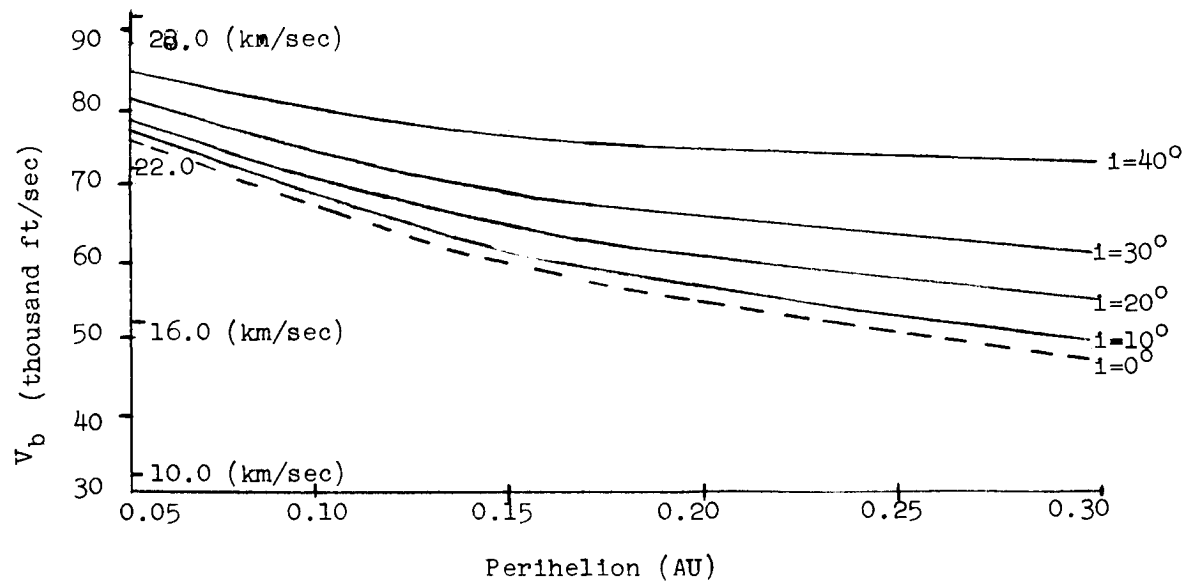

Figure 5A3.3 Injection velocity as a function of r_p and i

Table 5A5.1

Perihelion (AU)	Direct Flight Mission: Total Velocity Required (ft/sec)	Direct Flight Mission: Time of Flight (days)	Jupiter Fly-by Mission: Total Velocity Required (ft/sec)	Jupiter Fly-by Mission: Time of Flight (days)
0.5	40,000	120	46,500	1570
0.4	43,000	110	47,000	1520
0.3	48,000	95	47,500	1475
0.2	55,000	90	48,000	1420
0.1	66,500	75	48,500	1350
0.05	76,700	72.5	49,000	1310
Solar Impact	104,000	70	50,000	1270

While launch opportunities occur yearly for the Earth-Jupiter-Sun probe mission, long trip times, on the order of three years, decrease spacecraft reliability and present the hazard of having to go through the asteroid belt twice. In fact, as much as 400 days of the trip could be spent in the asteroid belt. In view of these uncertainties it is proposed that for the 0.2 AU regime direct flight missions be utilized. For flights in the regime 0.2 AU to 0.1 AU direct flight missions are technically feasible with existing boosters. It may be, however, that by 1970 the Jupiter fly-by technique will be developed not only for solar probe missions but also for 90^{o} out of the ecliptic missions, for Jupiter exploration, and for flights to the remote planets. If this is the case then economic considerations at that time may favor the Jupiter fly-by technique as the approach for exploring the near solar regime between 0.2 AU and solar impact.

Time considerations did not allow a study of possible uses of either Venus or Mercury for gravity assists to the Sun. However, the added complexity and weight penalties that might be required for accurate guidance to these planets may well rule them out also.

5B. Launch Vehicle

Launch vehicle ideal velocities required to obtain perihelions of interest are between 50,000 and 70,000 ft/sec. (See Fig. 5A2.4 and 5A3.3). The payload is a "Pioneer-like" spin stabilized spacecraft which weighs between 150 and 250 pounds. Thus, only those lauch vehicles which perform within these general weight and velocity constraints have been considered. General performance capabilities for several launch vehicles are shown in Fig. 5B1.1. This information has been compiled from several sources listed in thc references, but the bulk is from reference (6).

The cost of the launch vehicle is an equally important consideration. Table 5B1.1 lists the estimated 1970-1975 production costs of various launch vehicles which can perform within the weight and velocity ranges of interest. (The present Thor/Delta and Improved Thor/Delta are shown for reference use only.) It is apparent that launch vehicle costs for a 0.2 AU mission will be about 4 times as large as those of the present Pioneer (0.8 AU), and about 12 times as large for the 0.1 AU mission.

Figure 5B1.1 shows four vehicles whose performance characteristics penetrate the region of interest: Atlas/Centaur/Kick, Saturn IB/Centaur, Saturn IB/Centaur/Kick, and Saturn V. The Atlas/Centaur/Kick combination is the least expensive booster capable of the 0.2 AU mission. Unfortunately the kick stage referred to in Fig. 5B1.1 is a hydrogen-fluorine propelled 7000 lb. thrust vehicle which will not be available during this program. (It, in fact, may never be developed.) Thus, use of the Atlas/Centaur vehicle hinges upon the availability of an adequate kick stage, or stages.

A review of all the current kick stages revealed three satisfactory candidates. They are: (1) X-259-A3, the third stage on the existing Scout vehicle, (2) FW-4S, the fourth stage on the existing Scout vehicle, and (3) TE-364-3, the retro-rocket on the existing Surveyor lunar vehicle. All three of these are solid propellant rockets. Important specifications of these stages are summarized below.

	Stage Designation	Average Thrust(lbs)	Vacuum Isp-sec	Initial Weight(lbs)	Burnout Weight(lbs)
1.	X-259-A3	22,620	280	2780	200
2.	FW-4S	5,940	284	660	52
3.	TE-364-3	6,100	288	1585	130

Information contained in the above chart was used in the "rocket equation"

$$\Delta V = (I_{sp} \cdot g_o) \ln\left(\frac{W_1}{W_2}\right) \qquad 5B1.1$$

to obtain ideal velocities as a function of payload for each of these stages. The equations are:

Stage Designation	Equation	
X-259-A3	$\Delta V = 9050 \ln\left(\frac{2800+P}{220+P}\right)$	5B1.2
FW-4S	$\Delta V = 9150 \ln\left(\frac{680+P}{72+P}\right)$	5B1.3
TE-364-3	$\Delta V = 9260 \ln\left(\frac{1605+P}{150+P}\right)$	5B1.4

These equations allow 20 lbs for rocket to payload interstage structure in addition to P, the weight of the payload. The calculations are summarized in Table 5B1.2. Total launch vehicle velocities were obtained by adding the kick stage ideal velocity to the "correct" Atlas (SLV-3X)/Centaur velocity. Total velocities using the X-259-A3 are slightly higher than those using the TE-364-3 for payload wieghts above 200 lbs., and both are better than the FW-4S.

It is possible to obtain an additional increase in velocity by "stacking" various combinations of kick stages. The three combinations shown below are the most effective. Scaled sketches of these combinations are shown in Fig. 5B1.2.

	Combination A	Combination B	Combination C
Stage 3	TE-364-3	X-259-A3	X-259-A3
Stage 4	FW-4S	FW-4S	Te-364-3
Ignition Weight(lbs)	2375 + P	3600 + P	4500 + P

where P is payload weight

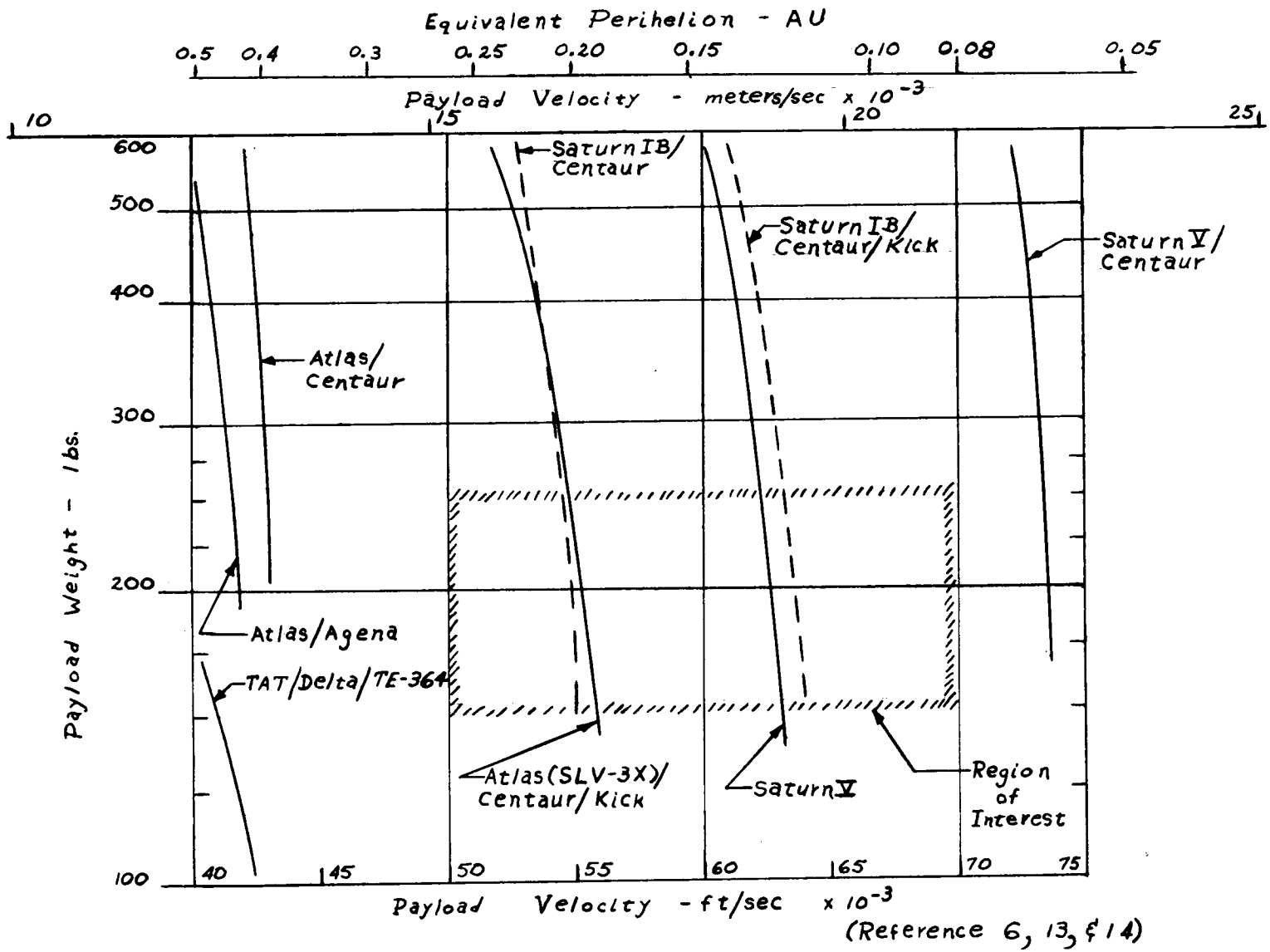

(Reference 6, 13, & 14)

Figure 5B1.1 Typical Booster Performance

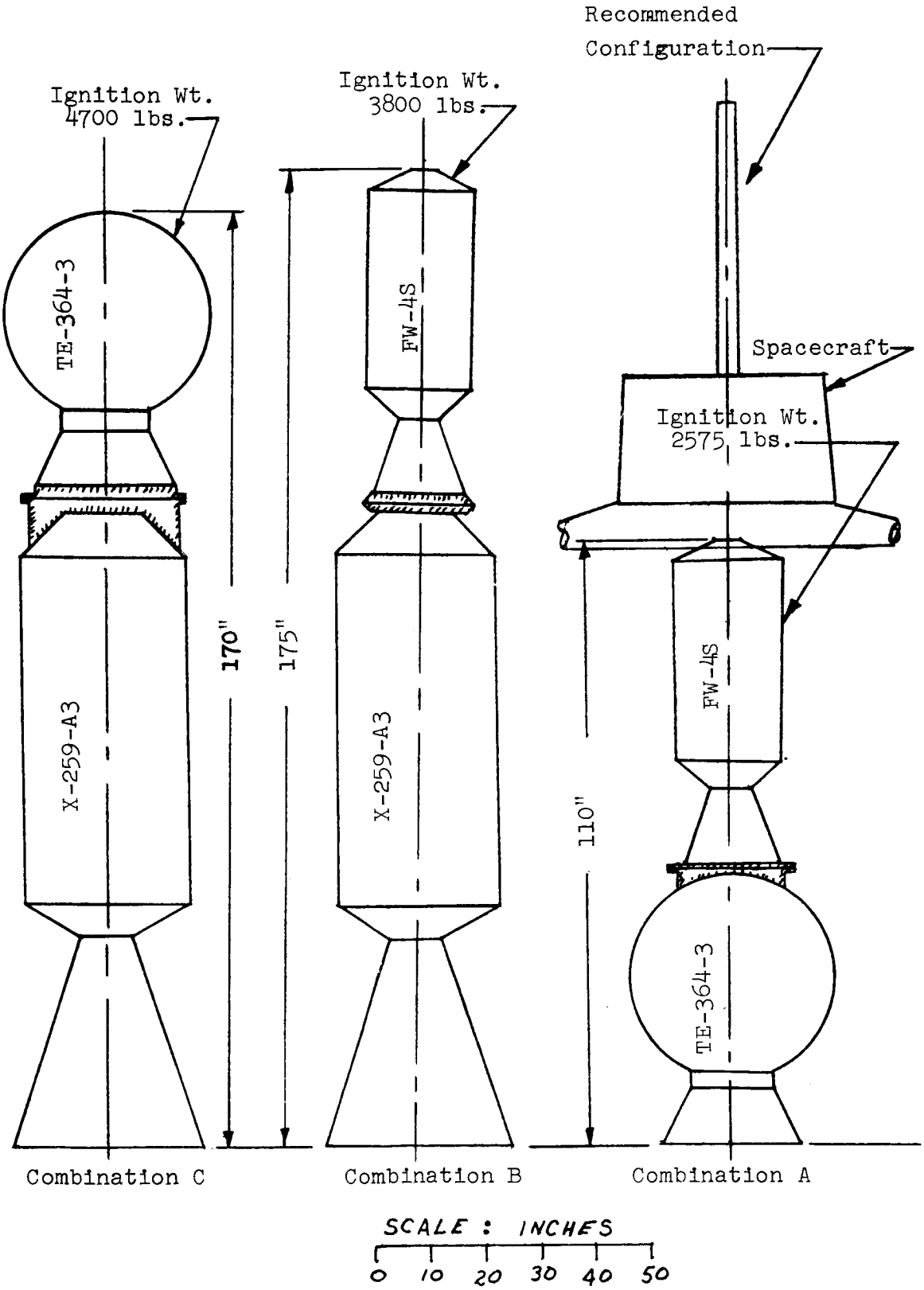

Figure 5B1.2 Possible Kick Stage Assembly Configurations

Table 5B1.1

ESTIMATED COSTS - LAUNCH VEHICLES

Vehicle	Production Cost* (in millions of dollars)
THOR/DELTA	2.5
TAT/DELTA/TE-364-3	3.5
ATLAS/AGENA	8.6
ATLAS/CENTAUR	12.0
ATLAS/CENTAUR/KICK**	16.0
SATURN IB/CENTAUR***	41.0
SATURN IB/CENTAUR/KICK**	45.0
SATURN V	125.0

* Does not include development costs

** A theoretical high energy kick stage which assumes use of a 7000 lb thrust hydrogen-fluorine propulsion system

*** The Titan III C/Centaur system utilizing two seven segment solid "strap-on" rockets has about the same cost and payload capability as the Saturn IB/Centaur system.

Table 5B1.2

Stage Designation	Payload wt. in lbs.	Ignition wt. in lbs.	Stage ΔV -ft/sec	Total ΔV -ft/sec
X-259-A3	400	3200	14,830	50,930
"	350	3150	15,450	51,650
"	300	3100	16,150	52,450
"	250	3050	16,970	53,370
"	200	3000	17,800	54,300
"	150	2950	18,850	55,400
"	100	2900	20,000	56,600
FW-4S	400	1080	7,720	48,520
	350	1030	8,350	49,250
	300	980	9,040	50,090
	250	930	9,910	51,110
	200	880	11,000	52,400
	150	830	12,390	53,900
	100	780	14,210	55,800
TE-364-3	400	2005	11,950	50,500
	350	1955	12,600	51,250
	300	1905	13,350	52,150
	250	1855	14,200	53,150
	200	1805	15,200	54,250
	150	1755	16,400	55,550
	100	1705	17,850	57,100

A comparison of the performance of these "combination kick stages" and the three single kick stages is shown below.

Number of Rockets	Stage Designation	Ignition Weight (Lbs) ‡	Total Vehicle Velocity - ft/sec ‡
2	Combination A	2575	56,000
2	Combination B	3775	56,100
2	Combination C	4675	55,700
1	FW-4S	880	52,400
1	TE-364-3	1805	54,250
1	X-259-A3	3000	54,300

‡ (These figures were derived on the basis of a 200 lb. payload, 20 lbs. of structure between the last stage and payload, and a 75 lb. structure between the third stage and fourth stage.) Combinations A and B both yield a velocity gain of about 1700 ft/sec over the best "single rocket" kick stage, and the velocity gain grows to about 2200 ft/sec for a 150 lb payload.

Combination A is the best of the "combination kick stages" for the following reasons:

a) delivers maximum velocity for payloads of 150-200 lbs
b) occupies smallest volume
c) contains minimum weight

The small volume of combination A will fit inside a modified Surveyor fairing while B and C would require a completely new fairing. The weight of Combination A reduces the task of distributing booster acceleration loads to the Centaur structure. (The Centaur structure needs to be reinforced whenever the weight it carries is greater than 3500 lbs.)

Performance characteristics of the Combination A assembly are tabulated in Table 5B1.3. The corresponding payload injection velocities for the Atlas (SLV-3X)/Centaur booster and the Saturn IB/Centaur booster are shown in Figures 5B1.3 and 5B1.4 respectively. The data is tabulated for two interstage (structure)weights, 50 lb and 100 lb, because the performance is rather sensitive to this parameter.

The best "single kick stage" of the three satisfactory candidates is the TE-364-3. The arguments offered for selection of this stage over the other two are identical to those arguements put forth for Combination A. In addition, the present Surveyor fairing would serve without modification.

The choice between the TE-364-3 kick stage and the Combination A kick stage assembly must include consideration of the velocity performance of each. The single kick stage has an obvious advantage in terms of size, weight, and reliability which it buys at the expense of performance. Typical performance parameters for the two kick stage candidates are shown below. (A payload of 160 lbs is assumed.)

Kick Stage	Burnout Velocity ft/sec	Orbit Perihelion AU	Orbit Inclination
Combination A	57,500	0.172 0.227	0° 15°
TE-364-3 (single stage)	55,300	0.194 0.256	0° 15°

The two stage Combination A weighs 800 pounds more than the single stage TE-364-3, but is still well within the structural weight limits of the Centaur. Other factors which favor the Combination A kick stage assembly are accessibility of the interstage structure and utilization of existing Pioneer attachment geometry. Fairing considerations favor slightly the choice of the single kick stage because the Centaur Surveyor fairing would fit this assembly. However, all things considered, the final choice is for the maximum performance vehicle, the Combination A kick stage assembly.

Payload fairing and interstage geometry are shown in Fig. 5B1.5. The existing Surveyor fairing must be extended 60 inches (80 inch extensions are permitted) to cover the Combination A kick stage and payload. A new spin table must be developed to fit on the Centaur (near Station 160.0). A spin table patterned after the Thor/Delta would weigh about 100 lbs. Spin table experience gathered from the Thor/Delta and Scout vehicles should make this a "state-of-the-art" design that requires little development testing. Centaur to third stage separation will be accomplished by an explosive band clamp and centrifugally opening "petal leaves". Third stage to fourth stage separation will be accomplished as it is presently being done on the Scout. The "spin-up" mechanism is a combination of several PET rockets arranged on the upper surface of the spin table. The exact number of PETS is determined by the spin moment of inertia and the desired angular velocity. A thrust dispersion analysis must be performed to determine the necessary spin rates, but there are no obvious reasons for spin velocities to exceed those of the Thor/Delta or Scout, i.e. 100 to 160 rpm.

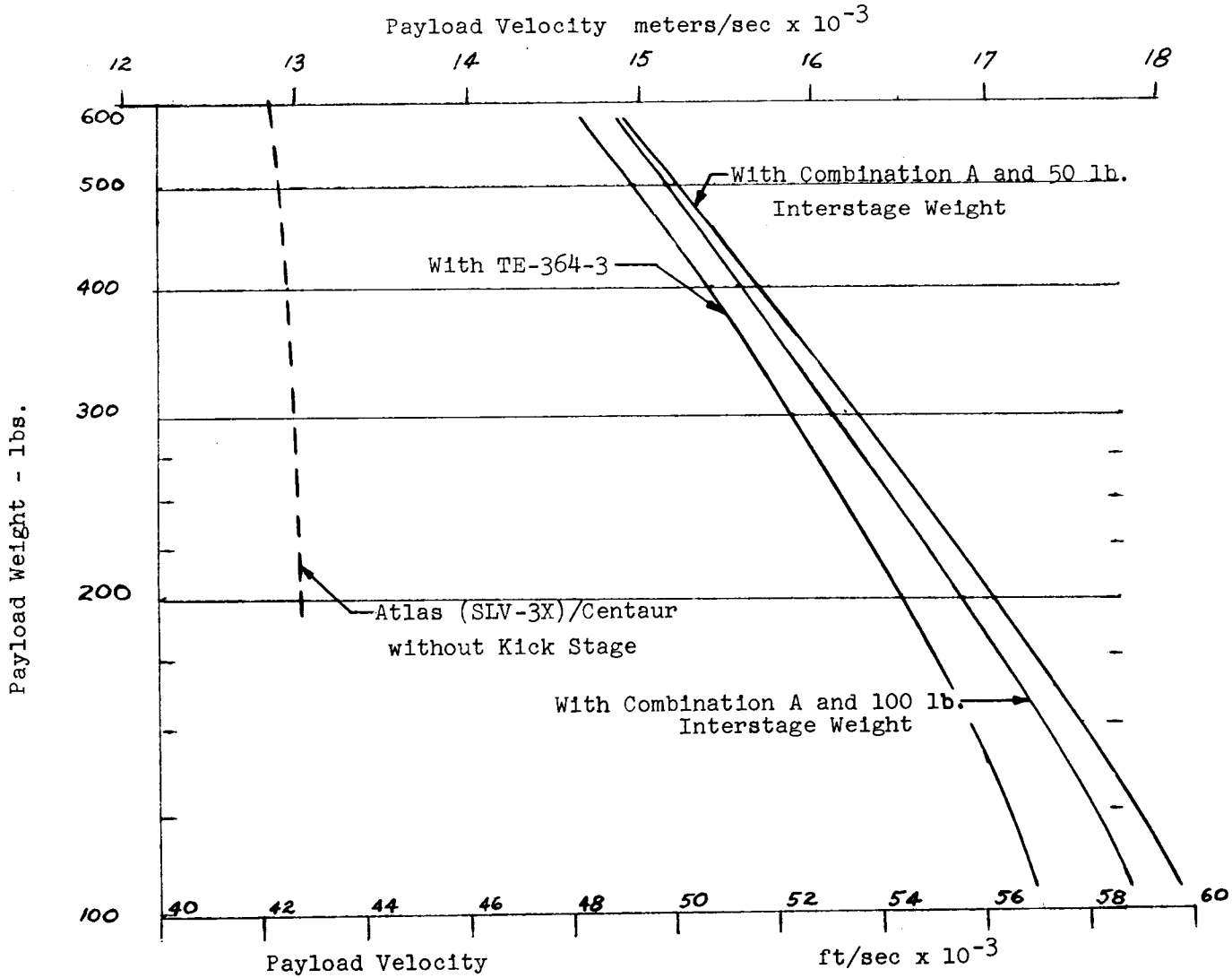

Figure 5B1.3 Payload Velocity with Atlas Booster

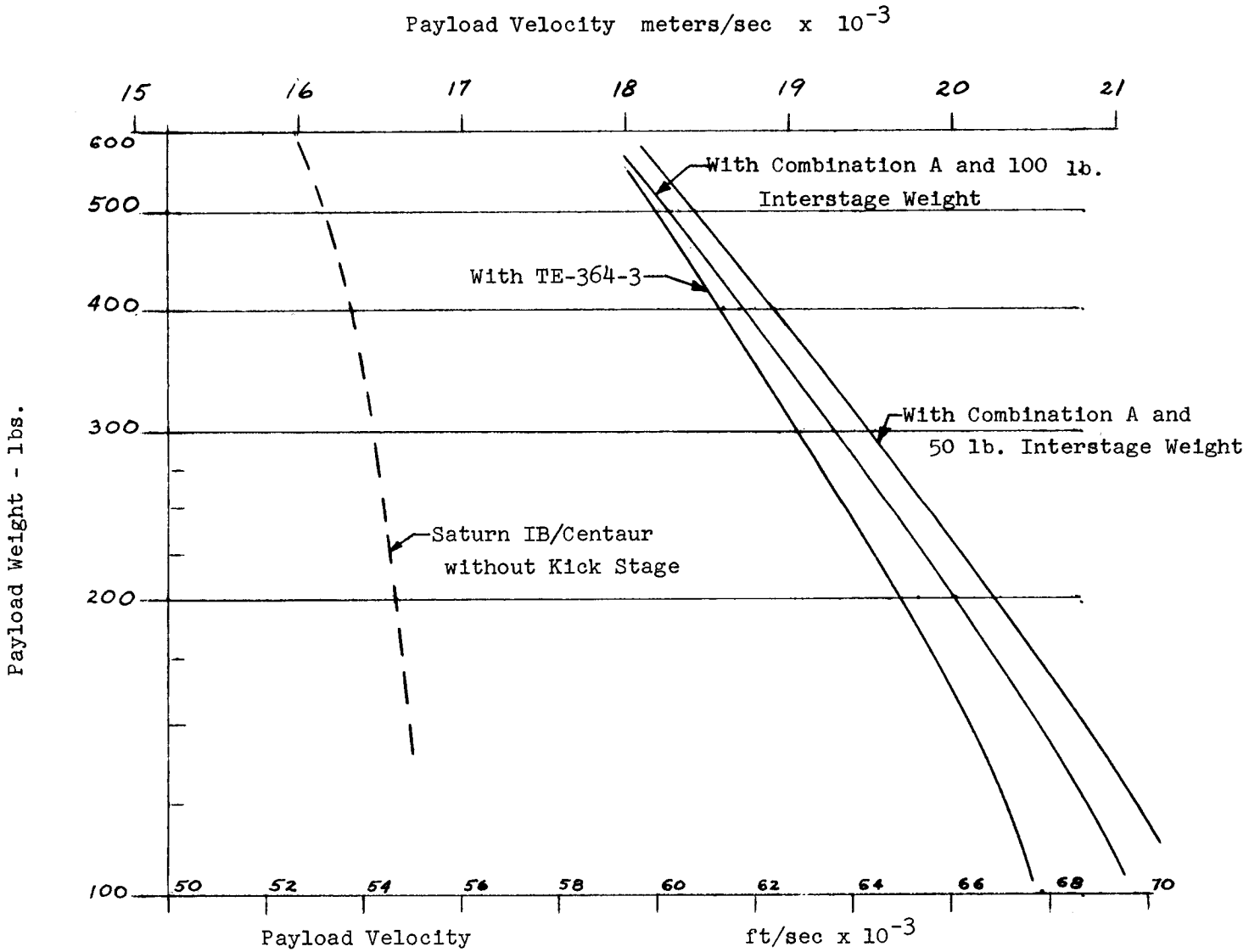

Figure 5B1.4 Payload Velocity with Saturn IB Booster

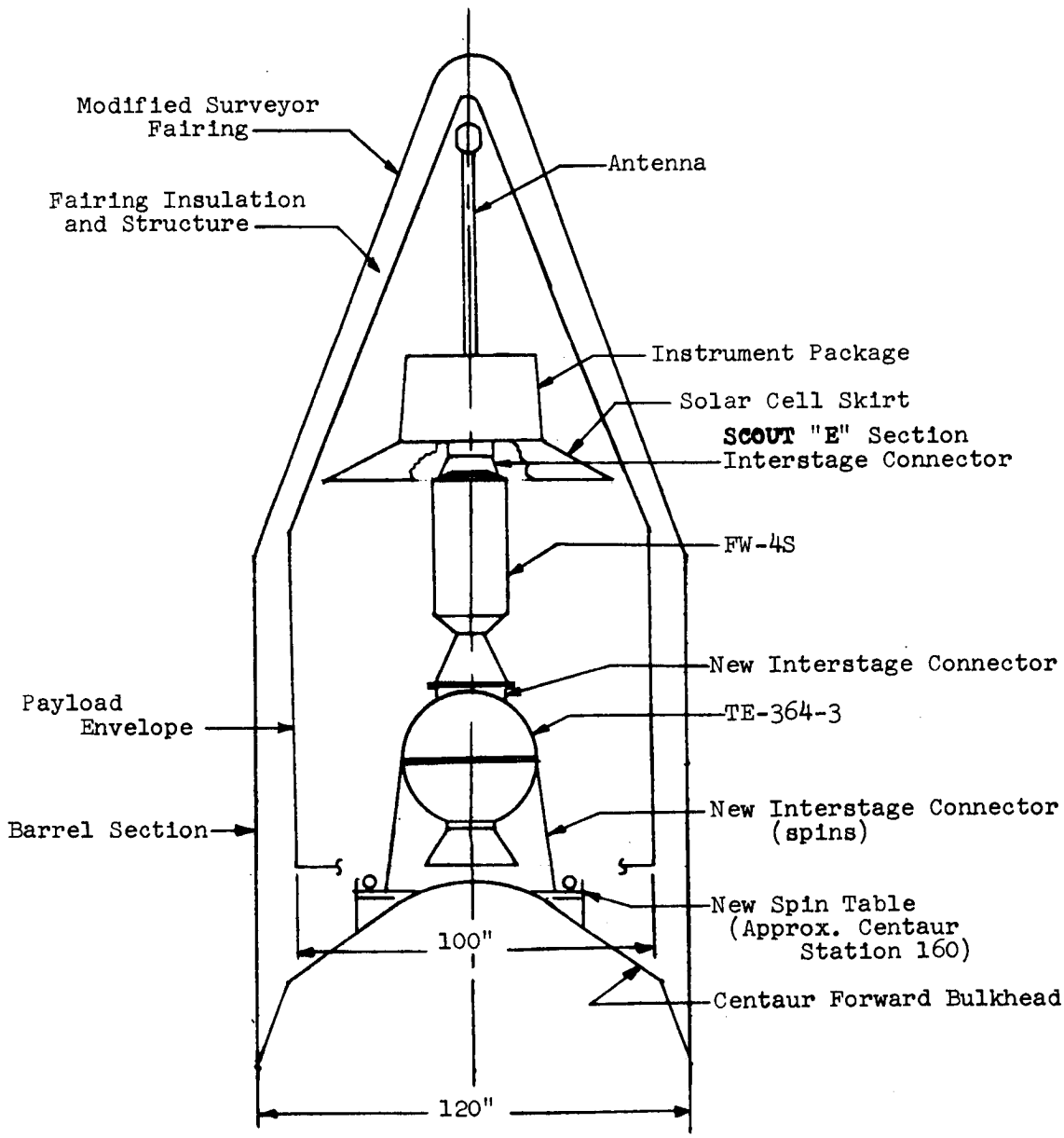

Figure 5B1.5 Fairing and Upper Stage Geometry

Table 5B1.3

COMBINATION A KICK STAGES IDEAL VELOCITIES
100 lb Interstage Structure

Payload wt. in lbs.	Ignition wt. in lbs.	Combination A ΔV - ft/sec	Total ΔV ft/sec
600	2975	12,120	48,520
500	2875	13,240	49,740
400	2775	14,420	51,120
300	2675	16,070	53,020
200	2575	18,430	55,530
100	2475	21,960	59,210
	50 lb. Interstage Structure		
600	2925	12,140	48,700
500	2825	13,340	49,920
400	2725	14,770	51,595
300	2625	16,520	53,545
200	2525	18,900	56,075
100	2425	22,650	59,975

A typical sequence of events for a direct ascent injection is shown for reference use below: (Atlas/Centaur/ TE-364-3/FW-4S)

Time (sec)	Event
00	Liftoff. Roll occurs for first 15 seconds
15	Pitch starts for zero-lift path
85	Maximum dynamic pressure
156	BECO-Booster engine cutoff
159	Booster package jettisoned
172	Centaur insulation jettisoned
223	Centaur payload fairing jettisoned (solar cell power available)
235	SECO-Sustainer engine cutoff
240	VECO-Vernier engine cutoff
241	Centaur stage separates
249	Centaur main engine start
625	Centaur cutoff
628	Centaur orientation
640	Spin up
641	Centaur package jettisoned
642	Third stage ignition
710	Third stage burnout
713	Third stage jettisoned
714	Fourth stage ignition
742	Maximum thrust acceleration (approximately 26 g's)
745	Fourth stage burnout
755	Fourth stage jettisoned

Typical Saturn IB/Centaur boost parameters are shown in Fig. 5B1.6. The peak values are comparable to those of the Atlas/ Centaur booster. Shock and vibration loads placed on the payload by the last stage (FW-4S) can be found in The Scout, reference (10).

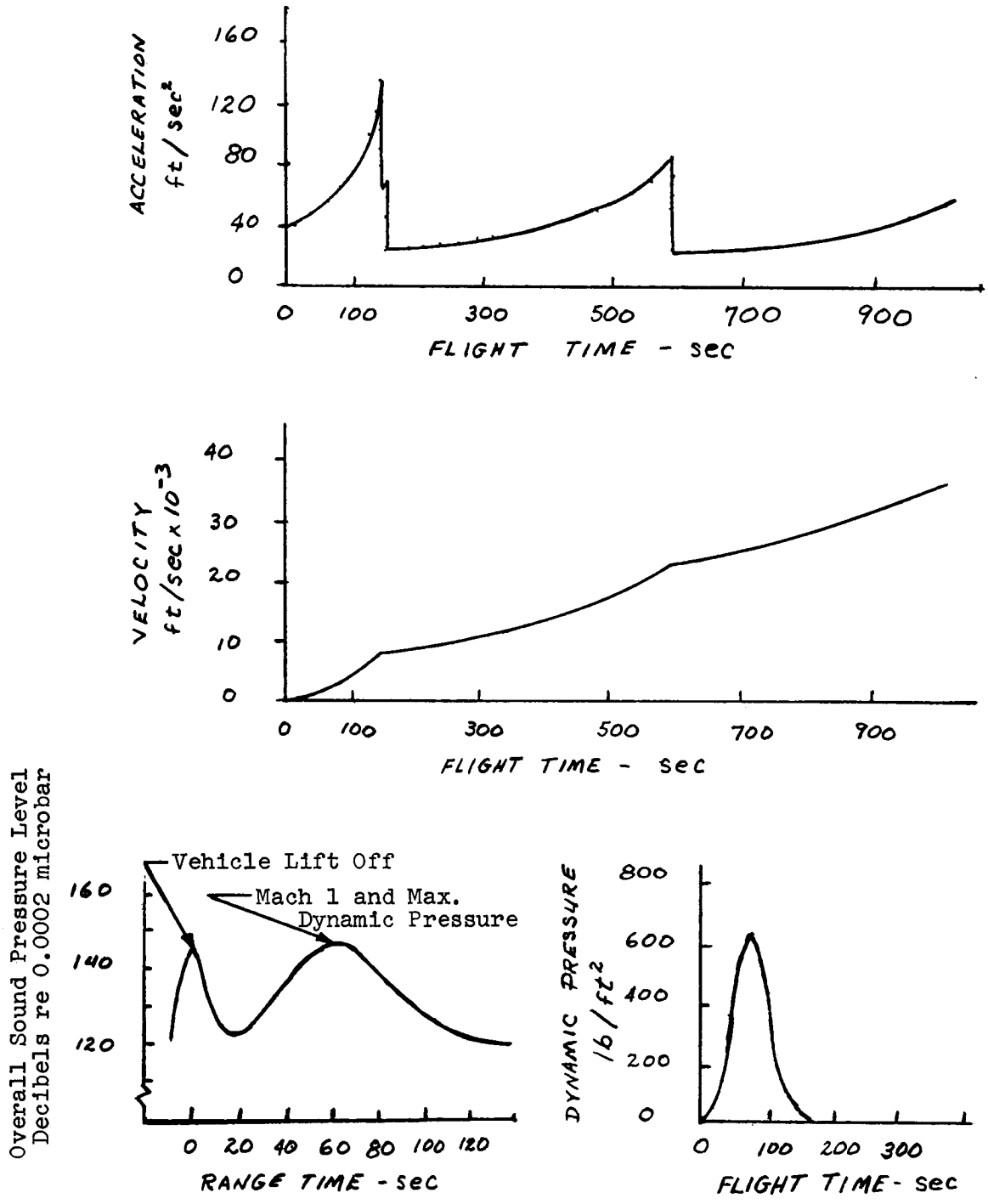

Figure 5B1.6 Typical Saturn IB/Centaur Trajectory Parameters

REFERENCES

1. Roy, A.E.: Foundations of Astrodynamics, The MacMillan Co., New York, 1965.
2. Battin, R.H.: Astronautical Guidance, McGraw-Hill Book Co., New York, 1964.
3. White, J.F., ed.: Flight Performance Handbook for Powered Flight Operations, John Wiley & Son, Inc., 1963.
4. Thomson, W.T.: Introduction to Space Dynamics, John Wiley & Sons, New York, 1961.
5. Niehoff, J.C.: An Analysis of Gravity Assisted Trajectories to Solar System Targets, American Institute of Aeronautics and Astronautics 3rd Aerospace Sciences Meeting, New York, 24-26 Jan. 1966, AIAA Paper No. 66-10.
6. Kovit, Bernard.: The Coming Kick Stage, Space/Aeronautics, p. 55-61, August, 1965.
7. Kolseth, J.B.: Thixotropic Propellant Would Cut Rocket Size, Space/Aeronautics, p. 86-87, Nov., 1965.
8. Perry, D.J.: Centaur Performance for Unmanned Mars Missions, an unpublished lecture delivered at Stanford in 1965.
9. Convair Division of General Dynamics, Atlas Familiarization Handbook, Report No. GDC-BG3 66-002, June, 1966.
10. LTV Aerospace Corporation, The Scout, October, 1965.
11. vonBraun, W.: Saturn Rocket Systems and Space Exploration, an unpublished lecture delivered at Stanford in 1965.
12. Philco Western Development Laboratories, Solar Probe Study, WDL-TR 2133, August, 1963.
13. 1966 NASA Authorization, U.S. Government Printing Office Publication 47-600-65-pt. 3-40.
14. Jorther, D., and Martinez, J.J.: System and Mission Considerations for a Radioisotope Propulsion System (POODLE), STL-5M-0024, a paper presented at an AIAA meeting, June, 1965.

VI. MECHANICAL DESIGN OF SPACECRAFT

6A. Spacecraft Configuration

6A1. Selection of Configuration

In order to select the spacecraft configuration, it was necessary to satisfy certain requirements established by termal control primarily, and power generation, experiments, and communication to a lesser degree. Many design alternatives were considered - for example, spinning or nonspinning vehicle, solar cells or solar thermoelectric or RTG power supplies, parabolic or fanbeam antenna, shielded or unshielded spacecraft, articulated or non-articulated concept, etc. The final spacecraft configuartion is presented in the following paragraphs.

6A2. Spacecraft Dimensions

An overall view of ICARUS is shown in Fig. 2D1.1 with dimensions given in Fig. 6A2.1 and Fig 6A2.2. The spacecraft consists essentially of a conical body containing the experiments of a conical solar cell array supplying the power. Differing power requirements for 0.1 AU and 0.2 AU perihelion missions necessitate changes in the solar cell array. This is discussed in detail in Section 6D.

6A3. Spacecraft Weight Data

The anticipated weight data for ICARUS is given in Table 6A3.1. The table is based on the 0.2 AU mission. For the 0.1 AU mission, the solar cell power supply and supporting structure increase 2.73 kg (6.0 lb) in weight, giving a total spacecraft weight of 74.26 kg (163.35 lb). Realizing that this report constitutes only a preliminary design for a flight in Spring 1971, many of the weights should be taken as engineering estimates. Nevertheless the data is believed to represent reasonable estimates, and clearly shows that a 0.1 - 0.2 AU mission spacecraft can be built for considerably less than 200 pounds gross weight.

Table 6A3.1

STRUCTURE	WEIGHT	
	kilograms	pounds
Bottom Equipment Platform	1.91	4.20
Top Equipment Platform	1.27	2.80
Thrust Cylinder	0.91	2.0
Interstage Support Ring	0.08	0.18
Payload Fitting	0.44	0.97
Antenna Supports	0.45	1.00
Wobble Damper	0.23	0.50

Table 6A3.1 (continued)

Solar Cell Connecting Ring	1.36	3.0
Solar Cell Supporting Structure	4.28	9.4
Hardware	0.55	1.2
	12.53	27.55
SOLAR CELL ARRAY		
Cells, Glass, etc.	6.82	15.0
	6.82	15.0
ORIENTATION		
Nitrogen Bottle and Support	1.35	2.97
Nitrogen	0.65	1.43
Valve (Solenoid)	0.2	0.44
Regulator	0.45	1.00
Nozzle	0.0045	0.01
Pressure Transducer	0.095	0.21
Pressure Switch	0.054	0.12
Plumbing and Supports	0.21	0.46
Logic	0.445	0.98
Fill Valve	0.09	0.21
Sun Sensors	0.5	1.10
	4.05	8.93
THERMAL CONTROL		
Bottom Louvers	1.28	2.82
Top Louvers	1.17	2.58
Insulation	2.50	5.50
Optical Solar Reflector	0.70	1.54
	5.65	12.44
ELECTRICAL POWER		
Battery	0.91	2.00
3 watt TWT Converter	0.46	1.01
100 watt TWT Converter	4.6	10.12
Power Conditioner	2.73	6.00
	8.70	19.13
ELECTRICAL DISTRIBUTION		
Cabling	1.82	4.00
	1.82	4.00

Table 6A3.1 (continued)

DATA HANDLING		
Central Data Process	5.45	12.00
	5.45	12.00
COMMUNICATIONS		
Receivers (2)	2.27	5.00
Transmitter Driver	1.36	3.00
3 watt TWT	0.36	0.79
20/50 watt TWT and Converter	3.19	7.00
100 watt TWT	1.14	2.50
Diplexers (2)	0.91	2.00
Tape Recorder	1.36	3.00
Coax Switches (6)	0.55	1.21
Power Divider	0.27	0.60
Fan-beam Antenna	0.915	2.00
Omnidirectional Antenna (2)	0.91	2.00
	13.23	29.10
TOTAL SPACECRAFT WEIGHT WITHOUT EXPERIMENTS	58.25	128.15
EXPERIMENTS		
Magnetometer Inboard	2.27	5.0
Magnetometer Sensor	0.34	0.75
Plasma Probe	2.0	4.4
Cosmic Ray	2.0	4.4
Neutron Phoswich Inboard	3.3	7.25
Neutron Phoswich Outboard	1.1	2.4
VHF Radio Propagation	2.27	5.0
	13.28	29.2
TOTAL SPACECRAFT WEIGHT	71.53	157.35

6A4. Spacecraft Mass Distribution and Moments of Inertia

Most of the necessary equipment for the opeation of ICARUS is mounted on the bottom and top platforms. The top plate carries only those components which must be provided a view outside the spacecraft; the equipment distribution is shown on Fig. 6A4.1. The bottom plate carries the remaining components, as shown on Fig. 6A4.2 and Table 6A4.1.

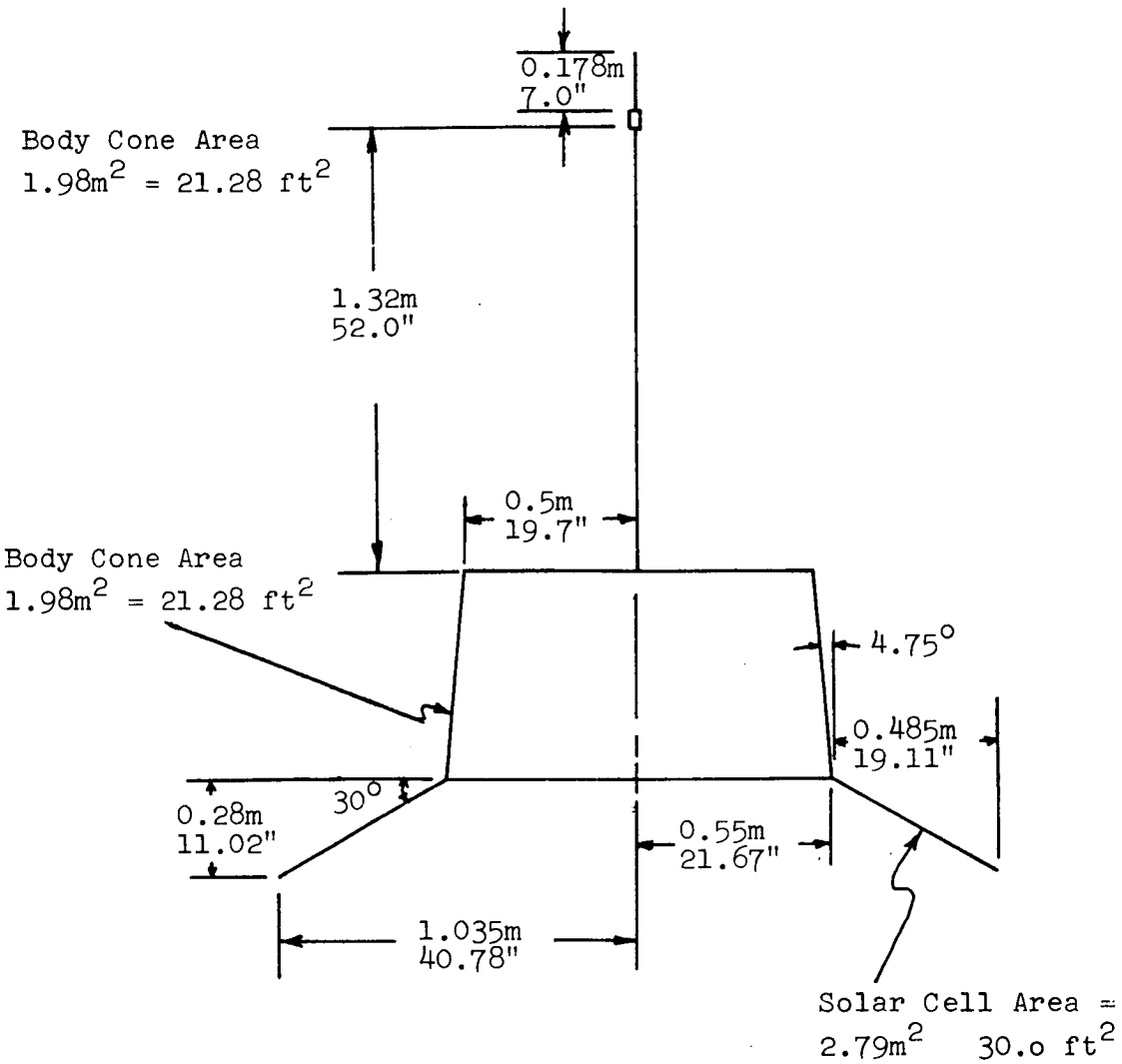

Figure 6A2.1 Dimensions for 0.2 AU Spacecraft

Since the spacecraft is spin stabilized, it must be both statically and dynamically balanced. Static balance means that the spacecraft center of gravity (c.g.) must be located on the spin axis, while dynamic balance implies that the line of maximum principal moment of inertia must be parallel to the spin axis. To help achieve these requirements, the weights on each plate have been positioned so that the equipment c.g. is on the spin axis. Furthermore, it is desirable to locate the nitrogen gas system c.g. at the spacecraft c.g. so that utilization of the gas will not change the location of the spacecraft c.g.

Figure 6A4.3 shows the location of the spacecraft c.g. for both the 0.1 and 0.2 AU missions. The moments of inertia with respect to axes through the c.g. are also recorded on that figure. (See Figure 7B1.2 for the ICARUS coordinate system.)

Table 6A4.1

Bottom Plate Equipment Identification Table

Equipment Number	Item	Equipment Number	Item
1	3 watt TWT	11	Diplexer
2	3 watt TWT & Power Converter	12	Coax Switch
3	Coax Switch	13	20 watt TWT & Power Converter
4	100 watt TWT	14	Coax Switch
5	100 watt TWT & Power Converter	15	Central Data Processor
6	Coax Switch	16	VHF Radio Propagation
7	Transmitter Driver	17	Battery
8	Power Divider	18	Tape recorder
9	Fluxgate Magnetometer	19	Diplexer
10	Neutron Phoswich (I)	20	Coax Switch
		21	Coax Switch

Table 6A4.1 (continued)

Equipment Number	Item	Equipment Number	Item
22	Power Conditioner	24	Receiver
23	Receiver		

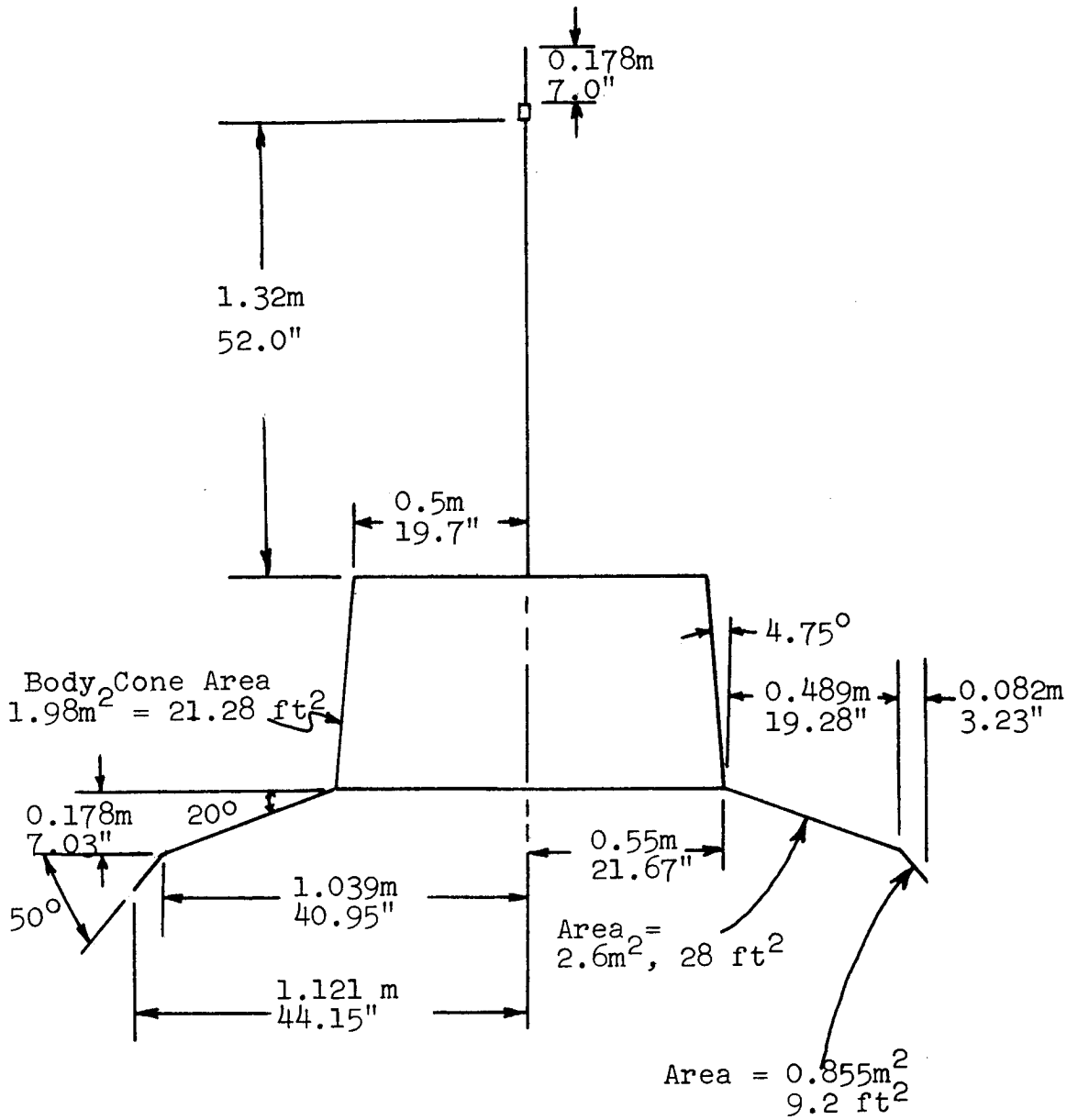

Figure 6A2.2 Dimensions for 0.1 AU Spacecraft

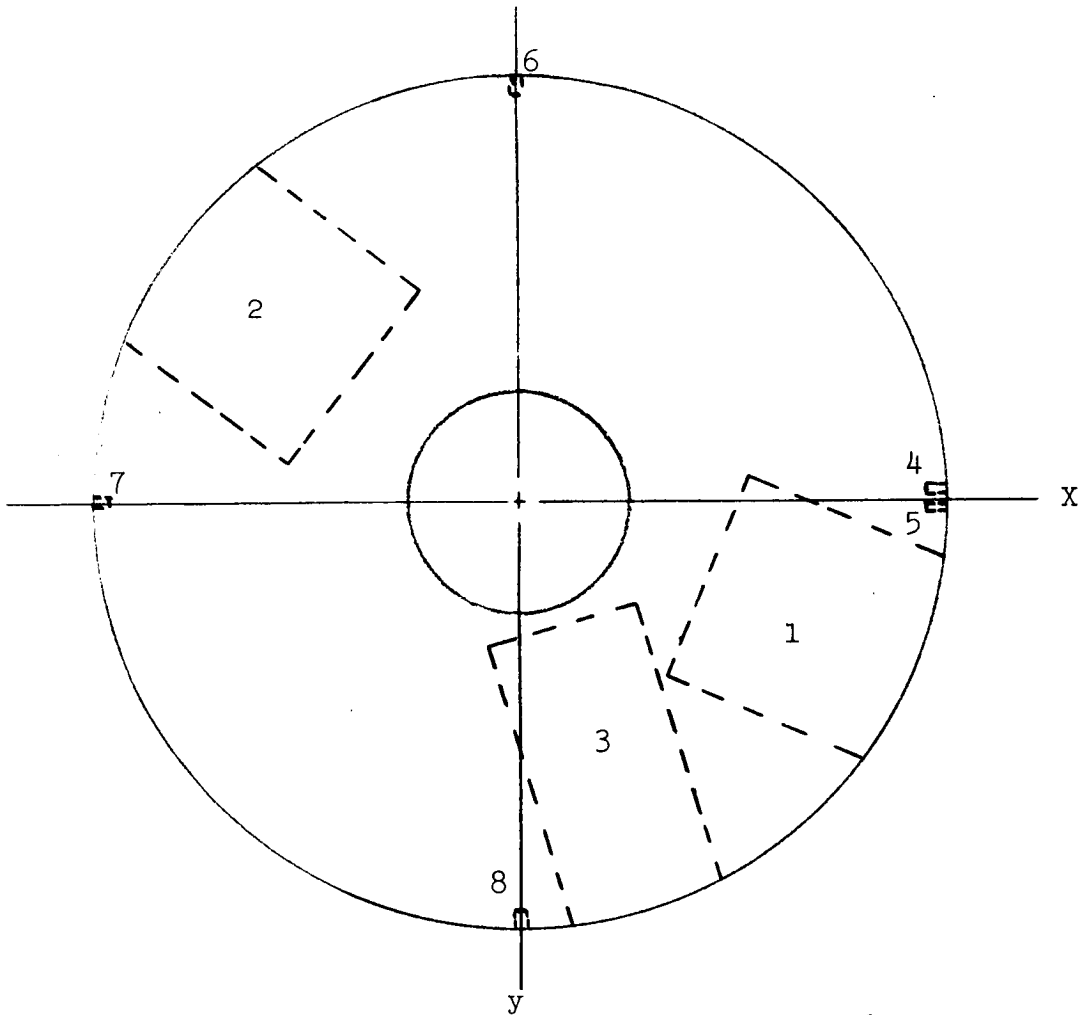

Total Weight of Equipment on Top Plate: 6.3 Kg

Equipment Number	Item	Equipment Number	Item
1	Cosmic Ray Probe	5	Sun Sensor
2	Plasma Probe	6	Sun Sensor
3	Neutron Phoswich (O1)	7	Sun Sensor
4	Sun Sensor	8	Sun Sensor

Figure 6A4.1 Top Equipment Plate

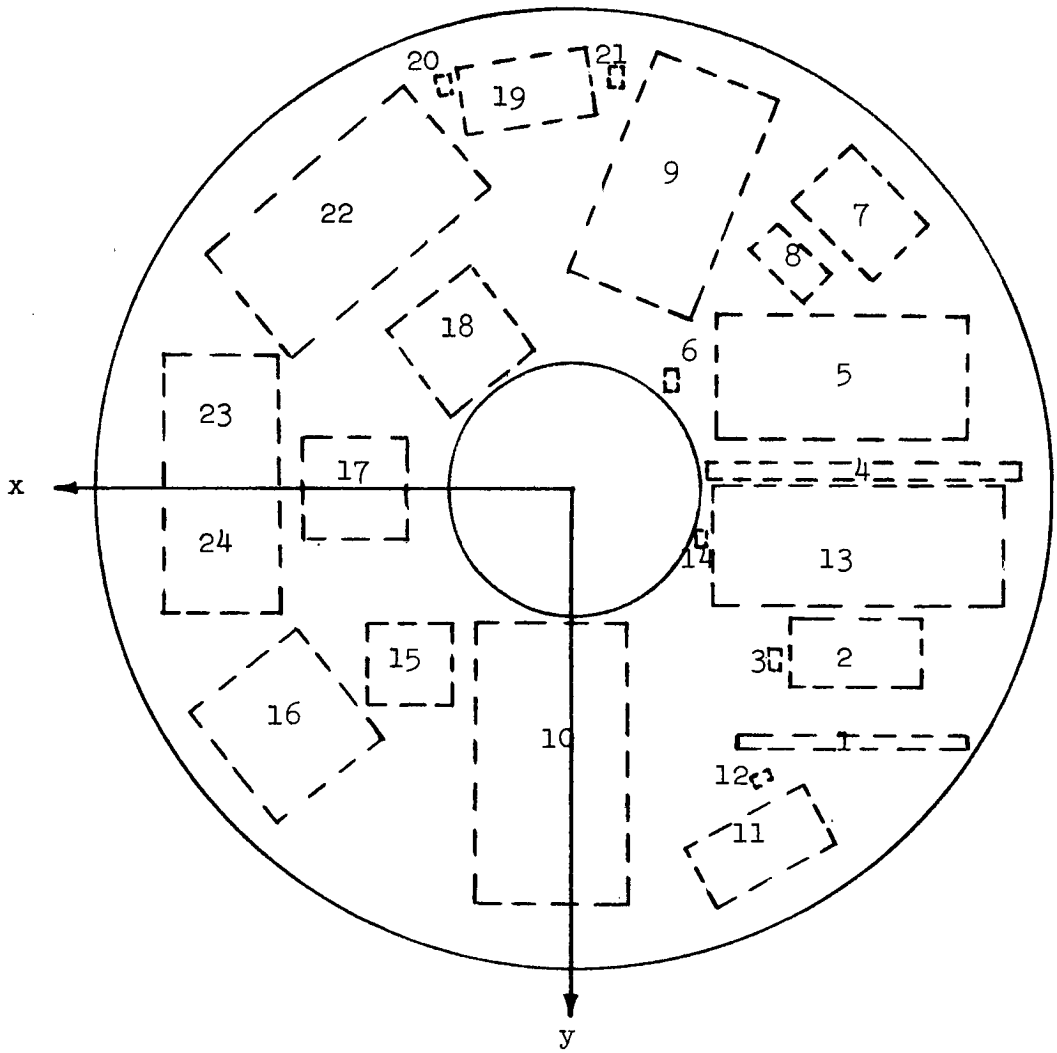

Total Weight on Bottom Equipment Plate: 34.93kg

Figure 6A4.2 Bottom Equipment Plate

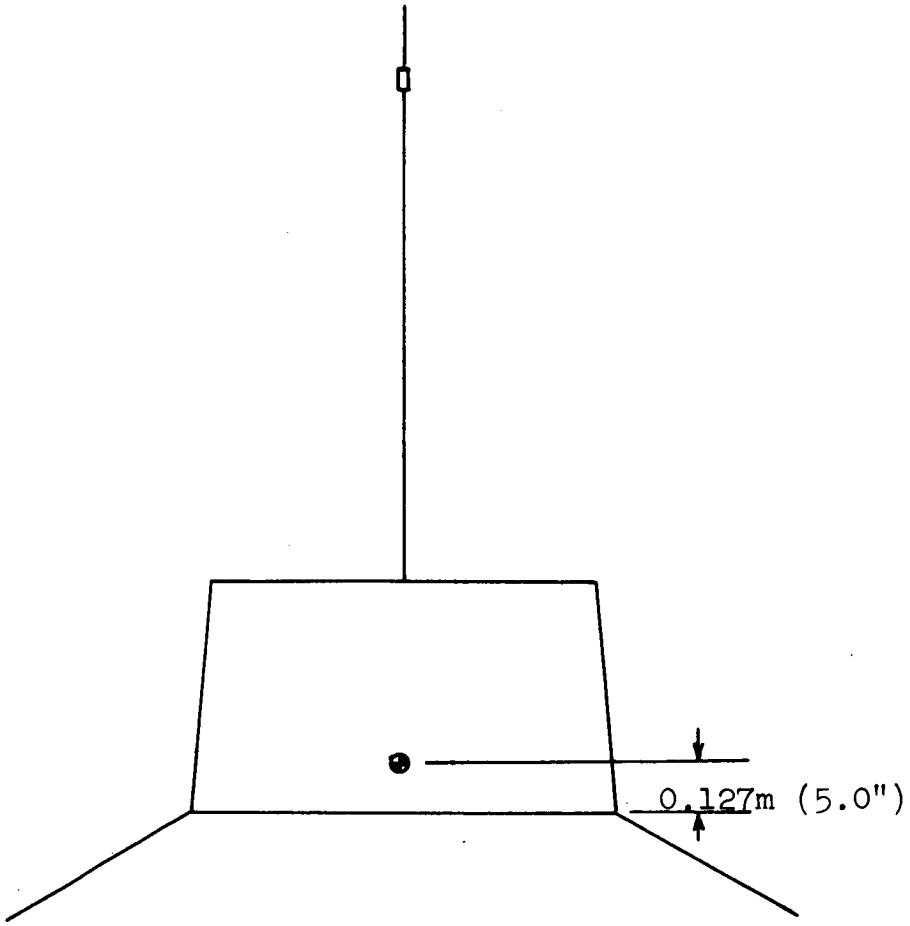

I_z = 15.5 kg m^2 = 53,000 lb in^2 = 11.4 slug ft^2

The c.g. location and moment of inertia values are approximately the same for both the 0.1 AU and the 0.2 AU Mission.

Figure 6A4.3 Spacecraft C.G. Location and Moment of Inertia

6B. Materials and Structural Design

6B1. Spacecraft Structural Materials

In structural design, the selection of materials is usually made on the basis of weight, strength, stiffness, cost and experience in the design and fabrication of the material. To do this properly, the designer must know the mechanical and physical properties of all potentially useful materials, how the conditions imposed by the environment to which they are subjected influence them, and their cost effectiveness in the fabricated system. For a solar probe spacecraft like ICARUS, the environmental conditions which are of interest to the structural designer are, aside from the usual ground handling and boost environments:

1. Magnetic fields
2. Vacuum
3. Radiation
4. Solar heating
5. Meteorites

In the following a brief description of each of the above environmental conditions and how they might be expected to influence material properties is given. The discussion will be limited to only those materials (metals, alloys and structural plastics) which have a reasonable probability of satisfying the solar probe mission requirements and are available to the designer. The candidate materials and some of their representative mechanical and physical properties are listed in Table 6B1.1.

Magnetic fields

The presence of magnetic fields of variable intensity and their influence on orientation dictates that the spacecraft structure be made of non-magnetic materials. All of the materials listed in Table 6B1.1 satisfy this requirement.

Vacuum

Some of the effects on materials associated with a very low pressure environment are:

1) Reaction of the surface with high energy atomic and molecular particles which causes loss of material through sputtering. This action can destroy some surface coatings, but results in no serious structural damage. However, the possible contamination of the spacecraft instruments and local environment makes such behavior undesirable.

Table 6B1.1 Material Properties

Material	σ_{tu} (ksi)	σ_{ty} (ksi)	σ_{cy} (ksi)	E (10^6 psi)	ν	ρ (lbs/in^3)	k (Btu/hr-ft-$^\circ$F)	α (10^{-6} in/in - $^\circ$F)
Be	70	50	50	42	.09	.067	104	6.4
Be - 38%Al	44	31	28	28	.15	.076	123	9
Al %75 - T6	72	63	64	10.3	.33	.101	76	12.9
Mg - Th Hk 31A-H24	34	26	20	6.5	.35	.065	60	15
Ti 6Al-4V	160	145	154	16	.28	.16	3.8	4.5
Reinforced Fiberglass Plastic	56	56		3.63	.113	.06	.23	12.5

σ_{tu} = Ultimate Tensile Strenght

σ_{ty} = Tensile Yield Stress

σ_{cy} = Compressive Yield Stress

E = Modulus of Elasticity

ν = Poisson's Ratio

ρ = Density

k = Thermal Conductivity

α = Coefficient of Thermal Expansion

2) Material lost by evaporation when the atmospheric density is sufficiently low. The loss of material by direct evaporation in space is insignificant for aluminum, beryllium and titanium (1). For magnesium it amounts to 4×10^{-2} in/yr at a temperature of 513°K.

3) Mechanical properties of the structural material are affected by the partial or complete loss of the surface film of gas which covers all materials at normal atmospheric pressures. Except for a small loss in fatigue life, no strengthening or weakening effect of vacuum on the mechanical properties of metals has been reported.

It had previously been assumed that, due to the above conditions, vacuum welding might be a problem, especially for similar metals (as defined by the periodic table). Recent experimental results seem to indicate that in order for this phenomenon to occur, a temperature of one-half the melting temperature, a bearing stress approaching the yield stress and a dwell time of approximately 10 minutes are required.

For organic structural materials degassing is a problem. Based on experimental evidence, however, the general conclusion seems to be that the structural properties of plastics are affected only in a minor way. Those plastics which have the lowest content of water and of solvents or plasticizers respond best to the vacuum environment. At any rate, manufacturing techniques adequately can assure the elimination of the outgassing phenomena.

Radiation

The major sources of penetrating particle radiation in space are: solar flare, primary cosmic rays and trapped radiation, like the Van Allen belts. Protons emitted during solar flare activity are considered to be the greatest hazard to solar probes. At high doeses a slight embrittlement of the material takes place, resulting in an increase in hardness and in strength and a decrease in creep rate. From the information available (1), the effect of this radiation on metals is expected to be negligible while most structural plastics have sufficient tolerance to operate a reasonable length of time. The radiation damage threshold for plastics Epoxy Resin Glass Fabric Laminate type is from 2×10^9 to 5×10^9 rad (1 rad = 10^5 ergs/kg)(2).

Ultraviolet radiation is not expected to limit the use of the candidate metals and structural plastics for space applications. Its principal effects on plastics is to cause surface degradation and an increase in solar absorptivity.

Again, surface degradation effects on successful operation of spacecraft instrumentation should be awaited.

Solar Heating

Some of the effects that the increasing temperature due to solar thermal radiation can have on material properties are

1) decrease in the strength properties (See Fig. 6B1.1 and Table 6B1.2)
2) decrease in the stiffness
3) cumulative creep deformation.

The effects of thermal gradients due to differential heating (the effect should be considerably reduced due to the use of a spinning spacecraft) can cause

1) thermal stress
2) thermal deformation and buckling
3) creep buckling
4) reduced vibration characteristics.

Special care must be taken in the design of the spacecraft to avoid joining materials of widely different coefficients of thermal expansion. This is a potential source of thermal stress. Also, since materials have characteristic maximum (see Fig. 6B1.2) and minimum operating temperatures, care must be taken to make sure that the temperature environment which the materials experience (it is expected to have a range of 123°K to 473°K) is within the material operating temperature limits.

Meteorites

The effect of meteorites is to cause erosion, spalling and perforation upon impact. The hazard presented by meteorite strikes is made difficult for the designer because of the many uncertainties in size, composition, weight, flux density and velocity of meteorite particles. Due to the low probability of perforation, the effect of meteorites may be omitted in the structural analysis.

Analysis of the space environmental conditions discussed above leads to the conclusion that except for the use of a derating factor on the strength and stiffness properties of materials, the effect of space enviroment need not be considered in the design of the spacecraft with the materials chosen. The structural design of the spacecraft is then dictated by instrumentation considerations, thermal control needs and the necessity to survive the boost environment.

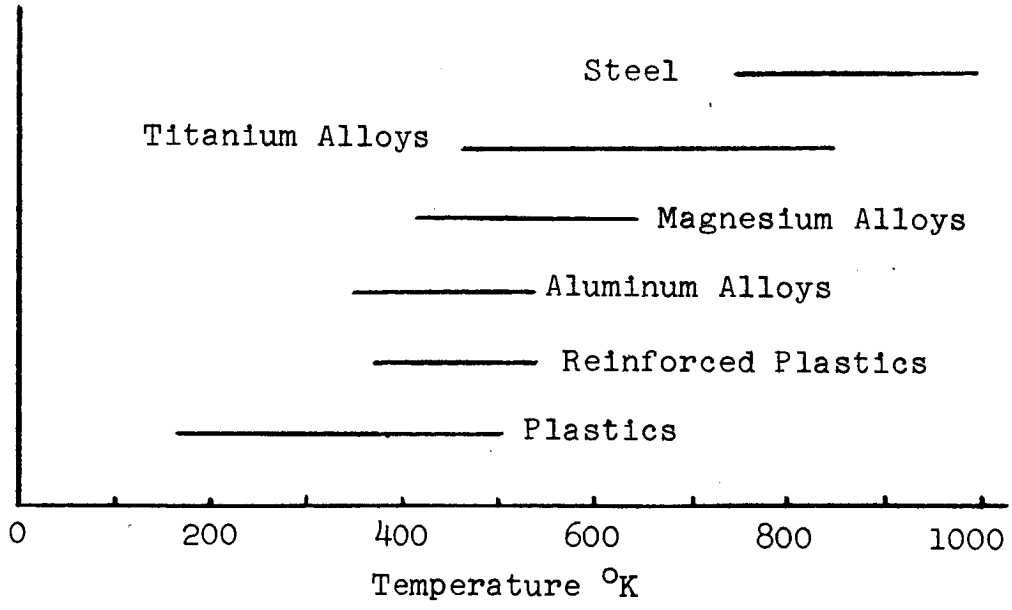

Figure 6B1.1 Maximum Operating Temperatures of Some Common Structural Materials

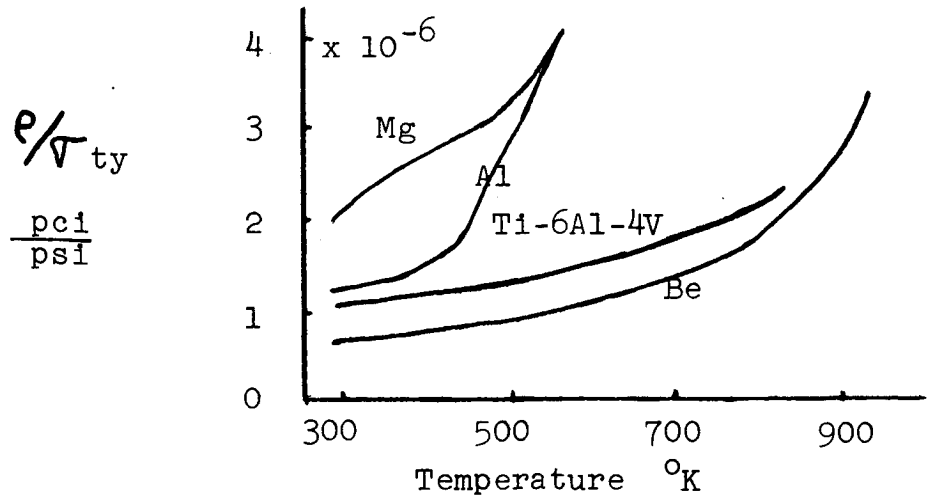

Figure 6B1.2 Comparative Tension Efficiencies

			77°K	297°K	478°K	700°K
E	(10^6psi)	L		29.1	30.0	16.9
		T		29.1	30.1	17.2
σ_{tu}	(ksi)	L	60.1	50.4	39.0	24.3
		T	58.8	50.9	39.7	24.1
σ_{ty}	(ksi)	L	41.8	36.6	30.9	21.0
		T	43.1	36.1	31.3	20.7
σ_{cy}	(ksi)	L		34.2	27.7	14.0
		T		34.3	28.4	14.4

Table 6B1.2 Variation of Mechanical Properties of Be-Al with Temperature

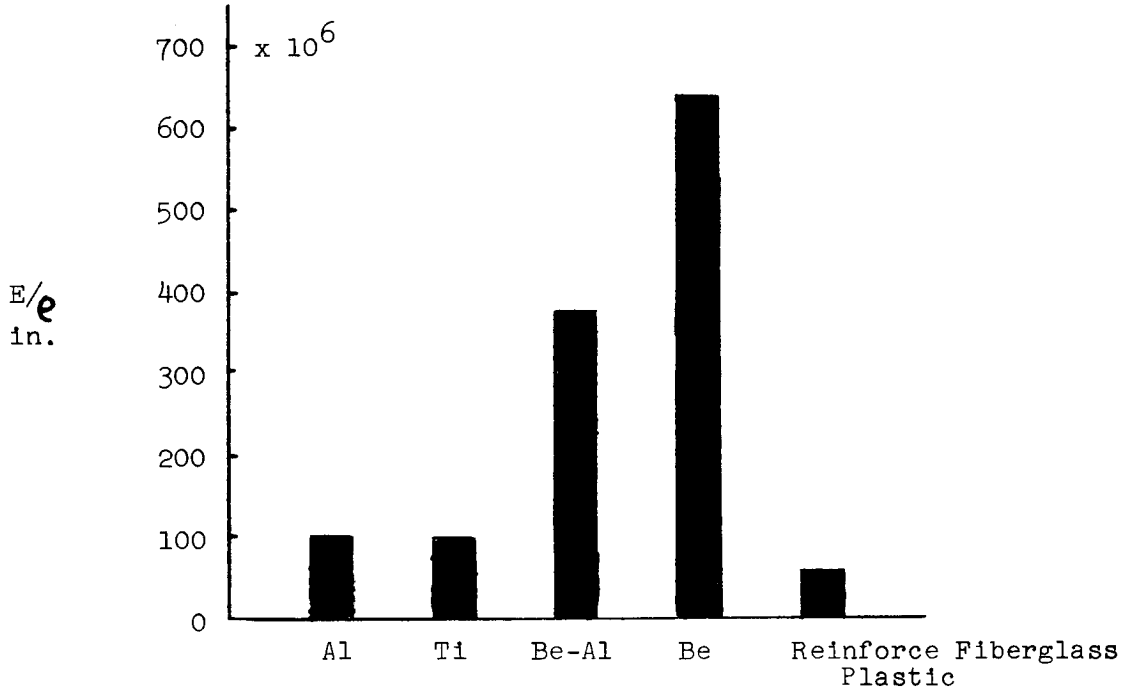

Figure 6B1.3 Stiffness Efficiency E/ρ (at room temperature)

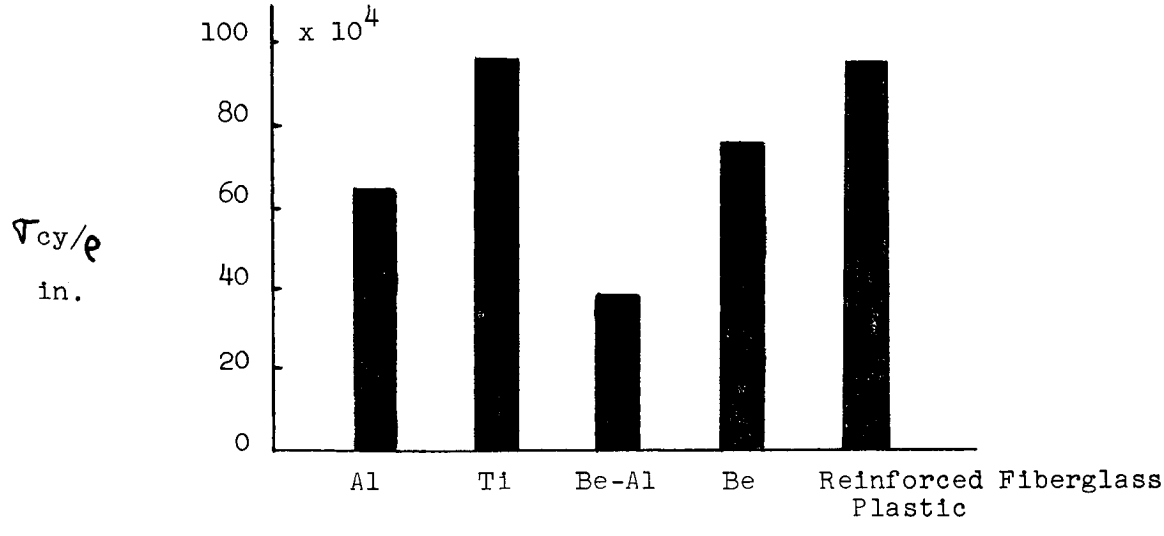

Figure 6B1.4 Compressive Strength Efficiency σ_{cy}/ρ (at room temperature)

The designer is thus permitted to choose structural materials on the basis of conventional requirements like stiffness, weight, strength, allowable temperature range, machinability and formability (see Ref. (3),(4) and (5)). If, for instance, a material with a high stiffness to weight ratio was being considered, the logical choice (from Fig. 6B1.3) would be beryllium of beryllium-aluminum. Similarly, on the basis of Fig. 6B1.4, the designer would choose fiberglass for high strength to weight considerations. Beryllium or beryllium-aluminum would have to be selected if a high thermal conductivity to weight ratio was desired and fiberglass if a low weight structural insulator was desired. Considerations like these (they will be discussed in detail for particular load and temperature environments) will govern the choice of structural materials for the spacecraft.

6B2. Structural Design

After the basic configuration of ICARUS was established as representing the best compromise between thermal, power and instrumentation considerations, the spacecraft structures group then directed its efforts toward achieving an efficient design. Due to the economic considerations involved in boosting the spacecraft into its desired orbit, every pound of structural weight which could be saved was worth approximately $200,000. In general the designer would like to design a spacecraft which provides adequate strength at minimum weight and cost. This leads to an evaluation of the structure and of the materials on a strength-weight basis. The optimum values in this relationship are zero weight and infinite strength. Since not much can be done in increasing the strength properties of the candidate materials, an attmept was made to design a minimum weight structure. One of the most obvious ways to accomplish this reduction in structural weight is to decrease the material thickness. Thin sections possess useful strength only if they are loaded in tension. To be able to use thin sections for other types of loading, it is necessary to

1) pressurize the structure internally
2) use sheet and stringer construction
3) use an integrally stiffened (waffle) construction
4) use sandwich construction

It was shown in the Materials section that beryllium possesses excellent stiffness/weight and good strength/weight properties. It can further be shown (6) that for bending and compression type loading the beryllium sandwich construction is the most efficient type of structure to use for a spacecraft. Its very high thermal conductivity also makes beryllium an excellent material to use in heat sink applications. Based on these considerations, beryllium was chosen as the main

structural material. Reinforced fiberglass plastic, because of its high strength/weight, good dielectric properties, excellent structural damping properties and low value of thermal conductivity, was chosen as the structural material for the antenna and where thermal insulation was required, as in the body cone.

A spacecraft must be designed to withstand the launch environment. The loads encountered here are the most severe imposed on the spacecraft. The principal loads arise from the steady-state and vibratory accelerations of the boosters while burning and maneuvering in atmospheric flight. Loadings of a secondary nature are due to noise, thermal cycling and shock of the type which might be encountered at ignition and also at stage separation. The design discussed below is based on the boost environment shown in Figs. 5B1.6 and Table 5B1.3 . The spacecraft is designed to withstand these loads without excessive deflection nor permanent deformation. If the loads are multiplied by a factor of safety of 1.5 to become design ultimate loads, then the structure must be capable of sustaining design ultimate loads without failure.

The discussion in the following sections deals with a description of the structural design which was selected. The structural analysis considerations pertaining to the major structural elements of this design are given in Appendix B The concepts of connections, joints and fittings are illustrated but the detailed design of these is beyond the scope of this preliminary design study.

The basic structural concept is shown in Fig. 2D1.2. Essentially, the structure consists of a beryllium thrust cylinder supporting two beryllium honeycomb sandwich equipment plates. The solar cells are mounted on an integrally stiffened beryllium cone which is attached to the bottom equipment plate. The conical body, which supports the super insulation and OSR (see section 6C1.) is made of reinforced fiberglass plastic sandwich construction and is attached to both equipment plates.

For reasons of thermal control, the body cone extends beyond the equipment plates. (See Fig. 2D1.2 and Fig. 6B2.1) The 0.127 m extension above the top plate provides 0.070 m for louvers and 0.057 m for shading. The 0.051 m extension beneath the bottom plate provides for louvers.

A detailed sketch of the body cone attachment is shown on Fig. 6B2.2. The connectors on the top plate will fit between the bimetallic springs of the louver system (see Fig. 6C3.2). Since the exterior insulation must not be disturbed, the connectors will be attached to the cone before the insulation

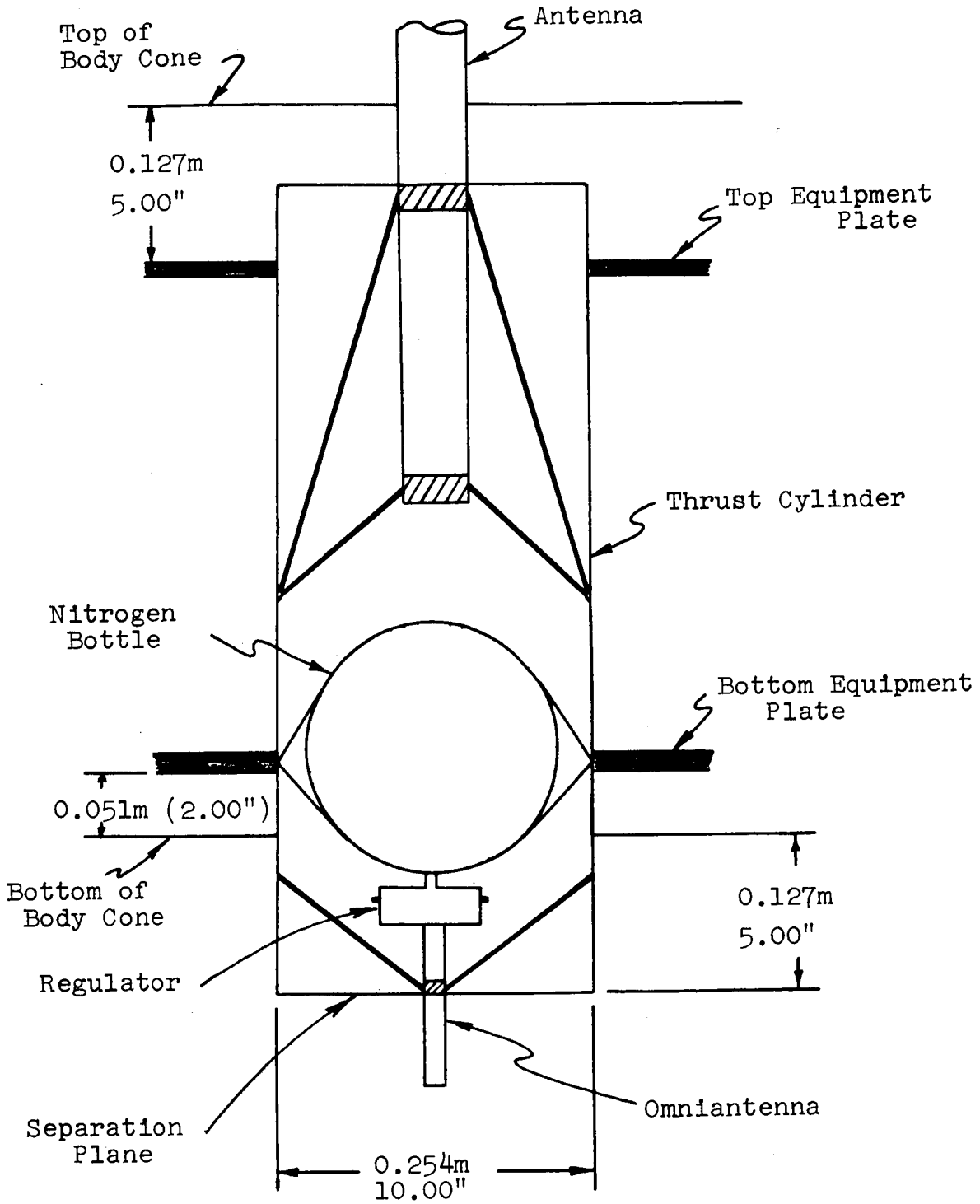

Figure 6B2.1 Detail of Thrust Cylinder

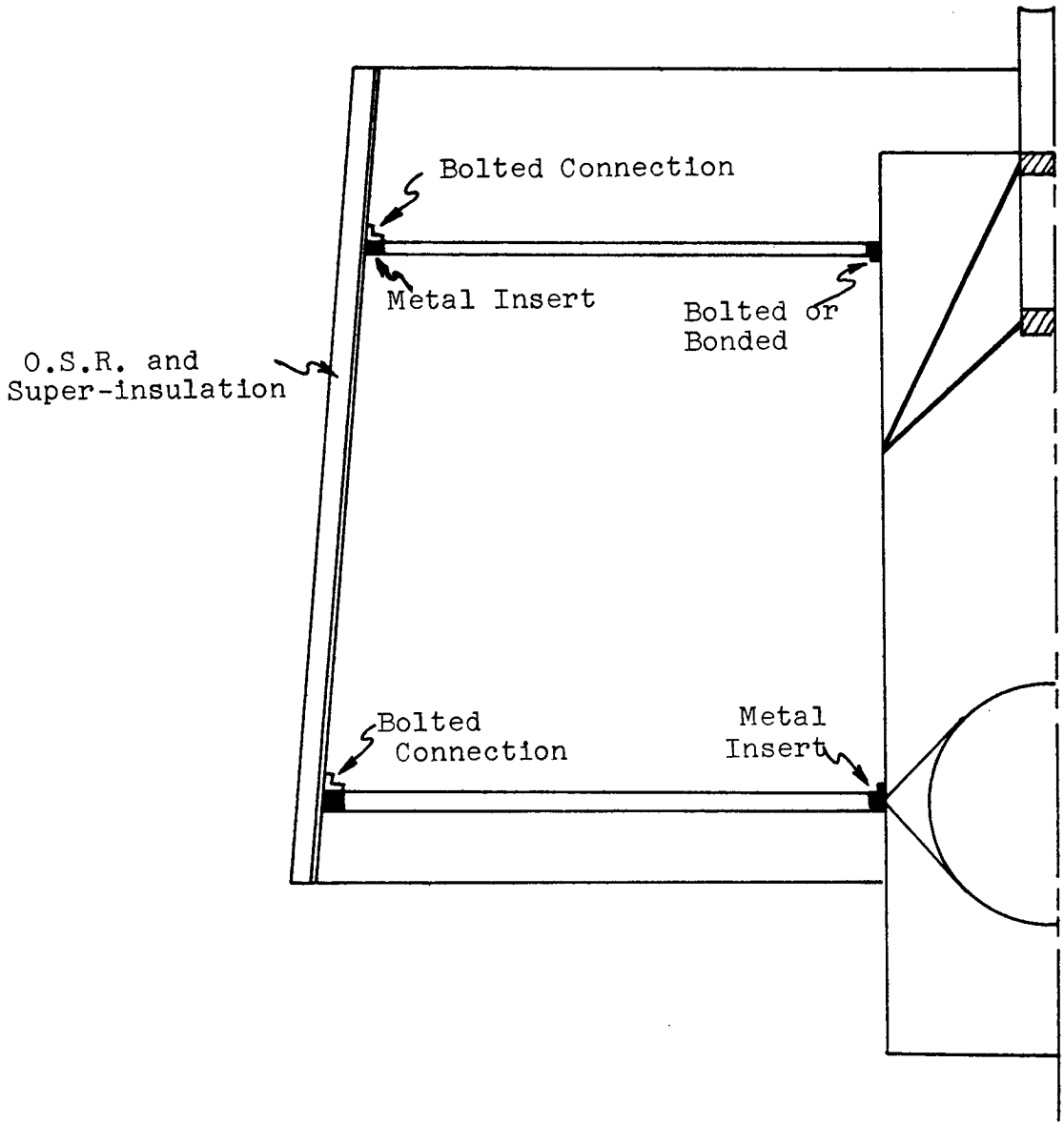

Figure 6B2.2 Body cone and Equipment Plate Connections

is wrapped. Then the necessary access to the internal equipment can be provided by disconnecting the plates and the connectors, removing the necessary sensor shades, and lifting off the entire body cone. This scheme leaves the spacecraft in a completely operating condition since no electrical connections are broken.

The equipment plates are attached to the thrust cylinder as shown in Fig. 6B2.2. The thrust cylinder is thickened in the regions around the plates because of the concentrated loades introduced into the cyliner by the plates. Welded connections are not used because either bolted or bonded connections provide increased structural damping.

The nitrogen gas system is supported inside the thrust cylinder as shown in Fig. 6B2.1. The regulator is positioned beneath the fiberglass filament-wound bottle, with the piping running through a small hole in the thrust sylinder out to the nozzle which is located as shown on Figure 2B3.1. The bottle will be supported by a webbing arrangement attached to the thrust cylinder. This positioning scheme will permit the c.g. of the gas system to be placed very near to the spacecraft c.g.

The high gain antenna is supported by six fiberglass struts which are attached to a stiffening ring on the thrust cylinder (see Fig. 6B2.1). The top three struts can be adjusted in length in order to align the antenna. If necessary, the antenna can be quickly removed by disconnecting the struts at either end.

One of the omni antannas (see Sec. 4B3.) will be connected to the nitrogen gas regulator, as shown on Fig. 6B2.1, and project o.1oo3 m (4 inches) beyond the thrust cyliner. It is not necessary that this antenna project beyond the solar cells.

The dual frequency VHF radio propagation experiment antenna will be placed on top of the magnetometer (see Fig. 2B3.1). This antenna will be constructed of beryllium wire.

The solar cell cone is attached to the bottom equipment plate as shown on Fig. 6B2.3. The connecting ring is constructed of fiberglass reinforced plastic and dimensioned so as to thermally separate the solar cell cone and the plate. (See Section 6C2.) A more efficient structural scheme would be to connect the solar cell substrate structure directly to the body cone. This would distribute the weight of this structure to both plates instead of only the bottom plate. The access and thermal control problem would now become more complicated, however, since the solar cells would have to

move with the cone and some electrical connections would be broken.

As mentioned in section 6B2.1 the solar cells are mounted on an integrally stiffened beryllium cone (see Fig. 6B2.4). Note that the circumferential stiffeners are inclined at an angle of 5° from the axis of revolution. This allows the stiffeners to serve a second function as solar shades protecting the back of the cone (see section 6C3). While the state of the art of beryllium fabrication is not as far advanced as aluminum, for example, it has already been demonstrated that forming of a beryllium shell structure can be accomplished; hence it will be possible to form the cone by successively forging, finish machining and chemical mining.

The thrust cylinder is mated to the interstage ring by the use of a payload clamp (see Fig. 5B1.5). The detailed design of the bottom of the thrust cyliner is not discussed here but it should be shaped so as to fit with the design of the interstage ring and clamp as given in the Scout Users Manual (7).

There were several other designs considered for ICARUS before arriving at the present choice. Because of the great premium placed on weight reduction of a space vehicle, designs that use a single item of structure for more than one purpose are highly desirable. From a structural efficiency viewpoint, the optimum design for ICARUS would have been to mount the equipment boxes on the sides of the spacecraft body. This design, though, could not be used for the 0.1 - 0.2 AU missions because of the extreme difficulties encountered in providing adequate thermal control in the vicinity of the Sun without an extensive redesign of the instrument packages.

It is recommended that the edge of the solar cell cone be flexibly attached to the shroud during the boost phase of the mission. This would considerably reduce the vibratory environment to which the spacecraft is subjected.

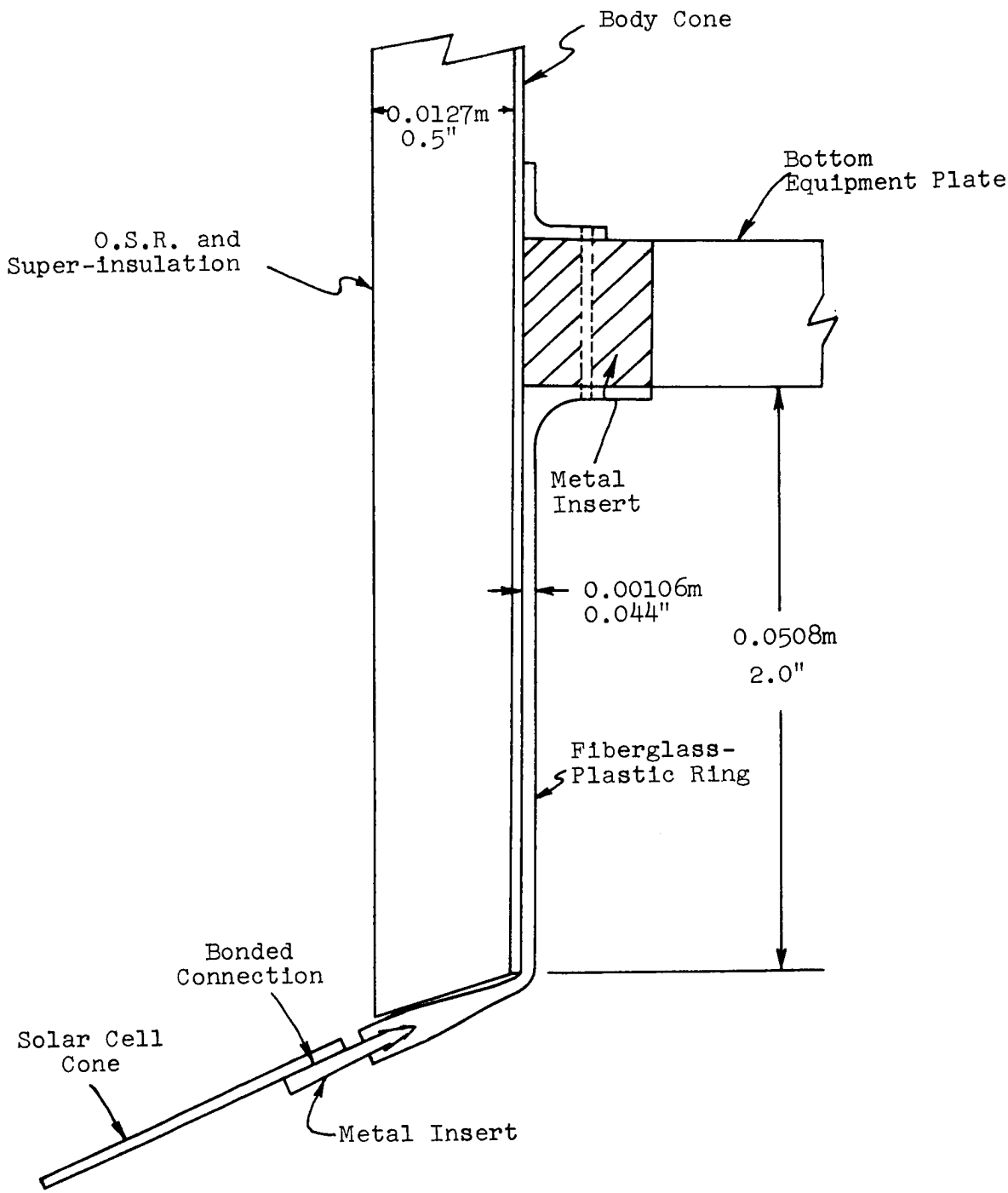

Figure 6B2.3 Solar Cell Cone Attachment

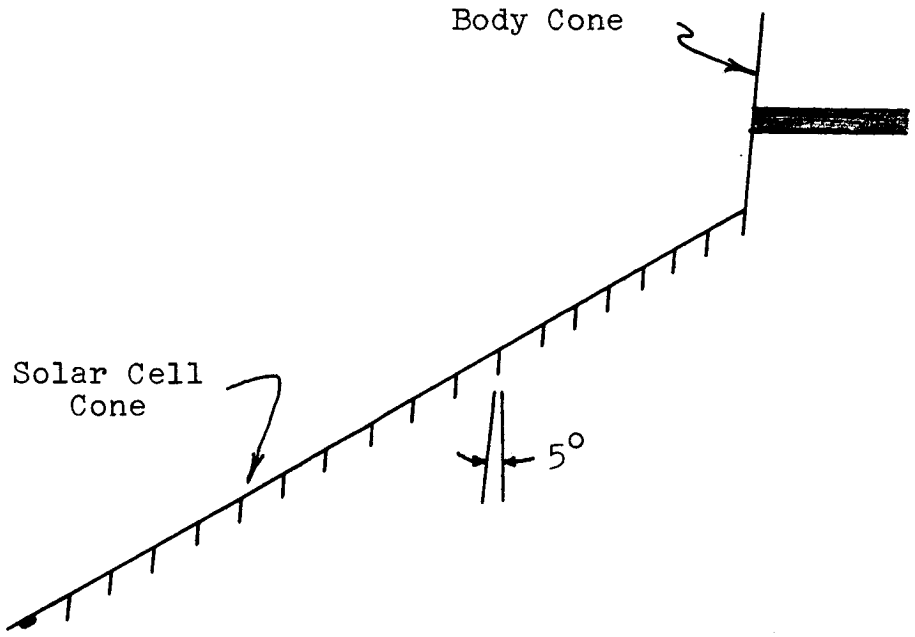

A. Section View of Solar Cell Cone

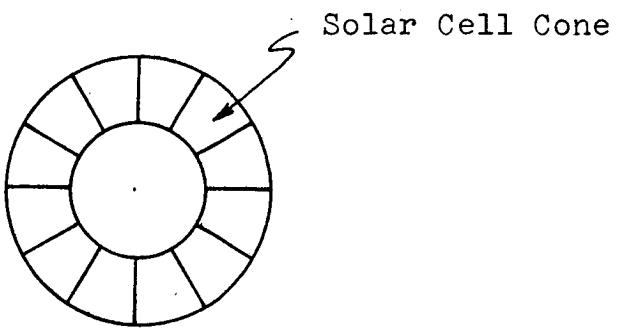

B. View of Radial Stiffness

Figure 6B2.4 Solar Cell Cone

6C. Thermal Control

6C1. Thermal Environment and System Requirements

The thermal control system for a spacecraft with a 0.2 AU or 0.1 AU perihelion orbit must be well designed in order to protect against the environment that will be encountered. The primary factor of the environment from the thermal control standpoint is the solar radiation. The solar radiation incident on one square centimeter normal to the Sun radiation at 1.0 AU is 0.14 W and at 0.10 AU is 14.0 w (8).

Other environmental factors are of a secondary nature or are of no importance as sources of thermal energy inputs to the system. However the selection of materials for use in the thermal control design must be made with due consideration given to the effect of micrometeorites, ultraviolet radiation and particle fields that may be encountered. The problem of alteration of optical properties of materials by high speed micron size particles has been investigated (13). The major problems from this type of particle exist in the region near Earth. A 50 percent degradation in optical properties may occur in a seven month period for a vehicle orbiting in the region near the earth(13). Since the ICARUS mission is of 150 days duration and only a very small fraction of that time will be in the region around 1.0 AU, particle impact is not expected to cause any significant optical property changes in the Optical Solar Reflector (OSR) surface (see Section 6C2). The effects of high-energy electrons, low-energy protons and ultraviolet radiation on OSR have been investigated (9). The results indicate that OSR will not experience significant degradation.

The primary function of the external thermal control system is to limit the thermal energy flow into and out of the vehicle between specified limits. The limit on thermal energy flow into the system is one of the controlling factors in sizing the radiating areas for waste energy rejection from the spacecraft.

The design of the internal thermal control system assures that the instrumentation and equipment aboard the spacecraft will be maintained within the limits specified by the experimenters. This control is accomplished by combining the techniques of active and passive temperature control along with careful selection of materials with desirable optical qualities.

6C2. Thermal Control Design - External

Two distinct solutions of the external thermal control problem exist. The first apprach is to establish a stationary shield in front of the spacecraft so that the vital elements of the system are protected from direct solar radiation. For a spin stabilized spacecraft the shield must be despun. The second approach is to encapsulate the vehicle with a protective shielding so thatthe entire vehicle may be spun. In light of the overall mission plan and design philosophy calling for a simple system with a minimum of articulated subsystems, the second solution was adopted.

The external thermal control design is based on reflecting a large portion of the incident solar radiation. Specularly reflecting surfaces are used in the design in such a way that the reflected energy is directed away from other parts of the spacecraft. The remaining portion of the incident radiation energy is absorbed by the outer layer of shielding material. A large portion of this energy is reradiated from the outer surface, and the remaining portion passes through into the interior of the spacecraft. A portion of the reradiated energy from the body of the spacecraft will strike the solar cell panel. The effect of the reradiated energy on the solar cell performance is discussed in Section 6D of this report. The important properties of the materials employed in external thermal control design are shown in Table 6C2.1. The materials employed are discussed later in this section of the report. The materials and shape of the vehicle were chosen in order to satisfy the conditions at the 0.10 AU perihelion.

Two thermal control materials are employed on the external portion of the body section of the spacecraft as shown in Fig. 6C2.1. The outer material is optical solar reflector and the inner material is alumized "H" film. (30 layers 1/2 mil aluminized "H" film with 3 mil dexiglas spacers) Some optical and physical properties of OSR (8) and aluminized "H" film (10) are presented in Table 6C2.1 and Fig. 6C2.1.

Thermal control analysis - External

The purpose of the thermal analysis of the external portion of the spacecraft is to establish the feasibility of maintaining the desired thermal environment. The feasibility of the design depends on first showning that the operating temperature of the thermal shielding is within the acceptable limits of the material. The second factor is to show that all the energy that enters the spacecraft may be radiated to space. This means determining the major sources of thermal energy

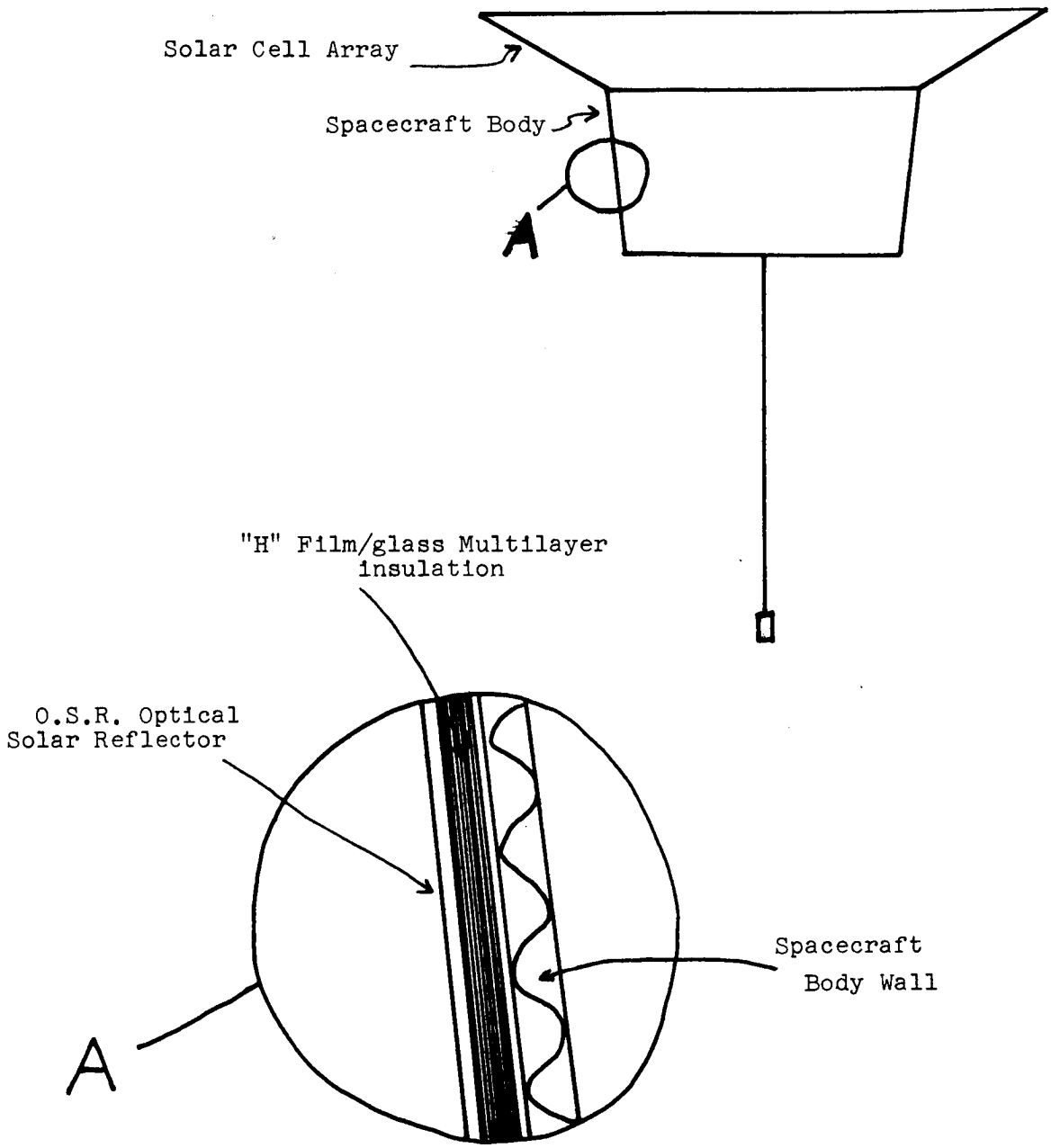

Figure 6C2.1 Spacecraft Body Thermal Control Design

Table 6C2.1

Optical And Physical Properties Of Thermal Control Materials

	Optical Solar Reflector - O.S.R	"H" Film/Glass Multi-layer Insul.	"H" Film/"Dexiglas"
		30 Shields $7.6X10^{-3}$ Cm Thick Spacers	10 Shields $2.3X10^{-2}$ Cm Thick Spacers
α_s	0.05	–	–
ϵ	@300°K - 0.81 @500°K - 0.71	–	–
α_s/ϵ	@300°K - 0.06 @500°K - 0.07	–	–
K $\frac{W}{Cm^o K}$		@500°K $5.0X10^{-6}$ @273°K $2.2X10^{-6}$	@500°K $5.5X10^{-6}$
Max. working temp. or Max. temp. for which data exist °K		610	600
Thickness Cm	0.0154	1.27	0.635
Weight/Unit Area Kg/m^2	0.33	*1.10	*0.65
Reference	(9) (12)	(10)	(10)

*Based on $\frac{1}{2}$ mill "H" film

feeding into the body of the spacecraft. The thermal inputs from external sources are determined in this section of the report and the internal energy balance is analyzed in section 6C3.

Equilibrium temperature of the body section as a function of Sun-craft distance.

In this section the following symbols have been used:

q_A	absorbed thermal energy	w
q_R	radiated thermal energy	w
S	solar constant @ 1.0 AU = 1.375×10^3 w/m^2	w/m^2
α_s	absorption of the exterior surface for solar energy	
A_s	cross sectional area exposed to sunlight	m^2
A_R	radiating area	
ϵ	emittance - total hemispherical - at equilibrium temperature	
S'	effective solar constant - accounts for reflected energy from solar cell skirt	
R	percentage of solar energy incident on solar cells that is reflected onto the body	
σ	Stefan-Boltzmann constant = 5.67×10^{-8} w/m^2	w/m^2
A	ref area, wall 1.98 m^2	m^2
A_c	conduction area	m^2
ℓ	conduction length	m
W	weight	kg
K	thermal conductivity or effective thermal conductivity	$\frac{w}{cm^oK}$

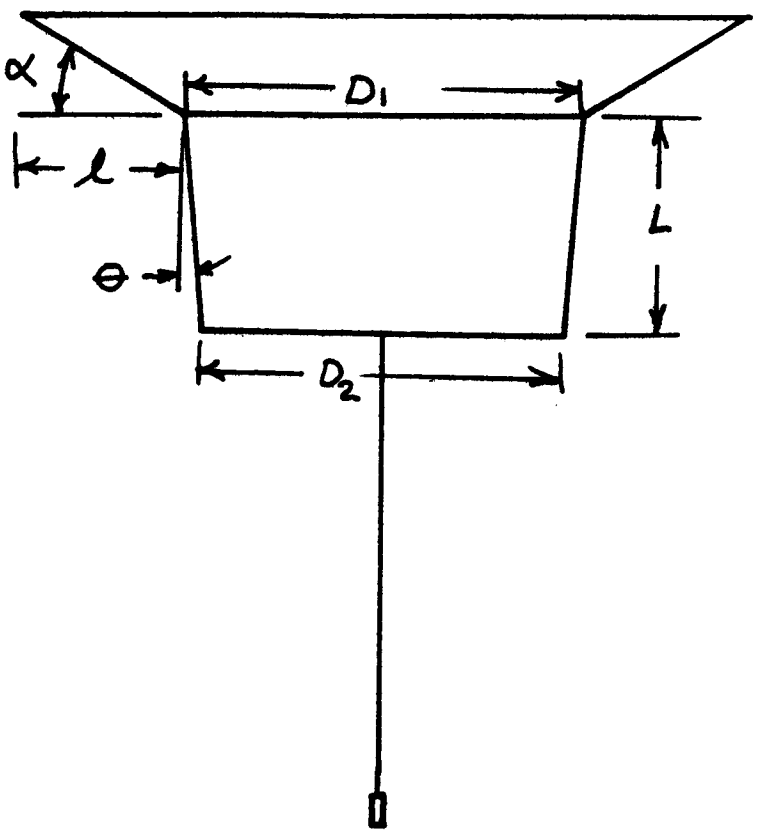

Figure 6C2.2 Geometry - Solar Cell Reflection on Body

If it is assumed that internal energy sources may be neglected (i.e. a well insulated body) and that the net interchange of energy between the solar cells and the body is small, the thermal energy balance equation is

$$q_A = q_R$$

Substituting for q_A and q_R and considering only the solar source (neglecting the earth's albedo etc.)

$$S' \alpha_s A_s = \sigma \epsilon A_R T^4 \qquad 6C2.1$$

Solving for the equilibrium temperature of the external surface:

$$T = \left(\frac{S' \alpha_s A_s}{\sigma \epsilon A_R} \right)^{1/4} \qquad 6C2.2$$

To account for the reflectance of the solar cell skirt the solar constant may be replaced by an effective solar constant (5).

$$S' = S\left(1 + \frac{\ell (\sin \alpha) \frac{D_1 + D_2}{2}}{\frac{D_1 + D_2}{2} L} R \right) \qquad 6C2.3$$

See Figure 6C2.2 for notation. Equation 6C2.3 accounts for the average added energy striking the body of the spacecraft due to the presence of the solar cell cone. The equation simply expresses by geometry the portion of the reflected energy that is intercepted by the body.

If ℓ is of the same magnitude as L, and if we assume a typical value of R to be 0.5,

$$S' = S\left(1 + \frac{\sin \alpha}{2} \right) \qquad 6C2.4$$

The area ratio may be expressed as

$$\frac{A_s}{A_R} = \frac{H (D_1 + D_2) 2 \cos \theta}{\pi 2 L (D_1 + D_2)}$$

$$\frac{A_s}{A_R} = \frac{1}{\pi} \cos \theta \qquad 6C2.5$$

Substituting Eqs. 6C2.4 and 6C2.5 into 6C2.2 gives the exterior surface equilibrium temperature

$$T = \left[S\left(1 + \frac{\sin \alpha}{2} \right) \frac{\alpha_s}{\sigma \epsilon} \frac{\cos \theta}{\pi} \right]^{1/4} \qquad 6C2.6$$

The body exterior surface temperature evaluated from eq. 6C2.6 is shown in Fig. 6C2.3 for the 0.1 AU and 0.2 AU designs.

The emissivity of the OSR was adjusted to account for the spectral distribution dependency on temperature (11).

Heat Transfer through Wall into Spacecraft Body

In designing the insulation, it is necessary to consider the heat transfer through the wall at both perihelion and aphelion. At the perihelion the spacecraft distance from the Sun is 0.1 AU and from Fig. 6C2.3 the external equilibrium temperature of the OSR is 493°K. The effective conduction per unit wall area of the body may be expresses as:

$$\frac{Q_c}{A} = \frac{KT}{x} \qquad 6C2.7$$

Employing 30 layer 1/2 mil aluminized "H" film with 3 mil dexiglas spacers as the insulation (see Table 6C2.1 for properties), and holding the interior temperature at 303°K, the effective condution into the body per unit body wall area is:

$$\frac{Q_c}{A} = \frac{(5.0 \times 10^{-6} \frac{W}{cm\,°K})(493-303)°K}{1.27\,cm} = 7.50\ W/m^2$$

At the aphelion the spacecraft distance from the Sun is 1.0 AU, and from Fig. 6C2.3, the external equilibrium temperature is 155°K. With the internal temperature held at 273°K, and employing Eq. 6C2.7, the effective conduction out of the body per unit body wall area is:

$$\frac{Q_c}{A} = \frac{(2.2 \times 10^{-6} \frac{W}{cm\,°K})(155-273)°K}{1.27\,cm} = -2.04\ W/m^2$$

For the spacecraft located at 0.2 AU, the 0.2 AU design body surface equilibrium temperature is 360°K and the effective conduction per unit body wall area is 2.25 w/m^2 into the body.

Conduction - Solar Cell Array

Another mechanism by which thermal energy is added to or removed from the body is the conduction from the solar cell array to the bottom equipment plate (see Fig. 6C2.4). The conduction per unit body wall area is

$$\frac{Q_c}{A} = \frac{K\,\Delta T\,A_c}{\ell\,A} \qquad 6C2.8$$

The conduction path is fiberglass with a thermal conductivity of 0.0043 $w/cm°K$. The solar cell array temperature for the 0.1 AU design is 473°K at 0.1 AU and the equipment plate temperature is 303°K.

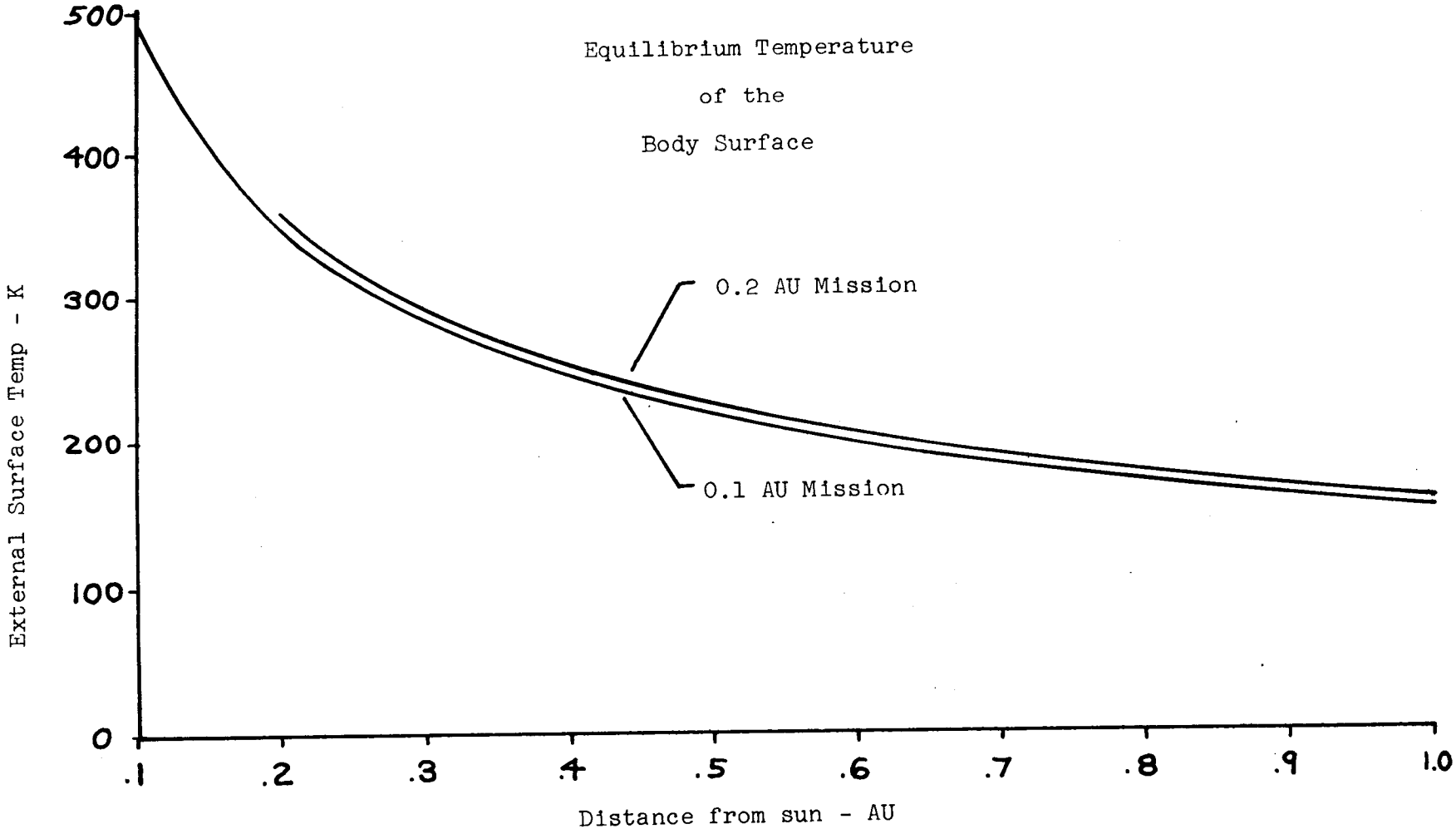
Equilibrium Temperature
of the
Body Surface
0.2 AU Mission
0.1 AU Mission
External Surface Temp - K
500
400
300
200
100
0
.1
.2
.3
.4
.5
.6
.7
.8
.9
1.0
Distance from sun - AU

Figure 6C2.3

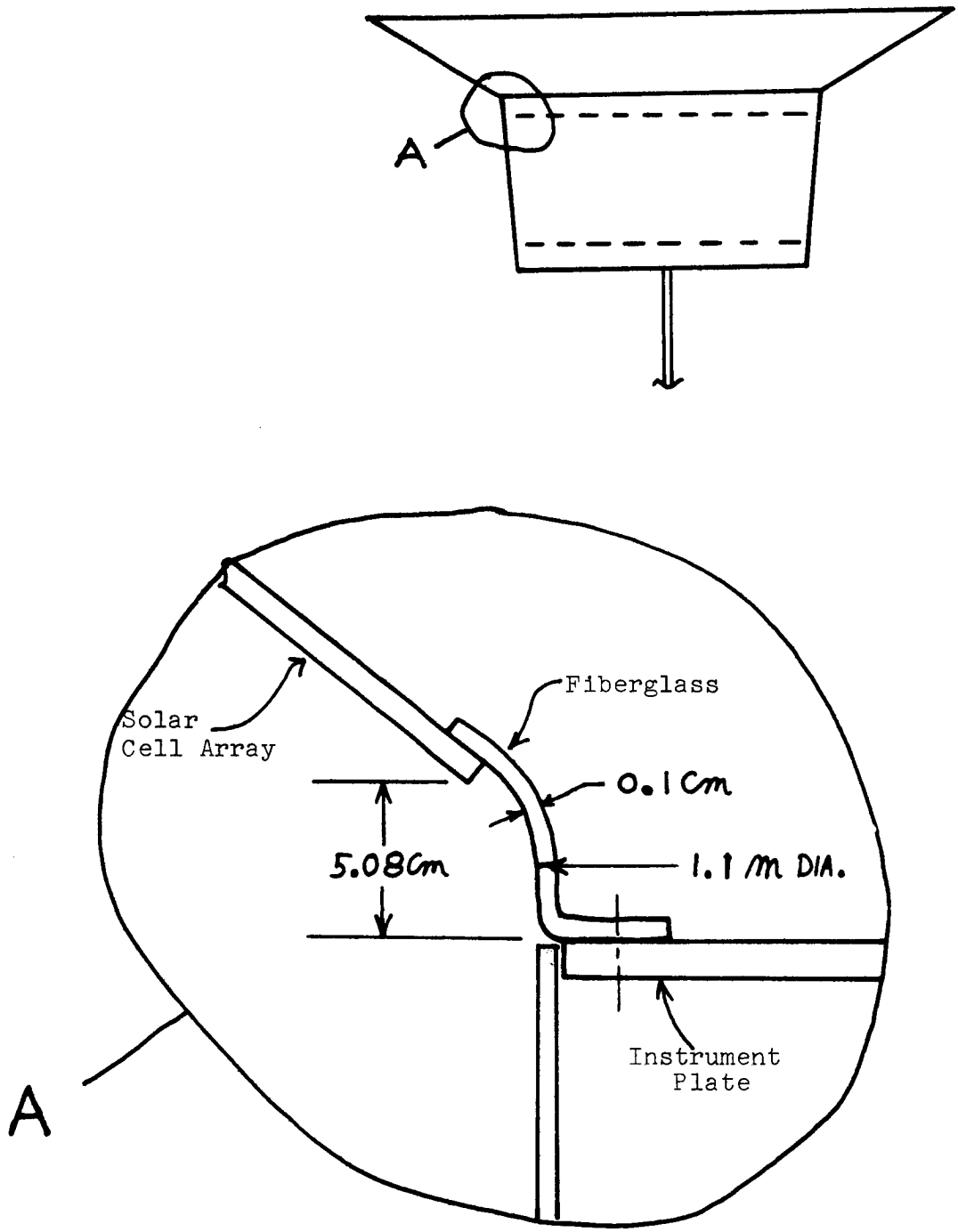

Figure 6C2.4 Conduction Path from Solar Cell Array

$$\frac{Q_c}{A} = \frac{\left(0.0043 \frac{W}{cm\,^\circ K}\right)(473-303)^\circ K\,(1.1\,m)(.1\,cm)}{(5.08\,cm)(1.98\,m^2)} = 2.51\ W/m^2$$

The solar cell array temperature at 1.0 AU is 150°K and the conduction loss per unit body wall area is 2.26 w/m^2. The solar cell array temperature for the 0.2 AU design is 400°K at 0.2 AU and 175°K at 1.0 AU. Again assuming the instrument plate temperature to be 303°K the conduction gain at 0.2 AU is 1.43 w/m^2, and the conduction loss at 1.0 AU is 1.89 w/m^2.

Conduction Fan-Beam Antenna

The antenna mast is protected by a covering of OSR. The equilibrium temperature will be 473°K at 0.1 AU, 400°K at 0.2 AU, and 150°K at 1.0 AU. Figure 6B2.1 shows the antenna connection. The thermal energy gain or loss may be determined from Eq. 6C2.8. The antenna and antenna supports are insulated with aluminized "H" film (10 layers of 1/2 mil aluminized "H" film see Figure 6C2.5). The conduction area consists of the six tubular members which make up the support. The tubes are fiberglass (thermal conductivity k = .0043 w/cm°K) of 0.75 cm O.D and 0.65 I.D. Three tubes are 0.13 m long and three tubes are 0.33 m long. For an average conduction path length and constant thrust cylinder temperature of 303°K equation 6C2.8 may be evaluated to give the heat flux, at 0.1 AU, into the body as:

$$\frac{Q_c}{A} = \frac{\left(0.0043 \frac{W}{cm\,^\circ K}\right)(473-303)^\circ K \frac{\pi}{4}\left(0.75^2\,cm^2 - 0.65^2\,cm^2\right)(6)}{\frac{(0.13+0.33)}{2}m \quad 1.98\,m^2}$$

$$= 1.06 \times 10^{-2}\ W/m^2$$

The conduction from the antenna into the body per unit body wall area at 0.2 AU is 0.61 x 10^{-2} w/m^2. The conduction from the body to the antenna per unit body wall area at 1.0 AU is -0.96 x 10^{-2} w/m^2. In addition to the conduction path, thermal energy will pass through the insultaion on the antenna support and antenna areas into the body of the spacecraft. The effective conduction into the body at 0.1 AU, through this insulation is then from eq. 6C2.8 (see table 6C2.1 for insulation properties)

$$\frac{Q_c}{A} = \frac{\left(5.5 \times 10^{-6} \frac{W}{cm\,^\circ K}\right)(473-303)\left[\frac{(0.13\,m+0.33\,m)}{2}\right](\pi\ 0.75\,cm)(6) + (5.7\,cm\ \pi)(.26\,cm)}{(0.635\,cm)(1.98\,m^2)}$$

$$= +0.59\ W/m^2$$

The effective conduction from the antenna into the body per unit body wall area at 0.2 AU is 0.35 w/m^2 and the loss from the body per unit body wall area at 1.0 AU is -0.53 w/m^2.

Conduction through Antenna Leads

The antenna mast contains thirty five electrical conductors which will also act as thermal energy conductors. The conductors are made of 0.04 cm diameter copper. The thermal energy conduction per unit body wall area at 0.1 AU is found by employing Eq. 6C2.8:

$$\frac{Q}{A} = \frac{\left(3.63 \frac{W}{cm\,^\circ K}\right)(473-303)^\circ K\,(35)(\pi\, 0.04^2)\,cm^2}{(25\,cm)(1.98\,m^2)(4)} = 0.55 \frac{W}{m^2} \quad 6C2.8$$

The conduction gain through the leads at 0.2 AU when the antenna temperature is 400°K is +0.30 w/m^2. The conduction loss through the leads at 1.0 AU where the antenna temperature is 150°K is -0.49 w/m^2.

External thermal control weight

Weight of OSR:

W = (area)(specific weight)
= $(1.98 m^2)(0.33 kg/m^2)$
= 0.66 kg

Weight of "H" film insulation:

W = $(1.98 m^2)(1.1\ kg/m^2)$
= 2.18 kg

Weight of antenna support and thrust ring covers insulation:

$$W = \left[(\pi\, 5.7cm)(26cm) + \left(\frac{0.13m + 0.33m}{2}\right)(\pi\, 0.75m)(6) + 2\left(\frac{\pi\, 25^2 cm^2}{4}\right)\right]\left[\frac{0.65kg}{m^2}\right] = 0.115\,kg$$

Total weight of the external thermal control system is:

W_{total} = 2.96 kg

Summary

The total thermal energy flow into and out of the system

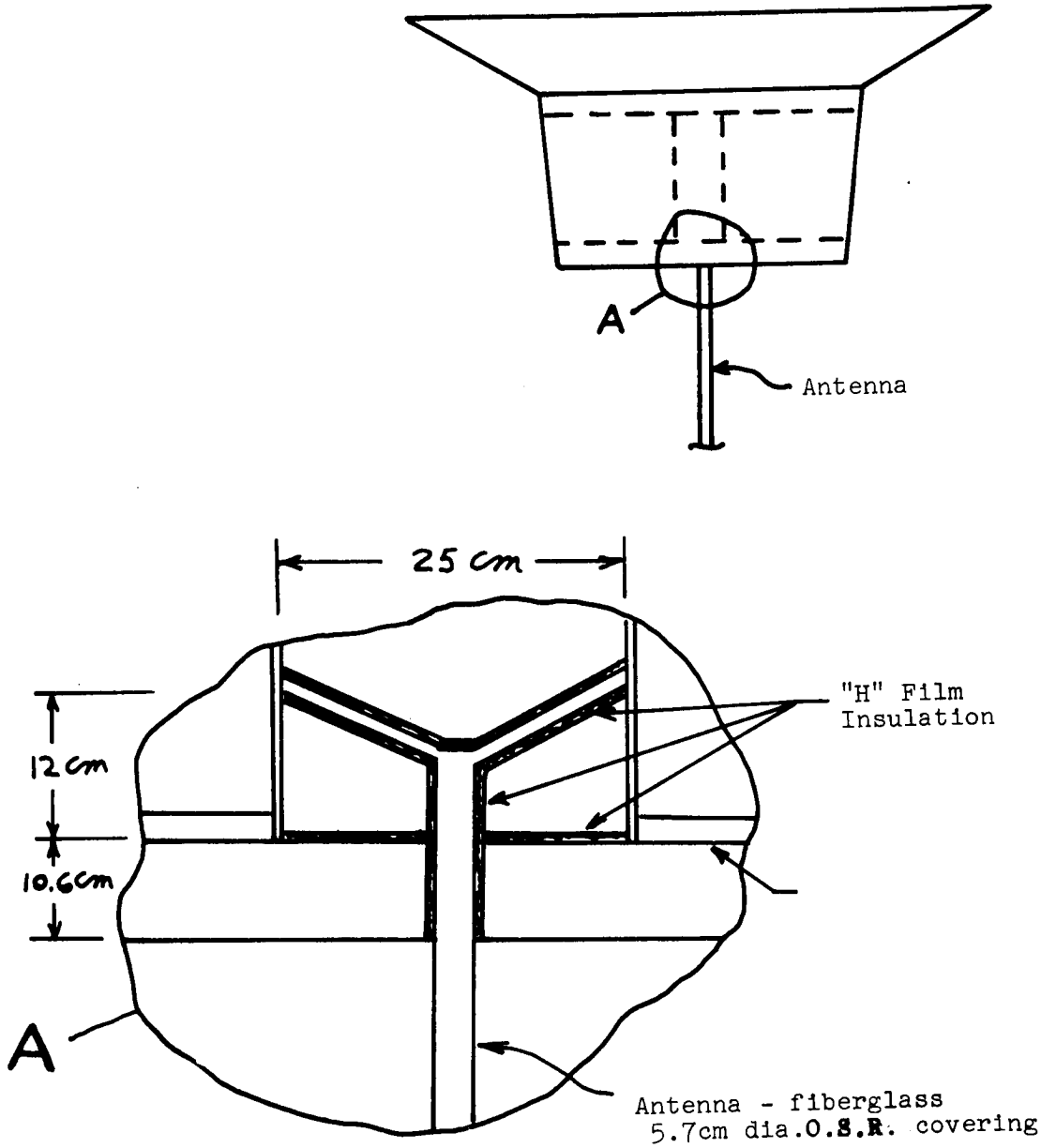

Figure 6C2.5 Antenna Support Conduction Path

is an important factor in the establishment of an acceptable energy balance as was indicated in section 6C1. For convenience this information is summarized below.

Method	w/m^2 Thermal Energy Flow based on body wall area @ 0.1 AU Design 0.1 AU	@ 0.2 AU Design 0.2 AU	@ 1.0 AU Design 0.1 AU	@ 1.0 AU Design 0.1 AU
Through wall of body	+7.50	+2.25	-2.04	-2.04
Solar cell array to body	+2.51	+1.43	-2.26	-1.89
Antenna to body	+1.15	+0.66	-1.03	-1.03
Sub Total	+11.16	+4.34	-5.33	-4.96
Estimated*	+11.16	+4.34	-5.33	-4.96
	+22.32	+8.68	-10.66	-9.92

(+) into spacecraft
(-) out of spacecraft

* To account for leakage through instrument window liners, insulation attachment, etc.

6C3. Main Compartment Thermal Control

Introduction

The instrument compartment is designed to maintain the temperature of the base plates of all instruments and electronics within the range 273°K to 323°K (0 to 50°C). An exception to this is that all 3 TWT bases are constrained to the range 253°K to 358°K (-20 to +85°C). The design discussed is satisfactory for missions to 0.1 AU. Modifications for missions with perehelion less than 0.1 AU are suggested.

All the equipment is mounted on the inside of two circular beryllium plates located at each end of the vehicle as shown in Fig. 2D1.2. On the outside of the plates are mounted active thermal control louvers much in the style of the current Pioneer, Mariner, and OGO. Bimetallic spiral

coils in thermal contact with the circular plates control the louvers. Barring a serious attitude control error, the louvered surface sees essentially black space although some account must be made for reradiation from the antenna, the back of the solar cell cone and the lip of the shield at the antenna end of the vehicle. The control system is designed to operate nominally for $\pm 2^{\circ}$ attitude control error with respect to the Sun-vehicle line at 0.1 AU.

Because of the great change in thermal inputs over the range of the mission, it is necessary to maintain a minimum electrical power dissipation within the craft when the distance from the Sun is greater than 0.25 AU. In this sense, all components of the vehicle capable of generating or dissipating electric power are part of the active thermal control of the vehicle.

Analysis

The details of the louvered plate construction are indicated in Fig. 6C3.2. The effective emissivity of the louvered portion of the mounting plates is given by (14):

$$\epsilon_{eff} = \epsilon_p \frac{1 - G(\theta)}{1 - (1 - \epsilon_p) G(\theta)} \qquad 6C3.1$$

where

$$G(\theta) = \frac{(F_{12} + F_{13} F_{32})(F_{21} + F_{23} F_{31})}{1 - F_{23} F_{32}} + F_{13} F_{31}$$

and the surfaces of the louvers are considered adiabatic and optically diffuse. ϵ_p is the emissivity of the plate itself and the F's are the configuration factors and are functions of the louver angle θ (see Fig. 6C3.4). When the louvers are closed ($\theta = 0$), Eq. 6C3.1 gives a misleading result. In this case, the shutters act as a single radiation shield and it is easy to verify that,

$$\epsilon_{eff} = \frac{\epsilon_s}{2 + \epsilon_s (\epsilon_p^{-1} - 1)} \qquad 6C3.2$$

where the more appropriate assumption is made that the louvers are isothermal rather than adiabatic. By coating the plate with one of several available black paints (e.g. Lowe Bros. No. 47,865 Black Base Enamel, or Parsons Optical Black Lacquer), it is possible to make $\epsilon_p \geq 0.95$.

ϵ_s is the emissivity of the shutters (assumed the same on both sides). Account must be made not only for the surface material and condition but also for the effect of spacing between the shutters or overlap of the shutters. Here it is assumed that the shutters are plated with silver with a 500 Å Al_2O_3 layer vapor deposited over it for protection (17). This

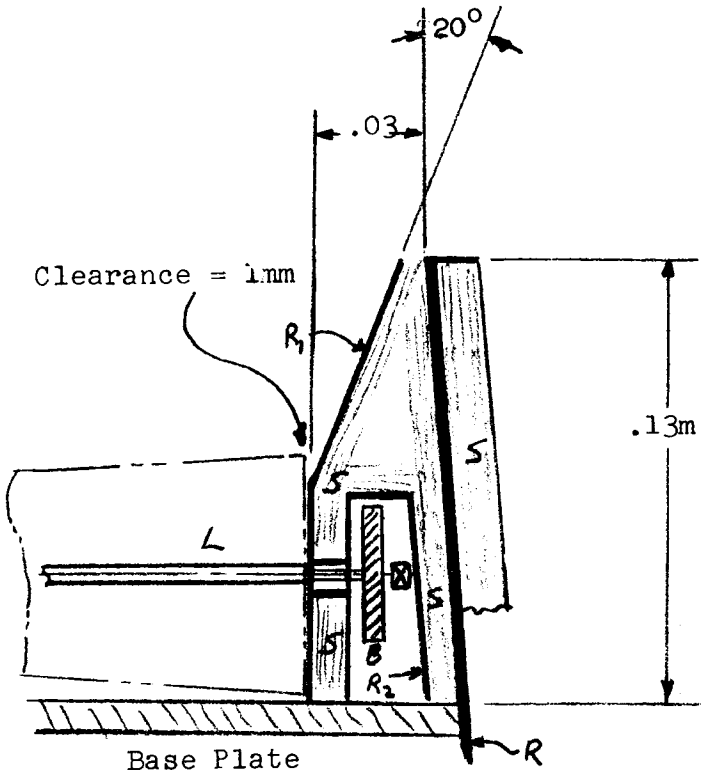

Section A-A (Top end - ½ scale)

S, super insulation
B, bimetal spring
L, louver, plated with Ag-Al_2O_3
R, reinforced plastic
R_1, plated with Ag-Al_2O_3
R_2, painted black

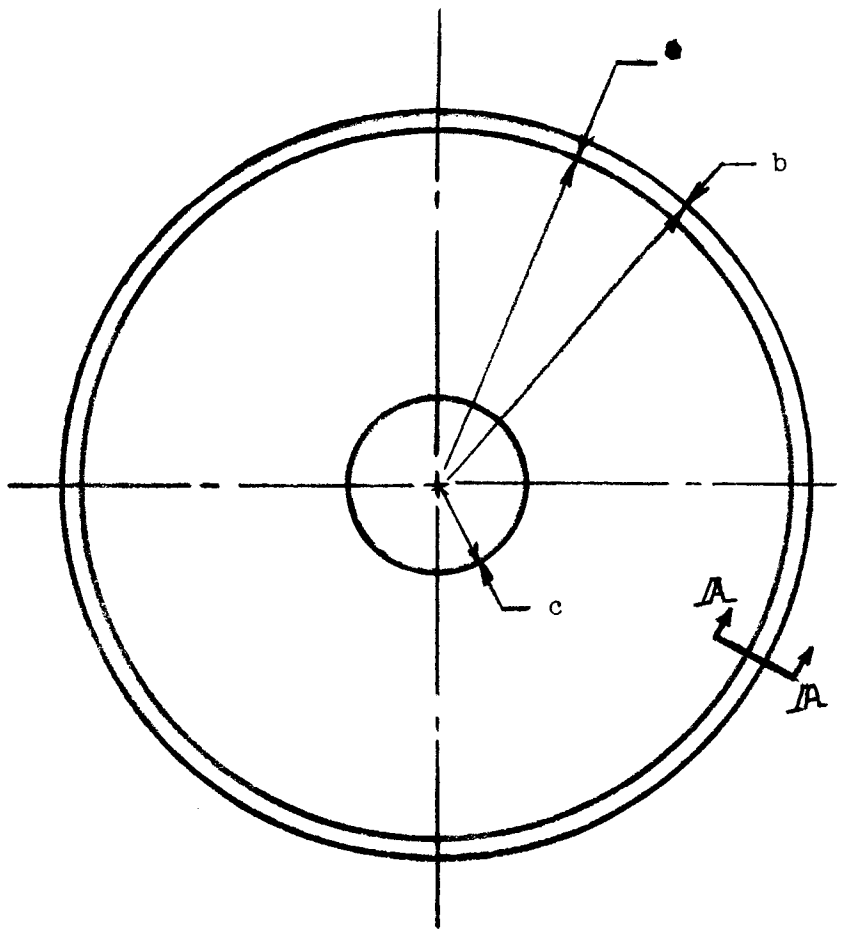

Figure 603.2 Details of Louver Arrangement
(page 1 of 2)

	Bottom End	Top End
radius a	0.52	0.47
radius b	0.55	0.50
raduis c	0.125	0.13
no. of louvers, N	47	43
weight/louver assembly (incl. bimetal spring, bearings)	0.028 kg	0.028kg
total weight	1.28 kg	1.17 kg
louver area, A	$0.80m^2$	$0.64m^2$
area of "black gap", A_{BG} $(2\pi(a + .125)x10^{-3}$	$4.05x10^{-3}m^2$	$3.76x10^{-3}m^2$
area of "black overlap", A_{BO} $(a-.125)(Nx10^{-3})$	$18.6x10^{-3}m^{-2}$	$14.6x10^{-3}m^2$
$\epsilon_s = 0.03(A_L-A_{BO})/A_L + A_{BO}/A_L$	0.053	0.052
ϵ_p	0.95	0.95
Closed		
$\epsilon_{eff} = \epsilon_s/[2+\epsilon_s(\epsilon_p^{-1}-1)]$	0.026	0.026
$Q_R = 310\frac{\omega}{m^2}\epsilon_{eff}A_L$ (273°K)	6.5w	5.1w
$Q_{BG} = 310\frac{\omega}{m^2}A_{BG}$	1.3w	1.1w
$Q_{END} = 2N(2.1\times10^{-2}\omega)$	2.0w	1.8w
$Q_R + Q_{BG} + Q_{END}$	9.8w	8.4w
Open		
ϵ_{eff}	0.72	0.72
$Q_R = 0.1(670)+(A_L-.1)(470)0.72$	284w	216w
Q_R/louver	6.0w	5.0w

TOTALS		
	Total area	$1.59m^2$
	Q (closed)	18.2 w
	Q (open)	500 w
	Weight	2.5 kg
	no. of louvers and actuators	90

Figure 6C3.2
(page 2 of 2)

surface should have $\epsilon \leq 0.03$. Aluminum, gold or copper could be used in place of silver but this will give a larger α_s -- which is only important if direct sunlight falls on the louvers due to an attitude control failure. It is assumed that careful construction of the louver system will allow the overlap between louvers to have no more of a degrading effect than would a "black" strip 0.1 cm wide between each louver. This "black" area is called "black overlap" in Fig. 6C3.2. The resulting ϵ_s is given by

$$\epsilon_s = 0.03\left(\frac{A_L - A_{BO}}{A_L}\right) + \frac{A_{BO}}{A_L} \qquad 6C3.3$$

where, A_L is the total louver area and A_{BO} is the "black overlap" area. The result is that $\epsilon_s \leq 0.053$ for the closed shutters. Equation 6C3.1 and 6C3.2 for these shutters give

$$\epsilon_{eff_{max.}} \geq 0.72 \quad at \quad \theta = 90°$$

$$\epsilon_{eff_{min.}} \leq 0.026 \quad at \quad \theta = 0° \qquad 6C3.3$$

The preceeding discussion assumes the louvers are thermally isolated from the base plates. A conservative correction for this effect is to take an additional heat rejection of 2.1×10^{-2} watts for each connection between the louvers and the spacecraft. There are two connections per louver. This figure was arrived at by assuming the connection was made by the equivalent of a 0.3 cm diameter reinforced plastic rod, 1 cm long, with the full temperature drop between the plate and the louver.

$$Q/connection = \frac{(\Delta T)kA}{l} = \frac{(273 - 230°K)(4.3 \times 10^{-3} \frac{w}{cm°K})}{1\ cm}$$

$$\cdot\frac{(0.3cm)^2\pi}{4} = 2.1 \times 10^{-2} w$$

230° K is the equilibrium temperature of the thermally isolated louvers. 4.3×10^{-3} w/cm°K is a typical thermal conductivity for reinforced plastic. Another louver loss which is significant when the louver is closed is due to the "black gap" between the end of the louver and the adjacent housing. The heat loss from this effect was calculated using an 0.1 cm gap at both ends of the louvers. Reference to Fig. 6C3.2 shows that the sum of the louver radiation losses (Q_R) plus conduction losses (Q_{END}) plus "black gap" losses (Q_{BG}) totals 18.2 watts for 1.59 m^2 of louver area with the plate at 273°K. This represents an overall effective emissivity of 0.037 -- considerably less than any current louver system. Values in the neighborhood of 0.12 are typical for closed louvers. It is the author's opinion that no serious attempts have been made to optimize louver design and that the emissivity of

0.037 is achievable. Should this prove not to be possible, two "fixes" are possible. A radioisotope heater with a thermal output of 20 to 40 watts could be added to the spacecraft without jeopardizing the thermal balance at 0.1 or 0.2 AU or the compartment equipment could be qualified for a lower temperature than 273°K (0°C). The weight of a radioisotope heater should be very small for this wattage since the isotope itself will produce 0.5 w/gram (Pu 238) or 2.3 w/gram (Cm 244). Pu 238 or Cm 244 are recommended as radioisotopes suited for this purpose if in fact radioisotope heaters are required.

The external thermal control system (Section 6C2) is designed so that the heat leak into the compartment through the sidewall is less than 22.3 w/m^2 at 0.1 AU and less than 10.7 w/m^2 out of the compartment at 1.0 AU. The heat leak through the portions of the top and bottom not covered by louvers is to be less than 4 w/m^2 out of the instrument compartment at 273°K.

In calculating the heat input at 0.1 AU it is necessary to include radiation from the antenna, radiation from the back side of the solar cell cone, and radiation from the lip of the shield at the antenna end. A portion of these radiations may enter the open louvers at 0.1 AU.

Item	Max. Thermal Input (w) at 0.1 AU
Antenna	39
Solar Cells	14
Shield	9
	62 x 0.72 = 45

In these calculations the antenna and inside of the shield are covered with specular surfaces with $\epsilon \leq 0.05$. The back of the solar cells is to have an effective emissivity of 0.05. Furthermore, the louvers are assumed to have $\epsilon = 0.72$ with respect to incident radiation. This is the value of ϵ for completely open louvers. A large thermal input at 0.1 AU comes from electric power dissipation and "windows" on the instruments and Sun sensors. Windows are openings in the outer wall through which Sun can enter the instrument compartment. These thermal inputs are summarized in Table 6C3.1

The limiting cases for thermal control are:

1) maintaining $T \geq 273°K(0°C)$ at 1.0 AU
2) maintaining $T \leq 323°K(50°C)$ at 0.1 AU

where T is the compartment temperature.

Table 6C3.1

Thermal Inputs From Instruments, Electronics, and Windows

Item	Notes	Window Area (Cm^2)	Electric Dissipation (watts)
Cosmic Ray		2.5	1.5
Neutron Phoswich		4.0	3.5
Plasma Probe		4.0	1.0
Magnetometer	1		3.5
UHF Radio Propagation			1.5
Total Experiments	9	10.5	11.0
Trans. Driver			2
3w TWT	2,9		13
20w TWT	2,3		40
50w TWT	2,3		100
100w TWT	2		122
Tape Recorder	8		1.3 - 2.3
Power Conditioner	4,9		5 - 26
Receivers	5,9		3
Data System	9		8
Total Electronics	9		31 - 163.3
Logic	9		0.2
Sun Sensors	6	1.0	
Total Orientation		5.0 - 7.0	0.2
Grand Total			
Minimum (1.0 AU)	6,9	15.5 - 17.5	42.2
Maximum (perihelion)	6	15.5 - 17.5	174.5
Window Thermal Equivalent			
1.0 AU	7		> 1
0.2 AU	7		17 - 19
0.1 AU	7		68 - 77

1. In-board portion only.
2. TWT plus driver; only one TWT used at any time.
3. 20 w and 50w TWT are physically the same unit.
4. Electric dissipation assumes 90% efficiency.
5. There are 2 receivers; both used continuously.
6. There are 5 to 7 sun sensors depending on mission.
7. Considering the windows to have $\varepsilon_T = 1.0$.
8. 1.3 watts on record, 2.3 on playback.
9. Items used in computing minimum powers.

Heat Balance at 1.0 AU (Compartment and base plate assumed to be at 273°K (0°C)

Outside Walls	-21 w
Louvers	-18 w
Other Areas	-2 w
Subtotal	-41 w
Electric Power Available	+42 w
Margin (sum total)	+1 w

Heat balance at 0.1 AU (Compartment base plates assumed to be at 303°K (30°C) except 0.1 m^2 at 333°K (60°C) under 100 w TWT)

Outside Walls	+44 w
Windows (23.5 cm^2)	+77 w
Radiation into louvers	+45 w
Electric dissipation	+174 w
subtotal	+340 w
Louver capacity	-500 w
Margin (sum total)	-160 w

For a mission to 0.2 AU, condition item (2) above is changed to (2) maintaining T 323°K (50°C) at 0.2 AU.

Heat Balance at 0.2 AU (compartment base plates assumed to be at 303°K (30°C) except 0.1 m^2 at 333°K 60°C) under the 100 w TWT)

Outside Walls	+17 w
Windows	+19 w
Radiation into louvers	+11 w
Electric Dissipation	+174 w
subtotal	+221 w
Louver capacity	-500 w
Margin (sum total)	-279 w

The antenna has a configuration as shown in Fig. 6C3.3. All of the surface of the antenna is covered with highly specular OSR with α_s = 0.05. Under the assumption that the antenna is small in diameter relative to the dimensions

of the plate, the heat flux from the antenna to the louvers on the top of the vehicle is given approximately by

$$Q = \alpha_s \frac{S}{\pi} Dh \tan^{-1} R \Big|_{R_1}^{R_2} \text{ watts}$$ (derivation given in Appendix C)

6C3.4

where α_s = the fraction of incident solar energy re-emitted diffusely

S = the solar constant

R = r/h

R_1 = r_1/h

R_2 = r_2/h.

For explanation of D, h, and r see Fig. 6C3.3

Substituting the appropriate values into Eq. 6C3.4 gives

$$Q = 780\ \alpha_s$$
$$= 39\ w \quad \text{for} \quad \alpha_s = 0.05$$

6C3.5

at 0.1 AU.

There is a thermal input to the louvers from the rim of the shield around the louvers at the upper end. This shield is made of very thin reinforced plastic and is thermally isolated from the outer walls by super insulation (see Fig. 6C3.3). However, because the Sun subtends a finite angle (particularly for close in missions) and because the craft may be slightly misaligned with the Sun (spin axis not perpendicular to the Sun-vehicle line), some Sun light will fall on the inside of the shield. The shield face is plated with silver with 500 Å of Al_2O_3 vapor deposited over it. This will give a very specular surface with $\alpha_s \simeq 0.05$. The shield cone is shaped so that at 0.1 AU, at least 99.95% of all the specularly reflected energy passes out of the vehicle. However, the 5% that is absorbed is reradiated in a diffuse fashion. The view factor of the shield cone to the louvers is 0.2 giving a possible thermal input at 0.1 AU of 9 watts.

The louvers on the bottom of the vehicle are exposed to radiation from the back of the solar cells. The amount of radiation into the louvers depends on the cone angle of the solar cell cone as well as its area, temperature and emissivity.

S, super insulation
B, base plate
L, louvers

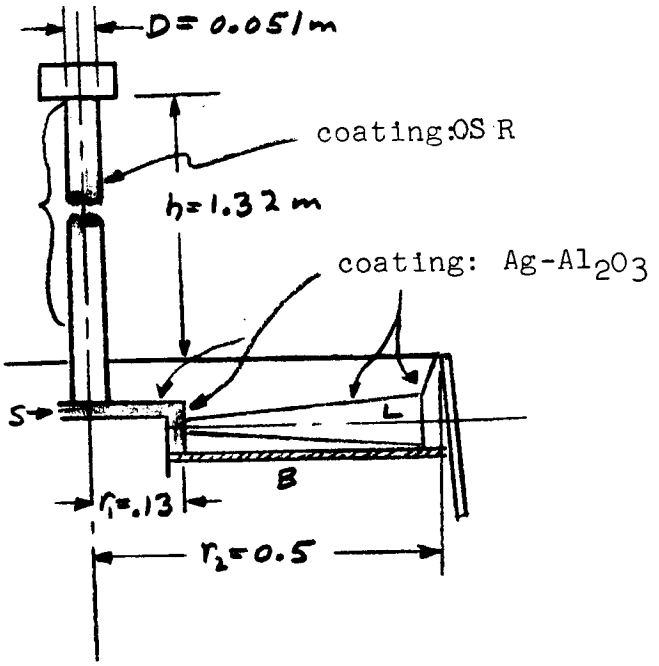

Figure 6C3.3 - Antenna Configuration, Shield Configuration - Thermal Input to Louvers (1/10 scale)

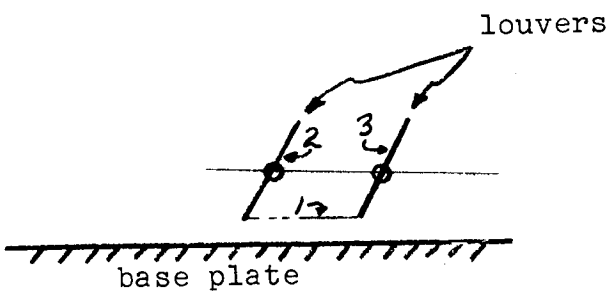

Figure 6C3.4 Louver View Factor Sketch

For most missions, the area of the cone is expected to be approximately 3 m^2 and at perihelion, the temperature will be less than 400°K (0.2 AU mission) or 473°K (0.1 AU mission). The emissivity as far as solar cell heat rejection is concerned will be approximately 0.9. However, because of the concentric polished beryllium stiffening rings on the solar cell cone, the effective emittance to the louvers will be approximately 0.05 (18). A graph of thermal input versus angle of the solar cell cone is given in Fig. 6C3.5. The large reduction in thermal input as a result of the stiffening ring construction is evident. On the 0.1 AU mission, in addition to the solar cell cone, there is a skirt of solar cells with an area of 0.85 m^2 (9.2 ft^2) The geometry of the skirt is given in Fig. 6C3.7. This skirt is designed to operate at the same temperature as a right cylindrical skirt. Thus, its pwer output corresponds to a right cylindrical skirt with 0.85 (cos 40°) = 0.65 m^2 (7 ft^2) of area. The view factor of the skirt shield to the louver area is 0.054. The flux from the Sun that falls on the inside of the shield as a result of the finite size of the Sun is

$$(0.5)(1.375 \times 10^5)\frac{w}{m^2}(\pi 1.04^2)\sin(0.9^\circ) = 3.65 \times 10^3 w$$

at 0.1 AU. (The centroid of one-half of the Sun disk makes an angle of 0.9° with the vehicle Sun line at 0.1 AU.) The specular reflections from the skirt shield do not strike the louver area, and are in fact almost completely rejected from the vehicle. The energy which is diffusely scattered is $(3.65 \times 10^{-3}$ w)(0.05) = 183 w. Hence, (183)(0.054) = 9.9 watts, is incident upon the louver area. In summary, the radiation incident upon the louver area is 4.5 w maximum for the 0.2 AU mission and 5.1 + 9.9 = 15 w maximum for the 0.1 AU mission.

Launch thermal control has been considered in only a very cursory fashion. The boost phase within the Centaur shroud lasts approximately 220 seconds. Sufficient insulation to prevent overheating of the instrument compartment solar cells can no doubt be attached to the shroud with little velocity increment penalty. The total burn time for all stages is in the neighborhood of 800 seconds. At the end of this interval the spacecraft will be in the sunlight with the spin-axis aligned essentially perpendicular to the Sun-vehicle line. At this point or before the electric power generation will be sufficient to prevent excessive cooling of the instrument package (see section 5B1).

The magnetometer at the top of the antenna boom must be maintained between 270°K and 370°K. Figure 6C3.6 indicates the geometry of this package as well as the thermal control elements. Heat flow by conduction between the instrument can

and the antenna is to be limited to $\pm$ 1 w. Using 8 layers of 0.5 mil. aluminized "H" film with 3 mil Dexiglass spacers covered with OSR, the heat leak through the walls will be approximately +0.36 watt at o.1 AU and -0.15 watt at 1.0 AU assuming internal temperatures of 370°K and 270°K respectively. The top surface, if painted black with $1.0 > \epsilon_T > 0.9$, will reject less than 2.4 w at 270°K and at least 7.3 w at 370°K. It is suggested that a 3.55 watt radioisotope heater be used to make up possible 3.55 w loss at 1.0 AU. Power dissipations of the magnetometer is negligible except that 3 watts is used when "flipping" the axis of the fluxgates.

Heat Balance

	1.0 AU	0.1 AU
leak from antenna	-1.00	+1.00
wall leak	-0.15	+0.36
radiator	-2.4(270°K)	-7.3(370°K)
radioisotope heater	+3.55	+3.55
	0.00	-2.40 w

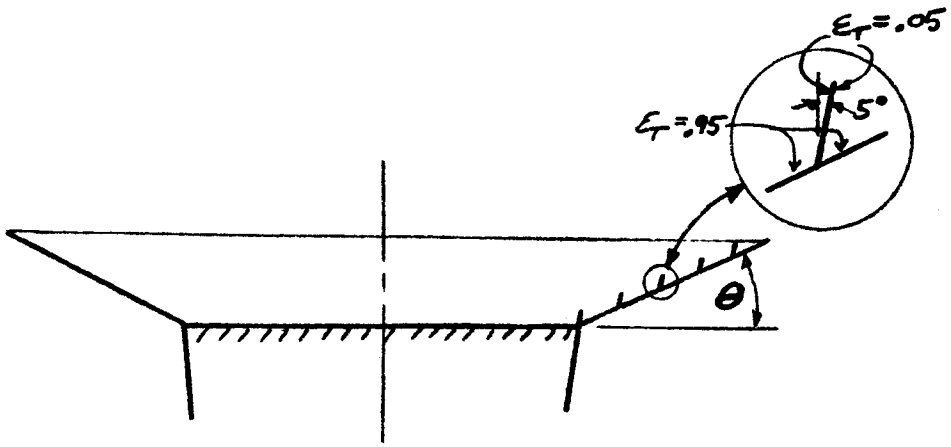

Figure 6C3.5 Thermal Input from Solar Cell Cone

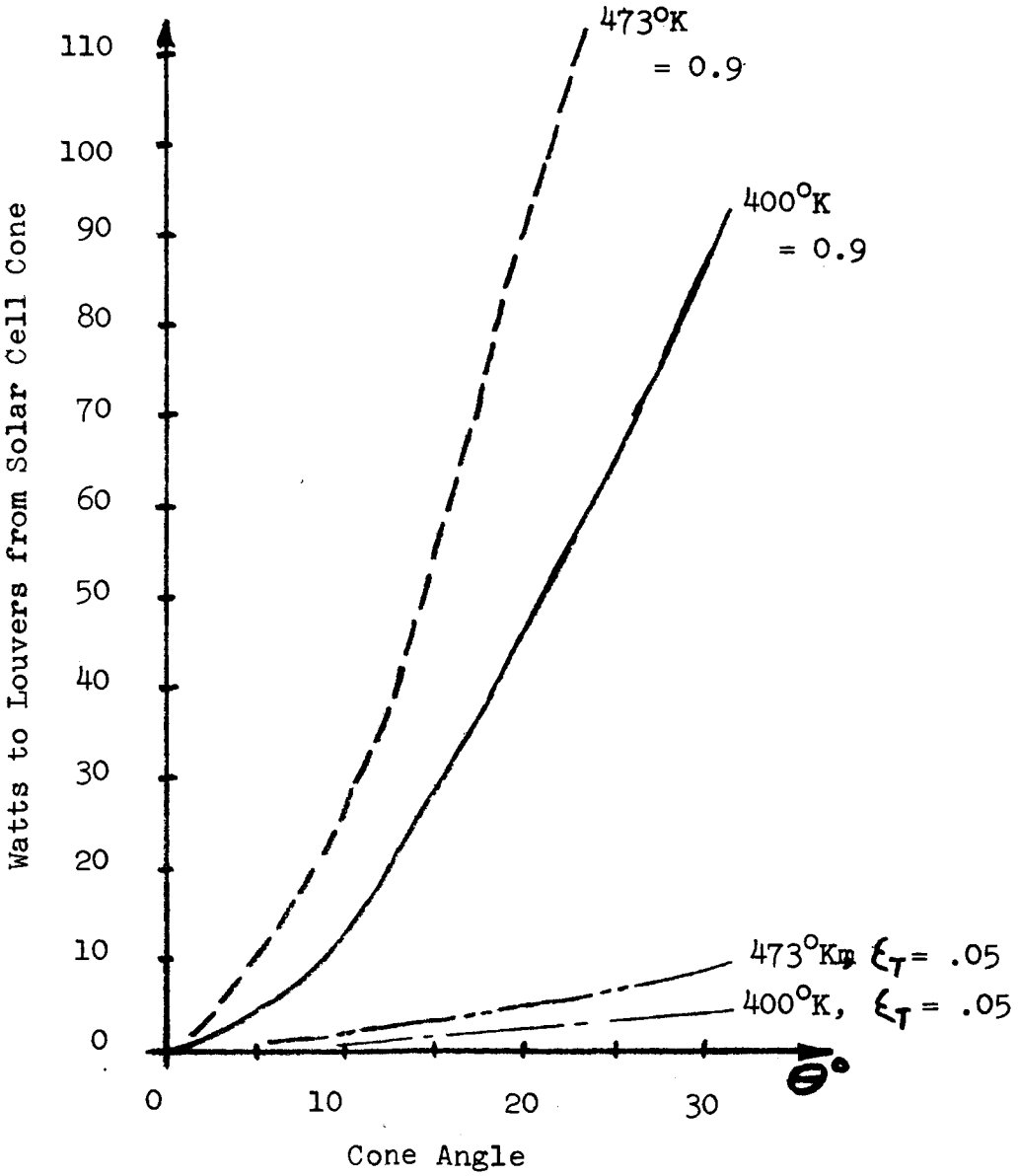

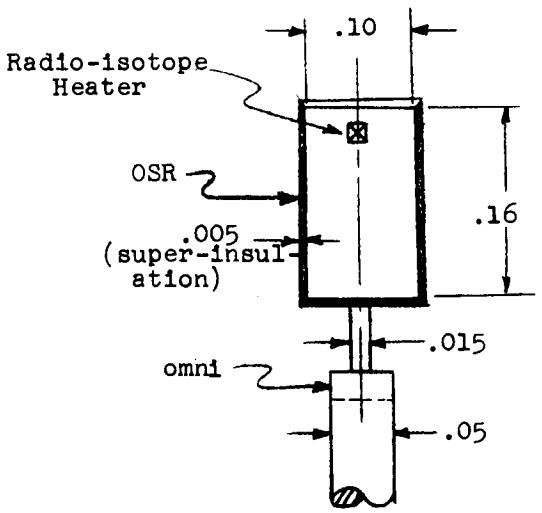

Figure 6C3.6 Magnetometer - Thermal Control
(dimensions in meters)

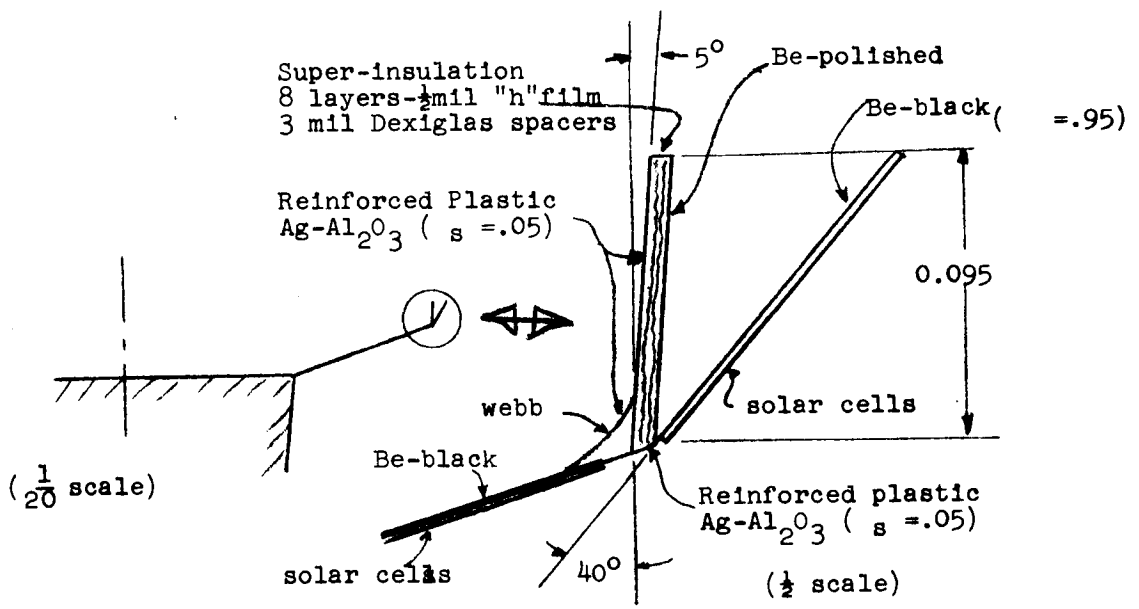

Figure 6C3.7 Detail of Solar Cell Skirt for 0.1 AU Mission

6D. Power Supply

6D1. Power Requirements

The power supply for the ICARUS missions is to provide all of the electrical energy for the spacecraft's experiment and communication equipment. It must also provide this energy in suitable form, in that the power conditioning equipment is considered as part of the power supply.

For the program of spacecrafts considered, the power required is 40 wattts (conditioned) at aphelion increasing to 240 watts at 0.3 AU. Between 0.3 AU and perihelion (either 0.2 AU or 0.1 AU) a minimum of 240 watts is required.

The minimum life of the power supply is to be long enough to assure required power at perihelion of the first orbit.

An imposed restriction on the power supply is that it not require articulation, despinning, or varying orientation of the spacecraft or its components. This restriction is considered to enhance the reliability of the system and lower its development time and costs.

6D2. Results

Many types of power supplies and combinations of power supplies were considered for the missions. These included solar cells, solar thermoelectric devices, solar thermoionic devices, radioisotope thermoelectric and thermoionic generators, fuel cells, and batteries. From these, silicon N/P solar cells were selected as the primary power supply. The main factors in the selection were weight, cost, and state-of-the art of the power supply.

In order to have initial power, for orientation of the spacecraft, and emergency power, in case the spacecraft should lose orientation, a 1.0 kg (2.2 lb) silver cadmium battery was also selected. This battery provides 73 watt-hours of power.

Although solar thermoelectric devices, GaAs solar cells, and radioisotope thermoelectric generators were not selected, very strong cases were presented for their use. These power supplies are discussed in section 6D4.

The power supply selected consists of a panel array of N/P silicon solar cells in the shape of a frustum of a cone, as shown in Figure 6D2.1. This design takes advantage of the facts that solar cell panels can be maintained at a lower temperature by tilting them away from the Sun, and that solar

cells are more efficient at low temperature. The increased efficiency compensates, in part, for the reduced incident solar radiation per unit area of cells.

Although the design concept is the same for all missions, each mission has a frustum array which is sized to optimize the solar cells' performance over the AU range anticipated. For the 0.2 AU perihelion mission, the design is shown in Figure 6D2.1A. It consists of a frustum array which makes an angle of 30° with respect to the Sun's rays, encompasses a total area of 2.8 meters^2 (30 ft^2), and weighs 11 kg (24 lb). The power delivered is shown in Figure 6D2.2. This design allows the spacecraft to attain perihelion while retaining the solar cell array at a temperature below 394°K (the maximum temperature reported for no thermal degradation (19).

The extreme variation of the solar intensity during the 0.1 AU perihelion mission necessitates using a primary power supply which is augmented by a degrading secondary supply available only during the first entry into perihelion. The power supply designed is shown in Figure 6D2.1B. It consists of a frustum array of cells which makes an angle of 20° with respect to the Sun's rays and has a total area of 2.6 meters^2 (28 ft^2). The maximum temperature attained by these cells is 473°K, which is below the reported temperature for permanent, total, thermal degradation (22). As the power provided by these cells is inadequate at high AU values, an additional frustum array of cells is used to provide power during the first entry into perihelion. This array (skirt) encompasses 0.85 meters^2 (9 ft^2) and makes an angle of 50° with respect to the Sun's rays. The total power delivered by the system is shown in Figure 6D2.2. Total panel weight is 13 kg (28 lb).

6D3. Analysis of Power Supply

An analysis of the performance of the solar cell array can be made by using an energy balance on a unit surface area of the panel. If, as a first approximation, it is assumed that there is no temperature decrease through the panel and that there is no thermal radiation interaction between the panel and the spacecraft or the panel and itself, then the resulting equation is

$$\frac{SC}{(AU)^2} A_s \alpha_f K = \sigma(\epsilon_f + \epsilon_b) T^4 + P$$

where: A_s ratio of projected area normal to Sun's rays to total area ($\frac{\sin\theta}{\pi}$ for frustum surface)

AU astronomical unit distance from Sun

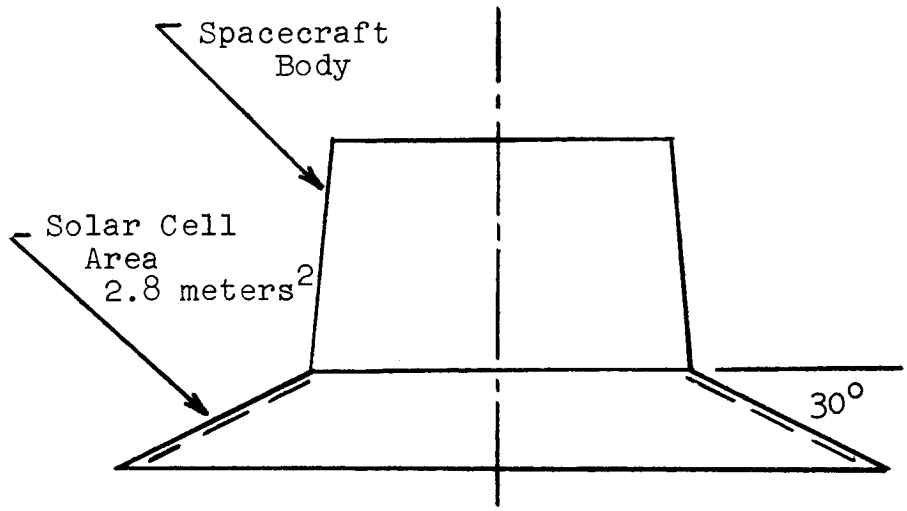

Spacecraft for 0.2 AU Mission

Figure A

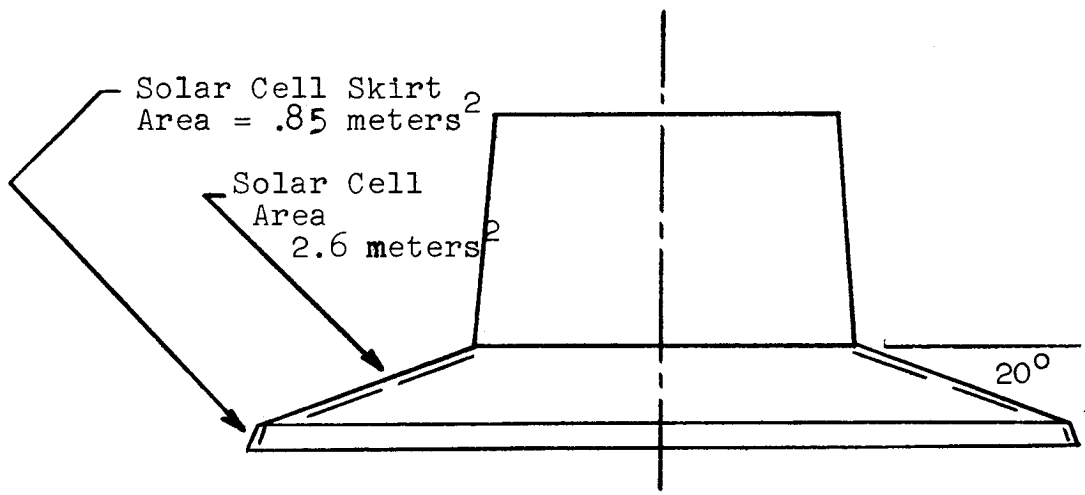

Spacecraft for 0.1 AU Mission

Figure B

Figure 6D2.1

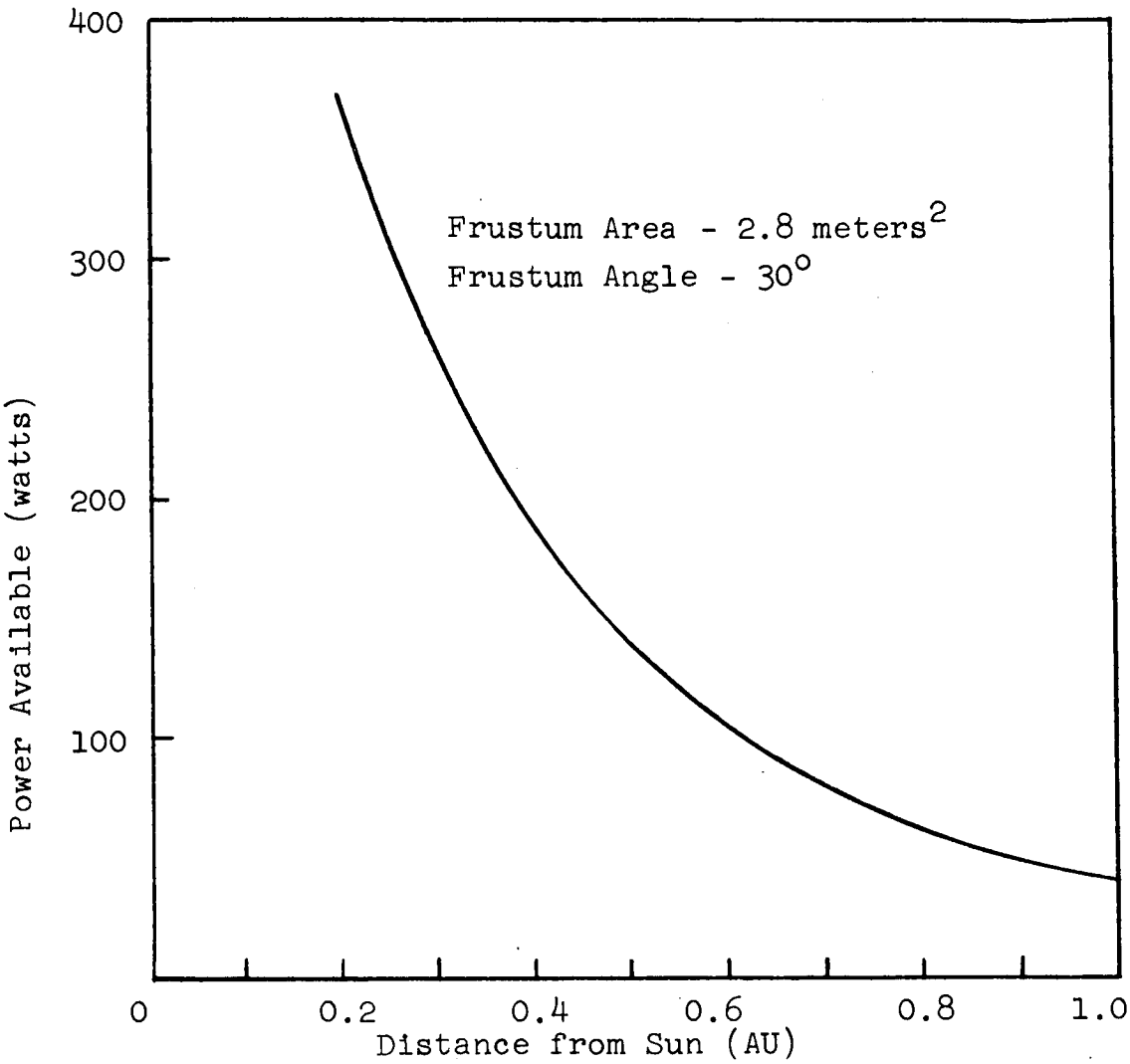

Figure 6D2.2 Power Available for 0.2 AU Mission

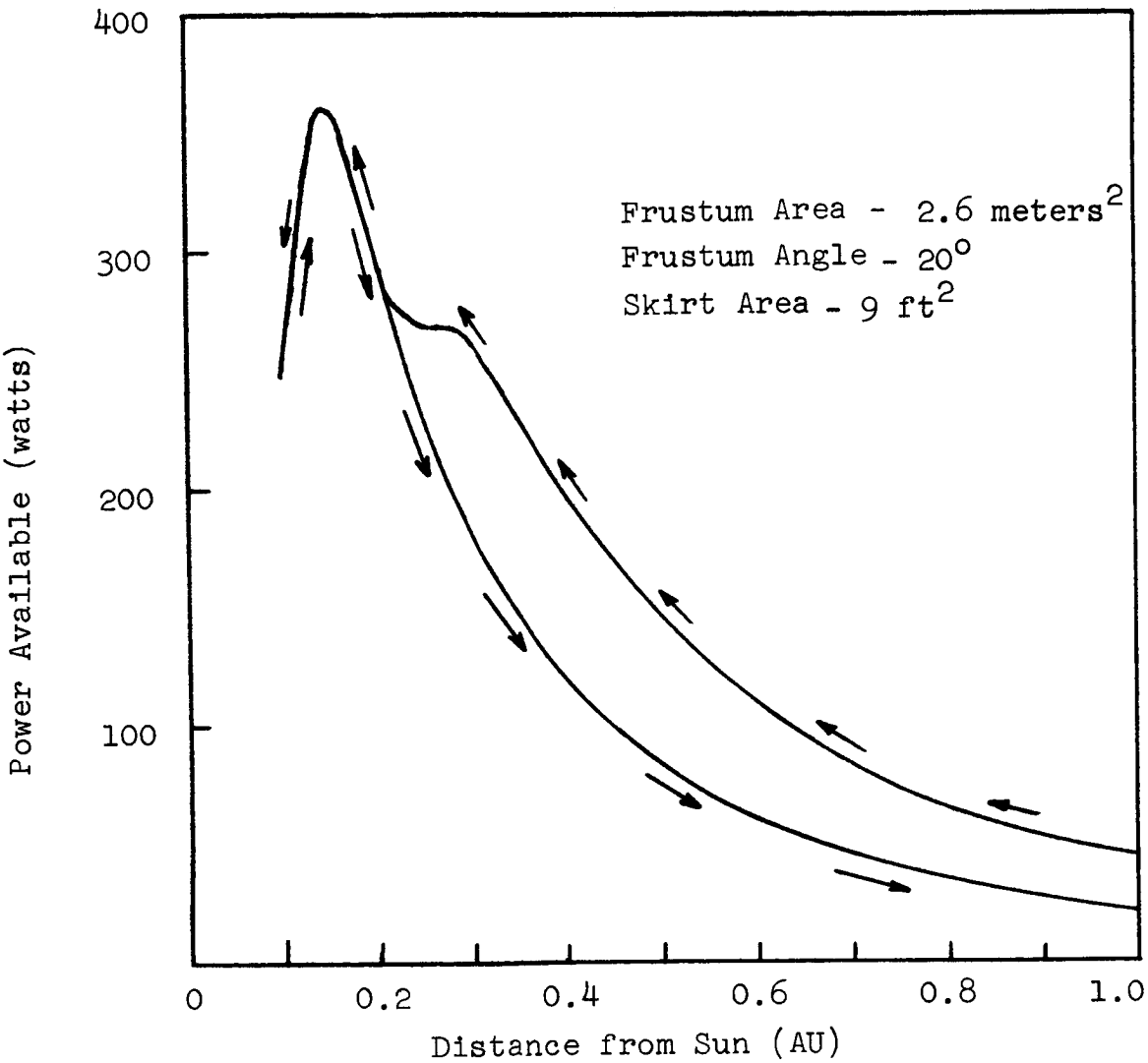

Figure 6D2.3 Power Available for 0.1 AU Mission

K empirical correction factor for small angles

P electrical power obtained per unit area of surface

SC solar radiation intensity per unit area at 1.0 AU (1400 watts/meter^2)

T temperature of panel

α_f averaged solar absorptivity of front side (solar cell side)

ϵ_f averaged emissivity of front side of panel

ϵ_b emissivity of back side of panel

θ angle between frustum surface and Sun's rays

σ Stefan-Boltazmann constant for radiation

The power obtained from a unit surface area of panel is given by the equation

$$P = \eta_b \eta_p \eta_T K A_s \frac{SC}{(AU)^2} \qquad 6D3.2$$

where the new symbols represent

η_b transmissibility of solar cell cover

η_p packing factor (actual solar cell area per unit surface area)

η_T thermal efficiency

Equations 6D3.1 and 6D3.2 indicate that, for a given design, the power and temperature are coupled,

$$\left(\frac{\alpha_f}{\eta_b \eta_p \eta_T} - 1\right) P = \sigma (\epsilon_f + \epsilon_b) T^4 \qquad 6D3.3$$

and are dependent on AU location and frustum angle selected.

The numerical values use in performing the numerical analysis were

$\alpha_f = 0.60$ ($\alpha_{\text{solar cell}} = 0.65$, $\alpha_{\text{area between cells}} = 0.2$)

$\epsilon_f = 0.80$ ($\epsilon_{\text{solar cell}} = 0.65$, $\epsilon_{\text{area between cells}} = 0.49$)

$\epsilon_b = 0.90$

$\eta_b = 0.92$

$\eta_p = 0.90$

which were considered representative (19). The thermal efficiency used was (19),

$$\eta_T = 15\%, \quad T \leq 196^{\circ}K$$
$$\eta_T(\%) = 24.17 - 0.0468T(^{\circ}K) \qquad 6D3.4$$

This efficiency is the most conservative of those reported. Many investigators have reported higher efficiencies existing over a larger temperature range (22,23).

Using the stated values, the power and temperature were calculated. The coupling of the two is shown in Fig. 6D3.1 with the maximum power calculated to be 200 watts/mt^2 (18.7 watts/ft^2). Figure 6D3.1 may be used to design a panel as its abcissa reflects the effects of AU location and frustum angle. The effect of varying these parameters upon the power produced is also shown in Fig. 6D3.2.

Varying the frustum angle not only changes the area ratio, As, it also changes the reflectivity characteristics of the solar cells. This effect has been evaluated experimentally by Johnston (20) using flat panels. Figure 6D3.3 indicates the values of K used in this analysis. Johnston's values have been modified to include the effect of the frustum's curvature.

$$K(\theta_{\text{this analysis}}) = K\left(\frac{\pi}{2} \cdot \theta_{\text{Johnston}}\right) \qquad 6D3.5$$

Upon reveiwing Fig. 6D3.1, it is noticed that varying the frustum angle is an effective way of obtaining a desired power available curve for a particular mission. This, then, becomes the design procedure for the power supply: Optimize the frustum angle so that the power available curve best fits the power required for the mission.

A limitation on the design selected is the maximum solar cell temperature allowed. It is reported that N/P silicon solar cells can withstand 394°K for long periods of time with no thermal degradation (19). It is also believed that the cells can withstand higher temperatures ($< 473^{\circ}$K) with little thermal degradation ($< 2\%$) if they are provided with high

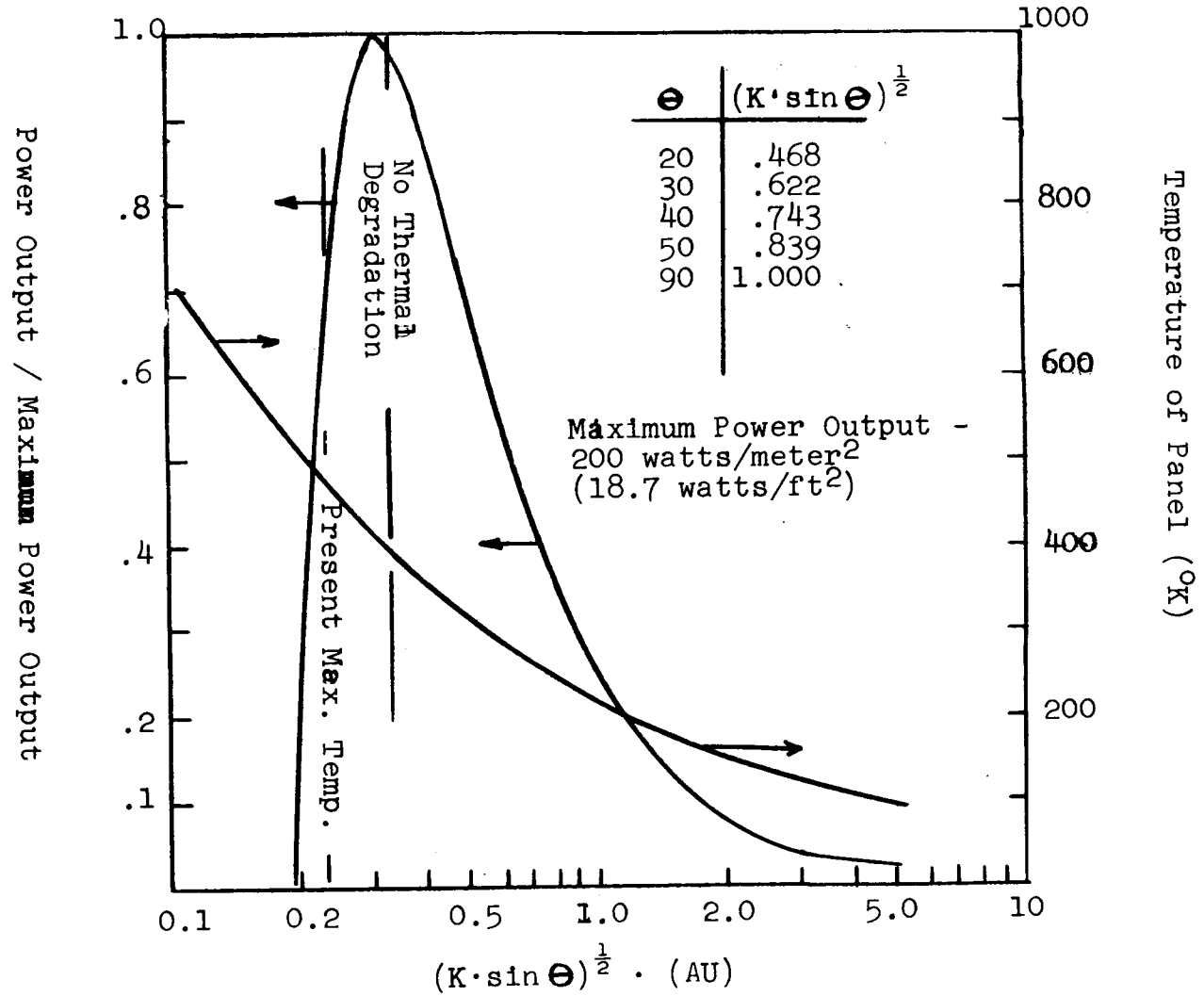

Figure 6D3.1 Effects of AU Location and Frustum Angle upon Panel Temperature and Power Output

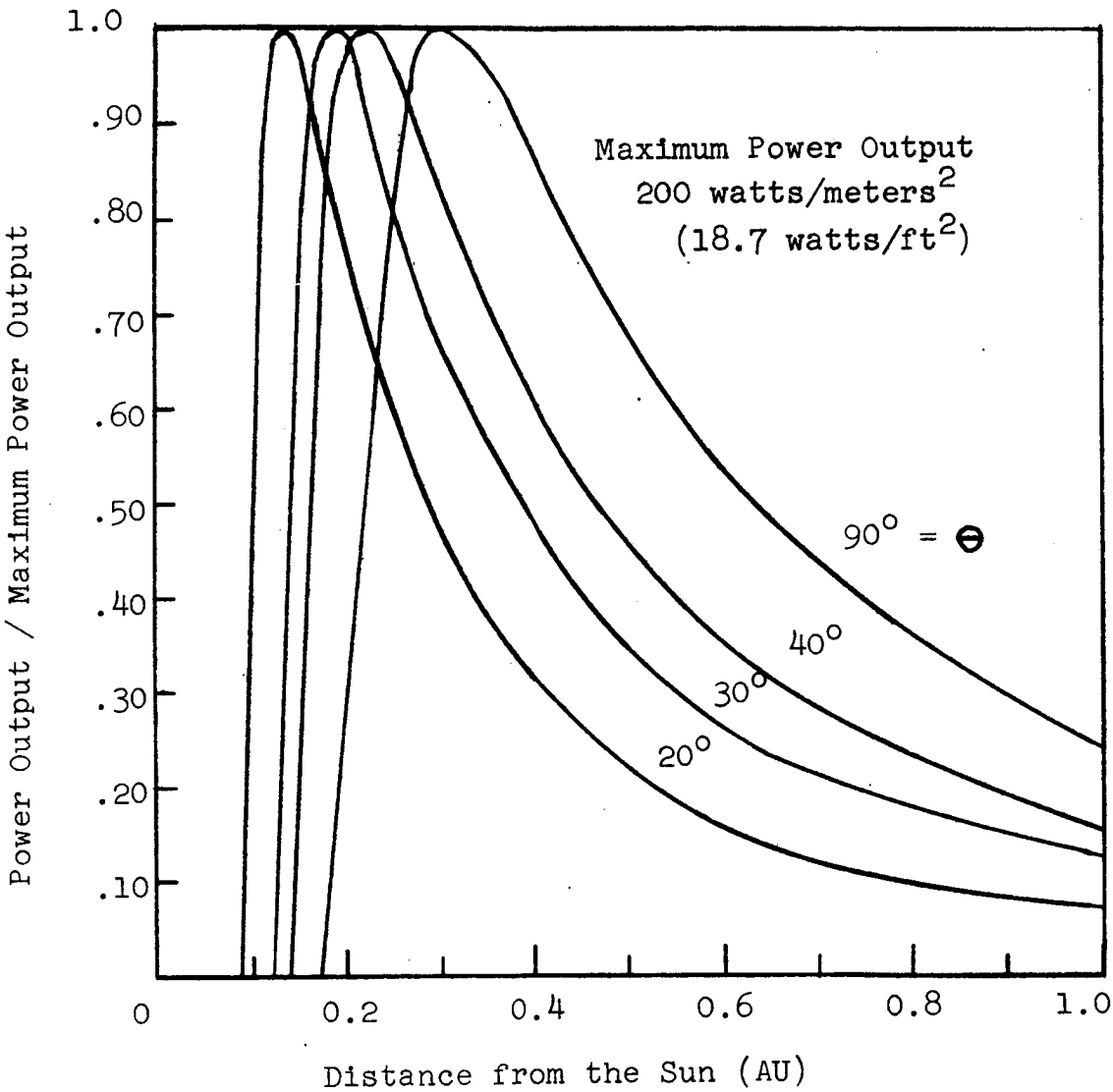

Figure 6D3.2 Effect of Frustum Angle - Θ Upon Power Output of Panel

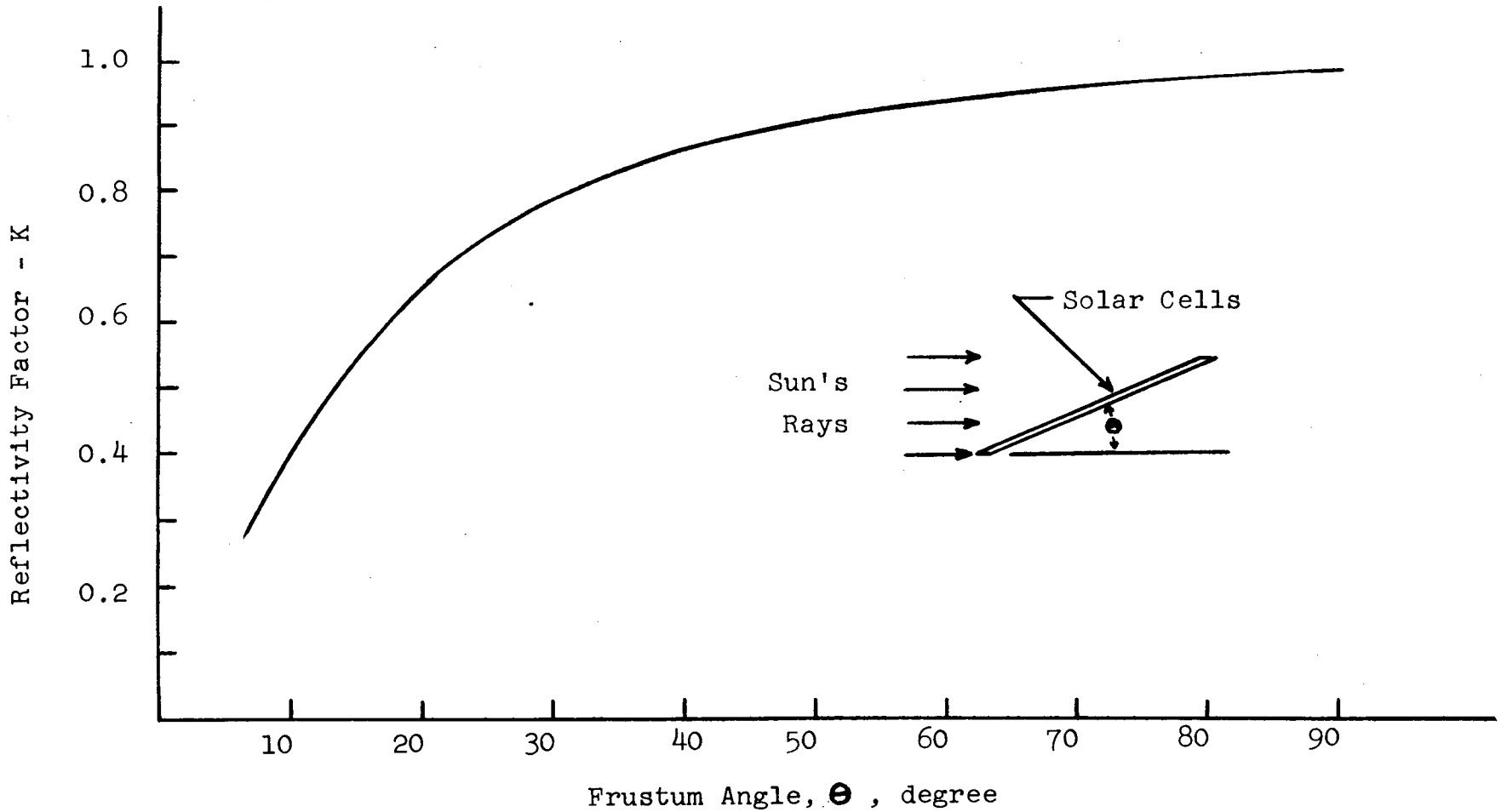

Figure 6D3.3 Effect of Frustum Angle on Reflectivity Factor - K

temperature contacts (22). In this analysis it was assumed that:

(1) If the cells were retained at a temperature less than 394°K, no thermal degradation was guaranteed (the ideal situation);

(2) If the cells were retained at a temperature less than 473°K, insignificant thermal degradation was present;

(3) If the cells exceeded 473°K, complete permanent degradation occurred.

As stated earlier, the maximum power per unit area is 200 watts/m^2 (18.7 watts/ft^2). However, before determining the solar cell area needed to provide the required power, the delivery losses and solar degradation of the power system must be determined. For this analysis delivery losses were estimated to be given by the representative values (19,23,25).

Diode and wiring loss	5%
Cell mismatch	4%
Random open circuit	6%
Power conditioning	10%

Thus the delivery efficiency was assumed to be 77.1%.

A major degradation of the power system is caused by solar radiation damage. Exact prediction of this damage is impossible although some insight can be obtained by assuming that the Sun's particle properties vary by an inverse square ratio with solar distance. The particle-time intensity calculated can then be correlated with known cell degradation information (24). An alternate approach is to use the calculated degradation caused by a major solar flare (23). As it is assumed that the cells will be provided with suitable cover glasses, the degradation caused by solar radiation is estimated to be 10% during the short lifetime of a mission (75 to 85 days to perihelion).

The total efficiency is, therefore, 69.4%. This implies that the maximum power delivered per unit area of solar cell surface is 13.9 watts/m^2 (13.0 watts/ft^2).

Figure 6D3.2 indicates that the power required for the 0.2 AU mission can be obtained by using a frustum angle of 30°. Using this angle, the cells attain a maximum temperature of 394°K; consequently there is no thermal degradation. A total cell area of 2.8 meters^2 (30 ft^2) is selected. The power available to the spacecraft is shown in Fig. 6D2.2. Total panel weight is 11 kg (24 lb).

The power requirements for the 0.1 AU mission cannot be satisfied by using only a single frustum array of solar cells. No angle exists which satisfies all of the power requirements, yet has satisfactory area and weight. The design selected consists of a primary power supply array of 2.6 meters^2 (28 ft^2) at an angle 20°. This array attains a maximum temperature of 473°K and is expected to survive the perihelion environment.

Supplementing the primary power is the power from a frustum skirt of .85 meters (9 ft^2) at an angle of 50°. (The area and angle are partly imposed by thermal considerations (see section 6C3) and are equivalent to an area of 0.65 meters at an angle of 90°.) The skirt provides additional power at large AU's. However, this power is available only during the first entry into perihelion.*

Since the solar cells are subjected to a wide range of temperatures and solar intensities, the output voltages and currents vary greatly during the mission. In order to provide a constant voltage bus for all equipment a dc-dc converter, using high speed switching transistors, is provided. The main bus regulator senses the power requirement of the craft and adjusts its pulse height and width in order to maintain a constant bus voltage.

A central power control unit provides for switching and distribution of power to the various experiments and communication equipment throughout the mission. Electronic current limiting is used to protect against a short circuit.

6D4. Alternate Power Supplies Considered

After evaluating all potential power supplies, N/P silicon solar cells were selected. However, there were other supplies that look promising and deserve consideration. These supplies are:

1. Solar thermoelectric panels augmenting solar cell panels
2. High temperature GaAs solar cells
3. Radioisotope thermoelectric generators

A solar thermoelectric generator uses heat produced by solar radiation to produce the temperature difference between the hot and cold junctions. A sandwich type construction is used, wherein the thermoelectric elements are bonded between two thin sheets. One surface, called the collector, is coated to produce a high solar absorptivity and a low

*High temperature at perihelion permanently degrade the skirt.

emissivity. This side of the panel is oriented toward the Sun, absorbs energy from it and produces the hot junction temperature. The heat absorbed is partially converted into electrical energy and the rest is transferred to the cold junction and radiated from the other side of the panel.

Solar thermoelectric panels have been successfully tested in earth orbit, and it has been analytically predicted that panels could be designed to produce 40 to 100 watts/ft^2 in the 0.1 AU to 0.3 AU range. These panels could survive boost environment and would weight 1.0 to 3.0 lb/ft^2 (6).

The designs considered consisted of solar thermoelectric panels supplementing a frustum N/P silicon solar cell array. The solar cells provided power in the 0.2 AU to 1.0 AU range and were the same design as the power supply selected for the 0.2 AU perihelion mission. The thermoelectric panels were used to provide power in the 0.1 AU to 0.2 AU range.

Two designs were considered. One design consisted of articulating solar thermoelectric panels shielding the solar cell frustum at low AU ranges. The other design consisted of a fixed solar thermoelectric skirt supplementing high temperature silicon solar cells (300^{o}C). It was proposed that if the thermal limitations imposed by the contacts and coverglass bonding materials could be eliminated, a solar cell could be developed which would withstand high temperature. Although the cell would yield no power at high temperature, it would be available to provide power when it cooled. These designs were rejected because of their need for articulation or need for high temperature cells, which are not available at present.

High temperature GaAs solar cells were also considered as a replacement for the N/P silicon cells. These cells offer higher efficiencies at elevated temperatures (7). They also withstand higher temperatures (673^{o}K) without failure (11), thereby relieving the necessity of a power augmentation skirt for low AU missions. GaAs cells were rejected for the mission because of their high cost (30 to 50 times that of N/P silicon cells) and the uncertainty of their future manufacture (9).

Due to the extremes in temperature and solar environment, a radioisotope thermoelectric generator was considered for the missions. The generator, being mounted internally, would not be subject to the surface degradations suffered by other systems. Two designs were investigated. One design used the RTG as the only power supply. The other used a small RTG to supplement a solar cell or solar thermoelectric supply. RTG's were rejected because of their heavy weight ($\sim$ 1 lb per watt), their cost, the availability of the desired isotope, and the difficulty of designing an efficient heat rejection system for an internally mounted RTG.

REFERENCES

1. Goetzel, C., Rittenhouse, J., and Singletary, J. eds.: Space Materials Handbook, ML-TDR-64-40, chpts. 15 and 18, 1965.
2. Rittenhouse, J., and Singletary, J.: Space Materials Handbook, Supplement 1 to the Second Edition, NASA SP-3025, Sect. 2.5, 1966.
3. Gerard, G.: An Evaluation of Structural Sheet Materials in Missile Applications, Jet Propulsion, p. 511, Aug. 1958.
4. Fern, R., Glass, R., Needham, R. and Steinburg, M.: Beryllium-Aluminum Alloys, Journal of Spacecraft, vol. 2, no. 1, p. 87, 1965.
5. Ormstrong, H. and Burns, A.: Structural Weight and Cost Comparison of Large Space Structures Employing Beryllium-Aluminum Alloys, Proceedings of the AIAA/ ASME Seventh Structures and Materials Conference, p. 338, April, 1966.
6. Spacecraft Structures, C.C. Osgood, Prentice-Hall, Inc., Englewood Cliffs, N.J., 1966.
7. The Scout, LTV Corporation, October, 1965.
8. Ordway, F.I., Gardner, J.P. and Sharpe, M.R.: Basic Astronautics, Prentice-Hall International,Inc., Englewood Cliffs, 1962
9. Breuch, R.A.: Exploratory Trapped Particle and Trapped-Particle-Plus-Ultraviolet Effects on the Optical Properties of Spacecraft Thermal Control Coatings, AIAA Paper no. 65-646 +
10. Streed, E.R., Cunningham, G.R., and Zierman, C.A.: Performance of Multilayer Insulation Systems for 300° to 800° Temperature Range, AIAA Paper no. 65-663.
11. VanVliet, Robert.: Passive Temperature Control in the Space Environment, The MacMillan Co., New York, 1965.
12. Streed, E.R.: Private Communication AMES Research Center, NASA Moffett Field, Calif.
13. Mirtich, M.J., Mark, H.: Alteration of Surface Optical Properties by High Speed Micron-Size Particles, Symposium on Thermal Radiation of Solids, NASA SP-55, 1965.
14. London, A.: Thermal Control of the Nimbus Satellite Control System, AIAA Unmanned Spacecraft Meeting, AIAA Publication no. CP-12, Los Angeles, March, 1965.
15. Breuch, R.A.: Exploratory Trapped-Particle and Trapped Particle Plus Ultraviolet Effects on Optical Properties of Spacecraft Thermal Control Coatings, AIAA Paper no. 65-646.
16. Zerlant, G.A., Carroll, W.F., and Gates, D.W.: Spacecraft Temperature-Control Coatings: Selection, Utilization, and Problems Related to the Space Environment, International Astronautical Federation Congress, Athens, Greece, Sept., 1965.

17. Hass, G., et al.: Solar Absorptance and Thermal Emittance of Aluminum Coated with Surface Films of Evaporated Aluminum Oxide, AIAA Thermophysics Specialist Conference, Monterey, Calif., Sept., 1965, AIAA Paper no. 65-656.
18. Fenn, R.W., Crooks, D.D. and Pasternak, R.C.: New Ductile Beryllium-Aluminum Wrought Alloys, Symposium on Newer Structural Materials for Aerospace Vehicles, Sp. Tech. Pub. no. 379, ASTM, 1965.
19. Solar Probe Study, Final Report, General Electric, NASA Contract NAS2 1359A, September, 1963.
20. Johnston, P.A.: Laboratory Experiments on the Performance of Silicon Solar Cells at High Solar Intensities and Temperatures, NASA TN D-2733.
21. Bifano, W.J.: Analysis of Solar Thermoelectric Flat-Plate Generators Operating in the Range 1.0 to 0.1 Astronomical Unit, NASA Technical Memorandum, Lewis Research Center, Cleveland, Ohio, to be published.
22. Shivoneu, Y.T.: GaAs Solar Cell Study: Final Report Materials Science Research Laboratory, Texas Instruments, 08-65-181, 1 December 1965.
23. Cobb, M.W., Cummings, W.S., and Fairbanks, J.W.: The Feasibility of a Programmed Heat Shield for Solar Cell Performance Control, Philco WDL Division, Contract NAS2-2564, October, 1965.
24. Cooley, W.C., and Janda, R.J.: Handbook of Space Radiation Effects on Solar Cell Power Systems, NASA SP 3003, 1963.
25. Solar Probe Study, Book B., Appendix 6, Power Philco WPL, Contract NAS-2-1397, 30 August 1963.

VII. ATTITUDE CONTROL AND STABILIZATION

7A. System Requirements

7A1. General Considerations

The attitude control system is designed to acquire the desired spacecraft orientation upon injection and maintain this orientation during the entire mission. It consists of sensors, controllers and actuators forming a closed loop system as described in section 7B. The orientation of ICARUS must satisfy the following constraints:

a. Orientation of the experiment sensors with respect to the Sun.
b. Orientation of the solar cells with respect to the Sun.
c. Orientation of the antenna with respect to Earth.

Constraint (a) is obviously overriding since the primary objective of the mission is to "look at the Sun". Thus the natural reference for experimental measurements is the vehicle-sun line. Some of the experiments require that the sensor heads scan the complete 360° in the vehicle orbit plane. This implies sensors mounted on a spinning platform, with spin axis reasonably close to the normal of the orbit plane. The maximum deviation allowed, from the experimental standpoint, is $\pm$ 5° (see section 3B2). The alternative, several sensors each looking in a different direction, has the disadvantages of added weight and possible offsets between sensors, while there is only a slight advantage in simultaneous measurements vs. measurements at most $\frac{1}{2}$ sec. apart.

In addition to the requirements listed above, simplicity and reliability were of prime importance in the choice of a configuration. It is most desirable that the spacecraft be capable, after the initial attitude acquisition is completed, of maintaining the desired attitude with a minimum of active control.

7A2. Choice of a Spin-stabilized Vehicle

Since the experiments require some spinning sensors, a major choice to be made was between spinning the entire vehicle or only parts of it. The main arguments for and against despinning the various components are listed in the table below.

Table 7A2.1

Despin	For	Against
Solar cells and thermal control elements	Weight is reduced	Requires continuous orientation along vehicle-sun line or hinged panels
Antenna	Less power required for communication	Orientation of a pencil beam toward Earth requires a star sensor, a bearing, a separate motor drive and an onboard short memory program
Whole vehicle except experiment sensors	Same as combination of above	Attitude is more sensitive to disturbance torques. Active control is needed at all times and is more difficult to achieve during communication blackouts, one of which occurs near perihelion

The completely spinning configuration chosen, with spin axis normal to the orbit plane, is an eminently stable system provided the spin axis is also the axis of maximum moment of intertia. It satisfies all the requirements listed in section 7A1 and avoids the problem of earth-tracking with a despun antenna by providing enough power to transmit with a fan-beam antenna. The attitude control system is required to provide the initial attitude acquisition, but will only be called upon to perform occasional corrections during the cruise phase. As described in the following sections, it is a very simple and reliable system, similar to the present Pioneer control system and with many identical components. It thus has the added advantages of being low-weight and flight-proven.

7A3. Accuracy Requirements

The experiments require a minimum accuracy of $\pm 5^{\circ}$ in the orientation of the spin axis with respect to the normal to the orbit plane. The antenna pointing requirements are more severe: $\pm 2.5^{\circ}$ (see section 4B5). However the orientation of the spin axis must be known within $\pm 1^{\circ}$ (see section 3B1) and the data reduction problem is greatly simplified if this is also the accuracy required for the spin axis orientation. Hence a $\pm 1^{\circ}$ requirement is adopted as no difficulty is anticipated in meeting it with the ICARUS

control system.

During communication blackout periods it is not possible to track the position of the spin axis in roll, since there is no radio link with Earth. To overcome this difficulty the spacecraft is designed, in the case of the .2 AU mission, so that the drift of the spin axis remain within $\pm 1^{o}$ during blackouts. For missions closer in, it may become necessary to provide for drift corrections. This is discussed in greater detail in section 7D2.

The spin rate was chosen at 100 rpm. Since this is the spin rate expected during the kick stage, and since it is also satisfactory for the experiments, spin-up or despinning devices are not needed.

7B. Sensors, Controller, and Activator

7B1. Introduction

The control system provides attitude control by means of cold gas expulsion through a nozzle located on the solar cell skirt. Gas release takes place on the basis of qualifying logic provided by radio command and solar sensors. The single nozzle orients the spacecraft in two dimensions using the gyroscopic principle therefore gas release must be synchronized (this is done through the solar sensors) with respect to the spin position as measured from the vehicle-sun line.

7B2. Sun Sensors and Configuration

Following the general techniques of present Pioneer, Sun sensors are placed on the spacecraft in the configuration as shown in Figure 7B1.1 (where Fig. 7B1.2 serves to establish spacecraft coordinates) with the object of performing the following functions:

a. Sun sensor E - A narrow beam view of the sun is specified and the sensor provides a reference pulse on each revolution of the spacecraft.

b. Sun sensor A and C - These Sun sensors are located on the x-axis at right angles to the nozzle lever arm. Sensor A has a general view in the +z direction as the vehicle spins about the z-axis while sensor C views in the -z direction. When connected through suitable logic these sensors control pitching maneuvers on initiation by radio command - a Type I orientation of the craft.

c. Sun sensor B and D - These Sun sensors are located on the y-axis. Each has a symmetrical field of view with the major view in the x-y plane. The logical selection of the appropriate sensor provides a means for performing roll maneuvers on radio command - a Type II orientation of the craft. Cross sections of the view angles for the Sun sensors are presented in Fig. 7B1.1.

Due to spacecraft spin the duty cycle of incident solar energy upon the sensors will be less than 100%, the view restriction shades further restrict incident energy but precautions must be taken to bond the sensors tightly to the spacecraft to give a good conduction path for the heat so as to limit the sensor temperature range from 343°K to 223°K.

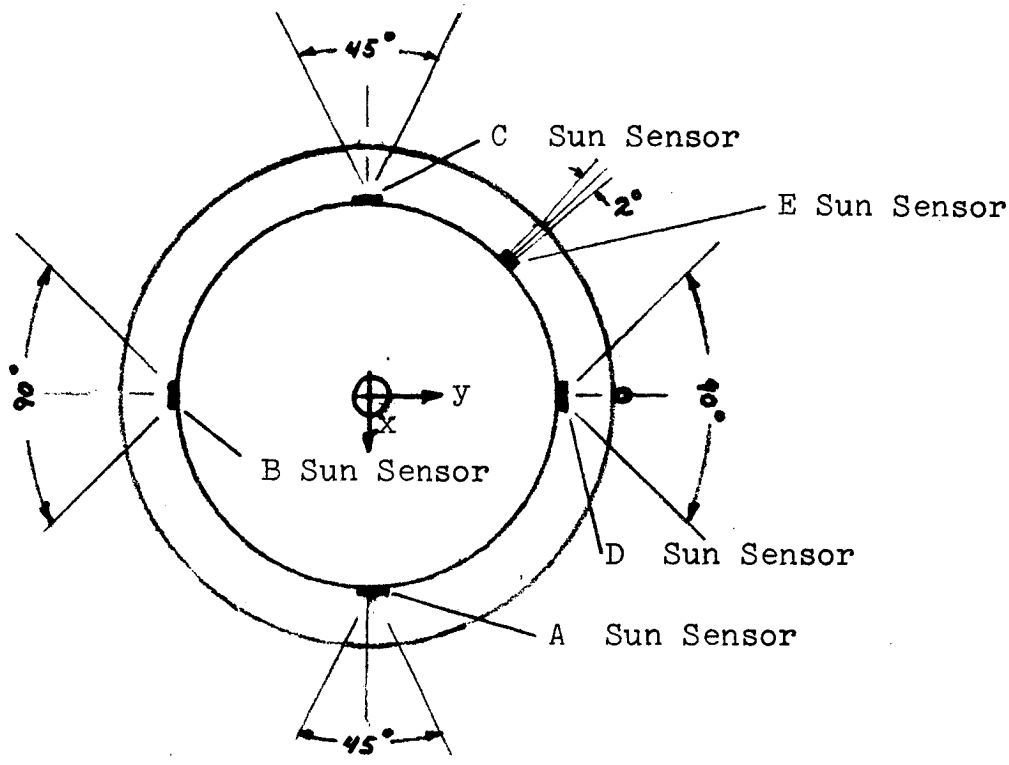

(a) In -z Direction

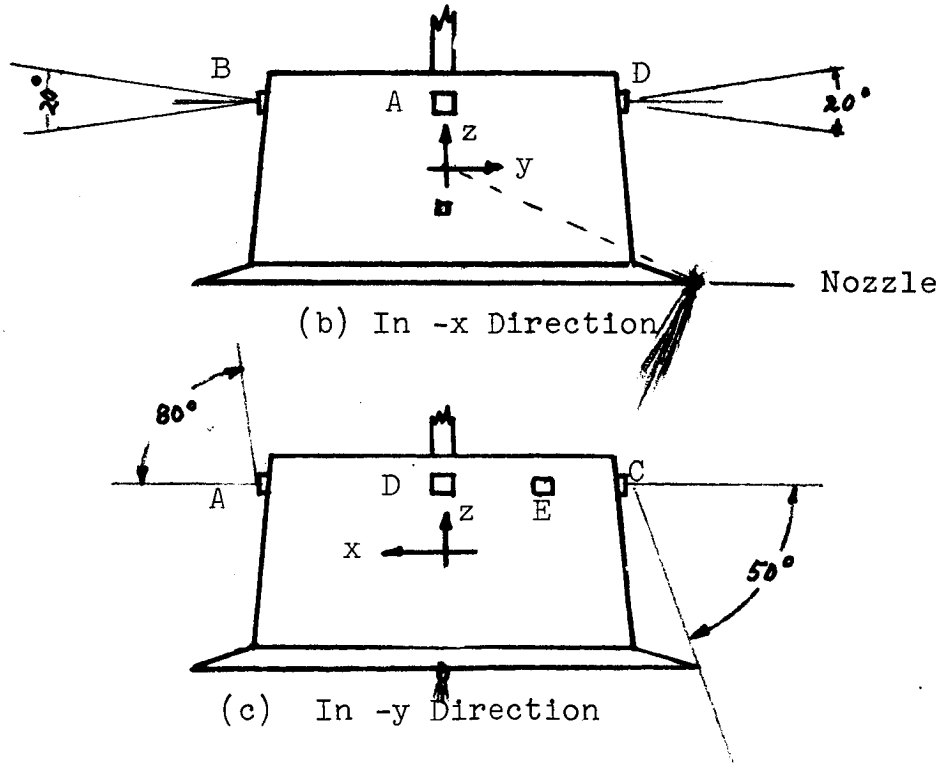

(b) In -x Direction

(c) In -y Direction

Figure 7B1.1 Sensor and Nozzle Views
Typical Angles

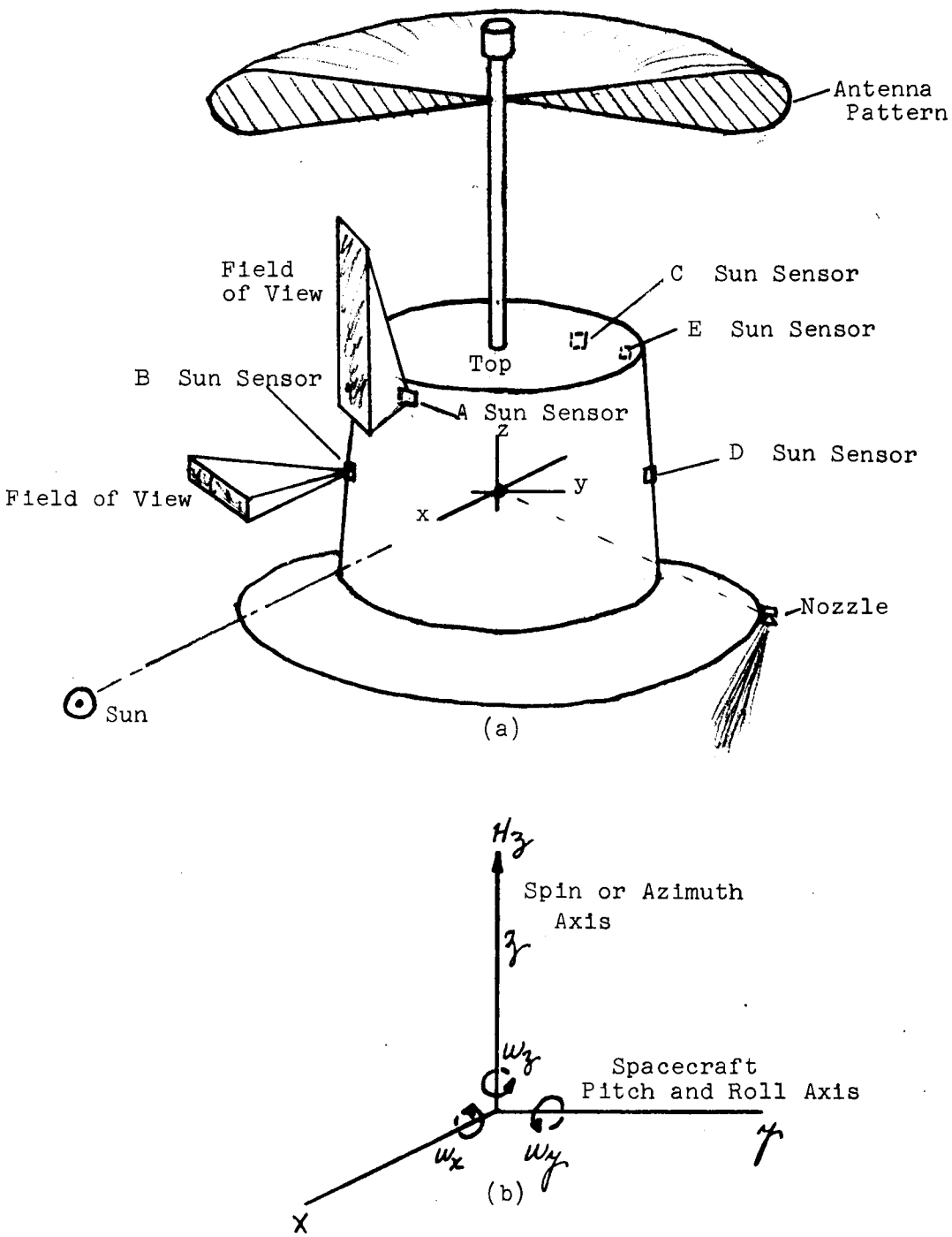

Figure 7B1.2 - Spacecraft Coordinates

7B3. Controller

Firing of the attitude control jet takes place on the basis of qualifying logic which includes the following signals:

a. Spacecraft readiness, e.g., launch complete,

b. Radio Command, e.g., Type I or II control mode specified, and

c. Sun Sensor Signals, e.g., during a Type II control mode logical qualifying of Sun Sensor D would provide a gas jet while this sensor sees the Sun thereby producing an increment of the roll angle about the y-axis in the positive direction.

Table 7B3.1 presents a general summary of sensor logic and resultant spacecraft maneuver.

Table 7B3.1

Qualified Sensor	Resultant Action
A only	Positive pitch increment
C only	Negative pitch increment
A and C	If, and only if, the integrated average solar incident energy on sensor A and C over one spin revolution is zero is it assumed that the pitch angle is zero and Type I control mode terminated
B only	Positive roll increment about vehicle-sun line
D only	Negative roll increment about vehicle-sun line

7B4. Actuator

Vehicle maneuvers are produced by actuation of a cold gas expulsion system. Cold gas (N_2 perhaps) is bottled at high pressure and released through a pressure regulator on the basis of qualifying logic as discussed in section 7B3. The quantity of gas required is based on an assumed specific impulse of 60 seconds. Filtering upon release is required to prevent clogging of lines or jet and contamination of

vehicle surfaces and sensor. Release of gas is obtained by a solenoid operated valve; therefore care must be taken to shield the experiments from any residual magnetic valve fields and also from the dynamic electromagnetic solenoid fields. In the present Pioneer the valve is located at the end of the boom adjacent to the nozzle; except for the afore mentioned reasons there is no objection to placing it elsewhere such as the equipment mounting platform of ICARUS. Power drain on actuation will be in the order of 10 watts with a maximum duty cycle of 90 degrees per revolution; with a spin rate of 100 rpm this will amount to 250 ms per second.

The nozzle lever arm must act through the center of mass of the system at right angles to the x-axis to avoid the undesirable mechanical couping resulting in excessive wobble buildup. It is assumed that the jet thrust produces a torque vector in the -x direction.

7C. Acquisition and Maneuver

The acquisition phase is initiated immediately after last stage burn out. The booster vehicle guidance system will have served to orient ICARUS with a spin axis essentially in the orbit plane at right angles to the vehicle-sun line. This means that solar cell power is immediately available without further spacecraft orientation if it is assumed that the most advantageous daily solar launch window has been selected.

A Type I maneuver will orient the spin line at right angles to the vehicle-sun line. It is important to note that this pitching maneuver is not terminated as soon as the non-active Sun sensor sees the Sun, but sufficient pitching must take place until both sensors A and C see the Sun equally (within a small pre-planned deadband). This technique (or its equivalent - such as a horizon seeker) becomes important near the Sun because the spacecraft views the Sun with such a large angle, e.g., at 0.1 AU the subtended angle to see the full sun diameter is 6 degrees. With the expected accuracy of injection the Type I maneuver should not last longer than 1 or 2 minutes. Orientation in pitch should inherently be within an accuracy of 1 or 2 degrees or less. Sufficient gas is carried to provide for a 20° re-orientation however.

A Type II maneuver will erect the spin axis perpendicular to the orbit plane. While the present Pioneer requires about 8 to 9 hours, since each erection pulse is radio commanded at a rate of 1 per minute, erection of ICARUS by 90 degrees can take place at a rate to assure completion in about 10 minutes if this is consistent with acquiring and analysing the engineering data to ascertain vehicle status for interested personnel. Following the nomenclature of section VIID1, the mass of gas required for an orientation of degrees of ICARUS is

$$M_{N_2} = \frac{\theta\, \omega_z I_z}{I_{sp}\, d} \qquad 7C1.1$$

which amounts to .5 kg for = 110° (20° pitch plus 90° roll) or .405 kg per 90° maneuver.

7.D. Cruise Phase

7.D1. Disturbance Torques

The major source of disturbance will be the solar radiation pressure (3,4). If there is an offset between the center of pressure and the center of mass (see Fig. 7D1.1) it will cause a torque about the pitch axis since there is symmetry about the spin axis. Hence the spin axis will tend to drift in roll (see Fig. 7D1.1 for axes and orbit coordinate system). The following numerical calculations, based on a .2 AU mission in the ecliptic plane, determine the maximum allowable offset between center of mass and center of pressure and the amount of gas needed during the cruise phase.

The rotation $\vec{d\alpha}$ of the spin axis during an interval of time dt, due to radiation pressure, occurs about the vehicle-sun line and is:

$$|\vec{d\alpha}| = \left|\frac{dH}{H}\right| = \frac{T\,dt}{I_z \omega_z} \qquad 7D1.1$$

where

$$T = \frac{P_o A b}{r^2} \quad \text{, radiation torque} \qquad 7D1.2$$

$P_o = 4.5 \times 10^{-6}$ N/m^2, radiation pressure at 1 AU
$A = 1.15$ m^2, projected spacecraft area
b = distance between center of mass and center of pressure, in meters
r = vehicle-sun distance, in AU
$I_z = 15.45$ kg m^2
$\omega_z = 10.5$ rad/sec

The total drift α during a blackout period (t_1, t_2) is:

$$\alpha = \left[\alpha_{x_o}^2 + \alpha_{y_o}^2\right]^{1/2} \qquad 7D1.3$$

where

$$\alpha_{x_o} = \int_{t_1}^{t_2} \cos\theta \, |\vec{d\alpha}| \qquad 7D1.4$$

$$\alpha_{y_0} = \int_{t_1}^{t_2} \sin\theta \, |\vec{d\alpha}| \qquad 7D1.5$$

Calculations show that the second communication blackout period, when the spacecraft is just past its perihelion, is the most severe. It occurs between the 91st and 96th day, and results in:

$$\alpha = 0.0082\ b$$

If for example the total drift during blackout is to remain below 0.5°, b must be less than 0.10 m. Such a requirement on the offset between center of mass and center of pressure is well within current practice. For future extension to a .1 AU mission the same calculations require that $b < 0.037$ m, which is still quite feasible.

The total angular impulse, J, due to radiation pressure, for one orbit at .2 AU and with b = 0.10 m, is

$$J = 30.7 \text{ N m sec}$$

The mass of gas required for control is

$$M = \frac{J}{I_{sp}\, d} \quad \text{per orbit} \qquad 7D1.6$$

Nitrogen is used for thrusting, with a specific impulse $I_{sp} = 60$ sec. The nozzle is placed at a distance d = 1.07 m from the center of mass. The total mass of gas needed to overcome only the solar radiation pressure is, for a mission of 1.5 orbits,

$$M_{N_2} = 0.075 \text{ kg}$$

Studies indicate that other sources of disturbances, such as gas leakage (assuming no malfunction), micrometeorite impact, Sun gravity gradient, internal moving parts, are orders of magnitude smaller than solar pressure (5). Even with a safety factor of 2 to account for other disturbances, the amount of gas needed during the cruise phase is only 30% of that for initial acquisition. The total mass, including a single 90° erection and initial acquisition, is

$$M_{N_2\ total} = 0.65\ kg$$

In comparison, the present Pioneer carries 0.395 kg of gas with an associated bottle and supporting structure of 0.79 kg.

7D2. Cruise Phase Attitude Control

If the offset b is kept within the calculated limit of section 7D1, corrections will not be needed more than once every 2-3 days. This may be reduced even further by the use of a small passive solar sail placed on top of the antenna and trimmed on the ground as with the present Pioneer.

The sequence of control pulses is identical to that used during the initial acquisition phase. It may be desirable in view of the possible extension to missions closer to the Sun to control pitch by means of temperature sensors on the solar cells. This would allow the solar cells to operate under the most favorable conditions, within the $\pm 5^{\circ}$ spin axis orientation required by the experiments.

The control of roll, which is commanded from Earth, and thus depends on a communication link, does not present any problem for the .2 AU mission. For closer missions, if a small enough b cannot be achieved, it is suggested that a short memory program for roll corrections during black out periods be provided. This program would be updated from the ground after sufficient information on the actual behavior of the spacecraft has been obtained. Another alternative which is more complex, but has the advantage of recording more accurately the spacecraft position, is the use of a star field sensor.

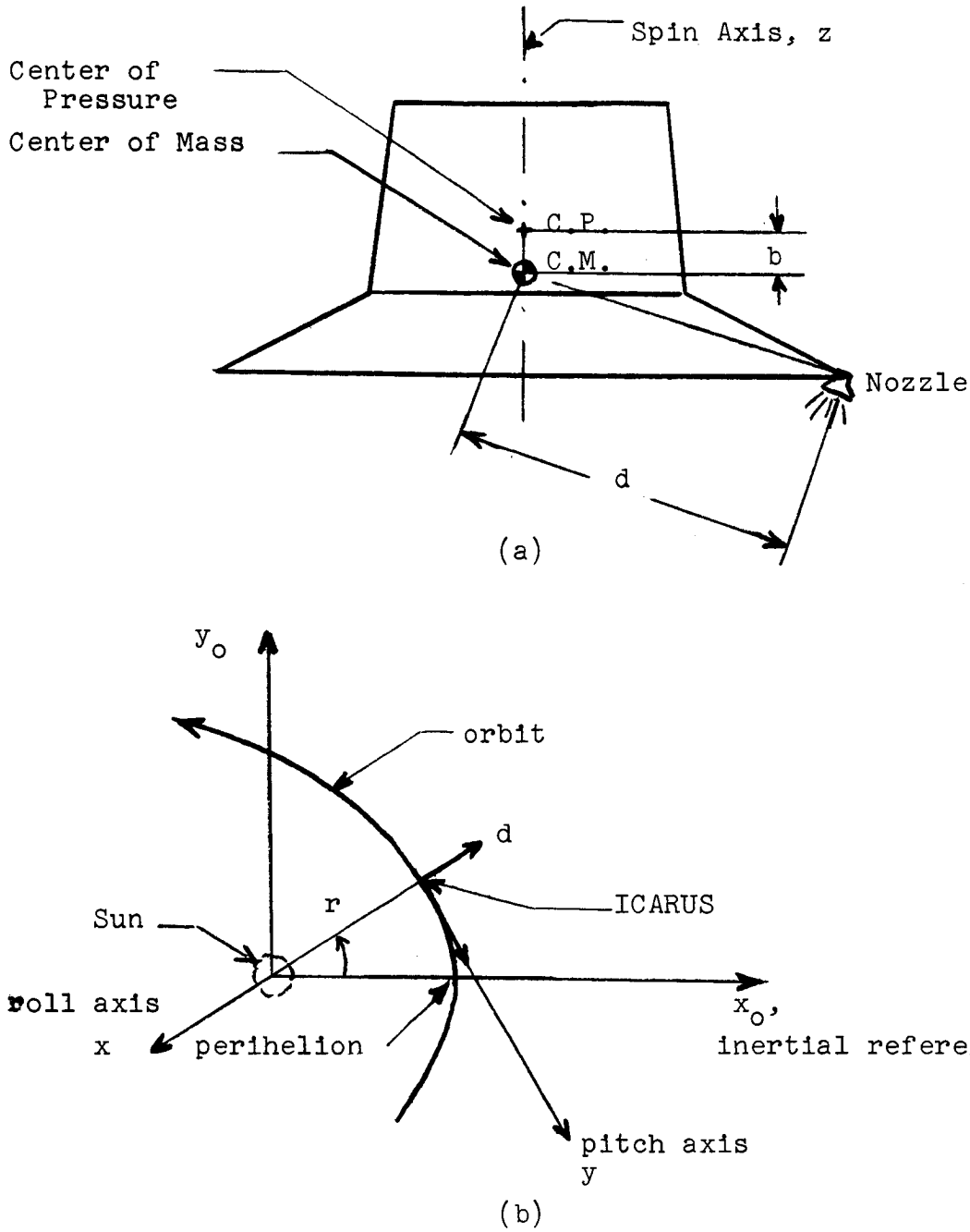

Figure 7D1.1 Orbit Plane Geometry for Calculation of Spin Axis Drift

REFERENCES

1. DeBra, D.B.: Principles and Developments in Passive Attitude Control, AAS Preprint no. 65-135, AAS/AAAS Special Astronautics Symposium, December 29, 1965.
2. Fedor, J.V.: Theory and Design Curves for A Yo-Yo De-Spin Mechanism for Satellites, NASA TN D-708, August, 1961.
3. Koella, H.H., ed.: Handbook of Astronautical Engineering, Section 14.222, McGraw-Hill, 1961.
4. Wolverton, R.W., ed.: Flight Performance Handbook for Orbital Operations, Section 6-1, Wiley, 1963.
5. deMoraes, C.A. and Gage D.D.: Mission Objectives and Design Considerations for a Scientific Solar Probe, AIAA Unmanned Spacecraft Meeting, Los Angles, March,1965.

VIII. PROGRAM DEVELOPMENT

In this chapter, a possible program of development and the corresponding costs are outlined. This program is based upon what is technically feasible and not upon actual governmental fundings or planning schedule.

8A. Program Schedules

Figures 8A1 and 8A2 summarise the program schedule.

The table below illustrates how the ICARUS program might be integrated with the existing PIONEER program.

Phase	Program	Program Duration	Cost
I	Present Pioneer (0.8 AU)	'65 - '69	NA
II	Pioneer Fe Cr (0.5 AU)	'69 - '70	NA
III	ICARUS, 4 flights (0.2 AU, 30° solar cell skirt; 2 in the elciptic, 2 out of the ecliptic)	'71 - '73	100/4
IV	ICARUS, 2 flights (0.1 AU, 20° solar cell skirt; 1 in and 1 out of the ecliptic)	'73 - '74	102/2

8B. Financial Developments

The costs presented here are based on information gathered from various space industries and similar space programs.

For cost analysis purposes, the ICARUS project can be conveniently subdivided into two programs: four missions to 0.2 AU perihelion and two missions to 0.1 AU perihelion. The costs involved in each of these programs include those for the spacecrafts, the experiments and the boosters.

The ICARUS spacecraft should be relatively inexpensive. It has no articulating or despun components. Consequently, it is believed that the four spacecrafts which obtain 0.2 AU will cost a total of 8 million dollars in addition to the 24 million dollars needed for research and development.

Assuming that a space experiment costs 1.2 million dollars per two shots, the total cost for the five experiments on the 0.2 AU missions is estimated to be 12 million dollars.

The booster for the 0.2 AU mission is the Atlas-Centaur with two "kick" stages. This boost system is estimated to cost 56 million dollars for four flights to the 0.2 AU (see Table 5B1.1).

The total cost for the 0.2 AU missions is summarized in the following table.

4 Flights to 0.2 AU

	Cost (Millions of dollars)
Spacecraft - Vehicle	8
R and D	24
Experiments	12
Boosters	56
Total	100
Cost per flight mission	25

The costs per spacecraft for the two missions to 0.1 AU may be estimated to be similar to those for the 0.2 mission except for the boosters. The two Saturn IB/Centaur/2 kick boosters cost 84 million dollars (see table 5B1.1).

2 Flights at 0.1 AU

	Cost (Millions of dollars)
Spacecraft - Vehicle	4
R and D	8
Experiments	6
Boosters	84
	102
Cost per flight mission	51

Figure 8A1.1 ICARUS Critical Program Milestone Dates

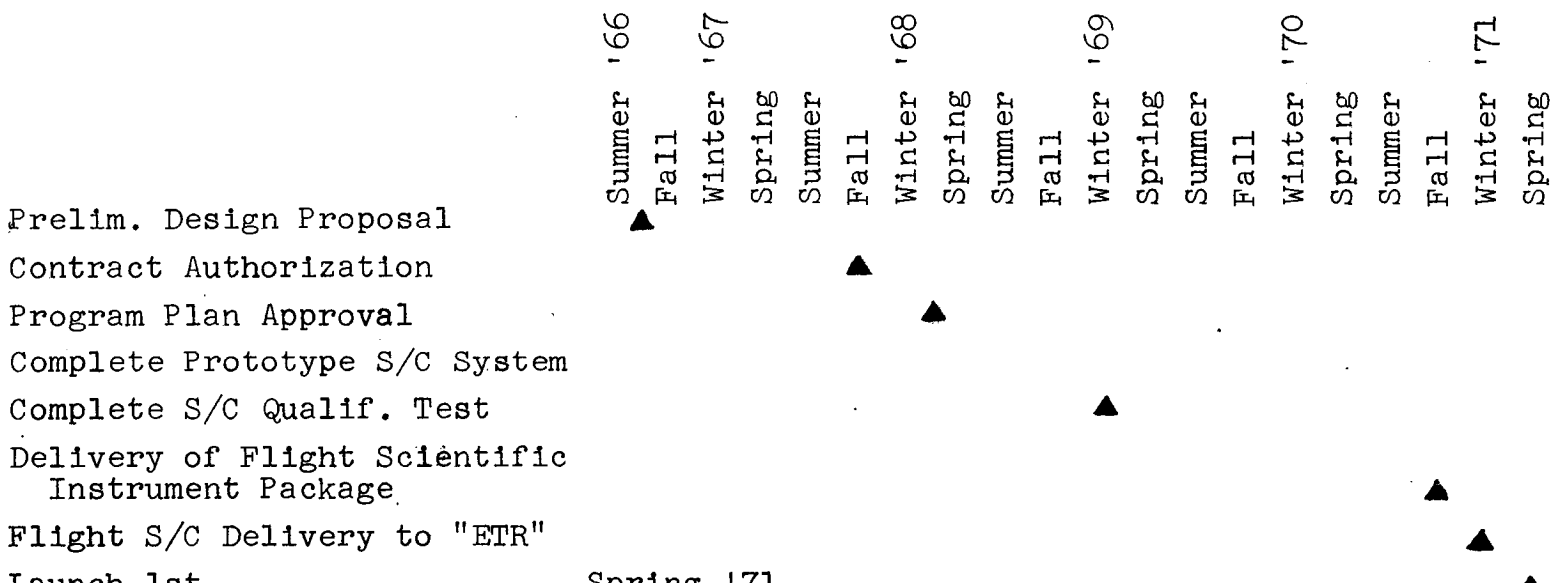

Figure 8A1.2 ICARUS - Program Schedule

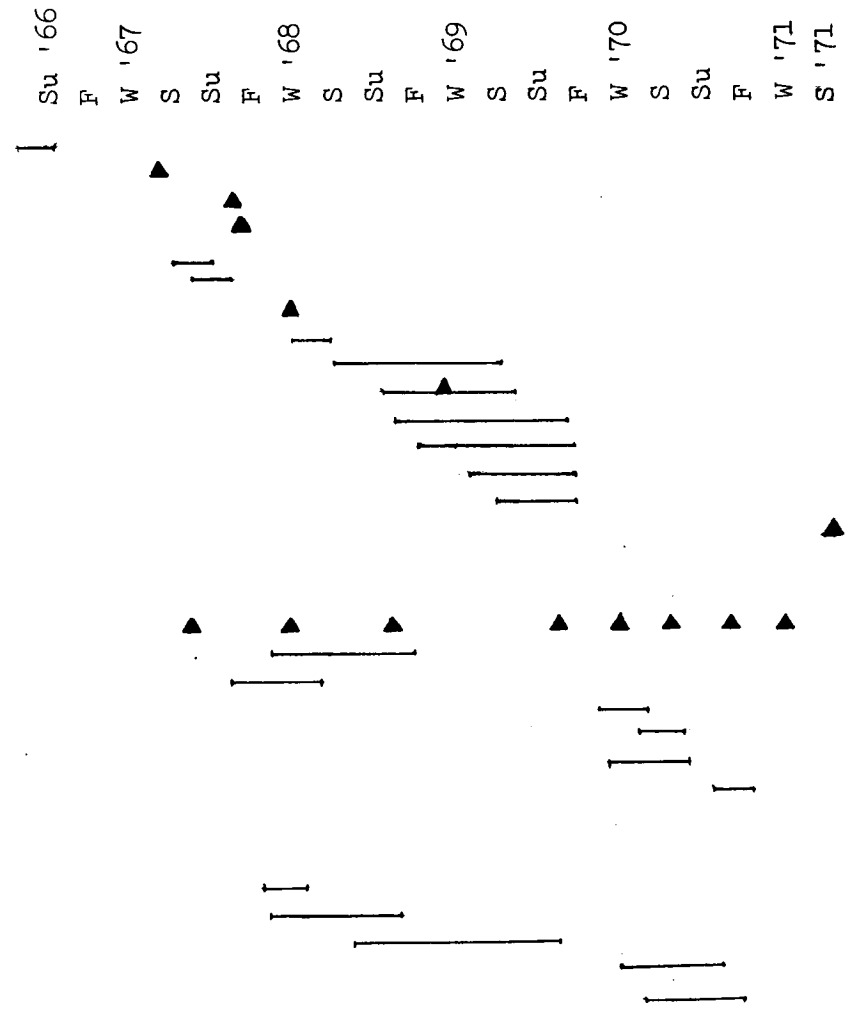

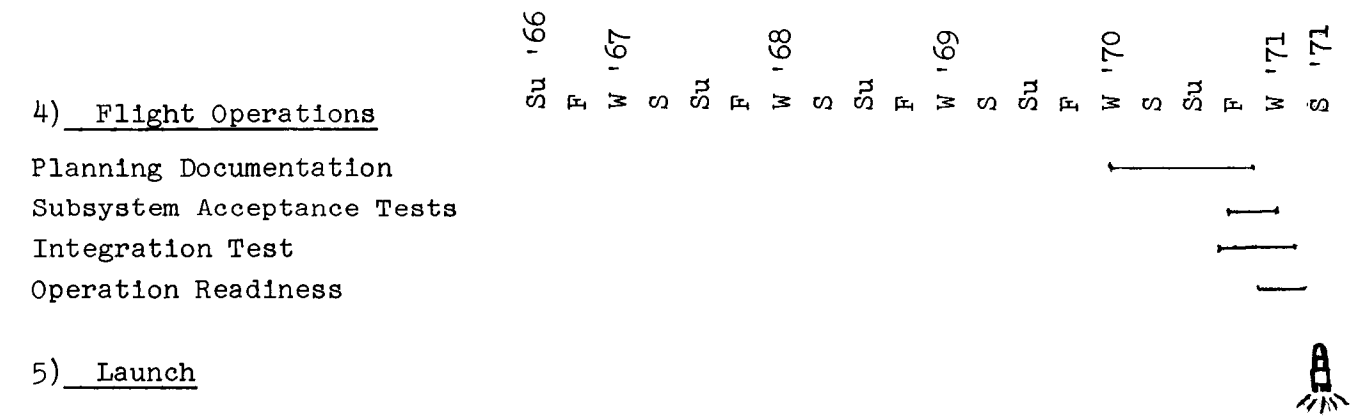
Su '66
F
W '67
S
Su
F
W '68
S
Su
F
W '69
S
Su
F
W '70
S
Su
F
W '71
S '71
4) Flight Operations
Planning Documentation
Subsystem Acceptance Tests
Integration Test
Operation Readiness
5) Launch

IX. GROWTH POTENTIAL AND FUTURE PROJECTS

There are many new problems associated with a solar mission to very small perihelions. The following sections point out some problems and possible solutions, in conjunction with the recommended developments in boosters, trajectories, experiments, communications and spacecraft.

9A. Experiments

The growth potential of the experiments depends primarily upon the ability of the vehicle to carry additional weight to the near vicinity of the Sun. Additional experiments have been described in Chapter 3 which, if placed near the Sun, would yield much more useful information which would aid in developing new and more realistic models of the universe.

The experiments which should be placed on board the spacecraft are listed in descending order of scientific merit in Table 3A1 in the body of this report. In addition, the electronic plasma probe should have a magnetic field added so that it could provide an additional sorting of the incoming particles.

9B. Communications

For close-in solar missions communications requirements change drastically. There is a loss of direct communication because of the near Sun. More data storage capacity will be necessary so that the data can be stored until direct communication becomes possible after the fly by. Use of high temperature electronics and high gain articulated antennas should be investigated.

9C. Trajectories and Boosters

The most difficult problems to be encountered on missions with very small perihelions are (1) the extremely high velocities the spacecraft must obtain and (2) the large change in incident solar flux experienced by the spacecraft. Section 9D, Spacecraft, will deal with the problem of solar flux so it will not be discussed here. Numerous schemes have been devised for achieving these very high velocities (see Fig. 5A2.4). The schemes fall into three broad categories: (1) Single impulse velocity increase, (2) planetary fly-bys, and (3) multiple impuse velocity changes (usually restricted to bi-elliptic transfers). These 3 methods are illustrated in Fig. 9C1.1.

A general discussion of bi-elliptic transfers is found in (1), and a good concise summary is contained in (2).

It appears that they do not offer any significant advantages over planetary fly-bys. The following chart compares booster velocity requirements and time of flight for all three methods for perihelions of 0.025 AU and 0.050 AU.

Perihelions of Interest	Orbit Parameters	Bi-elliptic transfer at 5 AU	Bi-elliptic transfer at 4 AU	Jupiter Fly-by	Direct Ascent
0.025AU	velocity	67,000 ft/sec	69,500 ft/sec	49,500 ft/sec	84,500 ft/sec
	trip time	1,665 days	1,240 days	1,290 days	67 days
0.050AU	velocity	65,500 ft/sec	68,000 ft/sec	49,000 ft/sec	76,700 ft/sec
	trip time	1,680 days	1,260 days	1,310 days	69 days

The bi-elliptic transfer at 4 AU yields a slightly shorter trip time but requires much higher velocities than does a Jupiter fly-by. In either case the trip time is approximately $3\frac{1}{2}$ years. A bi-elliptic transfer at 3 AU* is about 2,500 ft/sec cheaper than a direct ascent, but takes 2.35 years to complete. A Venus fly-by to the same perihelion gains about 6,000 ft/sec and is much faster.

Bi-elliptic transfers have less stringent guidance requirements than planetary fly-bys, but this advantage is more than offset by the disadvantages associated with carrying large quantities of propellant out to aphelion. The velocity to be added at a 4 AU aphelion to obtain a 0.05 AU perihelion, for example, is about 22,000 ft/sec. The engineering problems involved in storing this quantity of rocket propellants in space (especially cryogenics) for periods of 2 to 3 years are staggering. Planetary fly-bys, especially Jupiter, would also require mid-course velocity increments but these are small "guidance correction" impulses and can be accomplished with small amounts of cold gas.

In summary, the problems associated with bi-elliptic transfers to orbits with very small perihelions are worse than those associated with planetary fly-bys, and the bi-elliptic performance "gain" is much less than a planetary

*To a perihelion of 0.05 AU

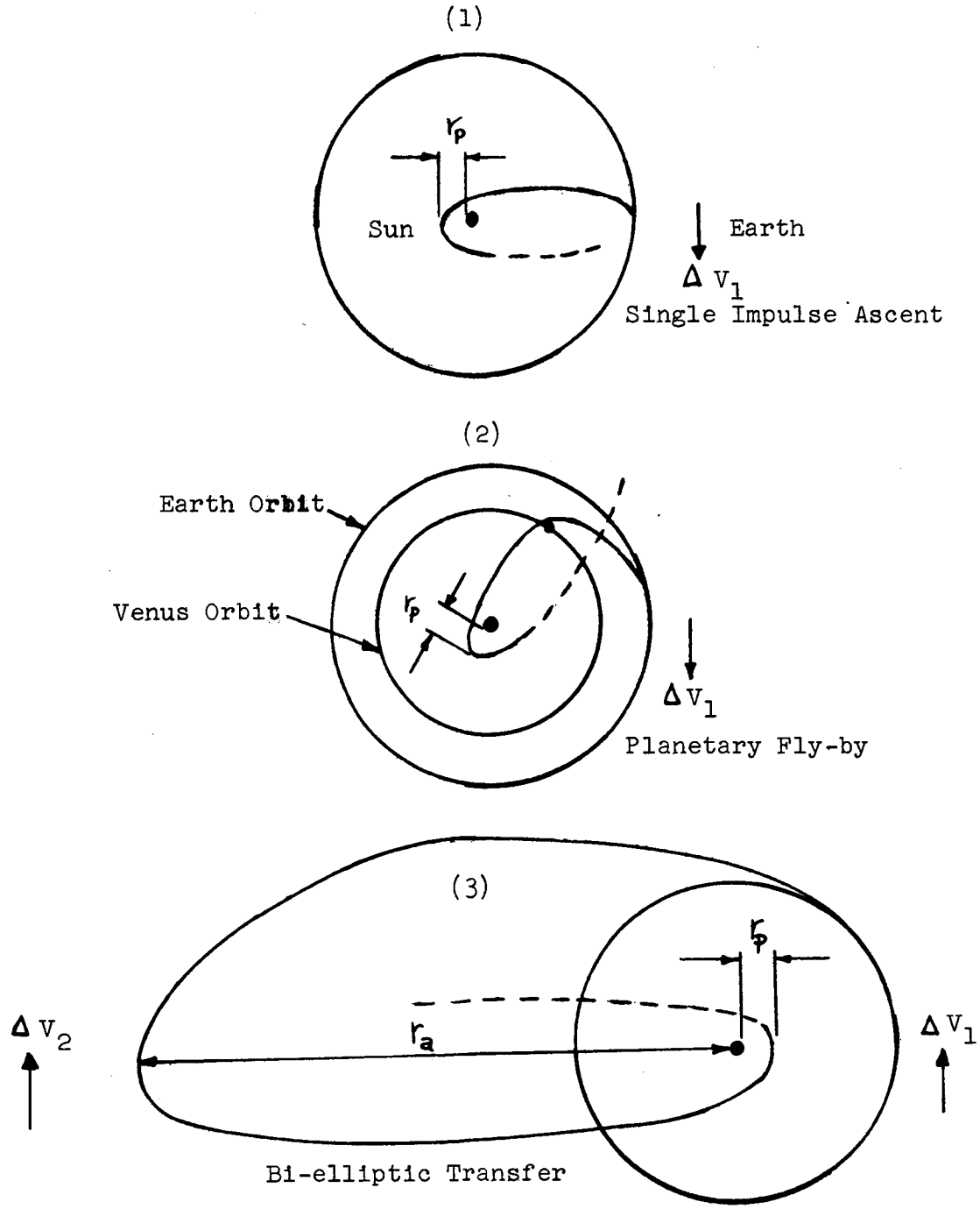

Figure 9C1.1 Methods of Obtaining Small Perihelion

fly-by.

The idea of trading trip time for launch vehicle velocity requirements to orbits very near the Sun is very attractive, however, if one considers planetary fly-bys. The summary in the above chart shows Jupiter fly-by savings of 35,000 ft/sec for a 0.025 perihelion and 27,700 ft/sec for a 0.050 perihelion. In both cases the Jupiter fly-by booster injection velocity requirements are about 49,000 ft/sec. The initial four stage ICARUS launch vehicle (Atlas/Centaur/TE-364-3/FW-4S) will lift a payload of more than 500 lbs. to this velocity, the Saturn IB/Centaur/Poodle will lift about 3700 lbs. to this velocity. (See ref. 3.) These launch vehicles can not lift any payload to a perihelion of 0.05 AU via a direct ascent. However the Saturn V/Centaur/Kick (the kick stage is a high performance 7,000 lb H_2/F_2 engine) or the Saturn V/Centaur/Poodle can lift significant payload weights via a direct ascent to velocities of interest. This information is summarized in the chart below.

Perihelion of 0.05 AU

Launch Vehicle	Payload Weight - lbs -	Estimated Booster Cost - $ million -	Method of Ascent
ICARUS	0	14	single impulse
ICARUS	580	14	Jupiter fly-by
Saturn IB/Centaur	0	41	single impulse
Saturn IB/Centaur	2200	41	Jupiter fly-by
Saturn IB/Centaur/ Poodle	0	44	"single"impusle
Saturn IB/Centaur/ Poodle	3700	44	Jupiter fly-by
Saturn V	0	125	single impulse
Saturn V	18000	125	Jupiter fly-by
Saturn V/Centaur	0	135	single impulse
Saturn V/Centaur	30000	135	Jupiter fly-by
Saturn V/Poodle	1400	128	"single" impulse
Saturn V/Poodle	28000	128	Jupiter fly-by

None of these booster configurations could launch any payload to 0.025 AU via a single impulse velocity increase, but the Jupiter fly-by payloads are essentially unchanged for smaller perihelions.

It is apparent from this summary that Jupiter fly-bys are economically very attractive for close solar probes. Thus it may be more economical to invest in the additional R & D to achieve high reliability components to survive a 3 - 4 year Jupiter fly-by mission to reach 0.025 AU than to invest in the very large and expensive Saturn V launch vehicles required for a direct flight to the same perihelion.

It is recommended that in 1970 a comparison be made of the relative costs of accomplishing the exploration of the solar regions between 0.2 AU and solar impact. It is technically feasible to accomplish the exploration between 0.2 AU and 0.1 AU using the ICARUS spacecraft boosted by the Saturn IB/Centaur/TE-364-3/FW-4S. If, however, by the early 1970's the reliability of equipment has improved sufficiently to achieve a high probability of successfully operating over a four year life time, then it may be preferable to combine the near solar probe mission with a number of other Jupiter fly-by missions such as flights which are 90° out of the ecliptic, and flights to the remote planets.

Future development of more advanced solar probes via Jupiter fly-by should first be aimed at developing a spacecraft which will survive over the extreme ranges of solar flux between aphelion and perihelion. This should be coupled with a major R & D program whose goal is to extend component lifetimes to 4 or 5 years. The booster can then be selected from the currently available types on the basis of minimum cost.

9D. Spacecraft

The ICARUS configuration will be unsatisfactory for missions to less than 0.07 AU perihelion. A more likely design for these missions would incorporate 3-axis stabilization and an elaborate heat shield arrangement. If a Jupiter fly-by trajectory is used an RTG power supply appears attractive. For direct transfer missions a combination power supply using retractable solar cells (4) plus solar thermoelectric seems possible. Recent research (2) indicates that electronic components may be built to operate at 700°K which would greatly reduce the thermal control problem. Due to high solar flux, experiments requiring a direct view of the Sun may require special provisions for cooling the sensing heads. One promising approach is to use mechanical sampling where the instrument is shielded except during the sampling period. There appear to be no serious structural problems for very close missions.

REFERENCES

1. Roy, A.D.: Foundations of Astrodynamics, The MacMillan Co., Inc., 1965.
2. Brasher, W.E. and Schall, E.M.: (TEXAS INSTRUMENT COMPANY), New Concepts for Close Solar Probe Mission, an unpublished paper delivered at Stanford in 1966.
3. Jortner, D. and Martinez, J.S.: System and Mission Considerations for a Radioisotope Propulsion System (POODLE). STL-517-0024, Presented at AIAA Propulsion Conference, Colorado, June 14-18, 1965.
4. Shivoner, Y.T.: GaAs Solar Cell Study: Final Report, Texas Instrument Technical Report no. 08-65-181, December, 1965 (Materials Science Research Lab.).

APPENDIX A

The Telemetry Problem

First, consider the problem of transmitting a single sensor output to the ground terminal. Let x(t) represent the amplitude of the sensor output over the time interval (O,T). Let z(t) represent the reconstructed waveform at the ground terminal. Ideally, we would like for z(t) to be identical to x(t), but this is not possible because of the inherent system noise. A number of systems might be proposed for accepting x(t) as the input (in the spacecraft) and providing the output z(t) (at the ground terminal). In order to compare these systems, a criterion of goodness must be chosen. A reasonable criterion of goodness is the integral squared error, i.e.

$$e = E\left\{ \int_0^T [x(t) - z(t)]^2 dt \right\} \qquad 1$$

and one system might be said to be better than another system if it results in less integral squared error.

Now, in space communications, digital systems are usually preferred to analog systems. A digital system requires that the waveform to be transmitted be given a digital representation, i.e. be represented by a vector. An excellent discussion of the problem of representing a waveform by a vector is given in Appendix B of reference (1).

We write

$$x(t) \doteq \sum_{j=1}^{N} x_j \cdot \alpha_j(t) \qquad 2$$

where the x_j are given by the reflections of x(t) onto the set of orthonormal basis functions

$$x_j = \int_0^T x(t)\, \alpha_j(t)\, dt \qquad 3$$

We now represent the waveform x(t) by the vector X where

$$X = \begin{bmatrix} x_1 \\ x_2 \\ \vdots \\ x_N \end{bmatrix} \qquad 4$$

Equation 2 is not an equality since, in general, an infinite number of basis functions are required. Hence, we incur the error

$$e_1 = E\left\{ \int_0^T \left[x(t) - \sum_{j=1}^{N} x_j \alpha_j(t) \right]^2 dt \right\} \qquad 5$$

when we represent the waveform x(t) by the vector X.

Now, to transmit the vector X to the ground terminal would require an infinite number of bits for each of the elements x_j, $j = 1, 2, \cdots, N$. Therefore, the usual procedure is to "quantize" each x_j into predetermined fixed levels. For example, if each x_j could be quantized into one of ten numbers by rounding off to the nearest integer. Hence, the vector X is transferred into the vector Y by the quantization process. This, of course, results in a second source of error, say e_2. The magnitude of this error depends on "fineness" of the quantization process.

Next, each element of the vector

$$Y = \begin{bmatrix} y_1 \\ y_2 \\ \vdots \\ y_N \end{bmatrix} \qquad 6$$

is coded into a sequence of binary symbols and transmitted to the ground station. Ideally, the output of the ground-based decoder, would be identical to the input to the spacecraft transmitted. However, in general, some decoding errors are introduced so that each y_j is decoded as z_j. (z_j is identical to y_j unless a decoding error is made.) Hence, the system noise in the communication channel introduces a third source of error.

The ground-based data processing equipment reconstructs the waveform

$$z(t) = \sum_{j=1}^{N} z_j \alpha_j(t) \qquad 7$$

from the z_j appearing at the output of the decoder. It can be shown (see reference (2)) that for most cases the three errors e_1, e_2 and e_3 are additive, i.e.

$$e = e_1 + e_2 + e_3$$

The magnitude of the first error e_1 can be minimized by the proper choice of the set of orthonormal basis functions $\phi_j(t)$. The errors e_2 and e_3 are related since increasing the number of quantization levels decreases e_2 but increases e_3 because more bits must then be transmitted in the same time interval which results in less energy per bit and more decoding errors. Therefore, an optimum trade-off that results in minimum mean squared error exists.

REFERENCES

1. Hancock, J. C. and Wintz, P. A.: Signal Detection Theory, McGraw-Hill Book Co., New York, N. Y.; 1966.

2. Totty, R. E.: Telemetry Errors, IEEE Trans., vol. IT-13, No. 4, December, 1966.

APPENDIX B

Structural Analysis

This appendix presents the preliminary design analyses of the following structural elements:

1) equipment plates
2) nitrogen bottle
3) thrust cylinder
4) body cone
5) radio propagation antenna
6) solar cell cone

Since this report represents a preliminary design study, each analysis is intended only to give reasonable engineering estimates for dimensions and weight. However, where appropriate, state-of-the-art plate and shell theory is utilized in conjunction with current material advances in order to approach an efficient design. The structural weight to total spacecraft weight ratio is indicative of the structural efficiency achieved.

Load factors of 30 in the longitudinal direction and 7 in the lateral directions are used to obtain maximum loading conditions. These load factors include a factor of safety of 1.5.

Equipment Plates

The equipment plates are analyzed as circular sandwich plates with a central hole, clamped at the inner edge, elastically supported at the outer edge, subjected to a uniform load on the top, and a line load around the outer edge. No exact analysis exists for this problem. However, it is possible to develop an approximate solution by means of Reissner's Principle, as follows:

Define:

$$U_p = \int_0^{2\pi} \int_a^R \left\{ \left(M_r K_r + M_\theta K_\theta \right) + \left[\frac{M_r^2 + M_\theta^2 - 2\nu_F M_r M_\theta}{2D(1-\nu_F^2)} \right] \right\} r \, dr \, d\theta$$

where U_p = Reissner functional for axisymmetric bending of a circular plate

a = radius of central hole

R = outer radius

$M_r (M_\theta)$ = radial (circumferential) bending moment

K_r = radial curvature = $\frac{d^2 w}{dr^2}$

K_θ = circumferential curvature = $\frac{1}{r} \frac{dw}{dr}$

w = plate deflection

ν_f = Poisson's ratio for face material

D = bending rigidity = $\frac{E t_F t_c^2}{2(1-\nu_f^2)}$

t_F = thickness of facings

t_c = thickness of core

Define:

$$U_s = \int_0^{2\pi} \frac{1}{2} \beta w^2 \Big|_{r=R} R \, d\theta$$

$$= \pi \beta R w^2 \Big|_{r=R}$$

where U_S = energy stored in the spring at the outer edge

β = spring constant for outer spring, $\frac{lb/in}{in}$

Define: $$V_p = -p\int_0^{2\pi}\int_a^R w r\, dr\, d\theta = -2\pi p\int_a^R w r\, dr$$

where V_p = potential energy of the uniform load

p = intensity of uniform load, $\frac{lb}{in^2}$

Define: $$V_N = -N\int_0^{2\pi} w\Big|_{r=R} R\, d\theta = -2\pi N R\, w\Big|_{r=R}$$

where V_N = potential energy of the outer edge line load

N = magnitude of line load, $\frac{lb}{in}$

Then the total Reissner functional is given by

$$F = U_p + U_S + V_p + V_N$$

The deflection and moments are assumed to be given by the following functions, which satisfy geometrical constraints and represent reasonable moment distributions:

$$w = w_0 \frac{(r-a)^2}{R^2}$$

$$M_r = M_0 = \frac{(R-r)^2}{R^2}$$

$$M_\theta = M_1 \frac{(R-r)^2}{R^2}$$

where w_0, $M_{0,1}$ are (as yet) undetermined coefficients.

If these assumptions are substituted into the expression for F, and the integrations are carried out, the resulting equation has the form

$$F = F(w_0, M_0, M_1) .$$

Reissner's principle states, in essence, that the "best" values for w_0, M_0 and M_1 are those values for which the function F has a stationary value. That is,

$$\frac{\partial F}{\partial w_0} = 0 , \quad \frac{\partial F}{\partial M_0} = 0 , \quad \frac{\partial F}{\partial M_1} = 0 .$$

Evaluating the above partial derivatives and setting them equal to zero furnishes three equations for the three unknowns w_0, M_0 and M_1. The final results are as follows:

$$w_0 = \frac{pR^4}{10D} \frac{(f_4 + 12 f_5 \frac{N}{pR}) f_3}{(f_1 + \nu_f f_2) f_1 + (\nu_f f_1 + f_2) f_2 + \frac{6}{5}\frac{BR^3}{D} f_2 f_3}$$

$$M_0 = \frac{5 w_0 D}{f_3 R^2} (f_1 + \nu_f f_2)$$

$$M_1 = \frac{5 w_0 D}{f_3 R^2} (\nu_f f_1 + f_2)$$

where $\alpha = \frac{a}{R}$

$$f_1 = 1 - 6\alpha^2 + 8\alpha^3 - 3\alpha^4$$

$$f_2 = (1-\alpha)^4$$

$$f_3 = 1 - 15\alpha^2 + 40\alpha^3 - 45\alpha^4 + 24\alpha^5 - 5\alpha^6$$

$$f_4 = 3 - 8\alpha + 6\alpha^2 - \alpha^4$$

$$f_5 = (1-\alpha)^2$$

For the bottom equipment plate used in ICARUS

$$a = 5 \text{ in}$$

$$R = 21.3 \text{ in}$$

$$\alpha = \frac{5}{21.3} = 0.235$$

distributed load = $77 + 4 = 81$ lbs

total area = $\pi\left[(21.3)^2 - (5)^2\right] = 1348 \text{ in}^2$

$$p = \frac{(81)(30)}{1348} = 1.8 \frac{\text{lb}}{\text{in}^2}$$

circumference = $2\pi(21.3) = 134$ in

$$N = \frac{30(10+15)}{134} = 5.6 \frac{\text{lb}}{\text{in}}$$

$t_f = 0.020$ in

$t_c = 0.60$ in

$$D = \frac{(42\times10^6)(0.020)(0.6)^2}{2(1-0.01)} = 1.53\times10^5 \text{ lb-in}$$

The outer edge spring for the bottom equipment plate is provided by the body cone and the top equipment plate. From (1) , page 62, the spring constant is determined to be

$$\beta = 2100 \frac{\text{lb}}{\text{in}^2}$$

The final results are as follows:

$$w_o = 0.0203 \text{ in}$$

$$M_o = 50 \text{ lb-in}$$

$$(\sigma_r)_{MAX} = \frac{M_o}{t_f t_c} = \frac{50}{(0.02)(0.6)} = 4{,}170 \text{ psi}$$

$$M.S. = \frac{70{,}000}{4{,}170} - 1 = \underline{\text{HIGH}}$$

The top equipment plate is dimensioned as follows:

$$t_F = 0.013 \text{ in}$$

$$t_c = 0.40 \text{ in}$$

Analysis shows that this plate is adequate for carrying its loading.

Nitrogen Bottle

The spherical gas bottle has a mean radius of 4 in. and will be designed for a burst pressure of 6,500 psi. It is to be made of fiberglass filament wound construction using S 994 glass (60% glass by volume). The ultimate tensile strength of this material is 321,000 psi. Due to the winding technique for a spherical surface, the design stress is reduced to .325 σ_{tu}. The stress in the spherical vessel is given by the following relationship:

$$\sigma = \frac{pR}{2t}$$

or solving for thickness,

$$t = \frac{pR}{2\sigma} .$$

With the values mentioned above,

$$t = \frac{(6500)(4)}{(2)(.325)(321{,}000)/1.5}$$

$$= .187 \text{ in}$$

where the factor of safety of 1.5 has been incorporated.

Given the density of the glass as $\rho = .072 \text{ lb} \times \text{in}^3$, the weight of the gas bottle is

$$W = \rho V$$

$$= \rho \frac{4}{3} \pi (R_o^3 - R_i^3)$$

$$= (0.072)(1.33)\pi (73.5 - 64)$$

$$W = 2.86 \text{ lb}$$

Thrust Cylinder

To find the critical thickness of the beryllium thrust cylinder, the assumption is made that the 7 in. length from the bottom to the lower equipment plate carries the total load. The total load is obtained by multiplying the spacecraft weight by the lingitudinal load factor,

$$P = (165)(30)$$
$$= 4950 \text{ lb}$$

The expression for the buckling load is given by (2)

$$P = 2\pi (.3) E t^2$$

On substituting $E = 42 \times 10^6$ psi and then equating the above two expressions, the thickness is obtained as

$$t = \left[\frac{4950}{(.6)\pi (42 \times 10^6)}\right]^{1/2}$$

$$= 0.0079 \text{ in}$$

Due to present manufacturing limitations, this thickness must be increased to

$$t = 0.030 \text{ in}$$

With this thickness, the weight of the cylinder is

$$W = \rho V$$
$$= \rho 2\pi R t h$$
$$= (0.067)(2\pi)(5)(0.030)(26)$$
$$= 1.64 \text{ lb}$$

The effect of the lateral acceleration is to cause a bending moment in the cylinder. The load acting through the c.g. is

$$P = (165)(7) = 1155 \text{ lb}$$

The critical bending moment for buckling is given by the expression

$$M_{CR} = .3\pi ERt^2$$

The actual bending moment is

$$M = Pd = 1155\,d$$

where d is the distance from the spacecraft c.g. to the bottom edge of the cylinder.

Equating these two relations yields the following expression for d:

$$d = \frac{(.3\pi)(42 \times 10^6)(5)(9 \times 10^{-4})}{11.55 \times 10^2}$$

$$= 154 \text{ in}$$

Since the actual moment arm is approximately 10 in., the cylinder is adequate with respect to bending action.

Body Cone

In order to provide adequate bending rigidity, the wall is of sandwich construction, with fiberglass facings and foam care. Plastic construction has been utilized for thermal considerations in this instance.

face thickness = $t_f = 0.005$ in

core thickness = $t_c = 0.20$ in

The material densities are as follows:

fiberglass (181 glass fabric) $\rho_f = 0.06 \frac{\text{lb}}{\text{in}^3}$

foam (polyeuroethane) $\rho_c = 0.0016 \frac{\text{lb}}{\text{in}^3}$

The body cone surface area is given by:

$$A = 1.98\ m^2$$

$$= 21.28\ ft^2 = 3065\ in^3$$

Total weight of body cone is given as follows:

$$W = A(2t_f\rho_f + t_c\rho_c)$$

$$= 3065\,[2(0.005)(0.06) + (0.20)(0.00116)]$$

$$= 2.55\ lb$$

Structural stability of the cone can be approximately analyzed by using (3) since the spacecraft body is essentially cylindrical. The following parameters must be evaluated:

$$Z_a = 2\left(\frac{a}{R}\right)\left(\frac{a}{t_c}\right)\sqrt{1-\nu_f^2}$$

$$r_a = \frac{\pi^2}{2(1-\nu_f^2)}\left(\frac{E_F}{G_c}\right)\left(\frac{t_F}{t_c}\right)\left(\frac{t_c}{a}\right)^2$$

$$k_{xa} = \frac{N_x/t_F}{E_f}\left(\frac{a}{t_c}\right)^2\frac{2(1-\nu_f^2)}{\pi^2}$$

where a = axial length of cylinder ≈ 16 inches
R = radius of cylinder ≈ 22 inches
ν_f = Poisson's ration for face material ≈ 0.10
E_f = modulus of elasticity of face material = 3.6×10^6 psi
G_c = shear modulus of core material ≈ 700 psi
N_x = axial compressive force, pounds per inch

$$Z_a = 2\left(\frac{16}{22}\right)\left(\frac{16}{0.20}\right)\sqrt{1-(0.1)^2} = 116$$

$$r_a = \frac{\pi^2}{2(1-0.01)}\left(\frac{3.6\times10^6}{7\times10^2}\right)\left(\frac{0.005}{0.20}\right)\left(\frac{0.20}{16}\right)^2$$

$$= 0.10$$

From Fig. 5, Reference (1),

$$k_{xa} = 10$$

$$\frac{N_x}{t_f} = (10)(3.6\times10^6)\left(\frac{0.2}{16}\right)^2\frac{\pi^2}{2(1-0.01)} = 27{,}900 \text{ psi}$$

This represents the critical stress for the fiberglass facings.

The body cone will be loaded primarily by the top and bottom equipment plates. That is, relative motion of the edges of the plates provides the mechanism for introducing forces in the body cone. The maximum allowable relative motion is approximated as follows:

$$\sigma_{CR} = 27{,}900 \text{ psi}$$

$$\epsilon_{CR} = \frac{\sigma_{CR}}{E} = \frac{2.79\times10^4}{3.6\times10^6} = 7.75\times10^{-3}$$

relative deflection = $\delta = \epsilon_{CR} L = (7.75\times10^{-3})(15.3)$

$$= 0.12 \text{ in}$$

The closed system of equipment plates and cone is quite stiff; thus, 0.12 inches of relative motion of the plate edges should never occur, and the body cone as designed is satisfactory.

Radio Propagation Antenna

This antenna consists of a beryllium wire which is seven inches long and 10 mils in diameter. The geometrical and physical properties are as follows:

density : $\rho = 0.067 \frac{lb}{in^3}$

modulus of elasticity : $E = 42\times10^6 \frac{lb}{in^2}$

moment of inertia : $I = \frac{\pi(0.010)^4}{64} = 4.91\times10^{-10} \text{ in}^4$

weight per unit length : $q = \pi(0.005)^2(0.067)$
$= 5.26 \times 10^{-6} \frac{lb}{in}$

First, considering the transverse acceleration of 7 g's and assuming that the antenna is a cantilever beam, the moment and stress are:

$$\text{Maximum moment} = \frac{7(5.26\times10^{-6})(7)^2}{2} = 9.02\times10^{-4}\ lb\text{-}in$$

$$\text{Maximum stress} = \frac{(9.02\times10^{-4})(0.005)}{4.91\times10^{-10}} = 9.18\times10^{3}\ psi$$

$$M.S. = \frac{70}{9.18} - 1 = \underline{\text{HIGH}}$$

The deflection at the end of the antenna is:

$$\delta = \frac{(7)(5.26\times10^{-6})(7)^4}{(8)(42\times10^{6})(4.91\times10^{-10})} = 0.536\ in$$

This deflection, while many times greater than the thickness, is much less than the length of the beam and is acceptable.

The antenna must also support its own weight, without buckling, during the 30 g longitudinal acceleration. The critical value of weight per unit length for a cantilevered bar under its own weight is given by

$$q_{CR} = \frac{7.837\,EI}{L^3}$$

$$= 4.59\times10^{-4}\ \frac{lb}{in}$$

$$M.S. = \frac{4.59}{5.26} - 1 = \underline{\text{HIGH}}$$

Solar Cell Cone

The solar cells are supported on an integrally stiffened beryllium conical frustum (see Fig. 6B2.4). The cone thickness is 0.018 inches; the stiffeners are 0.50 inches long and 0.030 inches thick. The total weight of the stiffened cone is 4.28 kg (9.4 pounds).

First consider the lateral load caused by the 7 g acceleration. An alternate solution to the actual complex problem is made possible by devising a substitute loading condition which is more severe on the structure but which admits a simple solution. If the cone can survive this more severe loading, it should be considered capable of surviving the actual load condition.

The critical question associated with the actual lateral load concerns the possible instability of the cone wall due to any compressive stresses in the wall. A more severe load state would consist of the load per unit area caused by lateral acceleration applied as a hydrostatic pressure. The critical value of the hydrostatic pressure is given in (4) as follows:

$$p_{CR} = \frac{0.74E}{\left(\frac{L}{\rho_{AVE}}\right)\left(\frac{\rho_{AVE}}{t}\right)^{5/2}}$$

where p_{CR} = critical value of hydrostatic pressure

L = slant length of cone = 22.1 inches

$$\rho_{AVE} = \frac{R_1 + R_2}{2\cos\alpha} = 62.5 \text{ in}$$

t = thickness of cone = 0.018 inches

Note that the thickness is taken as the thickness of the cone alone. This is conservative, since the stiffeners tend to give an effective thickness of 0.032 inches. Once again, if the severe load can be carried by the cone without stiffeners, then the stiffened structure will carry the actual load.

Substituting into the above equation:

$$p_{CR} = \frac{0.74(42 \times 10^6)}{\left(\frac{22.1}{62.5}\right)\left(\frac{62.5}{0.018}\right)^{5/2}} = 0.124 \frac{lb}{in^2}$$

The actual lateral load per unit area is:

$$p = \frac{7(10+15)}{(30)(144)} = 0.0405 \frac{lb}{in^2}$$

This is determined by taking the total weight of structure plus solar cells, multiplying by the lateral load factor, and dividing by the surface area of the cone. This load represents the lateral component of the following normal pressure:

$$p_{ACTUAL} = \frac{0.0405}{\cos 60^\circ} = 0.081 \frac{lb}{in^2}$$

$$M.S. = \frac{0.124}{0.081} - 1 = 0.53$$

Next consider the longitudinal loading caused by the 30 g acceleration. Since the solar cells are essentially hanging from the bottom equipment plate (see Fig. 6B2.3), the axial forces in the cone are tensile and lead to no instabilities. However, due to the displacements of the cone, compressive hoop forces are generated. Therefore, there exists the possibility of circumferential instability.

The detailed analysis of this problem is beyond the scope of this effort. However, several structural model analyses based on

1) a longitudinal element of the shell resting on an elastic foundation representing the remainder of the frustum,

2) the effective hoop contraction of a cylindrical shell segment due to differential axial loading (a problem analogous to the circumferential buckling of shells under thermal stress due to axially varying thermal gradients) and

3) the complete neglect of the effect of the integral stiffening in preventing such buckling

lead to the intuitive conclusion that the solar cell unit is capable of carrying the acceleration load without buckling.

REFERENCES

1. Timoshenko, S., and Woenowsky-Krieger, S.: Theory of Plates and Shells, McGraw-Hill Book Co., New York, 1959, Chpt. 1.

2. Weingarten, V. I., Morgan, E. J., and Seide, Paul: Elastic Stability of Thin Walled Cylindrical and Conical Shells Under Axial Compression, AIAA Journal, p. 500, March 1965.

3. Weingarten, V. I., Morgan, E. J., and Seide, Paul: Elastic Stability of Thin Walled Cylindrical and Conical Shells Under Combined External Pressure and Axial Compression, AIAA Journal, p. 913, May 1965.

4. Stein, Manuel, and Mayers, J.: Compressive Buckling of Simply Supported Curved Plates and Cylinders of Sandwich Construction, NACA TN 2601, 1952.

APPENDIX C

Derivation of Eq. 6C3.4

$$Q = \alpha_s \frac{S}{\pi} Dh \tan^{-1} R \Big|_{R_1}^{R_2} \qquad 6C3.4$$

where α_s = the fraction of incident radiation re-emitted diffusely.

S = the solar constant

$R = r/h$, $R_1 = r_1/h$, $R_2 = r_2/h$

D, h, r, see Fig. 6C3.3

Referring to Fig. 6C3.3 and Fig. A-1 immediately following, the heat flux from an elemental area on the antenna , to an elemental area on the top of the vehicle is given by

$$dQ_{d1,d2} \simeq i_1^{\circ} \frac{\sin\theta \cos\theta}{\pi S^2} dA_1 dA_2 \qquad (D \ll r)$$

assuming diffuse radiation of the flux i_1° . The total flux to the louver area is then

$$Q_{12} = i_1 \int_{r_1}^{r_2} r dr \int_0^{2\pi} d\psi \int_0^{\theta_0} \pi D d\alpha \left(\frac{\sin\theta \cos\theta}{\pi^2 S^2} \right)$$

Substituting: $S = r \sec\theta$, $d\alpha = r \sec^2\theta d\theta$ this becomes

since $\sin\theta_0 = \frac{h}{\sqrt{h^2+r^2}}$ the θ integration yields

$$Q_{12} = i_1^{\circ} D \int_{r_1}^{r_2} \frac{h^2 dr}{h^2+r^2}$$

Substituting $R = r/h$ this becomes

$$Q_{12} = i_1 Dh \int_{R_1}^{R_2} \frac{dR}{1+R^2} = i_1^{\circ} Dh \tan^{-1} R \Big|_{R_2}^{R_1}$$

If the antenna is assumed to be in thermal equilibream and only radiation heat transfer is considered. Then

$$i_1^{\circ} = \alpha_s \frac{S}{\pi}$$ and

$$Q_{12} = \alpha_s \frac{S}{\pi} Dh \tan^{-1} R \Big|_{R_2}^{R_1}$$

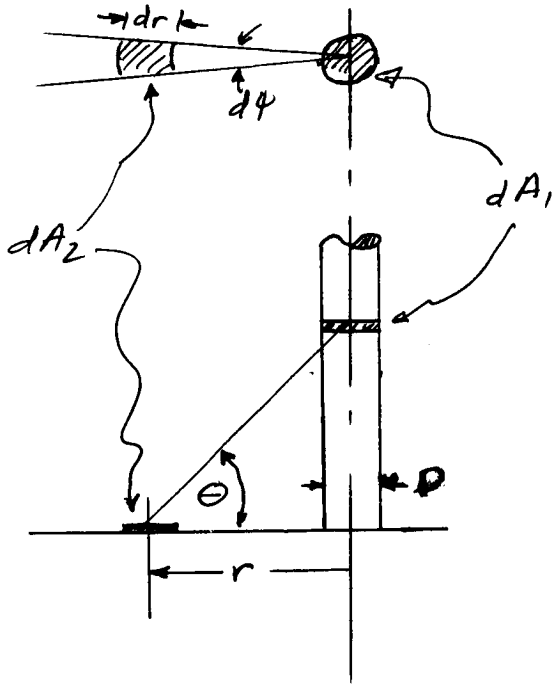

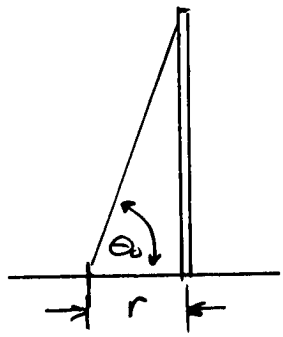

Figure A-1

APPENDIX D

LECTURE SERIES

Stanford Faculty	Topic
Bollay, Dr. William Engineering Dept.	(1) Objectives of the Course (2) Background on Previous System Engineering Projects (3) Available Booster Systems (4) Orbits and Trajectories
De Bra, Dr. Daniel Aeronautics & Astronautics	Stabilization
Lusignan, Dr. Bruce B. Electrical Engineering	(1) Objectives of the Course (2) Communications
Mayers, Prof. Jean Aeronautics & Astronautics	Structural Design
Sturrock, Dr. Peter Engineering Science	Nature of Solar Corona

NASA Lecturers	
Fimmel, Mr. Richard	Data Processing
Foster, Mr. John	Objectives of the Advanced Pioneer Project, Power Supplies
Iufer, Mr. Ernest	Magnetic Cleanliness
Lumb, Dr. Dale	Data Processing
Matthews, Mr. Howard	Present Pioneer Project
Sonnett, Dr. C. P.	Magnetometers
Streed, Dr. Elmer	Thermal Control
Wolfe, Dr. John	Charged Particle Counters (low to medium energies)

Visiting Lecturers	
Brasher, Mr. William Texas Instruments Corp.	High Temperature Solar Cells

Harris, Mr. S. Douglas Aircraft Corp.	Thor-Delta Vehicle
Jortner, Dr. D. T R W Corp.	Poodle Nuclear Rocket
Kirk, Mr. J. Douglas Aircraft	Thor-Delta Vehicle
McCracken, Dr. Kenneth Southwest Research Inst.	Charged Particle Counters (high energy)
Peake, Mr. Frank Douglas Aircraft Corp.	Thor-Delta Vehicle
Rittenhouse, Mr. John B. Lockheed Corp.	Materials Science
Schall, Dr. Edward M. Texas Instruments Corp.	High Temperature Solar Cells